# REGULATION OF MITOCHONDRIAL FUNCTION ON ANIMAL DISEASES

EDITED BY: Hui Zhang, Yung-Fu Chang and Jianzhu Liu
PUBLISHED IN: Frontiers in Veterinary Science

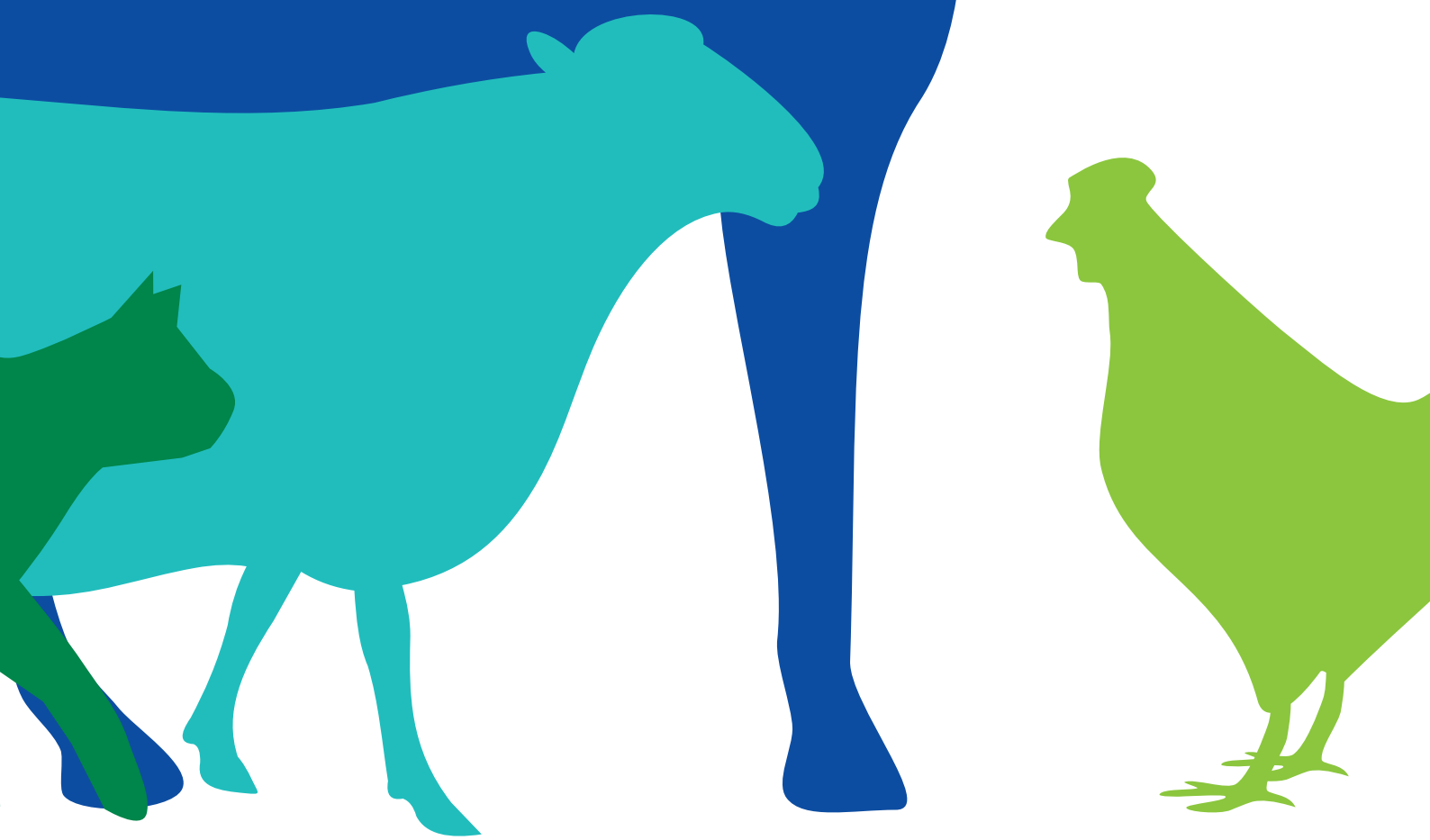

frontiers Research Topics

# frontiers



ISSN 1664-8714
ISBN 978-2-88976-545-4
DOI 10.3389/978-2-88976-545-4

## About Frontiers

Frontiers is more than just an open-access publisher of scholarly articles: it is a pioneering approach to the world of academia, radically improving the way scholarly research is managed. The grand vision of Frontiers is a world where all people have an equal opportunity to seek, share and generate knowledge. Frontiers provides immediate and permanent online open access to all its publications, but this alone is not enough to realize our grand goals.

## Frontiers Journal Series

The Frontiers Journal Series is a multi-tier and interdisciplinary set of open-access, online journals, promising a paradigm shift from the current review, selection and dissemination processes in academic publishing. All Frontiers journals are driven by researchers for researchers; therefore, they constitute a service to the scholarly community. At the same time, the Frontiers Journal Series operates on a revolutionary invention, the tiered publishing system, initially addressing specific communities of scholars, and gradually climbing up to broader public understanding, thus serving the interests of the lay society, too.

## Dedication to Quality

Each Frontiers article is a landmark of the highest quality, thanks to genuinely collaborative interactions between authors and review editors, who include some of the world's best academicians. Research must be certified by peers before entering a stream of knowledge that may eventually reach the public - and shape society; therefore, Frontiers only applies the most rigorous and unbiased reviews.
Frontiers revolutionizes research publishing by freely delivering the most outstanding research, evaluated with no bias from both the academic and social point of view. By applying the most advanced information technologies, Frontiers is catapulting scholarly publishing into a new generation.

## What are Frontiers Research Topics?

Frontiers Research Topics are very popular trademarks of the Frontiers Journals Series: they are collections of at least ten articles, all centered on a particular subject. With their unique mix of varied contributions from Original Research to Review Articles, Frontiers Research Topics unify the most influential researchers, the latest key findings and historical advances in a hot research area! Find out more on how to host your own Frontiers Research Topic or contribute to one as an author by contacting the Frontiers Editorial Office: frontiersin.org/about/contact

# REGULATION OF MITOCHONDRIAL FUNCTION ON ANIMAL DISEASES

Topic Editors:
**Hui Zhang,** South China Agricultural University, China
**Yung-Fu Chang,** Cornell University, United States
**Jianzhu Liu,** Shandong Agricultural University, China

**Citation:** Zhang, H., Chang, Y.-F., Liu, J., eds. (2022). Regulation of Mitochondrial Function on Animal Diseases. Lausanne: Frontiers Media SA.
doi: 10.3389/978-2-88976-545-4

# Table of Contents

frontiers | Frontiers in Veterinary Science

EDITORIAL
published: 17 June 2022
doi: 10.3389/fvets.2022.943860

# Editorial: Regulation of Mitochondrial Function on Animal Diseases

*Hui Zhang*[1], *Yung-Fu Chang*[2]* *and Jianzhu Liu*[3]*

[1] College of Veterinary Medicine, South China Agricultural University, Guangzhou, China, [2] College of Veterinary Medicine, Cornell University, Ithaca, NY, United States, [3] College of Veterinary Medicine, Shandong Agricultural University, Taian, China

**Keywords: regulation of mitochondrial function on animal diseases mitochondria, apoptosis, oxidative stress, energy metabolism, immune response**

**Editorial on the Research Topic**

**Regulation of Mitochondrial Function on Animal Diseases**

Mitochondria provide necessary energy for cells and participate in cell differentiation, cell information transmission, cell apoptosis, oxidative stress, and other processes (1). Meanwhile, mitochondria have the ability to regulate cell growth, cell cycles and play an essential role in the regulation of various animal diseases. When mitochondrial dysfunction occurs, it is accompanied by a series of diseases. This topic aims to study the regulatory role of mitochondria in the occurrence of various animal diseases. The 12 papers were collected in this topic, expounded on the role of mitochondria in controlling apoptosis, autophagy, oxidative stress, energy metabolism, signal transduction, and other aspects from different perspectives.

## MITOCHONDRIAL DAMAGE AND OXIDATIVE STRESS

Excessive ROS production can lead to mitochondrial membrane damage. Studies show that methionine-deficient broilers at 42 days of age have apparent kidney and liver damage with the change of mitochondrial structure and lipid metabolic disorders (Song et al.). Therefore, lipid metabolism disorder may be the secondary phenomenon of this pathological change, and mitochondrial damage is the first cause. Mitochondria are also affected by an excess of ROS, eventually leading to oxidative stress. Mitochondrial quality control (MQC) is essential for maintaining mitochondrial function. MQC is a safety mechanism of mitochondria, which can maintain the normal operation of mitochondrial biogenesis, mitochondrial division, mitochondrial fusion, and mitochondrial phagocytosis (2). In the study of vanadium (V) induced cardiac oxidative stress and mitochondrial quality control disorders in ducks, it was found that excessive V could cause cardiac oxidative stress in ducks, and V increased the levels of $H_2O_2$, MDA, and CAT, and the associated mitochondrial damage would also occur, leading to mitochondrial dysfunction (Xiong et al.).

## MITOCHONDRIA REGULATE APOPTOSIS AND AUTOPHAGY

Mitochondria-mediated signal transduction linked to an internal apoptosis pathway. P53 can interact with Bcl2 family members in the outer membrane of mitochondria, catalyze Bak activation and promote transcription-independent activation of Bax. Subsequently, activated Bak and Bax oligomerize in the outer membrane of mitochondria, inducing permeability. Caspase-9 is activated by signal transduction mediated by internal mitochondria, leading to activation of Caspase-3, thereby promoting apoptosis (3, 4). Conversely, Bcl2 inhibits the activation of Bax and Bak, thereby inhibiting apoptosis. Study showed that aflatoxin B1 (AFB1) inhibited

OPEN ACCESS

***Edited and reviewed by:***
*Domenico Bergero, University of Turin, Italy*

***Correspondence:**
*Yung-Fu Chang*
*yc42@cornell.edu.cn*
*Jianzhu Liu*
*liujz@sdau.edu.cn*

***Specialty section:***
*This article was submitted to Animal Nutrition and Metabolism, a section of the journal Frontiers in Veterinary Science*

***Received:*** *14 May 2022*
***Accepted:*** *03 June 2022*
***Published:*** *17 June 2022*

***Citation:***
*Zhang H, Chang Y-F and Liu J (2022) Editorial: Regulation of Mitochondrial Function on Animal Diseases. Front. Vet. Sci. 9:943860. doi: 10.3389/fvets.2022.943860*

the transcription of Bcl2 in broiler kidney tissue, promoted the transcription of P53, Bax, Bak1, CyC, Casp9, and Casp3, and induced renal cell apoptosis through the mitochondrial pathway. These findings suggest that AFB1 may activate mitochondrial-mediated apoptosis pathways (Tao et al.). With the addition of AFB1, it was found that the transcription of Bcl2 was reduced, and the expression levels of Casp3, Casp9, p53, Bak1, and Bax were observed to increase, while the addition of Herba extract (PCPE) had the opposite effect. These results highlight the involvement of AFB1 in mitochondria-related apoptosis (Nabi et al.). In addition, the study on the effects of dioxafimin (DQ) poisoning on mitochondrial apoptosis in duck liver also found that anti-apoptotic genes Parkin and Bcl2 were significantly up-regulated after DQ treatment, suggesting that anti-apoptotic factors play an important role in ducklings during acute DQ poisoning (Chen et al.). Adenosine triphosphate binding box subfamily C member 9 (ABCC9) protein is associated with bioelectrical control. The blocking of the KATP pathway controlled by G protein can significantly inhibit the proliferation and induce apoptosis of glioma and xenograft cells. In the study of down-regulated ABCC9 expression in canine breast cancer, it was found that ABCC9 and ABCC9 mRNA levels on the cell membrane of malignant tissues were significantly reduced, and ABCC9 expression was negatively correlated with cancer grade, and positive cells in the grade III cancer samples basically disappeared. This relationship may be due to the inhibition of KATP channels in cancer tissues (Hao et al.). Excessive V decreased the mRNA levels of Parkin, PINK1, P62, LC3B, and PGC-1α, NRF1, and TFAM, as well as the protein levels of PINK1 and PGC-1α, suggesting that excessive V could lead to biogenic damage of duck heart mitochondria, resulting in the defects of mitotic phagocytosis in myocardial cells. It is speculated that excessive V can seriously damage cardiac myocytes and mediate mitochondrial phagocytosis defects by inhibiting PINK1/Parkin signaling pathway (Xiong et al.).

## MITOCHONDRIA ARE INVOLVED IN ENERGY METABOLISM

The long chain enyl-CoA hydrase (OMIM 609015, EC 4.2.1.74), an enzyme that is integrated into the mitochondrial trifunctional proteins, is dysfunctional, and it remains to be seen whether genetic defects cause atypical myopathy in neonatal foals (Sander et al.). Glucose and serum-free fatty acid levels did not alter acute succinic acid (SUC) management, but lactic acid levels were significantly reduced in skeletal muscle. The results showed that SUC's explosive power increased did not depend on glycolysis and β -oxidation of fatty acids. After SUC treatment, ATP increased by increasing electron transport efficiency and oxidative phosphorylation. Moreover, SUC decreased NADH/NAD+ ratio, enhanced complex mitochondrial enzyme, increased creatine kinase (CK) activity, and increased skeletal muscle strength by increasing ATP production. Mitochondrial calcium levels strictly control mitochondrial ATP production, which stimulates complex III and ATP synthase on the electron transport chain to accelerate oxidative phosphorylation, and SUCNR1 activation has been shown to activate calcium signaling (Xu et al.). The proton drive drives the oxygen consumption of mitochondria, which is present in the inner membrane of mitochondria and drives the production of ATP. When the energy requirement of cells increases, the proton drive increases, increasing the oxygen consumption rate (OCR). OCR of vaccinated hens was significantly higher than that of unvaccinated hens, indicating an increase in the oxidative capacity of activated immune cells (Meyer et al.).

## MITOCHONDRIA PARTICIPATE IN ANTIVIRAL IMMUNITY

Mitochondria, which play a key role in apoptosis, become an important part of antiviral immunity. Novel mitochondrial proteins of mitochondrial antiviral signaling proteins (MAVS), as well as mitochondrial DNA and mitochondrial ROS, produced as sources of hazard-associated molecular patterns (DAMP), will be involved in antiviral immunity. The adaptive development of mitochondrial antiviral proteins in mammalian species was revealed, and the CARD domain of MAVS protein is highly conserved in mammals, which seems to be related to its participation in the adaptive immunity of the organism (Ahmad et al.).

It is also worth mentioning that Gao et al. determined the complete mitochondrial DNA (MT DNA) sequence of fluke lamiformis intermediates based on gene content and genome organization in Yaks of Qinghai-Tibet Plateau for the first time. Furthermore, the activation of TLR1/2/6/9/MyD88/NF-κB and TLR3/TRIF/IRF signal transduction pathways promotes the production of inflammatory factors, which provides a theoretical basis for the control of mastitis caused by *M. bovis* (Yang et al.).

Together, these results represent the latest data on the regulatory role of mitochondrial function in animal diseases. Despite all the existing literature and evidence on this extremely important topic, the papers published in this ebook clearly show mitochondria's role in controlling apoptosis, autophagy, oxidative stress, energy metabolism, signal transduction, and more. By the end of this book, the reader will understand the regulatory roles mitochondria play in animal disease.

## AUTHOR CONTRIBUTIONS

HZ, Y-FC, and JL wrote the article. All authors contributed to the article and approved the submitted version.

## REFERENCES


1. Herai RH, Negraes PD, Muotri AR. Evidence of nuclei-encoded spliceosome mediating splicing of mitochondrial RNA. *Hum Mol Genet*. (2017) 26:2472–9. doi: 10.1093/hmg/ddx142
2. Bouchez C, Devin A. Mitochondrial biogenesis and mitochondrial Reactive Oxygen Species (ROS): a complex relationship regulated by the cAMP/PKA signaling pathway. *Cells*. (2019) 8:287. doi: 10.3390/cells8040287
3. Bock FJ, Tait S. Mitochondria as multifaceted regulators of cell death. *Nat Rev Mol Cell Biol*. (2020) 21:85–100. doi: 10.1038/s41580-019-0173-8
4. Estaquier J, Vallette F, Vayssiere JL, Mignotte B. The mitochondrial pathways of apoptosis. *Adv Exp Med Biol*. (2012) 942:157–83. doi: 10.1007/978-94-007-2869-1_7


**Conflict of Interest:** The authors declare that the research was conducted in the absence of any commercial or financial relationships that could be construed as a potential conflict of interest.

frontiers in Veterinary Science

ORIGINAL RESEARCH
published: 11 August 2021
doi: 10.3389/fvets.2021.727766

# Effects of Acute Diquat Poisoning on Liver Mitochondrial Apoptosis and Autophagy in Ducks

*Jiaxin Chen*[1†], *Yalin Su*[1†], *Renzhao Lin*[1], *Fei Lin*[1], *Peng Shang*[2*], *Riaz Hussain*[3] *and Dayou Shi*[1*]

[1] College of Veterinary Medicine, South China Agricultural University, Guangzhou, China, [2] College of Animal Science, Tibet Agriculture and Animal Husbandry College, Linzhi, China, [3] Department of Pathology, Faculty of Veterinary and Animal Sciences, The Islamia University of Bahawalpur, Bahawalpur, Pakistan

Diquat (DQ) is an effective herbicide and is widely used in agriculture. Due to persistent and frequent applications, it can enter into aquatic ecosystem and induce toxic effects to exposed aquatic animals. The residues of DQ *via* food chain accumulate in different tissues of exposed animals including humans and cause adverse toxic effects. Therefore, it is crucial and important to understand the mechanisms of toxic effects of DQ in exposed animals. We used ducks as test specimens to know the effects of acute DQ poisoning on mechanisms of apoptosis and autophagy in liver tissues. Results on comparison of various indexes of visceral organs including histopathological changes, apoptosis, autophagy-related genes, and protein expression indicated the adverse effects of DQ on the liver. The results of our experimental trial showed that DQ induces non-significant toxic effects on pro-apoptotic factors like BAX, BAK1, TNF-α, caspase series, and p53. The results revealed that anti-apoptotic gene *Parkin* was significantly upregulated, while an upward trend was also observed for Bcl2, suggesting that involvement of the anti-apoptotic factors in ducklings plays an important role in DQ poisoning. Results showed that DQ significantly increased the protein expression level of the autophagy factor Beclin 1 in the liver. Results on key autophagy factors like LC3A, LC3B, and p62 showed an upward trend at gene level, while the protein expression level of both LC3B and p62 reduced that might be associated with process of translation affected by the pro-apoptotic components such as apoptotic protease that inhibits the occurrence of autophagy while initiating cell apoptosis. The above results indicate that DQ can induce cell autophagy and apoptosis and the exposed organism may resist the toxic effects of DQ by increasing anti-apoptotic factors.

**Keywords: diquat, liver, apoptosis, autophagy, ducks**

OPEN ACCESS

***Edited by:***
*Yung-Fu Chang,*
*Cornell University, United States*

***Reviewed by:***
*Fazul Nabi,*
*Lasbela University of Agriculture, Water and Marine Sciences, Pakistan*
*Fan Yang,*
*Jiangxi Agricultural University, China*

***Correspondence:**
*Peng Shang*
*nemoshpmh@126.com*
*Dayou Shi*
*shidayou@scau.edu.cn*

[†]*These authors have contributed equally to this work*

***Specialty section:***
*This article was submitted to Animal Nutrition and Metabolism, a section of the journal Frontiers in Veterinary Science*

***Received:*** *19 June 2021*
***Accepted:*** *12 July 2021*
***Published:*** *11 August 2021*

***Citation:***
*Chen J, Su Y, Lin R, Lin F, Shang P, Hussain R and Shi D (2021) Effects of Acute Diquat Poisoning on Liver Mitochondrial Apoptosis and Autophagy in Ducks. Front. Vet. Sci. 8:727766. doi: 10.3389/fvets.2021.727766*

## INTRODUCTION

Diquat (1,10-ethylene-2,20-bipyridinium, DQ) is a widely used non-selective herbicide that belongs to bipyridine (**Figure 1**) (1, 2). The toxicity of DQ is less different than that of other herbicides like paraquat (PQ) due to its rapid degradation in the environment. Although DQ is less toxic than other herbicides, there are still numerous adverse effects that are related to DQ. A previous report has indicated that accidental exposure to this herbicide during applications induces different toxic

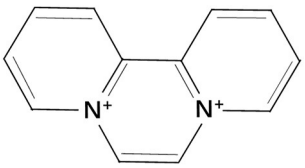


**FIGURE 1 |** The molecular structure of DQ.

effects (3). In addition, a previous study has shown that long-term exposure to DQ can increase the risk of Parkinson's disease in animals including public health (4). DQ can easily enter into aquatic ecosystem *via* direct discharge from production industry, agricultural sector, and runoff (5) and causes serious threats to fish (6), freshwater snails (7), ducks (8), and other aquatic animals. Peking ducks are mainly raised in rural areas of China, which are meat-based species. We choose the Peking ducks as our experiment animals because these animals have the closest connection with humans.

The liver is the target organ of DQ toxicity. The mechanism of liver injury induced by DQ is complex, but it is mainly related to reactive oxygen species (ROS). DQ can induce increased oxidative stress to produce a large number of superoxides and can alter different liver functional activities such as metabolism, detoxification, and immune response resulting in the production of a large number of ROS in the liver (9). The liver toxicity leads to hepatocyte degeneration, inflammation, mitochondrial dysfunction, and even apoptosis (10, 11). Oxidative stress can reduce glutathione (GSH) in the liver and can enhance the production of ROS to promote the activation of pro-apoptotic factors such as p53 and Bax leading to apoptosis (12). In the liver, the mitochondria are also affected by overproduction of ROS ultimately leading to oxidative stress. Studies have indicated that DQ can decrease the activities of mitochondrial complex I, II, III, and V in the liver and decrease the abundance of mitochondrial biosynthesis its related genes (*SIRT1*, *PGC1ATP*, and *TfAM*). Furthermore, oxidative stress can affect the activities of different antioxidant enzymes and interfere with the antioxidant defense mechanisms (13) in the liver and blood. It is reported that infants or piglets with underdeveloped antioxidant systems are more vulnerable to oxidative damage and liver diseases (14). The mechanisms of toxicity of DQ are still under debate. However, DQ induces its toxic effects in the liver through a variety of liver injuries.

Apoptosis is a process of cell death regulated by different genes, while autophagy is a self-protective process of degradation of its own components through the lysosomal system. Herbicides such as DQ and PQ can induce abnormal mechanisms of apoptosis and autophagy. A previous study has shown that different toxins can induce oxidative stress in mice and produce a large amount of ROS to promote DNA damage, upregulation of genes regulating cell cycle (CDKN1A, CDKN2C, and CDKN2D), and pro-apoptotic genes (*caspase-3* and *Bax*) eventually leading to promote apoptosis (15). Nitrite interferes with the expression of anti-apoptosis gene *Bcl2* and leads to apoptosis (16) by enhancing the expression of *caspase-3* and *Bax* genes in tissues. It has been recorded that aloe emodin can activate abnormal signals of apoptosis in the liver of zebrafish, promote the expression of p65, upregulate the proteases caspase-3 and Bax in p53 pathways while can downregulate Bcl2 in p53 pathway, and upregulate the expression of TNF-α and JNK in NF-κB that can induce inflammation and apoptosis (17). Different insecticides like fipronil can also promote the production of peroxisome that damages the DNA and mitochondria, causes the overexpression of Bax, and aggravates hepatocyte apoptosis (18). Furthermore, studies have reported that various drugs can cause hepatocyte apoptosis. The most commonly used anti-tuberculosis drug activates inflammatory corpuscles NLRP3 to upregulate the expression of p53, Bax, and Cleaved-Cas3, inhibit the expression of Bcl2, induce inflammation and apoptosis, and damage hepatocytes in rats (19). High concentrations of acetaminophen can reduce GSH resulting in increased oxidative stress and severe mitochondrial dysfunction, promoting the expression of key apoptotic factors, and promoting apoptosis (20, 21). A previous study has shown that increased concentrations of manganese (Mn) can induce neurotoxicity, increase the levels of glutathione peroxidase (GSH-Px), superoxide dismutase (SOD), and malondialdehyde (MDA), and promote the expression of p53, Bax, Bak, fas, and caspase-3 to induce apoptosis (22). A previous study has reported that cadmium affects the expression of IP3R1 receptor through $Ca^{2+}$ channels, induces DNA damage, and promotes the abnormal process of autophagy or apoptosis (23). Arsenic (As) and its methylation metabolites not only affect regulatory enzymes such as 2 (ERK2), p38, or c-jun to induce neuronal and neuroblastoma cell apoptosis through MAPK signaling pathways but also induce apoptosis through AMP-dependent protein kinase (AMPK)/mTOR signal pathways (24). The morphology of the mitochondria is also important in apoptosis (25, 26). The related proteins Drp1, Mfn1, and Mfn2, mitochondrial a-KGDH, that affect cell division and fusion are all related to the mitochondria (27). The mitochondria play a central role in the integration and circulation of intracellular death signals, such as oxidative stress and DNA damage (28, 29).

The mitochondria can cause cell injury or apoptosis by producing ROS, pro-inflammatory signals, or through mitochondrial membrane permeability. A little electron may escape from the mitochondrial electron transport chain resulting in the production of superoxide. The increased oxidant load also promotes the extra ROS produced by mitochondrial complex I to further enhance cell oxidative stress and promote cell death (30). In addition, ROS produced by the mitochondria can activate NLRP3, adaptation proteins ASC, and caspase-1 to form inflammatory bodies, and the accumulation of damaged mitochondria aggravates inflammation and leads to cell damage. The change of mitochondrial permeability is also an important cause of cell death, which leads to the dissipation of mitochondrial transmembrane potential and the cessation of oxonase. Furthermore, it leads to rapid necrosis of apoptotic (31). When apoptosis is induced by mitochondrial damage, the decrease of ATP produced by the mitochondria through respiratory chain or the increase of ROS will lead to the increase of autophagy (32). Moreover, the induction of autophagy affects

the circuit in which the mitochondria transmit lethal signals, protecting cells from other deadly stimuli (33). However, the relationship between autophagy and apoptosis affected by the mitochondria is complex. These two pathways are activated at the same time and can be regulated by the same factors such as Bcl-2 family proteins, cystatin (caspase), ATG proteins, and p53. On the other hand, autophagy and apoptosis are antagonistic to each other, and autophagy of damaged mitochondrial cells can reduce apoptotic signal transmission and protect normal cells.

The pathways through which DQ induces toxic effects are not clear. Therefore, it is interesting to speculate that DQ may induce harmful effects *via* induction of oxidative stress and increased level of apoptosis factors by regulating apoptosis and autophagy-related signal pathways like NF-κB, MAPK, and mTOR (34). Autophagy is beneficial to inhibit DQ-induced apoptosis and alleviate the effects of DQ poisoning (35). Therefore, the purpose of this study was to explore the relationship between liver injury and apoptosis and autophagy genes and proteins in ducks induced by acute DQ poisoning.

# MATERIALS AND METHODS

## Animals and Treatment

All the experiments were approved by the Animal Ethics Committee of South China Agricultural University (License Number: 2017A087) and were conducted following the ethical code of conduct for animal care and use. After 7 days of acclimatization, a total of 60 1-day-old Peking ducks were randomly divided into two groups including the control and treatment groups (feeding 100 mg/kg DQ on the first day). The ducks in the treatment group were exposed to DQ for 11 days. After weighing at day 11, ducks were anesthetized by injecting chloral hydrate through the intraperitoneal route. Blood was collected from the jugular vein for biochemical profile. The heart, liver, kidney, thymus, spleen, and bursa of fabric of the ducks were removed, weighed separately, and photographed, and the coefficient of each organ was calculated.

## Histopathological Examination

Liver tissue of 1 × 1 cm was cut and fixed in 4% paraformaldehyde solution. After that, all the tissues were processed and then embedded in paraffin for 24 h. Approximately 0.4 μm thick liver slices were obtained with the help of KEDEE KD2258 manual rotary microtome and were then stained with hematoxylin and eosin (H&E). Briefly, the paraffin slices were dewaxed in xylene solution for 20 min and then sequentially soaked in benzene alcohol, anhydrous ethanol I, anhydrous ethanol II, 95% alcohol I, 95% alcohol II, and 80% alcohol solution each for 10 min to remove xylene. After that, the slices were soaked in hematoxylin for 8 min, rinsed with water for 15 min, then shaken in the differentiation solution for ∼2 s, rinsed with water for 20 min again, and dyed again with eosin for 8 min. The dehydration and transparency procedures used in paraffin sections preparation were repeated. The residual liquid on the slice was removed, and neutral resin was dropped on slice, then sealed, and baked for more than 6 h. Finally, all the prepared sections were observed under light microscope (Y-TV55; NiKon, Japan) and photographed.

## RT-qPCR Analysis

The primer and sequences used for real-time PCR (RT-PCR) are shown in **Table 1**. Total RNA was lysed from 100 mg of the liver using RNA isolate reagents (Vazyme, China). Total RNA was separated with chloroform and precipitated with isopropanol. Ethanol was used to wash the residual isopropanol. Total RNA concentration was measured by Microvolume UV–Vis spectrophotometer (Nanodrop™ One; Thermo Fisher Scientific, Madison, WI, USA). Approximately 5 μg total RNA was reverse-transcribed into cDNA using HiScript III RT SuperMix for qPCR (Vazyme, China). The mixture contained 1 μl cDNA primer, and ChamQ University SYBR qPCR Master Mix (Vazyme, China) was used to perform RT-qPCR on the real-time PCR detection system (QuantStudio™ 5; Thermo Fisher Scientific, Waltham, MA, USA). The $2^{-\Delta\Delta(Ct)}$ method was used to calculate the relative gene expression level, and GAPDH was used as the internal reference gene. The results are expressed as normalize mRNA levels by reference gene.

**TABLE 1** | Primer sequences used for real-time PCR.

| Gene | 5′-primer (*F*) | bp | 3′-primer (*R*) | bp |
|---|---|---|---|---|
| *COL2A1* | GAGCGGAGACTACTGGATCG | 20 | TTCTTGTCTTTGGCCTTGCT | 20 |
| *BAK1* | CCGCTACCAACAGGAGAGAG | 20 | GCGTCGTACCGCTTGTTAAT | 20 |
| *BAX* | CTTCTGCTTCCAGACCAAGG | 20 | TCAGCGTGTTCTTCCTGTTG | 20 |
| *Bcl2* | GAGTTCTCCCGTCGCTACC | 19 | CGGTTCAGGTACTCGGTCAT | 20 |
| *Caspase-3* | CGGGTACGGATGTAGATGCT | 20 | GGGGCCATCTGTACCATAGA | 20 |
| *Caspase-9* | GAACTGGATCCGATGTGGAC | 20 | TTCCGTCCGTTCCATAAATC | 20 |
| *P53* | ACAGCAGACTCCTGGGAAGA | 20 | GGGGTATTCGCTCAGTTTCA | 20 |
| *LC3A* | GCTGGACAAGACCAAGTTCC | 20 | ACCCTCCCTGGACAGAAAGT | 20 |
| *LC3B* | TTCGAGAGCAGCATCCTACC | 20 | CCTTCTCGCTCTCGTACACC | 20 |
| *P62* | GGACCCACTTGTCTTCCAAA | 20 | AGCCTCTCGCAGTCCTGTAG | 20 |
| *Parkin* | TGATGGGCTTTGTGAAATGA | 20 | TTCAGCGTGACACAGAGGAC | 20 |
| *GAPDH* | GGTAGTGAAGGCTGCTGCTGATG | 23 | GGAGGAATGGCTGTCACCGTTG | 22 |

## Western Blot Analyses

The antibodies used for Western blot are shown in **Table 2**. Approximately 80 mg of the liver was lysed in RIPA lysis buffer (Meilunbio, China) and 1 mM protease inhibitor (PMSF) (Meilunbio, China) at 4°C, and the concentration was determined using the BCA protein concentration determination kit (Beyotime, China). After that, samples were diluted with 5× SDS-PAGE loading buffer and boiled for 8 min. An equal amount of protein sample (10 μg) was added and electrophoresed on a 12.5% SDS-polyacrylamide denaturing gel and then transferred to polyvinylidene fluoride membranes. After blocking with Tris buffered saline Tween (TBST) containing 5% skimmed milk powder for 1 h, primary antibodies were incubated with membranes for 16 h. After washing with TBST for three times, the membranes were blocked with secondary antibody for 1 h. Finally, an electrochemiluminescent liquid (ECL) (Meilunbio, China) was prepared to measure the signal imprinting. ImageJ software was used to calculate the gray value of each band and perform normalization processing.

**TABLE 2 |** Antibodies used for Western blot.

| Name | Company | Cat. no. | Concentration |
|---|---|---|---|
| Beclin 1 Rabbit pAb | ABclonal | A17028 | 1:1,000 |
| LC3B Rabbit pAb | ABclonal | A11282 | 1:1,000 |
| SQSTM1/p62 Rabbit pAb | ABclonal | A11483 | 1:1,000 |
| GAPDH Rabbit pAb | ABclonal | AC001 | 1:9,000 |
| Goat anti-Rabbit IgG (H&L) | Zenbio | 511203 | 1:5,000 |

## Statistical Analysis

Statistical analysis was performed on all data using GraphPad Prism 8.0 (GraphPad Inc., La Jolla, CA, USA) and SPSS for Windows (version 22; SPSS Inc., Chicago, IL, USA). The independent sample *t*-test was used to analyze the differences of the data between each group. Data were expressed as the mean ± standard deviation (SD). The data between different groups were analyzed by one-way analysis of variance (ANOVA) ($n = 2$, each repeated three times). Significance level was considered as $p < 0.05$, $p < 0.01$, and $p < 0.001$.

# RESULTS

## The Influence of DQ on Organ Index and Serum Biochemistry

The indexes of the heart, liver, kidney, and spleen were significantly higher in treated ducks (**Figure 2**) than in the control group ($p < 0.05$). The results showed no significant difference in the index of the cloacal bursa and thymus ($p > 0.05$) as compared with ducks of the control group.

The results of serum biochemical examination are shown in **Table 3**. The results showed that DQ reduces the serum

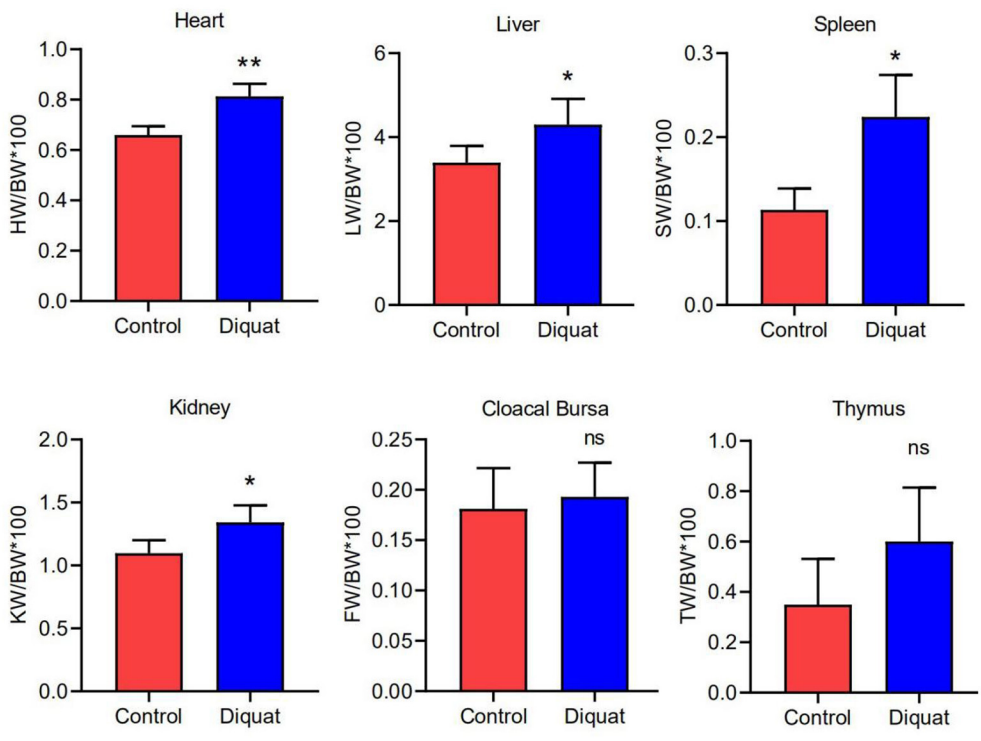


**FIGURE 2 |** The organ index of the heart, liver, spleen, kidney, cloacal bursa, and thymus. Error bars indicate standard error of the mean ($n = 4$). "ns" and "*" indicate the level of significance. ("ns" means no significant difference, $^*p < 0.05$, $^{**}p < 0.01$ compared with the control conditions).

**TABLE 3 |** Serum biochemical index.

| Parameter | Units | Control ($n = 3$) | Diquat ($n = 3$) | $p$ |
|---|---|---|---|---|
| Ca | Mmol | 1.88 ± 0.20 | 1.35 ± 0.09 | <0.05 |
| P | mmol | 2.49 ± 0.92 | 1.70 ± 0.21 | ns |
| TG | mmol | 1.00 ± 0.32 | 0.37 ± 0.13 | <0.05 |
| TC | mmol | 7.81 ± 2.79 | 4.74 ± 0.44 | ns |
| TP | g/L | 22.03 ± 3.84 | 18.27 ± 0.87 | ns |
| T-Bil | μmol/L | 50.57 ± 11.27 | 27.57 ± 6.14 | <0.05 |
| γ-GT | U/L | 4.47 ± 1.05 | 2.97 ± 0.67 | ns |
| ALP | U/L | 1,459 ± 223.70 | 891.90 ± 191.20 | <0.05 |
| ALT | U/L | 64.27 ± 2.30 | 77.30 ± 16.52 | ns |
| AST | U/L | 54.20 ± 1.02 | 35.07 ± 2.83 | <0.001 |
| ALB | g/L | 7.97 ± 0.90 | 6.20 ± 0.36 | <0.05 |
| GLU | mmol | 7.21 ± 2.43 | 8.18 ± 1.50 | ns |
| γ-GT/ALT | | 0.070 ± 0.018 | 0.038 ± 0.001 | <0.05 |

*"ns" indicates the level of significance, and it means no significant difference.*

levels of calcium (Ca), phosphorus (P), triglyceride (TG), total protein (TP), total cholesterol (TC), albumin (ALB), γ-glutamyl transpeptidase (γ-GT), alkaline phosphatase (ALP), aspartate aminotransferase (AST), and total bilirubin (T-Bil) as compared with the control group. Among them, Ca, TG, ALB, ALP, and T-Bil are significantly reduced ($p < 0.05$), and AST is extremely significantly reduced ($p < 0.01$).

## The Effect of DQ on Liver Histopathology

In general, there were no obvious pathological changes in the liver of treated and untreated control groups (**Figure 3**). The basic liver structure of the control group and the DQ treatment group was normal and clear. No inflammatory response was observed in the portal area and liver parenchyma. Histologically, the liver cells of the control group were slightly enlarged, and the accumulation of eosinophilic glycogen material was observed in the cytoplasm. In the DQ treatment group, a large number of vacuoles (shown by black arrows) were observed in the liver cells, which were diffusely distributed. In liver sections of DQ, treated duck's fatty infiltration was obvious indicating that the drug may cause liver fat metabolism disorders.

## The Effect of DQ on Cell Apoptosis

Compared with the control group, the expression of apoptosis-related genes is recorded as indicated in **Figure 4**. The expression level of caspase-3 decreased significantly, and the expression of Bax increased significantly. In addition, there was no significant difference in the expression of *Bak1*, *Bcl2*, *p53*, and *Caspase9* genes. In these genes, only *Caspase9* showed an upward trend, and the others showed a downward trend.

## The Effect of DQ on Autophagy

The changes of autophagy-related genes and proteins in the ducks treated with DQ are shown in **Figure 5**. As compared with the control group, there was no significant difference in the expression of *LC3A*, *LC3B*, and *p62* genes, in which *LC3A* and *LC3B* increased non-significantly, and E3 ubiquitin ligase gene

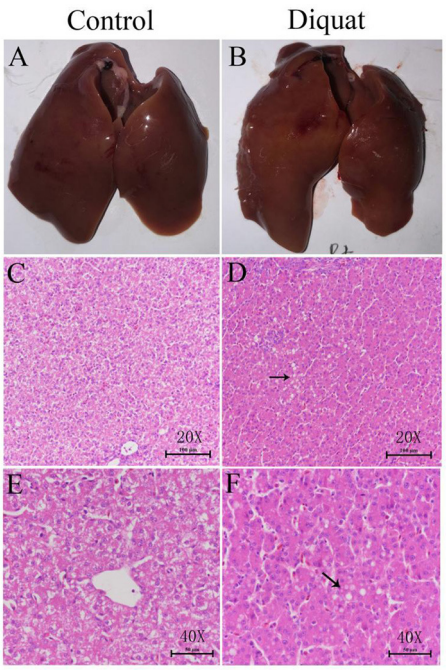


**FIGURE 3 |** The effect of diquat on the liver. **(A)** The liver of the control group. **(B)** The liver of the DQ treated group. **(C)** Control group (HE, 20×). **(D)** DQ treated group (HE, 40×). **(E)** Control group (HE, 40×). **(F)** DQ treated group (HE, 40×).

*Parkin* increased significantly. The protein expression like LC3B decreased significantly, while Beclin 1 increased significantly.

# DISCUSSION

Different histopathological changes in liver sections of treated ducks were observed in our experimental study. Previously, various pathological lesions such as widening of the alveolar septum with inflammatory cells, narrowing and atrophy of the alveolar sac and proliferation of collagen fiber in the lungs, and swelling and necrosis of renal tubular epithelial cells and telangiectasia in the kidneys have been reported (36). Inflammation of cardiomyocytes accompanied by inflammatory cell infiltration in the heart and focal inflammatory cell infiltration in the brain tissue have also been reported (37). In DQ exposed patients, the values of serum creatine and urea nitrogen were significantly increased suggesting severe renal function abnormalities (38). Mild bilateral patchy consolidation at the hilar in the lungs has been observed (39). The lungs mainly involve the alveolar epithelium, which may initially cause acute alveolitis and then pulmonary fibrosis (34). The inflammatory spots around the pleura gradually expand into plaques over time and developed into pulmonary fibrosis (40). Studies have found that the injection of DQ in pigs can increase the expression of mitochondria-related proteins including Pink1, Parkin, and LC3B in the intestine. It is suggested that DQ can induce mitochondrial autophagy (41). Previously, it has

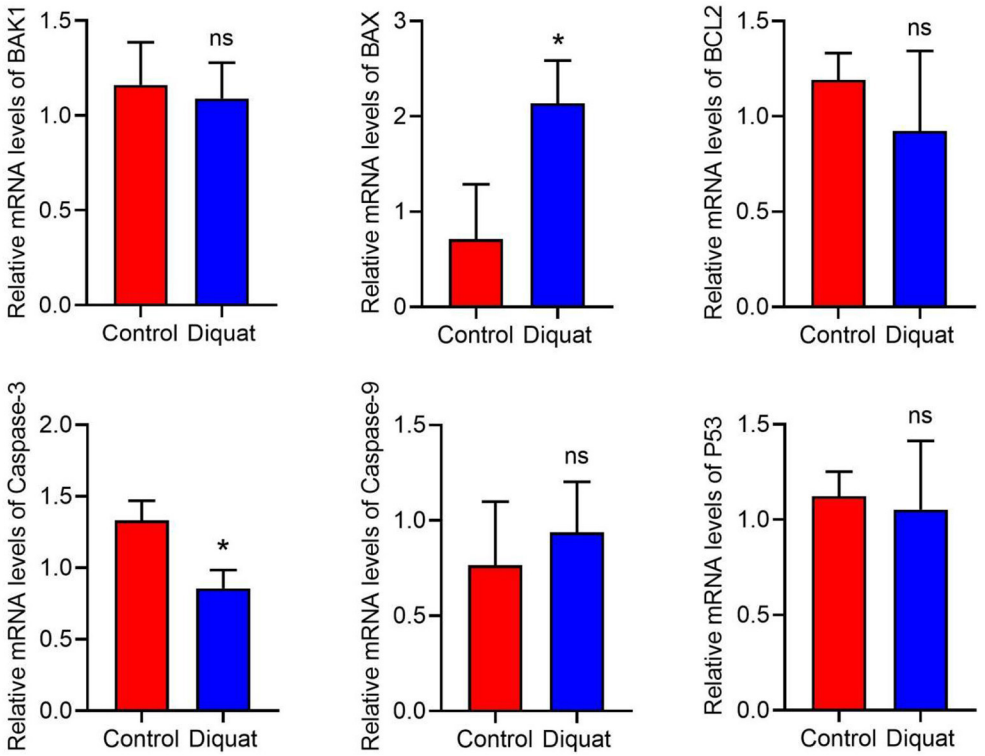


**FIGURE 4 |** The expression of apoptotic genes in the liver. DQ affects the mRNA expression levels of apoptosis-related genes in liver, including BAK1, BAX, Bcl2, Caspase-3, Caspase-9, and P53. "ns" and "*" indicates the level of the Significance. ("ns" means no significant difference, $^*p < 0.05$ compared to the control conditions).

also been found that DQ can reduce the activity of SOD and GSH-Px in the intestinal mucosa and increase the contents of MDA (42, 43), suggesting that PQ causes oxidative stress in the intestine. *In vivo* and *in vitro* studies have shown that the oxidative stress caused by DQ can damage the integrity of the intestinal epithelial barrier that is manifested by the destruction of tight junctions (TJ) and reduction of epithelial cell viability (44–47). Different studies have indicated manifestations of DQ toxicity as decreased TER and increased FD4 flux (48), high serum lipopolysaccharide levels, and diamine oxidase activity in piglets (43). DQ reduces the activity of AHR in the spleen, causing oxidative damage to the spleen. The decreased activity of SOD and CAT suggests decreased antioxidant functions in the spleen (49). Long-term exposure to DQ had toxic effects on the reproductive system (50–52) that is manifested by reducing the quality of germ cells affecting early embryo development (53). Long-term ingestion of DQ in rats and dogs can induce cataracts (54). Dose-dependent axonal degeneration has been observed in dorsal root ganglion neurons (55). In addition, the production of nitric oxide and superoxide anion free radicals was significantly increased, and lipid peroxidation increased, suggesting that PQ causes neurotoxicity (56).

The central vein around the liver cells showed vacuolar degeneration with punctate necrosis due to exposure to DQ (36). The activity of total antioxidant capacity, SOD, and GSH-Px in the liver of piglets injected with DQ decreased suggesting lower status of the liver's antioxidant capacity. There were significant differences in the expression of liver mRNA and lncRNA. GNMT is highly expressed, and GCK is downregulated. These results indicate that DQ can affect glucose metabolism in the liver and reduce weight gain (57). It can also increase the accumulation of glutathione peroxidase (GPX) activity and MDA in the plasma and liver; increase the activity of AST, alanine aminotransferase, and T-Bil concentrations; and increase the relative liver weight, indicating that DQ causes liver damage (10). DQ increases Ca efflux due to the weakened ATP-dependent Ca chelation of liver microsomes (58). DQ-induced liver lipid peroxidation is manifested as increase in 11-, 12-, and 15-hydroxyeicosatetraenoic acid. DQ can also activate inflammatory cells, leading to the synthesis and release of certain pro-inflammatory cytokines like TNF-α, IL-1β, and IL-6 (59).

As a commonly used herbicide, DQ mainly destroys plant cells to achieve the purpose of weeding by inducing redox cycle, releasing ROS and nitric oxide and inhibiting the effect of NADPH. However, it is the herbicidal principle that causes serious damage to the nervous system, liver, kidney, heart, and lungs of animals or humans, while the liver is the main source of ROS, and it has become the target of DQ (60). Liver injury has a prodigious impact on the organism, which can directly lead to an increase in morbidity

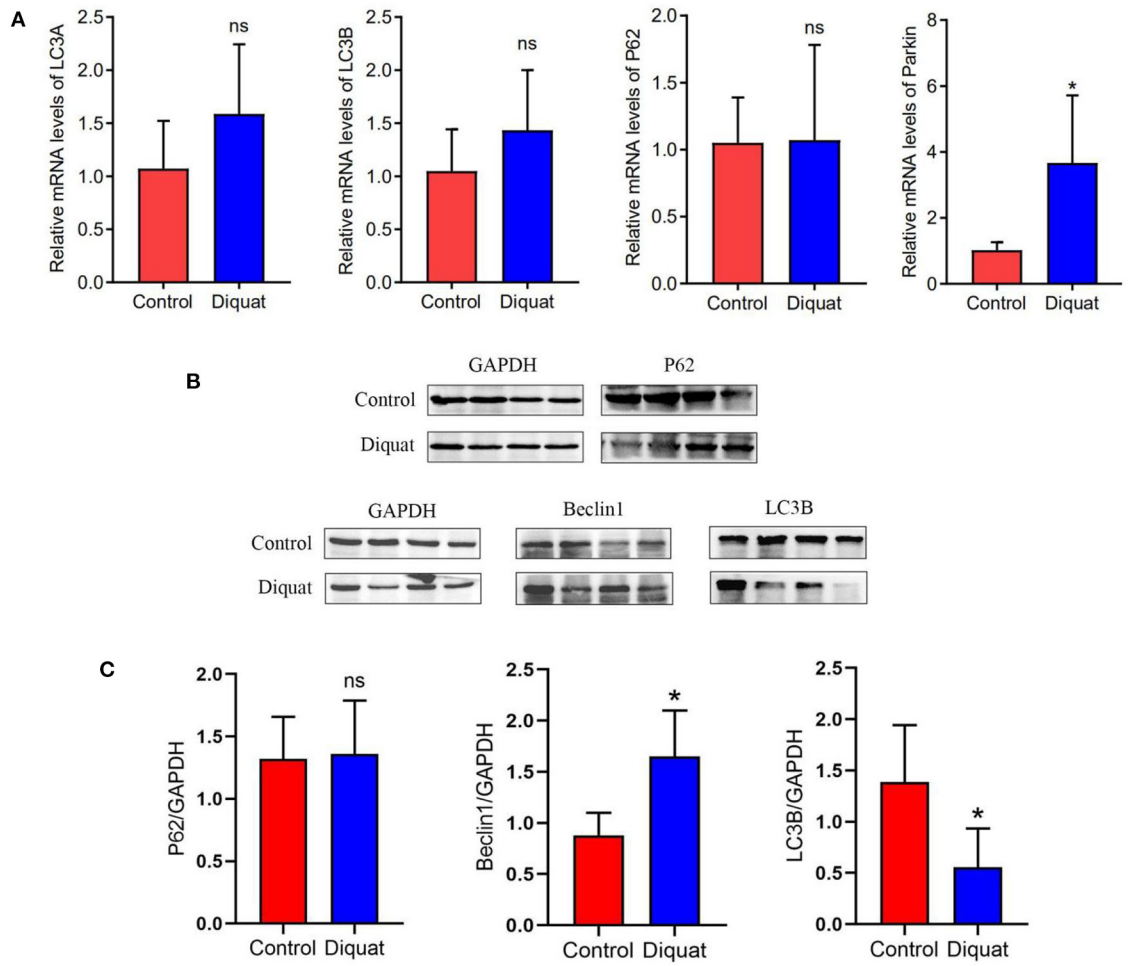


**FIGURE 5 |** The expression of autophagy genes and proteins in the liver. **(A)** Autophagy mRNA gene expression: LC3A, LC3B, and P62. **(B)** Western blot detects protein expression bands: P62, Beclin 1, and LC3B. **(C)** The level of the protein expression: P62, Beclin 1, and LC3B. "ns" and * indicates the level of the significance. ("ns" means no significant difference, $^*p < 0.05$ compared to the control conditions).

and mortality of terrestrial and aquatic animals, especially birds (61).

Many studies have been conducted on DQ-induced liver injury, which mainly focus on oxidative stress, apoptosis, and autophagy. Previous studies have shown that DQ induces liver redox cycle to produce superoxide while inhibit the production of antioxidant enzymes, so that antioxidant enzymes are not enough to resist liver damage caused by oxidation. Secondly, the endoplasmic reticulum and mitochondria can regulate apoptosis and autophagy, while damaged mitochondria initiate autophagy mechanism to inhibit the release of cytochrome c (Cyt-c) and induce apoptosis. Damaged mitochondria can also reduce the accumulation of ROS, which inhibit the division of the mitochondria and prevent it from degradation by autophagy (62).

In the specific effect of DQ on the liver, some scholars have found that the content of glutathione disulfide (GSSG) can reflect the liver injury induced by DQ, while previous studies have shown that DQ leads to a sharp increase in the content of GSSG in the liver (12, 63). DQ can also increase the level of serum ALT and AST and decrease the level of anti-apoptosis factor Bcl2, which indicates hepatocyte apoptosis and injury (64). When DQ is put into the waters of fish fry, it was found that biosynthesis of protein and RNA was increased, while ATK/mTOR signal, SREBP pathway, and caspase pathway were activated. It was considered that this change was closely related to the increase of protein and mRNA, which further confirmed the occurrence of oxidative stress and apoptosis in fish (65–67). It is also found that intraperitoneal injection of DQ in piglets affects the MAPK signal pathway that leads to acute oxidative stress and increase lipids, antioxidant metabolites, and peroxide MDA in the liver (68), so it indicates that DQ can destroy cell lipids and induce cell death. Some scholars have found that DQ-induced oxidative stress can promote the production of $H_2O_2$ in the mitochondria, depolarize the mitochondria, and inactivate iron and sulfur in the mitochondria containing aconitase and other

proteins, resulting in mitochondrial damage (69–72). Previous studies have found that mitochondrial damage and induced mitochondrial release of apoptosis and oxidation-related proteins can promote apoptosis. Oxidative stress induces the release of Cyt-c from the mitochondria that is the key factor of apoptosis, while the antioxidant enzyme Gpx4 can eliminate lipid peroxides in the mitochondria to inhibit the production of Cyt-c and reduce apoptosis (73). DQ can also affect the caspase signal pathway by inducing oxidative stress to produce ROS and enhance the activities of caspase-3 and caspase-9 in the liver tissue (74–78). It is found that there is a relationship between Bax/Bcl-2 and caspase. With the increase of Bax/Bcl-2 ratio, caspases are also gradually activated, which can promote apoptosis (79). It was also found that the activity of mitochondrial complex I was inhibited and ATP was consumed, which proved the destructive effect of DQ on the mitochondria. In addition, it is found that mitochondrial dysfunction and reduced apoptosis by inhibiting NF-KB and p53 signal pathways are the main pathways for DQ to induce inflammation and apoptosis. Secondly, some studies have found that the release of Smac/Diablo, endonuclease G, and other intermembrane space proteins after permeation of mitochondrial outer membrane can promote cell apoptosis by activating cystatin. A large amount of $H_2O_2$ is produced by the mitochondria, which further induces the production of ROS to aggravate the oxidative stress of cells that leads to further apoptosis (80).

Our research results are somewhat consistent with the above research results. In our study, we did not find that DQ had significant effects on pro-apoptotic factors BAX, BAK1, TNF-α, caspase series, and p53, but they showed an upward trend all together. The anti-apoptotic genes *Parkin* and *Bcl2* were significantly upregulated, indicating that anti-apoptotic factors in ducklings play an important role in the period of acute DQ poisoning. It is well-known that the production of a large number of ROS can destroy the function of the mitochondria. Some studies have suggested that it may convert the apoptosis pathway into necrosis, thus showing the increase of inhibitory apoptosis factors. Previous studies have shown that *Parkin* gene not only plays an anti-apoptotic role but also inhibits the pro-apoptotic pathway of p53 (81, 82). In our study of autophagy factor, we found that DQ significantly upregulated the protein expression of autophagy factor Beclin 1 in the liver. The key autophagy factors LC3A, LC3B, and p62 showed an upward trend at the gene level, but the protein expression of LC3B and p62 decreased; it may be due to the effect of pro-apoptotic components such as apoptotic proteases during translation, which initiated apoptosis and inhibited the occurrence of autophagy at the same time (62). Most evidence shows that autophagy is the protective mechanism of cell initiation. Autophagy can inhibit apoptosis when autophagy is upregulated; similarly, apoptosis can also reduce autophagy. Therefore, we believe that acute duck poisoning has a significant effect on the liver. On the one hand, it activates the apoptosis and anti-apoptosis system, which proves that there is apoptosis in hepatocytes. On the other hand, the autophagy protection system was activated, and it was found that the autophagy and apoptosis system inhibited each other.

## DATA AVAILABILITY STATEMENT

The raw data supporting the conclusions of this article will be made available by the authors, without undue reservation.

## ETHICS STATEMENT

The animal study was reviewed and approved by Animal Ethics Committee of South China Agricultural University (License Number: 2017A087).

## AUTHOR CONTRIBUTIONS

JC, YS, RL, and FL were responsible for the study conception and design. RH and DS revised the manuscript. JC, YS, PS, and DS were involved in the drafting of the manuscript. All authors contributed to the article and approved the submitted version.

## FUNDING

The study was supported by the Natural Science Foundation of Guangdong Province (2021A1515011010) and Science and Technology Major Project of Tibet Autonomous Region (XZ202101ZD0005N).

## REFERENCES

1. Wang XH, Souders CL, Zhao YH, Martyniuk CJ. Mitochondrial bioenergetics and locomotor activity are altered in zebrafish (*Danio rerio*) after exposure to the bipyridylium herbicide diquat. *Toxicol Lett*. (2018) 283:13–20. doi: 10.1016/j.toxlet.2017.10.022
2. Yastrub TO, Omelchuk ST, Yastrub AM. Dermal absorption of diquat and potential occupational risk. *Wiad Lek*. (2020) 73:1459–64. doi: 10.36740/WLek202007127
3. Fortenberry GZ, Beckman J, Schwartz A, Prado JB, Graham LS, Higgins S, et al. Magnitude and characteristics of acute paraquat- and diquat-related illnesses in the US: 1998-2013. *Environ Res*. (2016) 146:191–9. doi: 10.1016/j.envres.2016.01.003
4. Pouchieu C, Piel C, Carles C, Gruber A, Helmer C, Tual S, et al. Pesticide use in agriculture and Parkinson's disease in the AGRICAN cohort study. *Int J Epidemiol*. (2018) 47:299–310. doi: 10.1093/ije/dyx225
5. Magalhães N, Carvalho F, Dinis-Oliveira RJ. *Human and Experimental Toxicology of Diquat Poisoning: Toxicokinetics, Mechanisms of Toxicity, Clinical Features, and Treatment*. London: SAGE Publications (2018).
6. Souders CN, Liang X, Wang X, Ector N, Zhao YH, Martyniuk CJ. High-throughput assessment of oxidative respiration in fish embryos: advancing adverse outcome pathways for mitochondrial dysfunction. *Aquat Toxicol*. (2018) 199:162–73. doi: 10.1016/j.aquatox.2018.03.031
7. Bouetard A, Besnard AL, Vassaux D, Lagadic L, Coutellec MA. Impact of the redox-cycling herbicide diquat on transcript expression and antioxidant enzymatic activities of the freshwater snail Lymnaea stagnalis. *Aquat Toxicol*. (2013) 126:256–65. doi: 10.1016/j.aquatox.2012.11.013

8. Sewalk CJ, Brewer GL, Hoffman DJ. Effects of diquat, an aquatic herbicide, on the development of mallard embryos. *J Toxicol Environ Health A*. (2000) 62:33–45. doi: 10.1080/009841000050201659
9. Sánchez-Valle V, Chávez-Tapia NC, Uribe M, Méndez-Sánchez N. Role of oxidative stress and molecular changes in liver fibrosis: a review. *Curr Med Chem*. (2012) 19:4850. doi: 10.2174/092986712803341520
10. Chen YP, Gu YF, Zhao HR, Zhou YM. Dietary squalene supplementation alleviates diquat-induced oxidative stress and liver damage of broiler chickens. *Poultry Sci*. (2021) 100:100919. doi: 10.1016/j.psj.2020.12.017
11. Yang L, Yu Z, Hou J, Deng Y, Zhou Z, Zhao Z, et al. Toxicity and oxidative stress induced by T-2 toxin and HT-2 toxin in broilers and broiler hepatocytes. *Food Chem Toxicol*. (2016) 87:128–37. doi: 10.1016/j.fct.2015.12.003
12. Wu KC, Zhang Y, Klaassen CD. Nrf2 protects against diquat-induced liver and lung injury. *Free Radic Res*. (2012) 46:1220–9. doi: 10.3109/10715762.2012.700709
13. Zhang H, Chen Y, Chen Y, Jia P, Ji S, Xu J, et al. Comparison of the effects of resveratrol and its derivative pterostilbene on hepatic oxidative stress and mitochondrial dysfunction in piglets challenged with diquat. *Food Funct*. (2020) 11:4202–15. doi: 10.1039/D0FO00732C
14. Jia P, Ji S, Zhang H, Chen Y, Wang T. Piceatannol ameliorates hepatic oxidative damage and mitochondrial dysfunction of weaned piglets challenged with diquat. *Animals (Basel)*. (2020) 10:239. doi: 10.3390/ani10071239
15. Huang B, Chen Q, Wang L, Gao X, Zhu W, Mu P, et al. Aflatoxin B1 induces neurotoxicity through reactive oxygen species generation, DNA damage, apoptosis, and S-phase cell cycle arrest. *Int J Mol Sci*. (2020) 21:517. doi: 10.3390/ijms21186517
16. El-Nabarawy NA, Gouda AS, Khattab MA, Rashed LA. Effects of nitrite graded doses on hepatotoxicity and nephrotoxicity, histopathological alterations, and activation of apoptosis in adult rats. *Environ Sci Pollut Res Int*. (2020) 27:14019–32. doi: 10.1007/s11356-020-07901-6
17. Quan Y, Gong L, He J, Zhou Y, Liu M, Cao Z, et al. Aloe emodin induces hepatotoxicity by activating NF-κB inflammatory pathway and P53 apoptosis pathway in zebrafish. *Toxicol Lett*. (2019) 306:66–79. doi: 10.1016/j.toxlet.2019.02.007
18. Sayed AA, El-Desouky MA, Ibrahim KA. Garlic and allopurinol attenuate hepatic apoptosis induced by fipronil in male albino rats. *Regul Toxicol Pharmacol*. (2019) 107:104400. doi: 10.1016/j.yrtph.2019.05.025
19. Zhang Y, Qu X, Gao H, Zhai J, Tao L, Sun J, et al. Quercetin attenuates NLRP3 inflammasome activation and apoptosis to protect INH-induced liver injury *via* regulating SIRT1 pathway. *Int Immunopharmacol*. (2020) 85:106634. doi: 10.1016/j.intimp.2020.106634
20. Feng Y, Cui R, Li Z, Zhang X, Jia Y, Zhang X, et al. Methane alleviates acetaminophen-induced liver injury by inhibiting inflammation, oxidative stress, endoplasmic reticulum stress, and apoptosis through the Nrf2/HO-1/NQO1 signaling pathway. *Oxid Med Cell Longev*. (2019) 2019:7067619. doi: 10.1155/2019/7067619
21. Cao P, Sun J, Sullivan MA, Huang X, Wang H, Zhang Y, et al. Angelica sinensis polysaccharide protects against acetaminophen-induced acute liver injury and cell death by suppressing oxidative stress and hepatic apoptosis *in vivo* and *in vitro*. *Int J Biol Macromol*. (2018) 111:1133–9. doi: 10.1016/j.ijbiomac.2018.01.139
22. Zhang K, Zhu Y, Wang X, Zhao X, Li S, Teng X. Excess manganese-induced apoptosis in chicken cerebrums and embryonic neurocytes. *Biol Trace Elem Res*. (2017) 180:297–305. doi: 10.1007/s12011-017-0992-4
23. Rani A, Kumar A, Lal A, Pant M. Cellular mechanisms of cadmium-induced toxicity: a review. *Int J Environ Health Res*. (2014) 24:378–99. doi: 10.1080/09603123.2013.835032
24. Garza-Lombo C, Pappa A, Panayiotidis MI, Gonsebatt ME, Franco R. Arsenic-induced neurotoxicity: a mechanistic appraisal. *J Biol Inorg Chem*. (2019) 24:1305–16. doi: 10.1007/s00775-019-01740-8
25. Burke PJ. Mitochondria, bioenergetics and apoptosis in cancer. *Trends Cancer*. (2017) 3:857–70. doi: 10.1016/j.trecan.2017.10.006
26. Srinivasan S, Guha M, Kashina A, Avadhani NG. Mitochondrial dysfunction and mitochondrial dynamics-the cancer connection. *Biochim Biophys Acta Bioenerg*. (2017) 1858:602–14. doi: 10.1016/j.bbabio.2017.01.004
27. Abate M, Festa A, Falco M, Lombardi A, Luce A, Grimaldi A, et al. Mitochondria as playmakers of apoptosis, autophagy and senescence. *Semin Cell Dev Biol*. (2020) 98:139–53. doi: 10.1016/j.semcdb.2019.05.022
28. Green DR, Kroemer G. The pathophysiology of mitochondrial cell death. *Science*. (2004) 305:626–9. doi: 10.1126/science.1099320
29. Kaufmann SH, Earnshaw WC. Induction of apoptosis by cancer chemotherapy. *Exp Cell Res*. (2000) 256:42–9. doi: 10.1006/excr.2000.4838
30. Sinha K, Das J, Pal PB, Sil PC. Oxidative stress: the mitochondria-dependent and mitochondria-independent pathways of apoptosis. *Arch Toxicol*. (2013) 87:1157–80. doi: 10.1007/s00204-013-1034-4
31. Green DR, Galluzzi L, Kroemer G. Mitochondria and the autophagy-inflammation-cell death axis in organismal aging. *Science*. (2011) 333:1109–12. doi: 10.1126/science.1201940
32. Gomes LC, Di Benedetto G, Scorrano L. During autophagy mitochondria elongate, are spared from degradation and sustain cell viability. *Nat Cell Biol*. (2011) 13:589–98. doi: 10.1038/ncb2220
33. Wrighton KH. Autophagy: shaping the fate of mitochondria. *Nat Rev Mol Cell Biol*. (2011) 12:344–5. doi: 10.1038/nrm3116
34. Park A, Koh HC. NF-kappaB/mTOR-mediated autophagy can regulate diquat-induced apoptosis. *Arch Toxicol*. (2019) 93:1239–53. doi: 10.1007/s00204-019-02424-7
35. Choi SE, Park YS, Koh HC. NF-kappaB/p53-activated inflammatory response involves in diquat-induced mitochondrial dysfunction and apoptosis. *Environ Toxicol*. (2018) 33:1005–18. doi: 10.1002/tox.22552
36. Sun YQ, Yuan L, Gao HB, Yao DQ, Chen QS, Tian YP. Establishment and evaluation of acute diquat poisoning model in Wistar rats. *Zhonghua Lao Dong Wei Sheng Zhi Ye Bing Za Zhi*. (2019) 37:342–6. doi: 10.3760/cma.j.issn.1001-9391.2019.05.005
37. Wu YZ, Kan BT, Wang WJ, Zhang ZC, Jia JE, Li XQ, et al. The experimental study of diquat on the half-Lethal dose and pothological injuny of related organs in wistor rats. *Zhonghua Lao Dong Wei Sheng Zhi Ye Bing Za Zhi*. (2018) 36:813–18. doi: 10.3760/cma.j.issn.1001-9391.2018.11.004
38. Xing J, Chu Z, Han D, Jiang X, Zang X, Liu Y, et al. Lethal diquat poisoning manifesting as central pontine myelinolysis and acute kidney injury: a case report and literature review. *J Int Med Res*. (2020) 48:300060520943824. doi: 10.1177/0300060520943824
39. Safaei AA, Dadashzadeh P. Acute kidney injury in patients with paraquat intoxication; a case report and review of the literature. *J Renal Inj Prev*. (2016) 5:203–6. doi: 10.15171/jrip.2016.43
40. Yu G, Kan B, Jian X, Wang J, Sun J, Song C. A case report of acute severe paraquat poisoning and long-term follow-up. *Exp Ther Med*. (2014) 8:233–6. doi: 10.3892/etm.2014.1727
41. Cao S, Wu H, Wang C, Zhang Q, Jiao L, Lin F, et al. Diquat-induced oxidative stress increases intestinal permeability, impairs mitochondrial function, and triggers mitophagy in piglets. *J Anim Sci*. (2018) 96:1795–805. doi: 10.1093/jas/sky104
42. Lv M, Yu B, Mao XB, Zheng P, He J, Chen DW. Responses of growth performance and tryptophan metabolism to oxidative stress induced by diquat in weaned pigs. *Animal*. (2012) 6:928–34. doi: 10.1017/S1751731111002382
43. Yin J, Liu M, Ren W, Duan J, Yang G, Zhao Y, et al. Effects of dietary supplementation with glutamate and aspartate on diquat-induced oxidative stress in piglets. *PLoS ONE*. (2015) 10:e0122893. doi: 10.1371/journal.pone.0122893
44. Jiao N, Wu Z, Ji Y, Wang B, Dai Z, Wu G. L-glutamate enhances barrier and antioxidative functions in intestinal porcine epithelial cells. *J Nutr*. (2015) 145:2258–64. doi: 10.3945/jn.115.217661
45. Liu F, Cottrell JJ, Furness JB, Rivera LR, Kelly FW, Wijesiriwardana U, et al. Selenium and vitamin E together improve intestinal epithelial barrier function and alleviate oxidative stress in heat-stressed pigs. *Exp Physiol*. (2016) 101:801–10. doi: 10.1113/EP085746
46. Liu J, Zhang Y, Li Y, Yan H, Zhang H. L-tryptophan enhances intestinal integrity in diquat-challenged piglets associated with improvement of redox status and mitochondrial function. *Animals (Basel)*. (2019) 9:1045. doi: 10.3390/ani9050266
47. Zheng P, Yu B, He J, Yu J, Mao X, Luo Y, et al. Arginine metabolism and its protective effects on intestinal health and functions in weaned piglets under oxidative stress induced by diquat. *Br J Nutr*. (2017) 117:1495–02. doi: 10.1017/S0007114517001519
48. Wijtten PJ, van der Meulen J, Verstegen MW. Intestinal barrier function and absorption in pigs after weaning: a review. *Br J Nutr*. (2011) 105:967–81. doi: 10.1017/S0007114510005660

49. Wu X, Cao W, Jia G, Zhao H, Chen X, Wu C, et al. New insights into the role of spermine in enhancing the antioxidant capacity of rat spleen and liver under oxidative stress. *Anim Nutr*. (2017) 3:85–90. doi: 10.1016/j.aninu.2016.11.005
50. Gupta RK, Miller KP, Babus JK, Flaws JA. Methoxychlor inhibits growth and induces atresia of antral follicles through an oxidative stress pathway. *Toxicol Sci*. (2006) 93:382–9. doi: 10.1093/toxsci/kfl052
51. Gupta RK, Schuh RA, Fiskum G, Flaws JA. Methoxychlor causes mitochondrial dysfunction and oxidative damage in the mouse ovary. *Toxicol Appl Pharmacol*. (2006) 216:436–45. doi: 10.1016/j.taap.2006.06.013
52. Gupta RK, Aberdeen G, Babus JK, Albrecht ED, Flaws JA. Methoxychlor and its metabolites inhibit growth and induce atresia of baboon antral follicles. *Toxicol Pathol*. (2007) 35:649–56. doi: 10.1080/01926230701459960
53. Zhang JQ, Gao BW, Wang J, Wang XW, Ren QL, Chen JF, et al. Chronic exposure to diquat causes reproductive toxicity in female mice. *PLoS ONE*. (2016) 11:e0147075. doi: 10.1371/journal.pone.0147075
54. Clark DG, Hurst EW. The toxicity of diquat. *Br J Ind Med*. (1970) 27:51–5. doi: 10.1136/oem.27.1.51
55. Fischer LR, Glass JD. Oxidative stress induced by loss of Cu,Zn-superoxide dismutase (SOD1) or superoxide-generating herbicides causes axonal degeneration in mouse DRG cultures. *Acta Neuropathol*. (2010) 119:249–59. doi: 10.1007/s00401-009-0631-z
56. Djukic M, Jovanovic MD, Ninkovic M, Stevanovic I, Curcic M, Topic A, et al. Intrastriatal pre-treatment with L-NAME protects rats from diquat neurotoxcity. *Ann Agric Environ Med*. (2012) 19:666–72. doi: 10.1108/09653561211278761
57. Wang J, Li ZX, Yang DD, Liu PQ, Wang ZQ, Zeng YQ, et al. Diquat determines a deregulation of lncRNA and mRNA expression in the liver of postweaned piglets. *Oxid Med Cell Longev*. (2019) 2019:9148535. doi: 10.1155/2019/9148535
58. Tsokos-Kuhn JO, Smith CV, Hughes H, Mitchell JR. Liver membrane calcium transport in diquat-induced oxidative stress *in vivo*. *Mol Pharmacol*. (1988) 34:209–14.
59. Smith CV, Hughes H, Lauterburg BH, Mitchell JR. Oxidant stress and hepatic necrosis in rats treated with diquat. *J Pharmacol Exp Ther*. (1985) 235:172–7.
60. Karuppagounder SS, Ahuja M, Buabeid M, Parameshwaran K, Abdel-Rehman E, Suppiramaniam V, et al. Investigate the chronic neurotoxic effects of diquat. *Neurochem Res*. (2012) 37:1102–11. doi: 10.1007/s11064-012-0715-3
61. Avanzo JL, de Mendonca CJ, Pugine SM, de Cerqueira CM. Effect of vitamin E and selenium on resistance to oxidative stress in chicken superficial pectoralis muscle. *Comp Biochem Physiol C Toxicol Pharmacol*. (2001) 129:163–73. doi: 10.1016/s1532-0456(01)00197-1
62. Kaminskyy VO, Zhivotovsky B. Free radicals in cross talk between autophagy and apoptosis. *Antioxid Redox Signal*. (2014) 21:86–102. doi: 10.1089/ars.2013.5746
63. Madhu C, Gregus Z, Klaassen CD. Marked interanimal differences in susceptibility of Sprague-Dawley rats to diquat-induced oxidative stress in the liver: correlation with hepatic uptake of diquat. *J Pharmacol Exp Ther*. (1992) 263:1003–8.
64. Chen Y, Chen Y, Zhang H, Wang T. Pterostilbene as a protective antioxidant attenuates diquat-induced liver injury and oxidative stress in 21-day-old broiler chickens. *Poult Sci*. (2020) 99:3158–67. doi: 10.1016/j.psj.2020.01.021
65. Luu W, Sharpe LJ, Stevenson J, Brown AJ. Akt acutely activates the cholesterogenic transcription factor SREBP-2. *Biochim Biophys Acta*. (2012) 1823:458–64. doi: 10.1016/j.bbamcr.2011.09.017
66. McCuaig LM, Martyniuk CJ, Marlatt VL. Morphometric and proteomic responses of early-life stage rainbow trout (*Oncorhynchus mykiss*) to the aquatic herbicide diquat dibromide. *Aquat Toxicol*. (2020) 222:105446. doi: 10.1016/j.aquatox.2020.105446
67. Porta C, Paglino C, Mosca A. Targeting PI3K/Akt/mTOR signaling in cancer. *Front Oncol*. (2014) 4:64. doi: 10.3389/fonc.2014.00064
68. Doan N, Liu Y, Xiong X, Kim K, Wu Z, Bravo DM, et al. Organic selenium supplement partially alleviated diquat-induced oxidative insults and hepatic metabolic stress in nursery pigs. *Br J Nutr*. (2020) 24:1–11. doi: 10.1017/S0007114520000689
69. Chen L, Yoo SE, Na R, Liu Y, Ran Q. Cognitive impairment and increased Abeta levels induced by paraquat exposure are attenuated by enhanced removal of mitochondrial H(2)O(2). *Neurobiol Aging*. (2012) 33:432.e15-26. doi: 10.1016/j.neurobiolaging.2011.01.008
70. Cantu D, Fulton RE, Drechsel DA, Patel M. Mitochondrial aconitase knockdown attenuates paraquat-induced dopaminergic cell death *via* decreased cellular metabolism and release of iron and H(2)O(2). *J Neurochem*. (2011) 118:79–92. doi: 10.1111/j.1471-4159.2011.07290.x
71. Cantu D, Schaack J, Patel M. Oxidative inactivation of mitochondrial aconitase results in iron and H2O2-mediated neurotoxicity in rat primary mesencephalic cultures. *PLoS ONE*. (2009) 4:e7095. doi: 10.1371/journal.pone.0007095
72. Czerniczyniec A, Karadayian AG, Bustamante J, Cutrera RA, Lores-Arnaiz S. Paraquat induces behavioral changes and cortical and striatal mitochondrial dysfunction. *Free Radic Biol Med*. (2011) 51:1428–36. doi: 10.1016/j.freeradbiomed.2011.06.034
73. Liang H, Ran Q, Jang YC, Holstein D, Lechleiter J, McDonald-Marsh T, et al. Glutathione peroxidase 4 differentially regulates the release of apoptogenic proteins from mitochondria. *Free Radic Biol Med*. (2009) 47:312–20. doi: 10.1016/j.freeradbiomed.2009.05.012
74. Zhang H, Chen Y, Chen Y, Jia P, Ji S, Xu J, et al. Comparison of the effects of resveratrol and its derivative pterostilbene on hepatic oxidative stress and mitochondrial dysfunction in piglets challenged with diquat. *Food Funct*. (2020) 11:4202–15. doi: 10.1039/d0fo00732c
75. Liu B. Role of oxidative stress and antioxidants in thiram-induced tibial dyschondroplasia. *Pak Vet J*. (2021) 41:1–6. doi: 10.29261/pakvetj/2020.094
76. Qamar H. Recovery of chickens affected with tibial dyschondroplasia by application of grape seed extract through downregulating ca2 gene and enhancing liver functions. *Pak Vet J*. (2019) 39:527–33. doi: 10.29261/pakvetj/2019.076
77. Qamar H. Effect of grape seed extract on tibial dyschondroplasia incidence, liver weight, and tibial angiogenesis in chickens. *Pak Vet J*. (2020) 40:187–94. doi: 10.29261/pakvetj/2019.109
78. Bakr AF, Abdelgayed SS, EL-Tawil OS, Bakeer AM. Assessment of ginger extract and ginger nanoparticles protective activity against acetaminophen-induced hepatotoxicity and nephrotoxicity in rats. *Pak Vet J*. (2019) 39:479–86. doi: 10.29261/pakvetj/2019.060
79. Luo Z, Zhu W, Guo Q, Luo W, Zhang J, Xu W, et al. Weaning induced hepatic oxidative stress, apoptosis, and aminotransferases through MAPK signaling pathways in piglets. *Oxid Med Cell Longev*. (2016) 2016:4768541. doi: 10.1155/2016/4768541
80. Tretter L, Adam-Vizi V. Generation of reactive oxygen species in the reaction catalyzed by alpha-ketoglutarate dehydrogenase. *J Neurosci*. (2004) 24:7771–8. doi: 10.1523/JNEUROSCI.1842-04.2004
81. Kanapathipillai M. Treating p53 mutant aggregation-associated cancer. *Cancers (Basel)*. (2018) 10:154. doi: 10.3390/cancers10060154
82. Alves DCC, Checler F. Parkin: much more than a simple ubiquitin ligase. *Neurodegener Dis*. (2012) 10:49–51. doi: 10.1159/000332803


**Conflict of Interest:** The authors declare that the research was conducted in the absence of any commercial or financial relationships that could be construed as a potential conflict of interest.

frontiers in Veterinary Science

ORIGINAL RESEARCH
published: 22 September 2021
doi: 10.3389/fvets.2021.722567

# Methionine Deficiency Affects Liver and Kidney Health, Oxidative Stress, and Ileum Mucosal Immunity in Broilers

*Baolin Song*[1,2], *Min Fu*[1], *Fang He*[1], *Huan Zhao*[1,3], *Yu Wang*[1], *Qihang Nie*[1] *and Bangyuan Wu*[1,3]*

[1] College of Life Sciences, China West Normal University, Nanchong, China, [2] Department of Infectious Diseases and Public Health, Jockey Club College of Veterinary Medicine and Life Sciences, City University of Hong Kong, Hong Kong SAR, China, [3] Key Laboratory of Southwest China Wildlife Resources Conservation, Ministry of Education P. R. China, Nanchong, China

Methionine (Met) is the first limiting amino acid in broiler diets, but its unclear physiological effects hamper its effective use in the poultry production industry. This study assessed the effect of a Met-deficient (MD) diet on chicken liver and kidney health, exploring the associated mechanisms of antioxidant capacity and ileum mucosal immunity. Seventy-two broilers were administered either the control diet (0.46% Met in starter diet, 0.36% Met in grower diet) or the MD diet (0.22% Met in starter diet, 0.24% Met in grower diet). Liver and kidney samples were collected every 14 days for anatomical, histological, and ultrastructural analyses, accompanied by oxidative stress assessment. Meanwhile, T- and B-lymphocyte abundance and essential cytokine gene expression were measured in the ileum, the center of the gut–liver–kidney axis. Signs of kidney and liver injury were observed morphologically in the MD group at 42 days of age. Furthermore, aspartate aminotransferase, alanine aminotransferase, creatinine, and uric acid levels were decreased in the MD group compared with the control group, accompanied by decreased superoxide dismutase activity, increased malondialdehyde content, decreased numbers of T and B lymphocytes, and decreased cytokine expression in the ileum, such as IL-2, IL-6, LITAF, and IFN-γ. These results suggest that MD can induce kidney and liver injury, and the injury pathway might be related to oxidative stress and intestinal immunosuppression.

**Keywords: methionine deficiency, broilers, liver and kidney injury, antioxidant function, ileum mucosal immunity**

OPEN ACCESS

***Edited by:***
*Jianzhu Liu,*
*Shandong Agricultural University, China*

***Reviewed by:***
*Siaka Seriba Diarra,*
*University of the South Pacific, Fiji*
*Jing Wang,*
*Beijing Academy of Agriculture and Forestry Sciences, China*

***Correspondence:**
*Bangyuan Wu*
*wby2008@cwnu.edu.cn*

***Specialty section:***
*This article was submitted to Animal Nutrition and Metabolism, a section of the journal Frontiers in Veterinary Science*

***Received:*** *09 June 2021*
***Accepted:*** *17 August 2021*
***Published:*** *22 September 2021*

***Citation:***
*Song B, Fu M, He F, Zhao H, Wang Y, Nie Q and Wu B (2021) Methionine Deficiency Affects Liver and Kidney Health, Oxidative Stress, and Ileum Mucosal Immunity in Broilers. Front. Vet. Sci. 8:722567. doi: 10.3389/fvets.2021.722567*

## INTRODUCTION

As the first limiting amino acid in broiler diets and a potential mediator of the immune response, methionine (Met) supplementation is required in poultry production (1). Consumption of a Met-deficient (MD) diet has shown to decrease the body weight, growth speed (2), and abdominal fat (3) in broilers, while appropriate Met supplementation can promote egg production (4) and peripheral blood immunity (5). The chicken body reacts sensitively to Met, which affects feather growth at different ages and causes metabolic changes (6). Many studies have explored more effective use of Met in poultry diets, not just to meet the nutritional needs of the chicken but also as a health product. Assessing the physiological functions of Met through diets supplemented with various MD levels has revealed several negative phenomena. Fouad and El-Senousey (7) reported that an MD

diet increased the percentage of abdominal fat due to increased fatty acid synthase and hormone-sensitive lipase activities, lipid accumulation in the liver, and decreased hepatic lipid catabolism (8). The reason why would such fatty acid-related metabolic disorder happen is still unclear. However, since we understand that Met residue is an endogenous substrate in antioxidant defense system and oxidative stress is closely related to fatty acid metabolic gene changes (9), it is possible that Met mainly induces such liver abnormalities in this pathological way. Specifically, oxidative stress is often marked by decreased activities of antioxidant enzymes such as aspartate aminotransferase (AST), alanine aminotransferase (ALT), alkaline phosphatase (ALP), and glutamyl transferase (GGT), which allow downstream oxidation products to attack tissue cells, the first targets of which are mainly parenchymal cells in the liver and renal cells in the kidney (10). Within the cell, the initial stress phase is thought to induce fatty acid metabolism gene changes that result in the structural collapse of mitochondria, microsomes, and peroxisomes (11). Therefore, oxidative stress-related pathology analysis in organelle, cell, and organ levels under MD is urgently needed and might reveal a new injury mechanism that would be helpful for understanding Met and its use as a feed supplement.

Recent studies have reported that the gut–liver–kidney axis plays a vital role in many metabolic diseases, including non-alcoholic fatty liver and steatohepatitis (12, 13). However, the liver and kidney are not the only pathological recipients. Digested substrates in the gut are also able to change the consistency of the intestinal content and induce imbalance in the gut microbiota, which leads to abnormal food digestion. Mucosal immunity, which plays a protective role against pathogenic bacteria, would be impaired, allowing entry of microbial endotoxins into the bloodstream and finally to the liver, where bile is produced and influenced. Following bile secretion into the gut, food and microbes would be influenced for a second time. At the core of this loop, a balanced microbial composition can protect a healthy host from metabolic disorders (14, 15). This process is achieved *via* the bloodstream and is guarded by intestinal mucosal immunity. So, we cannot exclude mucosal immunity as a potential factor affecting the Met pathological process and it would also bring us new ideas about this nutrient. Although increased intestinal cell apoptosis has been reported for broilers consuming MD diets (16), suggesting a possible mucosal immunosuppression, we still understand few about the exact immunity status, especially in the ileum, the cross point in such gut–liver–kidney axis.

In the current study, basal diets were formulated according to a study by Wu et al. (17), in which consumption of an MD diet induced significant immunosuppression in the intestine, and a study by Peng et al. (8), in which significant hepatic fat accumulation was observed using 0.24–0.26% Met in the starter diet and 0.26–0.28% Met in the grower diet. The control Met level was set according to National Research Council (NRC) standards and Mirzaaghatabar et al. (18), who suggested that 0.42–0.45% Met in the starter diet and 0.33–0.40% Met in the grower diet were safe levels. The aim of the study was to assess the kidney and liver health of broilers under MD at the organ, cell, and organelle level, in order to elucidate the pathway of oxidative stress-induced injury. Furthermore, the study aimed to investigate ileum mucosal immunity in broilers under MD, including T-lymphocyte subsets, abundance of B lymphocytes, and essential cytokine expression. The study findings provide new insight into pathological knowledge of MD in broilers.

# MATERIALS AND METHODS

## Animal Use and Experimental Design

All animal experiments were approved by the Animal Welfare Committee of China West Normal University in accordance with the Laboratory Animal Guidelines for Ethical Review of Animal Welfare (China). This study used a total of 72 one-day old broiler chicks ($43 \pm 2$ g, male) obtained from Cobb Germany (Wiedemar, Germany). The broilers were randomly divided into two treatment groups (control and MD) with six replicates per treatment group and six broilers in each replicate. Six broilers in each replicate were housed in experimental cages (12 cages in total, $2 \times 1 \times 0.8$ $m^3$ length/width/height) with free access to feed and water. The room temperature was $28^{\circ}C \pm 2^{\circ}C$ (day) and $19^{\circ}C \pm 2^{\circ}C$ (night). The experimental period lasted 42 days. Peripheral blood, liver, kidney tissue, and ileum samples were collected on days 14, 28, and 42.

This study first designed starter and grower basal diets composed of ground yellow corn and soybean meal plus supplemental energy, vitamins, and mineral elements, which meet the NRC nutritional standards for broilers, except Met. After calculating the Met content, the basal diets were then used for the MD group, while additional 0.24% and 0.12% DL-Met were added to the starter and grower diets for the control group, respectively. The component details and calculated nutrient levels in these diets are shown in **Table 1**.

## Morphological Observation

### Body Weight

A total of 12 broilers were randomly chosen at 7, 14, 21, 28, 35, and 42 days for body weight to avoid the sample number change by the weekly chicken euthanasia. The body weight data were gained using an electronic scale, and the weekly weight gain were calculated shown in **Table 2**.

### Anatomical, Histological, and Ultrastructural Observations

At 14, 28, and 42 days of age, 12 broilers in each group were randomly chosen and euthanized before being photographed using a color video camera (3CCD; Nikon, Shanghai, China). After anatomical observation, the kidneys and liver were excised and fixed in 4% paraformaldehyde solution for histological observation. After rinsing with water, the samples were dehydrated in a graded series of absolute ethanol (50, 70, 80, 90, and 100%), cleared with benzene twice, followed by saturation and embedding in paraffin. Sections 5 μm thick (10 slices per sample) were prepared and stained with hematoxylin and eosin. A 4XC-W light microscope (Olympus, Tokyo, Japan) was used to observe histological changes in the liver and kidney, and images were edited using Image-Pro software (Media Cybernetics, Rockville, MD, USA). At 42 days of age, kidney

**TABLE 1 |** Diet components of the control and Met deficiency group (%).

| Ingredient | Met deficiency diet | | Control diet | |
|---|---|---|---|---|
| | Starter diet 1 to 21 days | Grower diet 22 to 42 days | Starter diet 1 to 21 days | Grower diet 22 to 42 days |
| Ground yellow corn | 56.0 | 59.9 | 56.0 | 59.9 |
| Soybean meal | 26.6 | 22.2 | 26.6 | 22.2 |
| Soybean oil | 2.76 | 3.60 | 2.76 | 3.60 |
| Maize gluten | 7.09 | 7.71 | 7.09 | 7.71 |
| Fish meal | 3.00 | | 3.00 | |
| Monocalcium phosphate | 1.43 | 1.47 | 1.43 | 1.47 |
| Limestone | 1.45 | 1.33 | 1.45 | 1.33 |
| Mineral and vitamin premix # | 1.00 | 1.00 | 1.00 | 1.00 |
| Salt | 0.12 | 0.24 | 0.12 | 0.24 |
| Choline chloride | 0.10 | 0.12 | 0.10 | 0.12 |
| L-Lysine (54.6%) | 0.10 | 0.19 | 0.10 | 0.19 |
| L-Threonine (98.5%) | 0.05 | 0.06 | 0.05 | 0.06 |
| L-Valine (98.0%) | 0.03 | 0.03 | 0.03 | 0.03 |
| DL-methionine | 0.00 | 0.00 | 0.24 | 0.12 |
| Bentonite | 0.24 | 0.12 | 0.0 | 0.0 |
| Nutrient level (%) | | | | |
| ME, MJ/kg | 12.39 | 12.79 | 12.39 | 12.79 |
| Crude Protein | 21.17 | 19.72 | 21.17 | 19.72 |
| Lysine | 1.19 | 1.08 | 1.19 | 1.08 |
| Methionine | 0.22 | 0.24 | 0.46 | 0.36 |
| Met+Cys | 0.46 | 0.49 | 0.70 | 0.61 |
| Ca | 0.85 | 0.77 | 0.85 | 0.77 |
| Non-phytate P | 0.44 | 0.40 | 0.44 | 0.40 |

*#The premix was made with the following ingredients: iodine, 156 mg; selenium, 25 mg; biotin, 25 mg; folic acid, 167 mg; thiamine, 333 mg; riboflavin, 800 mg; pyridoxine, 417 mg; cobalamin, 2.5 mg; nicotinamide, 6.91 g; calcium, 300 g; chloride, 1.0 g; retinol, 1,200,000 IU; cholecalciferol, 400,000 IU; menadione, 333 mg; calcium pantothenate, 2.0 g; choline chloride, 40 g; iron, 5.0 g; copper, 1.5 g; manganese, 10.0 g; and zinc, 7.0 g. All values presented above were calculated using AMINODat ® 5.0.*

**TABLE 2 |** Body weight changes of broilers in the control and methionine deficiency group.

| Experimental time | Body weight gain in the control group (g) | Body weight gain in the methionine-deficient group (g) | SEM | *p*-value | Sample number |
|---|---|---|---|---|---|
| 7 days | 135.22 | 128.85 | 0.758 | 0.755 | 72 |
| 14 days | 295.77 | 277.42 | 3.227 | 0.158 | 60 |
| 21 days | 415.35 | 370.28* | 9.554 | 0.032 | 60 |
| 28 days | 552.43 | 507.42** | 17.251 | 0.009 | 48 |
| 35 days | 625.72 | 535.64** | 26.758 | 0.001 | 48 |
| 42 days | 705.55 | 601.42** | 29.105 | 0.000 | 36 |

*Body weight gain data are shown as the mean in the table. The sample numbers were 12 at all the experimental times mentioned above. Significant differences are labeled with * or **, *$p < 0.05$, compared with the control group, **$p < 0.01$, compared with the control group.*

and liver samples were collected for ultrastructural observation. The samples were fixed in 2.5% glutaraldehyde, post-fixed in 2% veronal acetate-buffered $OsO_4$, dehydrated with alcohol, and embedded in Araldite resin. Sections 65–75 nm thick were placed in uncoated copper grids and stained with uranyl acetate and 0.2% lead citrate. Images were collected using an H-600 transmission electron microscope (Hitachi, Tokyo, Japan) and edited using Image-Pro software.

## Metabolic Function Assessment Through Peripheral Blood

Peripheral blood was collected from chickens every 14 days, from which the serum was obtained. Related enzyme activities, such as aspartate transaminase (AST), alanine transaminase (ALT), alkaline phosphatase (ALP), and gamma-glutamyltransferase (GGT), were determined by ultraviolet spectrophotometry, using a microplate reader and colorimetric methods. Serum

was also used to assess creatinine (Cr), uric acid (UA), and blood urea nitrogen (BUN) levels using the sarcosine oxidase method, enzyme colorimetry, and urease method, respectively. All methods were performed using reagent kits purchased from Nanjing Jiancheng Bioengineering Institute (Nanjing, China).

## Determination of Antioxidant Ability of Kidney and Liver

Every 14 days, fragments of collected kidney and liver samples were homogenized and centrifuged at 3,500 rpm for 10 min. The supernatant was collected and superoxide dismutase (SOD), catalase (CAT), and glutathione peroxidase (GSH-Px) activities were determined using the hydroxylamine method (for SOD) and colorimetric methods (CAT and GSH-Px). Additionally, glutathione (GSH) content was measured using a spectrophotometric method and malondialdehyde (MDA) content was determined using the thiobarbituric acid (TBA) method. All methods were performed using reagent kits purchased from Nanjing Jiancheng Bioengineering Institute.

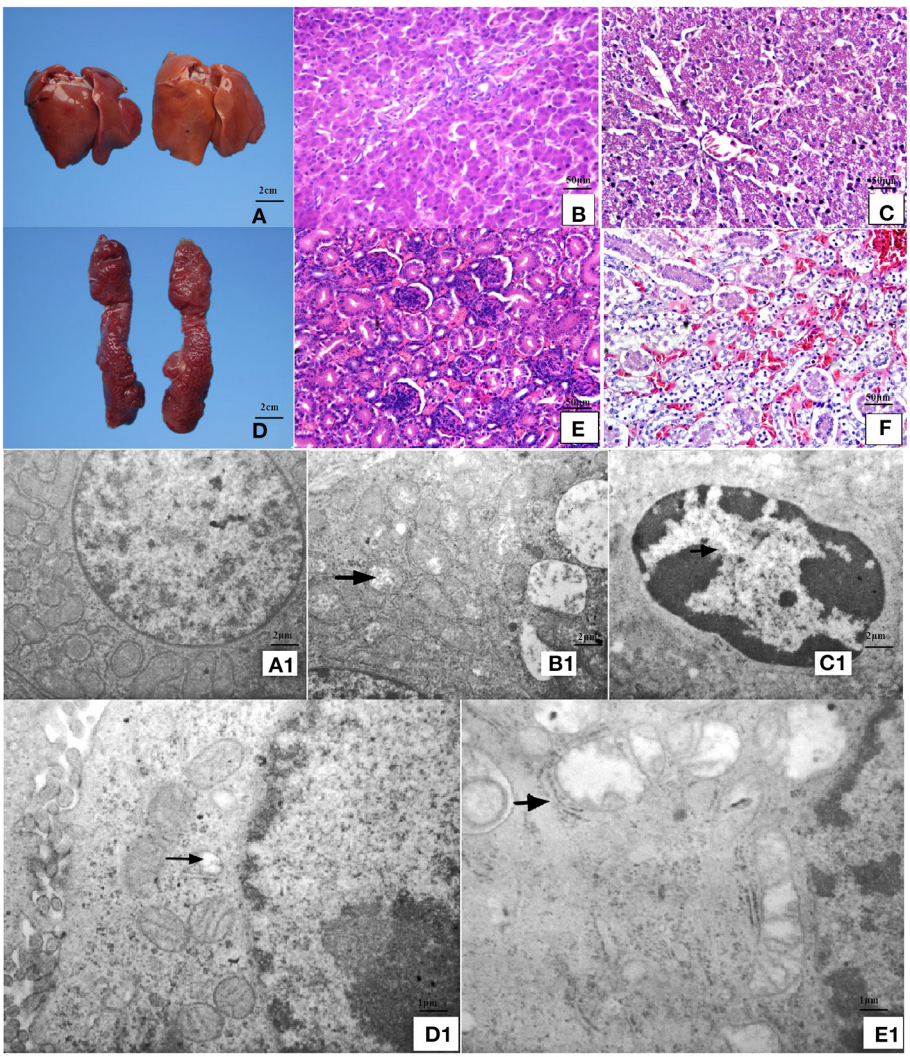


**FIGURE 1 |** Anatomical, histopathological, and ultrastructural observations of liver and kidney. **(A)** The liver was swollen, blunt-edged, and yellow and **(D)** the kidney was swollen in the MD group (right side of panels) at 42 days of age compared to the control group (left side of panels). **(C)** Severe granular degeneration in liver cells was observed in the MD group at 42 days of age (H&E staining ×400) compared to **(B)** the control group (H&E staining ×400). **(F)** Vacuolar degeneration was observed in kidney cells with lots of liquid entry into the cytoplasm in the MD group at 42 days of age (H&E staining ×400) compared to **(E)** the control group (H&E staining ×400). **(A1)** Hepatocytes in the control group possessed clear bilayer lipid membranes and normal organelles (TEM×12,000). **(B1)** The mitochondria of hepatocytes in the MD group were swollen or vacuolated with degenerating cristae (left arrow) (TEM×12,000). **(C1)** The chromatin of hepatocytes in the MD group was condensed (left arrow) (TEM×25,000). **(D1)** Renal cells in the control group possessed normal organelles (TEM×25,000). **(E1)** The mitochondria of hepatocytes in the MD group were swollen or vacuolated with degenerating cristae (left arrow) (TEM×25,000). MD, methionine deficiency; H&E, hematoxylin and eosin; TEM, transmission electron microscopy.

## Assessment of Intestine Mucosal Immunity

### Detection of T-Lymphocyte Subsets in Ileum

Isolation of intraepithelial lymphocytes (IELs) from the ileum was carried out as described by Montufar-Solis and Klein (19) and Todd et al. (20). Briefly, ileum samples were dissected, washed with D-Hank's buffer, cleaned with phosphate-buffered saline (PBS) without $Ca^{2+}$ and $Mg^{2+}$, and digested using a solution consisting of ethylenediaminetetraacetic acid (EDTA), dithiothreitol (DDT), and PBS. After incubation at 37°C followed by centrifugation, the cells were collected and analyzed by flow cytometry.

Resendiz-Albor's isolation method was used to obtain lamina propria lymphocytes (LPLs) from the ileum (21). Briefly, after IELs were collected, the samples were treated with EDTA, cleaned, and transferred to centrifuge tubes containing collagenase, fetal bovine serum (FBS), and gentamicin. After shaking and centrifugation, the suspension containing the lamina propria cells was filtered and centrifuged again, after which the LPLs were collected and prepared for flow cytometry.

The collected IELs and LPLs were made into a cell suspension and transferred into the flow tube. Mouse anti-chicken CD4-FITC (MCA2164F), CD3-SPRD (8200-13), and CD8-RPE (GTX74921) antibodies were added in turn, and stained in the dark at 4°C for 30 min. After washing with PBS, 500 μl of PBS was added to the flow tube and cells were detected by using a BD FACS flow cytometer (Becton, Dickinson and Company, Franklin Lakes, NJ, USA) for 1 h. Lymphocyte subset data were calculated as the number of target positive cells in the whole group of T cells by percentage.

### Detection of B Cells by Immunohistochemistry (IHC)

Paraffin sections of ileum samples were deparaffinized, blocked for endogenous peroxidase by incubating with 3% $H_2O_2$, boiled with 0.01 M sodium citrate buffer for 20 min, and cooled at room temperature. The slices were subsequently incubated in 5% bovine serum albumin (BSA), and then incubated with mouse anti-chicken immunoglobulin (Ig) A antibody followed by incubation with biotinylated secondary antibody goat anti-mouse Ig (GNBP2-34648B, Novus Biologicals, Little Rock, CO, USA). Finally, the slices were incubated with streptavidin-biotin complex at 37°C. After washing, the slices were stained with DAB-$H_2O_2$, counterstained with hematoxylin, dehydrated in ethanol, and sealed with neutral gum. The number and distribution of IgA-positive cells in the ileum were observed under a light microscope. Five slices were made for each intestinal segment of each broiler, and the same parts of the ileum were analyzed in each slice. Images were collected and edited using Image-Pro software.

### Detection of CD19 by ELISA

Ileum segments were treated using the same method as described above. CD19 content was detected in the sample homogenate using the CD19 ELISA kit (Jianglai Biological Co., Ltd., Shanghai, China), according to the manufacturer's instructions. The absorbance (OD) of the treated sample was measured at 450 nm and the CD19 level was calculated using a standard curve.

### Detection of Cytokine Expression by qRT-PCR

Ileum segments stored at −195.8°C were ground with liquid nitrogen until a uniform powder was obtained. Total RNA

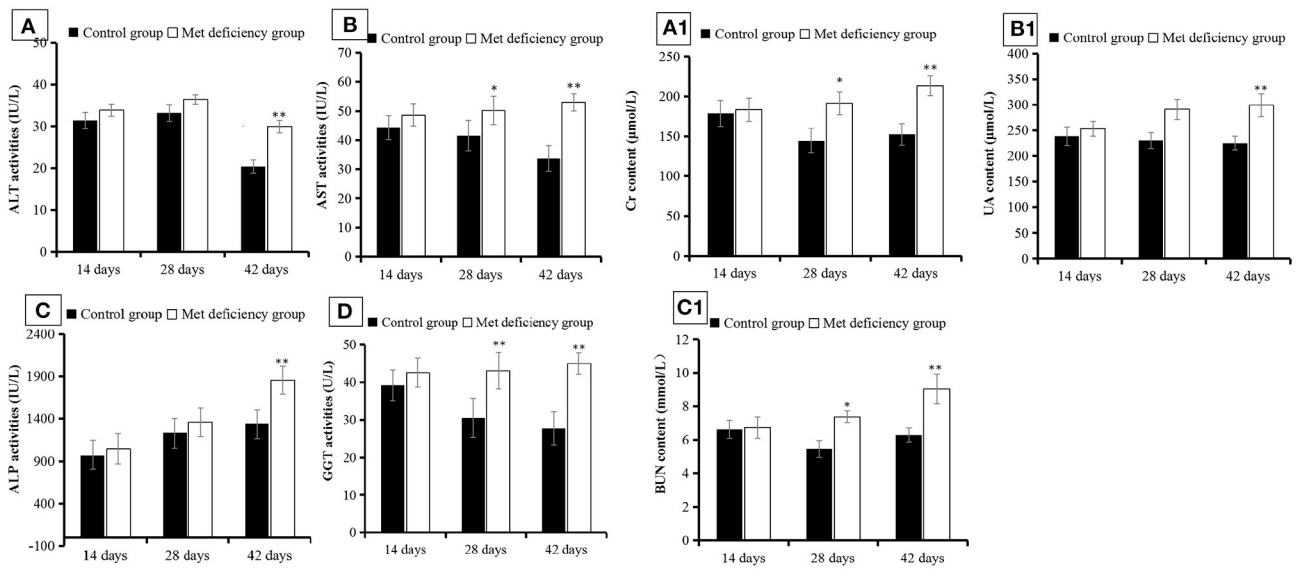


**FIGURE 2 |** Liver and kidney function detection. The activities of **(A)** ALT, **(B)** AST, **(C)** ALP, and **(D)** GGT were significantly ($p < 0.05$, $p < 0.01$) increased at 42 days of age in the MD group compared to the control group. Levels of **(A1)** Cr, **(B1)** UA, and **(C1)** BUN were all significantly ($p < 0.05$ or $p < 0.01$) increased at 28 or 42 days of age in the MD group compared to the control group. ALT, alanine transaminase; AST, aspartate transaminase; alkaline phosphatase; GCT, gamma-glutamyl transferase; MD, methionine deficiency; Cr, creatine; UA, uric acid; BUN, blood urea nitrogen.

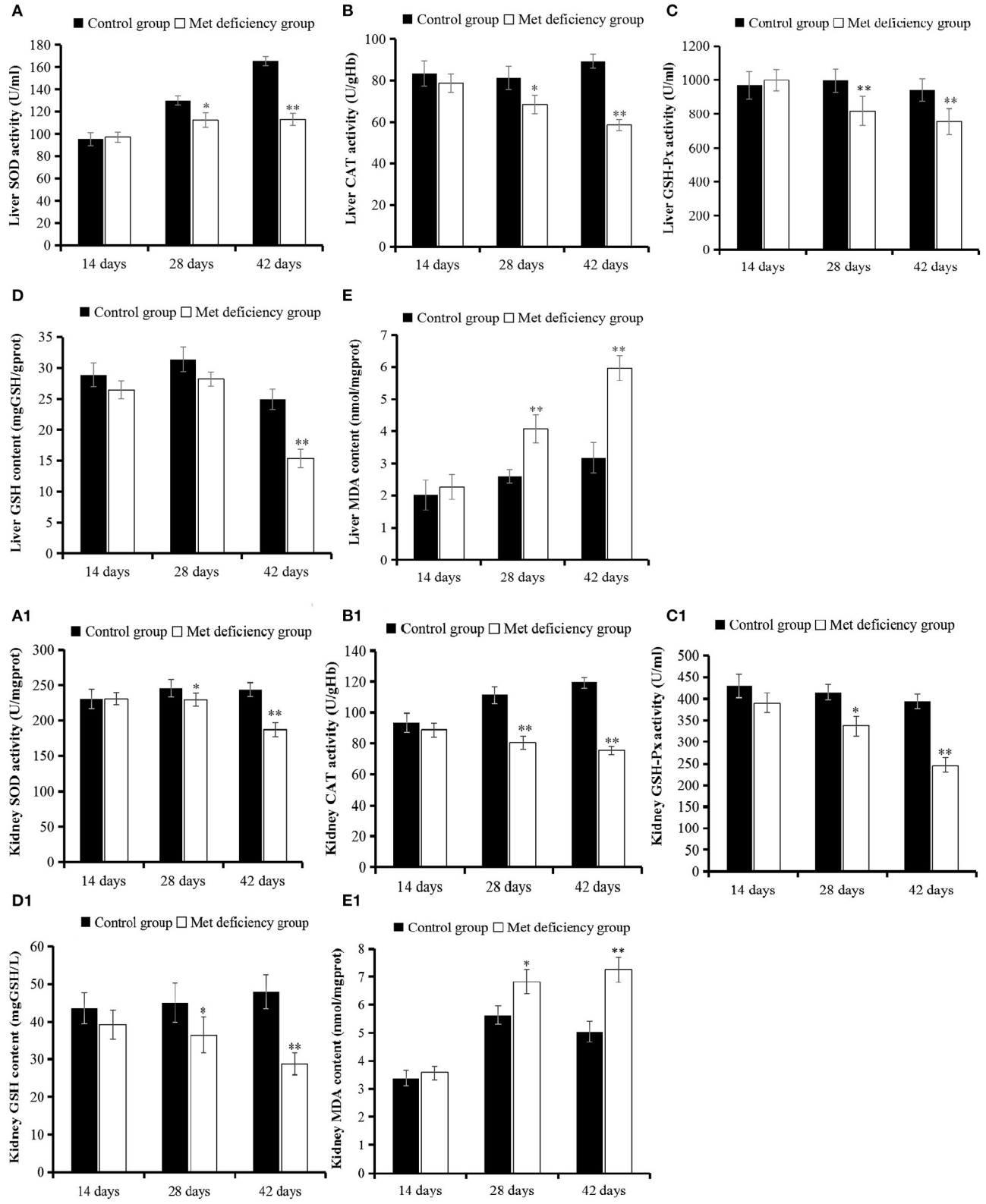


**FIGURE 3 |** Oxidative stress evaluation in liver and kidney. The activities of SOD, CAT, and GSH-Px in liver **(A–C)** and kidney **(A1–C1)** were all significantly ($p < 0.05$ or $p < 0.01$) decreased at 28 or 42 days of age in the MD group compared to the control group. **(D** and **D1)** The level of antioxidant substrate GSH decreased in the MD group at 42 days of age compared to the control group. **(E** and **E1)** The level of oxidation product MDA increased significantly in the MD group at 28 or 42 days of age. SOD, superoxide dismutase; CAT, catalase; GSH-Px, glutathione peroxidase; MD, methionine deficiency; MDA, malondialdehyde; GSH, glutathione.

was isolated using RNAiso Plus (Takara Bio, Kumatsu, Japan) and reverse transcribed to cDNA using the Prim-Script™ RT Reagent Kit (Takara Bio). cDNA was used as the PCR template. Oligonucleotide primers were designed using Primer 5 software and synthesized by Takara Bio (Dalian, China), as shown in **Table 1**. The qRT-PCR reactions (25 μl total volume) included 12.5 μl of SYBR® Premix Ex Taq™ II (Takara Bio, Japan), 1 μl of forward and 1 μl of reverse primers, 8.5 μl of RNase-free water (Tiangen Biotech, Co., Ltd., Beijing, China), and 1 μl of cDNA. A C1000 Touch Thermal Cycler (Bio-Rad, Hercules, CA, USA) was used to perform qRT-PCR. The thermal cycling conditions were as follows: 95°C for 3 min, followed by 44 cycles of 95°C for 10 s, Tm of the specific primer pair for 30 s, and 95°C for 10 s, followed by 72°C for 10 s. Melting curve analysis displayed only one peak for each PCR product. Chicken β-actin was used as the internal reference housekeeping gene. Gene expression values from the control group samples at 14, 28, and 42 days were used to calibrate gene expression values for MD group samples. Expression fold changes were calculated using the $2^{-\Delta\Delta CT}$ method, as described by Ochshorn et al. (22). The details of cytokine mRNA expression detection using primers and normalization primer sequences are provided in **Supplementary Table 1**.

## Statistical Analysis

Statistical analysis was performed using Microsoft Excel and IBM SPSS Statistics v19 software (IBM Corp., Armonk, NY, USA). Differences between treatment groups were analyzed by independent sample *t*-test, and the results are presented as mean ± standard deviation (SD). Differences between means were assessed, and values of $p < 0.05$ were considered significant, while values of $p < 0.01$ were considered extremely significant between the control and MD groups.

# RESULTS

## Growth Performance of Broilers Was Negatively Affected by MD

Although the body weight gains of broilers in both control and MD groups increased continuously for 42 days, the upward trend of data in MD groups is suppressed significantly showing a body growth inhibition. The mean weight gain data in the control group begin to be significantly higher than them in the MD group from 14 days of age ($p < 0.05$), and the difference finally reaches a very significant level from 21 days of age ($p < 0.01$).

## Mitochondrial Damage, Cell Degeneration, and Organ Swelling Induced by MD in Liver and Kidney

Chicks fed an MD diet for 42 days exhibited liver and kidney injury (**Figure 1**). Anatomical observations revealed that the liver was swollen, blunt, round-edged, turbid, lusterless, and grayish-yellow, as shown in **Figure 1A**. These features were speculated to be correlated with granulosis or steatosis, which was supported by the histological and ultrastructural observations. The liver cells were disordered with severe granular degeneration into the cytoplasm (**Figure 1C**), accompanied by distortion and swelling of the mitochondria (**Figures 1B1,C1**). The histological observations of the kidney were more meaningful than the anatomical observations. Only slight swelling and blunt edges were observed in the kidney (**Figure 1F**), but histological examination revealed extreme vacuolar degeneration

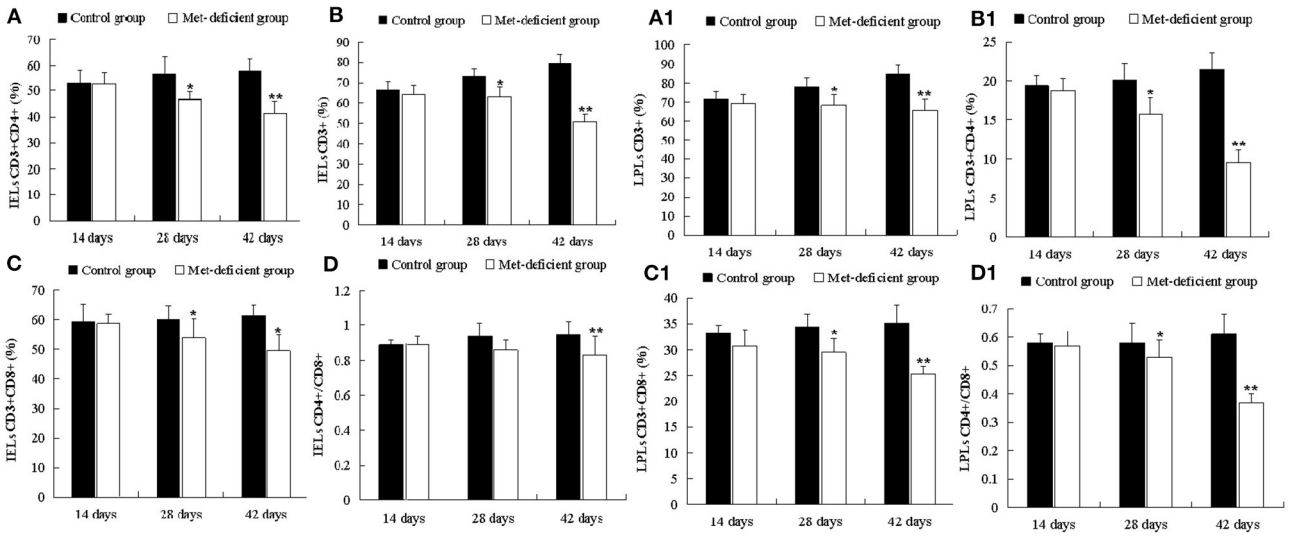


**FIGURE 4 |** Changes in the abundance of ileac CD3+, CD3+CD4+, CD3+CD8+, and CD4+/CD8+ T IELs and LPLs in broilers. At 28 and 42 days of age, the CD3+ **(B)**, CD3+CD4+ **(A)**, and CD3+CD8+ **(C)** IEL populations in the MD group were significantly decreased ($p < 0.05$ or $p < 0.01$), and the CD4+/CD8+ **(D)** IEL population was significantly decreased ($p < 0.01$) at 42 days of age compared to the control group. At 28 and 42 days of age, the CD3+ **(B1)**, CD3+CD4+ **(A1)**, CD3+CD8+ **(C1)**, and CD4+/CD8+ **(D1)** LPL populations in the MD group were significantly lower than those in the control group ($p < 0.05$ or $p < 0.01$). IELs, intraepithelial lymphocytes; LPLs, lamina propria lymphocytes; MD, methionine deficiency.

and hyperemia in renal tubule cells, accompanied by serious degeneration of mitochondria (**Figures 1D1,E1**). All liver- and kidney-related morphological observations indicated severe injury at the organ, cell, and organelle levels.

## MD Leads to Metabolic Disorder in Growing Chicks

AST ($p < 0.05$) and GGT ($p < 0.01$) activities were significantly higher in the MD group than in the control group at 28 days of age and continued to increase over the experimental period ($p < 0.01$) (**Figures 2B,D**). ALT and ALP activities did not differ significantly between the treatment groups at 28 days of age ($p > 0.05$), but were significantly higher in the MD group at the end of the experimental period compared to the control group ($p < 0.01$) (**Figures 2A,C**). This indicated that liver injury was aggravated over time, concentrated mostly between 28 and 42 days of age. In addition, Cr, BUN, and UA serum levels in the MD group also increased significantly compared to the control group, reaching maximum values at 42 days of age ($p < 0.01$) (**Figures 2A1–C1**). These results indicated severe renal cell injury.

## MD Leads to Oxidative Stress in Liver and Kidney of Growing Chicks

As shown in **Figure 3**, the level of oxidation product MDA significantly increased in both the liver and kidney of the MD group at 42 days of age compared to the control group ($p < 0.01$). However, the activities of antioxidant enzymes SOD, GHS-Px, and CAT and the level of antioxidant GSH were significantly decreased at 42 days of age ($p < 0.01$) in the MD group compared to the control group.

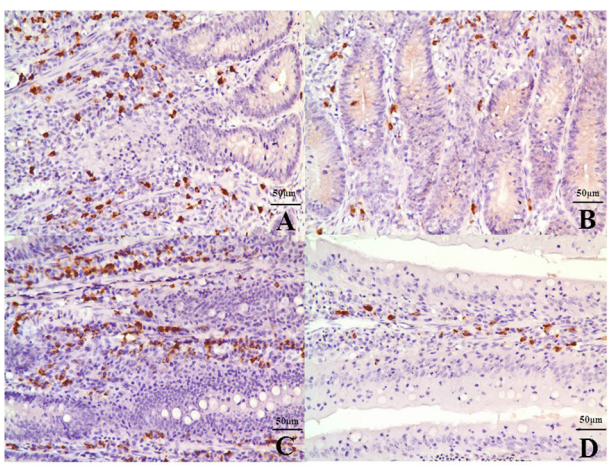


**FIGURE 5 |** IgA-positive B cells in the submucosa and lamina propria in the villi of the ileum at 42 days of age. **(A)** The ileac submucosa of the control group (400×, bar = 50 μm). **(B)** The quantity of B cells in the ileac submucosa of the MD group was significantly decreased (400×, bar = 50 μm). **(C)** The lamina propria in the villi of the ileum in the control group (400×, bar = 50 μm). **(D)** The quantity of B cells in the lamina propria in the villi of the ileum in the MD was significantly decreased (400×, bar = 50 μm). MD, methionine deficiency.

## MD Inhibits Ileum Intraepithelial and Lamina Propria T-Cell Immunity Establishment in Growing Chicks

As shown in **Figures 4A–D**, the percentages of IELs CD3+, CD3+CD4+, and CD3+CD8+ in the MD group decreased significantly at 28 ($p < 0.05$) and 42 days of age ($p < 0.01$) compared to the control group. Furthermore, the percentage of IELs CD4+/CD8+ was significantly decreased ($p < 0.01$) at 42 days of age. These results suggested that MD affected the abundance of IEL subsets and reduced the ability of the chick immune system to defend against pathogens. Moreover, LPLs constitute part of the mucosal immune response. The LPL subsets demonstrated similar trends to those of the IEL subsets. LPL CD3+, CD3+CD4+, and CD3+CD8+ percentages were significantly lower in the MD group at 28 days of age than in the control group ($p < 0.05$), while the percentage of LPLs CD4+/CD8+ in the MD group was significantly lower than that in the control group at 42 days of age ($p < 0.01$) (**Figures 4A1–D1**).

## MD Limits the Activation, Proliferation, and Number of B Cells in the Ileum of Growing Chicks

The IHC results revealed that IgA-positive B cells were mainly distributed in the submucosa and lamina propria in the villi of the ileum (**Figures 5A–D**) with similar numbers of B cells in both treatment groups at 14 days of age. However, the number of B cells in the MD group decreased significantly at 28 ($p < 0.05$) and 42 days of age ($p < 0.01$) compared to the control (**Supplementary Figure 1**). Cell inactivation is indicated by mass suppression of cytokine expression. As shown in **Supplementary Figure 2**, the mRNA expression of IL-2, IL-6, IL-10, IL-17, IFN-γ, and LITAF decreased significantly at 28 ($p < 0.05$) and 42 days of age ($p < 0.01$) in the MD group compared to the control group.

# DISCUSSION

Met supplementation for broilers is important before 42 days of age, when they are growing quickly and establishing immunity. Peng et al. (8) reported that broiler consumption of an MD diet with 0.3% Met increased lipid accumulation in the liver by decreasing hepatic lipid catabolism, which concurred with reported findings of liver weight gain in broilers with a 0.2% Met diet (23) and abnormal increased triglyceride levels and decreased lipoprotein-cholesterol levels in serum of broilers with a 0.3% Met diet (24). For the kidney, the organ most closely related to the liver, renal cell apoptosis in broilers was upregulated through the P53–P21 cancer gene pathway with consumption of a 0.3% Met diet (25). Our study starts with MD diets containing 0.24 and 0.26% Met in the starter and grower diets, respectively. So, the pathological changes revealed in this study would not be aggravated significantly due to Met content differences.

The study demonstrated the effect of MD on the growth performance of broilers. Growth speed under MD was significantly reduced, which was consistent with the conclusion

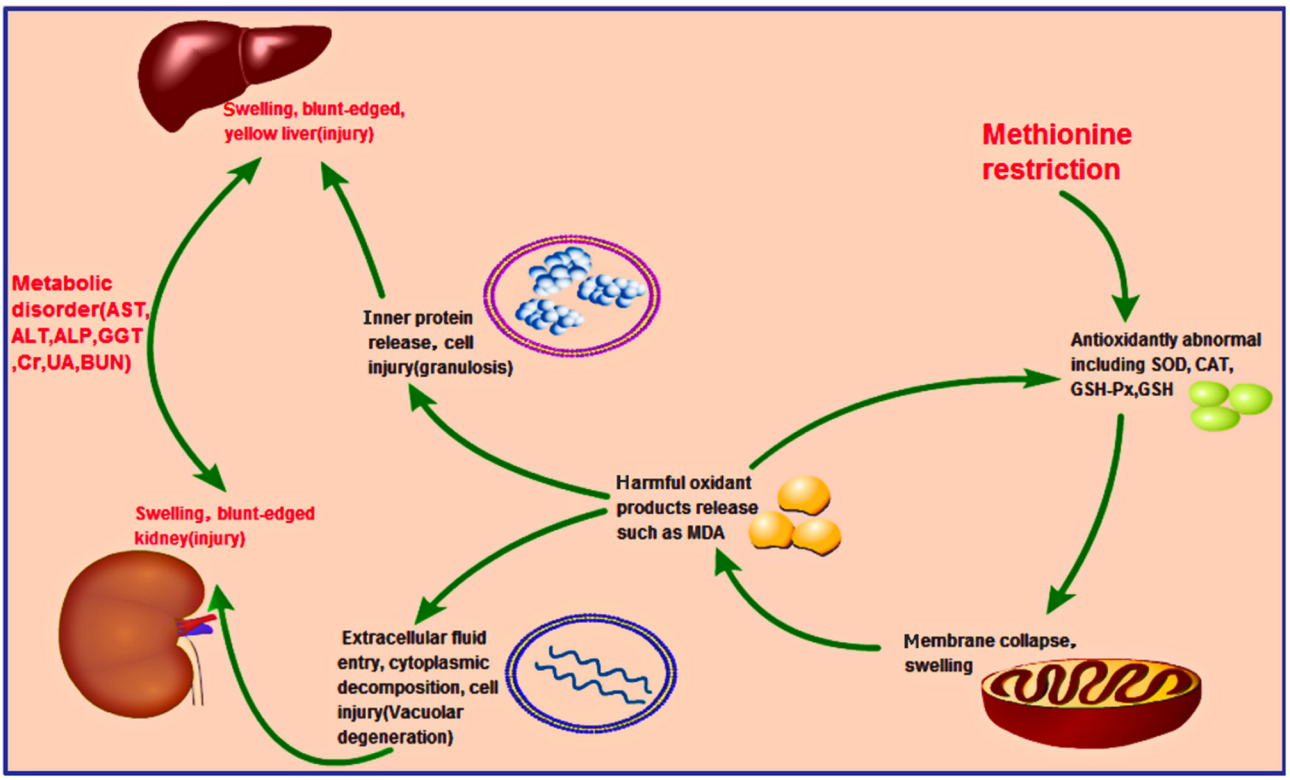


**FIGURE 6 |** Hypothesized pathology of methionine deficiency in the liver and kidney, reflecting induced oxidation stress. Methionine deficiency can decrease the activities of antioxidant enzymes such as SOD, CAT, GSH-Px, and GSH. The mitochondria, where many oxidation-related chemicals such as MDA exist, would be damaged, resulting in their release into the cytoplasm due to membrane collapse. Other organelles in the liver and kidney would then be harmed, releasing lots of proteins and changing the osmotic pressure, causing granulosis degeneration (liver) and vacuolar degeneration (kidney), respectively. Prolonged methionine deficiency could induce liver and kidney injury, finally leading to metabolic disorder.

that a 0.2% Met diet would be harmful for chicken growth and meat quality (26). This demonstrates that the broiler chicken metabolism was affected apparently. Through morphological observations, it is found that the kidney and liver were both swollen, blunt-edged, and turbid, and the kidney had turned yellow (**Figure 1**), suggesting that both organs were injured and significant lipid accumulation might have occurred in the liver, which may also reflect the lipid metabolism disorder found before this study (24). However, the histopathological results indicated granulosis in the liver rather than steatosis (**Figure 1**), suggesting that lipid accumulation was not as severe as previously thought. In contrast, the granulosis and mitochondrial fold destruction found *via* ultrastructural observations suggested more serious metabolic disorder led by mitochondrial injury. This can also be supported by indicators (27, 28) including ASL, ALT, ALP, and GGP activities in the liver (**Figure 2**), and Cr, UA, and BUN levels in the kidney (**Figure 2**). Because only when destructive injury happens such as mitochondrial collapse can these contents be released instead of lipid accumulation inside liver cells. So, the lipid metabolic disorder may be the secondary phenomenon of such pathological changes while mitochondrial injury is induced first. As mentioned by a study (8), lipid metabolism-related gene changes can be influenced in a moderate level by oxidative stress. We need to discuss further whether the mitochondrial injury achieved a significant oxidative stress.

The study findings suggested some latent reasons, including the occurrence of oxidative stress. Met is also known as the precursor of succinyl-CoA, homocysteine, cysteine, creatine, and carnitine (29), some of which are essential substrates for antioxidant molecules, such as GSH. These molecules prevent oxidative stress (30), which is extremely harmful to cells and may cause cell death and tissue damage. We analyzed more key enzymes and products in the antioxidant loop to obtain a broader view of oxidative status in broilers. As shown in **Figure 3**, the GSH content in the liver and kidney decreased significantly ($p < 0.05$) from 14 days of age and complies with the results of a study by Swennen et al. (31). Furthermore, significant lower ($p < 0.01$) antioxidant enzyme activities (SOD, CAT, and GSH-Px) in the liver and kidney were detected in growing chicks in the MD group than in the control group at 42 days of age (**Figure 3**). Moreover, levels of the oxidation product MDA increased significantly ($p < 0.01$) at 42 days of age in the MD group (**Figure 3**). This evidence clarifies the existence of oxidative stress in broilers. These findings might explain the results of mitochondrial membrane potential collapse (**Figure 1**) and metabolic disorder (**Figure 2**), because structural alterations

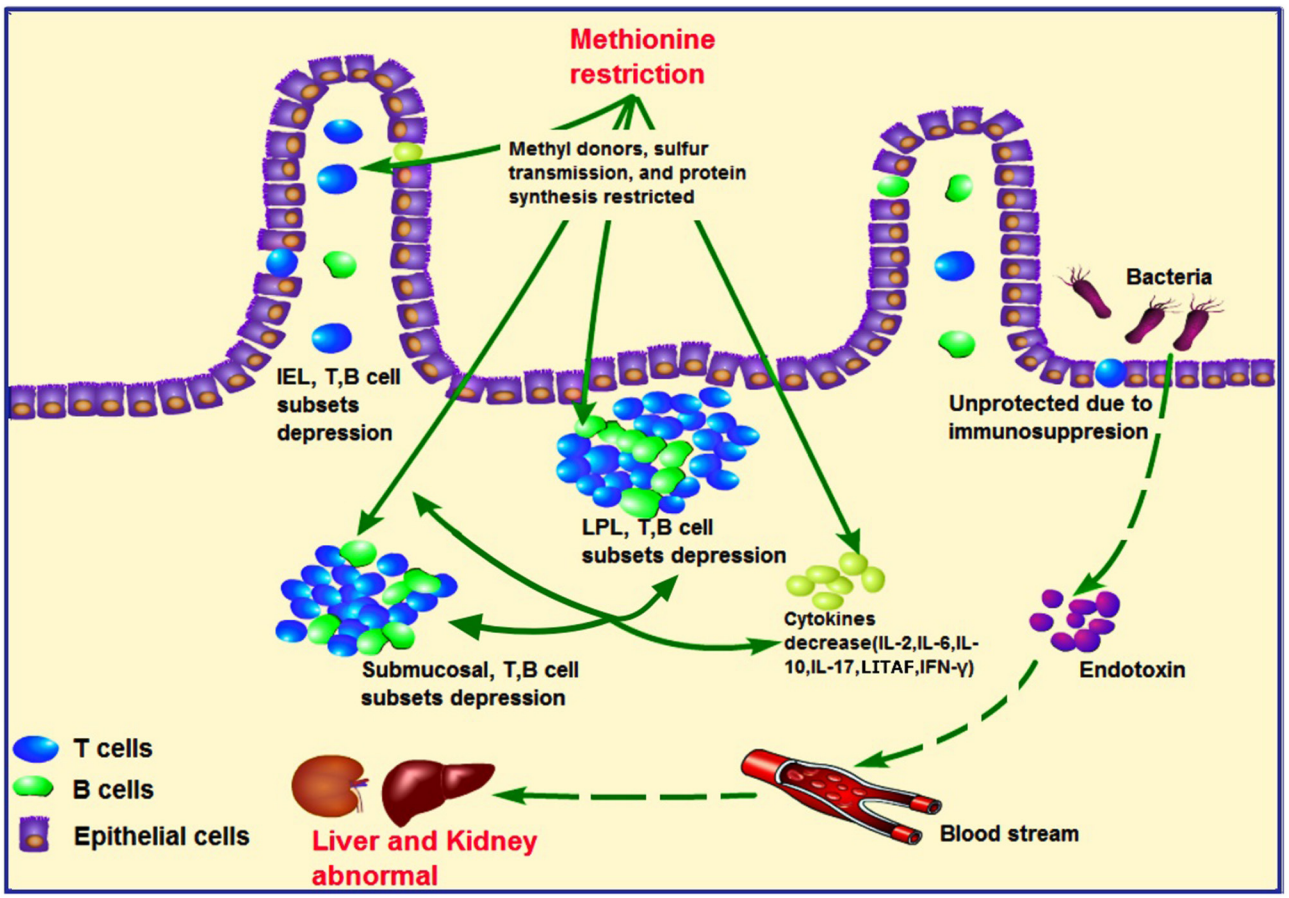


**FIGURE 7 |** Hypothesized pathology of methionine deficiency in ileum mucosal immunity, and the latent pathway of liver and kidney injury. Methionine, an important methyl donor and source of sulfur, might influence protein synthesis and affect intestinal immunity. Under methionine deficiency, IELs and LPLs and submucosal T- and B-cell subsets were suppressed, which could be partially responsible for decreased levels of cytokines such as IL-2, IL-6, IL-10, LITAF, and IFN-γ. These phenomena contribute to ileum mucosal immunosuppression. As intestinal immunity plays a central role in the gut–liver–kidney axis, uncontrolled harmful bacteria might lead to abnormal liver and kidney function due to secretion of endotoxins. IELs, intraepithelial lymphocytes; LPLs, lamina propria lymphocytes.

of proteins and mitochondrial DNA (32) are the initial part of oxidative stress. The discussed possible pathway is shown in **Figure 6**.

The kidney and liver injury found in the current study might also be correlated with compromised immunity in the ileum. MD has been shown to decrease the immune function of chicks. MD can inhibit the development the bursa of Fabricius (33), while increasing cell apoptosis and cell cycle arrest in the spleen, accompanied by oxidative stress (17). However, studies investigating the immunity of the intestine under these conditions are lacking. In addition, further evidence has shown that crosstalk occurs between intestinal mucosal immunity and gut microbes. When the intestinal immune bridge breaks, kidney metabolism disorders may result (34, 35). In our study, the abundances of IEL and LPL subsets were found to be decreased in the MD group (**Figure 5**), including CD3+, CD4+, or CD8+ cells (**Figure 4**), in agreement with reported findings of their T-cell function (36). In addition, IL-2, IL-6, IL-10, IL-17, LITAF, and IFN-γ (**Supplementary Figure 2**) expression also decreased significantly in the MD group, suggesting impaired activating ability and efficiency of ileum mucosal immunity. This was also supported by the activation, proliferation, and number of B cells in the MD group (**Supplementary Figure 1**). So, in regard to cytokine content decrease and LEL and LPL lymphocyte depression, the LEL and LPL subset suppression occurs in the MD broilers. The mechanism responsible for such changes might be related to Met's function as a methyl donor and its involvement in sulfur transmission and protein synthesis, which could cause abnormal gene expression and cell death (37). The ileum is where blood from the intestine returns to the liver through the portal vein. Due to severe immunosuppression found in this key location, we suggest that intestinal immunosuppression played a role in the observed liver and kidney abnormalities. Therefore, we hypothesize that MD-induced liver and kidney injury might also be achieved *via* a second pathway by the gut–liver–kidney axis described also in **Figure 7**.

In conclusion, MD directly affects the growth performance of broilers reflected by suppressed growth rate. The physiological

mechanisms responsible may be related to liver and kidney injury due to metabolic disorder achieved *via* increased oxidative stress in these organs and mucosal immunosuppression in the ileum. Additional studies investigating mucosal immunity or microbes between metabolic organs and the gut are warranted to better evaluate Met diet standards.

## DATA AVAILABILITY STATEMENT

The datasets presented in this study can be found in online repositories. The names of the repository/repositories and accession number(s) can be found in the article/**Supplementary Material**.

## ETHICS STATEMENT

The animal study was reviewed and approved by The Animal Welfare Committee of China West Normal University.

## AUTHOR CONTRIBUTIONS

BS: Conceptualization, Validation, and Formal Analysis. MF, FH, and HZ: Methodology. YW, QN and HZ: Software. BS and MF: Investigation. YW and QN: Data Curation. BS and BW: Writing—Original Draft Preparation and Visualization. BW and HZ: Writing—Review and Editing. BW: Supervision. All authors contributed to the article and approved the submitted version.

## FUNDING

This study is supported by the program for the Fundamental Research Funds of China West Normal University (Project No. 20A003), the Meritocracy Research Funds of China West Normal University (Project No. 17YC349), and the Education Department of Sichuan Province (Project No. 17ZB0425).

## ACKNOWLEDGMENTS

We would like to thank the co-workers of China West Normal University for their assistance in performing the experiments and analysis. We would also like to thank Editage (www.editage.com) for English language editing.

## SUPPLEMENTARY MATERIAL

The Supplementary Material for this article can be found online at: https://www.frontiersin.org/articles/10.3389/fvets.2021.722567/full#supplementary-material

## REFERENCES

1. Jankowski J, Ognik K, Całyniuk Z, Stepniowska A, Konieczka P, Mikulski D. The effect of different dietary ratios of lysine, arginine and methionine on protein nitration and oxidation reactions in turkey tissues and DNA. *Animal.* (2021) 15:100183. doi: 10.1016/j.animal.2021.100183
2. Zeng QF, Zhang Q, Chen X, Doster A, Murdoch R, Makagon M, et al. Effect of dietary methionine content on growth performance, carcass traits, and feather growth of Pekin duck from 15 to 35 days of age. *Poult Sci.* (2015) 94:1592–9. doi: 10.3382/ps/pev117
3. Elamin Ahm ME, Abbas TE. Effects of dietary levels of methionine on broiler performance and carcass characteristics. *Int J Poult Sci.* (2011) 10:147–51. doi: 10.3923/ijps.2011.147.151
4. Fouad AM, Ruan D, Lin YC, Zheng CT, Zhang HX, Chen W, et al. Effects of dietary methionine on performance, egg quality and glutathione redox system in egg-laying ducks. *Br Poult Sci.* (2016) 57:818–23. doi: 10.1080/00071668.2016.1222603
5. Bouyeh M. Effect of excess lysine and methionine on immune system and performance of broilers. *Ann Biol Res.* (2012) 3:3218–24.
6. Sanchez-Roman I, Barja G. Regulation of longevity and oxidative stress by nutritional interventions: role of methionine restriction. *Exp Gerontol.* (2013) 48:1030–42. doi: 10.1016/j.exger.2013.02.021
7. Fouad AM, El-Senousey HK. Nutritional factors affecting abdominal fat deposition in poultry: a review. *Asian-Australas J Anim Sci.* (2014) 27:1057–68. doi: 10.5713/ajas.2013.13702
8. Peng JL, Bai SP, Wang JP, Ding XM, Zeng QF, Zhang KY. Methionine deficiency decreases hepatic lipid exportation and induces liver lipid accumulation in broilers. *Poult Sci.* (2018) 97:4315–23. doi: 10.3382/ps/pey317
9. Drazic A, Miura H, Peschek J, Le Y, Bach NC, Kriehuber T, et al. Methionine oxidation activates a transcription factor in response to oxidative stress. *Proc Natl Acad Sci U S A.* (2013) 110:9493–8. doi: 10.1073/pnas.1300578110
10. Sánchez-Valle V, Chávez-Tapia NC, Uribe M, Méndez-Sánchez N. Role of oxidative stress and molecular changes in liver fibrosis: a review. *Curr Med Chem.* (2012) 19:4850–60. doi: 10.2174/092986712803341520
11. Li S, Tan HY, Wang N, Zhang ZJ, Lao L, Wong CW, et al. The role of oxidative stress and antioxidants in liver diseases. *Int J Mol Sci.* (2015) 16:26087–124. doi: 10.3390/ijms161125942
12. Tripathi A, Debelius J, Brenner DA, Karin M, Loomba R, Schnabl B, et al. The gut–liver axis and the intersection with the microbiome. *Nat Rev Gastroenterol Hepatol.* (2018) 15:397–411. doi: 10.1038/s41575-018-0011-z
13. Wiest R, Albillos A, Trauner M, Bajaj JS, Jalan R. Targeting the gut-liver axis in liver disease. *J Hepatol.* (2017) 67:1084–103. doi: 10.1016/j.jhep.2017.05.007
14. Compare Compare D, Coccoli P, Rocco A, Nardone OM, De Maria S, Cartenì M, et al. Gut–liver axis: the impact of gut microbiota on non-alcoholic fatty liver disease. *Nutr Metab Cardiovasc Dis.* (2012) 22:471–6. doi: 10.1016/j.numecd.2012.02.007
15. Holmes E, Li JV, Athanasiou T, Ashrafian H, Nicholson JK. Understanding the role of gut microbiome–host metabolic signal disruption in health and disease. *Trends Microbiol.* (2011) 19:349–59. doi: 10.1016/j.tim.2011.05.006
16. Ruan T, Li L, Lyu Y, Luo Q, Wu B. Effect of methionine deficiency on oxidative stress and apoptosis in the small intestine of broilers. *Acta Vet Hung.* (2018) 66:52–65. doi: 10.1556/004.2018.006
17. Wu B, Cui H, Peng X, Fang J, Cui W, Liu X. Pathology of spleen in chickens fed on a diet deficient in methionine. *Health.* (2012) 04:32–8. doi: 10.4236/health.2012.41007
18. Mirzaaghatabar F, Saki AA, Zamani P, Aliarabi H, Hemati Matin HR. Effect of different levels of diet methionine and metabolisable energy on broiler performance and immune system. *Food Agric Immunol.* (2011) 22:93–103. doi: 10.1080/09540105.2010.530249
19. Montufar-Solis D, Klein JR. An improved method for isolating intraepithelial lymphocytes (IELs) from the murine small intestine with consistently high purity. *J Immunol Methods.* (2006) 308:251–4. doi: 10.1016/j.jim.2005.10.008
20. Todd D, Singh AJ, Greiner DL, Mordes JP, Rossini AA, Bortell R, et al. new isolation method for rat intraepithelial lymphocytes. *J Immunol Methods.* (1999) 224:111–27. doi: 10.1016/S0022-1759(99)00015-0
21. Reséndiz-Albor AA, Esquivel R, López-Revilla R, Verdín L, Moreno-Fierros L. Striking phenotypic and functional differences in lamina propria lymphocytes from the large and small intestine of mice. *Life Sci.* (2005) 76:2783–803. doi: 10.1016/j.lfs.2004.08.042

22. Ochshorn Y, Shira AB, Jonish A, Lessing JB, Pauzner D, Ezer O, et al. Quantitative fluorescence polymerase chain reaction (QF-PCR) for rapid prenatal diagnosis of aneuploidy. *Am J Obstet Gynecol.* (2004) 191:S44–S44. doi: 10.1016/j.ajog.2004.10.026
23. Carew LB, McMurtry JP, Alster FA. Effects of methionine deficiencies on plasma levels of thyroid hormones, insulin-like growth factors-I and -ii, liver and body weights, and feed intake in growing chickens. *Poult Sci.* (2003) 82:1932–8. doi: 10.1093/ps/82.12.1932
24. Nukreaw R, Bunchasak C, Markvichitr K, Choothesa A, Prasanpanich S, Loongyai W. Effects of methionine supplementation in low-protein diets and subsequent re-feeding on growth performance, liver and serum lipid profile, body composition and carcass quality of broiler chickens at 42 days of age. *J Poult Sci.* (2011) 48:229–38. doi: 10.2141/jpsa.010064
25. Song B, Zeng Q, Liu Y, Wu B. Effect of methionine deficiency on the apoptosis and cell cycle of kidney in broilers. *Res Vet Sci.* (2021) 135:228–36. doi: 10.1016/j.rvsc.2019.09.013
26. Hakamata Y, Watanabe K, Amo T, Toyomizu M, Kikusato M. Characterization of mitochondrial content and respiratory capacities of broiler chicken skeletal muscles with different muscle fiber compositions. *J Poult Sci.* (2018) 55:210–6. doi: 10.2141/jpsa.0170141
27. Petrosillo G, Portincasa P, Grattagliano I, Casanova G, Matera M, Ruggiero FM, et al. Mitochondrial dysfunction in rat with nonalcoholic fatty liver: involvement of complex I, reactive oxygen species and cardiolipin. *Biochim Biophys Acta.* (2007) 1767:1260–7. doi: 10.1016/j.bbabio.2007.07.011
28. Granata S, Zaza G, Simone S, Villani G, Latorre D, Pontrelli P, et al. Mitochondrial dysregulation and oxidative stress in patients with chronic kidney disease. *BMC Genomics.* (2009) 10:388. doi: 10.1186/1471-2164-10-388
29. Martínez Y, Li X, Liu G, Bin P, Yan W, Más D, et al. The role of methionine on metabolism, oxidative stress, and diseases. *Amino Acids.* (2017) 49:2091–8. doi: 10.1007/s00726-017-2494-2
30. Blachier F, Mariotti F, Huneau JF, Tomé D. Effects of aminoacid-derived luminal metabolites on the colonic epithelium and physiopathological consequences. *Amino Acids.* (2007) 33:547–62. doi: 10.1007/s00726-006-0477-9
31. Swennen Q, Geraert PA, Mercier Y, Everaert N, Stinckens A, Willemsen H, et al. Effects of dietary protein content and 2-hydroxy-4-methylthiobutanoic acid or DL-methionine supplementation on performance and oxidative status of broiler chickens. *Br J Nutr.* (2011) 106:1845–54. doi: 10.1017/S0007114511002558
32. Jaeschke H, McGill MR, Ramachandran A. Oxidant stress, mitochondria, and cell death mechanisms in drug-induced liver injury: lessons learned from acetaminophen hepatotoxicity. *Drug Metab Rev.* (2012) 44:88–106. doi: 10.3109/03602532.2011.602688
33. Wu B, Cui H, Peng X, Fang J, Cui W, Liu X. Pathology of bursae of Fabricius in methionine-deficient broiler chickens. *Nutrients.* (2013) 5:877–86. doi: 10.3390/nu5030877
34. Zeuzem S. Gut-liver axis. *Int J Colorectal Dis.* (2000) 15:59–82. doi: 10.1007/s003840050236
35. Fu ZD, Cui JY. Remote sensing between liver and intestine: importance of microbial metabolites. *Curr Pharmacol Rep.* (2017) 3:101–13. doi: 10.1007/s40495-017-0087-0
36. Takahashi K, Ohta N, Akiba Y. Influences of dietary methionine and cysteine on metabolic responses to immunological stress by Escherichia coli lipopolysaccharide injection, and mitogenic response in broiler chickens. *Br J Nutr.* (1997) 78:815–21. doi: 10.1079/BJN19970197
37. Bunchasak C. Role of dietary methionine in poultry production. *J Poult Sci.* (2009) 46:169–79. doi: 10.2141/jpsa.46.169


**Conflict of Interest:** The authors declare that the research was conducted in the absence of any commercial or financial relationships that could be construed as a potential conflict of interest.

frontiers in Veterinary Science

ORIGINAL RESEARCH
published: 08 October 2021
doi: 10.3389/fvets.2021.750937

# *Penthorum chinense* Pursh Compound Ameliorates AFB1-Induced Oxidative Stress and Apoptosis via Modulation of Mitochondrial Pathways in Broiler Chicken Kidneys

*Weilai Tao*[1†], *Zhenzhen Li*[1], *Fazul Nabi*[1†], *Yu Hu*[1], *Zeyu Hu*[1] *and Juan Liu*[1,2,3*]

[1] College of Veterinary Medicine, Southwest University, Chongqing, China, [2] Chinese Veterinary Herbal Drugs Innovation Research Lab, University Veterinary Science Engineering Research Center in Chongqing, Chongqing, China, [3] Immunology Research Center, Medical Research Institute, Southwest University, Chongqing, China

OPEN ACCESS

**Edited by:**
*Hui Zhang,*
*South China Agricultural University, China*

**Reviewed by:**
*Shu-cheng Huang,*
*Henan Agricultural University, China*
*Ali Raza Jahejo,*
*Shanxi Agricultural University, China*
*Harish Menghwar,*
*University of Saskatchewan, Canada*

***Correspondence:**
*Juan Liu*
*liujrc@163.com*

[†]*These authors have contributed equally to this work*

**Specialty section:**
*This article was submitted to Animal Nutrition and Metabolism, a section of the journal Frontiers in Veterinary Science*

**Received:** *31 July 2021*
**Accepted:** *31 August 2021*
**Published:** *08 October 2021*

**Citation:**
*Tao W, Li Z, Nabi F, Hu Y, Hu Z and Liu J (2021) Penthorum chinense Pursh Compound Ameliorates AFB1-Induced Oxidative Stress and Apoptosis via Modulation of Mitochondrial Pathways in Broiler Chicken Kidneys. Front. Vet. Sci. 8:750937. doi: 10.3389/fvets.2021.750937*

Aflatoxin B1 (AFB1) is a carcinogenic mycotoxin widely present in foods and animal feeds; it represents a great risk to human and animal health. The aim of this study was to investigate the protective effects of *Penthorum chinense* Pursh compound (PCPC) against AFB1-induced damage, oxidative stress, and apoptosis via mitochondrial pathways in kidney tissues of broilers. One-day-old chickens ($n = 180$) were randomly allocated to six groups: control, AFB1 (2.8 mg AFB1/kg feed), positive drug (10 mLYCHT/kg feed), and PCPC high, medium, and low-dose groups (15, 10, and 5 ml PCPC/kg feed, respectively). AFB1 treatment reduced weight gain and induced oxidative stress and kidney damage in broiler tissues; however, PCPC supplementation effectively enhanced broiler performance, ameliorated AFB1-induced oxidative stress, and inhibited apoptosis in the kidneys of broilers. The mRNA expression levels of mitochondria-related apoptosis genes (Bax, Bak, cytochrome *c*, caspase-9, and caspase-3) were significantly increased, whereas *BCL2* expression level decreased in the AFB1 group. Supplementation of PCPC to the AFB1 group significantly reversed the changes in mRNA expression levels of these apoptosis-associated genes compared to those in the AFB1 group. The mRNA levels of *NRF2* and *HMOX1* in the kidneys of the AFB1 group were significantly reduced compared to those in the control group, whereas PCPC significantly increased the *NRF2* and *HMOX1* mRNA levels. AFB1 decreased the levels of Beclin1, LC3-I, and LC3-II and increased P53 levels in the kidney compared to those in the control, whereas PCPC significantly reversed these changes to normal levels of autophagy-related genes compared to those in the AFB1 group. In conclusion, our findings demonstrated that PCPC ameliorated AFB1-induced oxidative stress by regulating the expression of apoptosis-related genes and mitochondrial pathways. Our results suggest that PCPC represents a natural and safe agent for preventing AFB1-induced injury and damage in broiler tissues.

**Keywords: *Penthorum chinense* Pursh compound, kidney, broilers, aflatoxin B1, apoptosis, autophagy, mitochondrial DNA**

## INTRODUCTION

Aflatoxins are carcinogenic mycotoxins produced by *Aspergillus* fungi, among which aflatoxin B1 (AFB1) is the most toxic and widely present in various foods and feeds and represents a serious risk to human and animal health (1, 2). AFB1 produced by moldy feed causes liver, kidney, and other organ damage and inhibits the immune function of the body which considerably affects the growth performance of livestock and poultry, thereby causing huge losses to the livestock and poultry breeding industry globally (3–5). Moreover, AFB1 and its metabolites (AFM1) may accumulate in meat products, which represents a serious risk to human health (6).

The kidneys are vital organs that perform many functions including removal of waste from the blood, regulation of the dynamic balance of water and electrolytes, and urine production (7–10). The absorbed mycotoxins are removed directly through urine and it is excreted in droppings in the poultry; however, the mycotoxin residues in the kidney pose animal and human threat, since the kidney cells are directly damaged by AFB1, and increase cell apoptosis and death. The liver and kidney are considered to be the main target organ of AFB1 with signs of liver injury, hepatic histological lesions, and renal atrophy (11, 12); however, recent studies have also shown that after consumption of feed rich in AFB1, the accumulation of AFB1 and AFM1 in the kidneys may cause damage to the kidneys in broiler chickens (*Gallus gallus domesticus*) (13). The toxic effects of AFB1 are mainly mediated via oxidative stress; AFB1 induces the formation of free radicals and inhibits the production of antioxidant enzymes, which leads to an imbalance between oxidation and anti-oxidation and increases oxidative damage (14).

Apoptosis involves programmed cell death, which plays an important role in maintaining normal tissue homeostasis. However, excessive apoptosis leads to the development of various diseases (15). AFB1, which accumulates in the kidneys, may induce kidney cell apoptosis via cytotoxicity (16). Autophagy is an efficient mechanism via which host cells resist cytotoxicity and it plays a crucial role in maintaining organism homeostasis in both physiological and pathological situations (17). Autophagy is closely related to apoptosis; therefore, AFB1 may exert toxic effects by inducing oxidative stress generation and cell apoptosis and by regulating autophagy in the chicken kidneys.

*Penthorum chinense* Pursh is a compound preparation (PCPC) composed of traditional Chinese herbal medicines such as *P. chinense* Pursh, *Bupleurum*, Yinchen, and licorice. The main ingredient *P. chinense* Pursh has antioxidant and anti-liver cancer activities (18), and may exert therapeutic effects and reduce adverse effects via the synergistic effect of multiple active ingredients from different plant parts (19–21). PCPC may prevent damage caused by AFB1 in broilers by inhibiting kidney oxidative stress and cell apoptosis (22). Mitochondrial injury is closely related to several diseases. Induction of autophagy increases the threshold for cell death and inhibits apoptosis. Autophagy can protect kidney cell mitochondria from damages and maintain cellular bioenergetics. However, the most advantageous approach for alleviating the toxic effects of AFB1 on kidney cells of chickens with traditional Chinese medicine has not been reported. Therefore, the aim of this study was to explore the mitochondrial autophagy to understand the underlying mechanism of AFB1 causing kidney apoptosis and drugs exertion effects. In this study, kidneys of chickens were selected to investigate the toxic effects of AFB1 and explore the efficacy of PCPC for alleviating mycotoxin-mediated toxicity.

## MATERIALS AND METHODS

### Preparation of PCPC and Positive Drug YCHT (Yin-Chen-Hao Tang) Extract

#### Preparation of PCPC

PCPC (20 g *P. chinense* Pursh, 20 g *Bupleurum*, 4 g Yinchen, and 4 g licorice; Chongqing, Renjihong Pharmaceutical Co., Ltd.) was added to 480 ml deionized water, after which the volatile oil was extracted and collected at 140°C following filtration. Subsequently, 480 ml deionized water was added to the residue at 140°C, following decoction for 1 h which was filtered, and 480 ml of deionized water was added again to decoct for 1 h. The solution was then combined with the three water extracts. Next, 3.84 l of 60% ethanol was added to the water-extracted residue and extracted for 10 min under ultrasonication at 125 W and 50°C. The volatile oil, water, and alcohol extracts were concentrated in a rotary evaporator to 48 ml (equivalent to 1 g herb $ml^{-1}$) and then stored at 4°C.

#### Preparation of YCHT Extract

YCHT was prepared according to the description in "ShanghanLun" (23). First, 54 g Yin Chen was decocted using 3.6 L deionized water, and the solution volume was reduced to 1.8 L, after which samples of 27 g gardenia and 18 g rhubarb were added. The mixture was decocted for 30 min and filtered through a bandage. Subsequently, the filtrate was concentrated under vacuum to 100 ml (equivalent to 1 g herb $ml^{-1}$) and stored at 4°C.

### Experimental Design, Birds, and Sample Collection

A total of 180 Cobb broilers (age, 1 day) were purchased from a commercial hatchery (Daan, Zigong, Sichuan, China; License No. 1510304017011579). All experimental protocols were performed in accordance with animal ethics guidelines and approved by the Institutional Animal Care and Use Committee (IACUC) of Southwest University (IACUC-20201203). All birds were maintained under standard hygienic conditions, ambient temperature was set at 33°C and 60% humidity during the experimental period. After 1 week of adaptive feeding, they were randomly assigned to the following groups ($n = 30$ per group): control; AFB1; positive drug (YCHT group); and PCPC high-, PCPC medium-, and PCPC low-dose groups. All groups were fed AFB1 (MACKLIN, Shanghai, China) at 2.8 mg/kg feed except for the control group; the positive drug group was fed YCHT at 10 ml/kg feed, and the PCPC high-, medium-, and low-dose groups were fed normal feed containing 15, 10, and 5 ml/kg PCPC until the end of the experiment (28 days), respectively. All birds had free access to feed; diet and body growth parameters

were recorded during each week of the experiment, and serum and kidney samples were collected on the 28th day of the experiment. The birds were euthanized without anesthesia via cervical dislocation; all birds were weighed, and kidney index was calculated using the following formula:

$$\text{Organ index} = \frac{\text{organ mass } (g)}{\text{body weight } (100\,g)}$$

## Histopathological and Serum Analyses

Kidney samples were stained using hematoxylin and eosin (H&E; Solar Bio, Beijing, China). In brief, part of the broiler kidney tissue was fixed in 10% formaldehyde solution for more than 24 h; placed in running water overnight; and then the kidney sample was dehydrated in a series of ethanol, turned transparent in xylene, and embedded in paraffin. The tissue samples were cut into 5-μm sections, placed on glass slides, stained with H&E, sealed with neutral resin, and the pathological changes in the kidney tissues were observed under an optical microscope (Zeiss upright microscope Axio Scope A1; Carl Zeiss, Oberkochen, Germany). Serum urea and uric acid (UA) levels in broilers were analyzed using an automatic biochemical analyzer.

## Oxidative and Autophagy Assay

Kidneys samples (total six samples) were collected and immediately frozen in liquid nitrogen at −80°C. The kidney ($n$ = 6) samples were added to phosphate-buffered saline (pH 7.4) (kidney and PBS volume 1:9), fully homogenized using a tissue homogenizer, and centrifuged (4°C, 3,000 rpm for 20 min). The superoxide dismutase (SOD), malondialdehyde (MDA), Beclin1, LC3-I, and LC3-II levels in the kidney tissues were analyzed using a commercial kit according to the manufacturer's instructions (Xiamen Huijia Biological Technology Co., Ltd., Xiamen, China).

## RNA Isolation and Quantitative Real-Time Reverse Transcription-Polymerase Chain Reaction (RT-qPCR)

Kidney tissue samples were collected from each group, ground in liquid nitrogen, and then homogenized in TRIzol reagent (1 ml trizol for 50 mg kidney sample) (Win Biosciences, Beijing, China) to extract the total RNA. cDNA was synthesized from the RNA using a Trans Gen cDNA kit (Biotech Co., Ltd., Beijing, China) according to the manufacturer's instructions. Reverse transcription was performed at 42°C for 60 min and 95°C for 3 min; cDNA synthesis was performed in a 20-μl reaction mixture consisting of oligo (dT)18, 2×ES Reaction Mix, and 5 μg RNA.

The mRNA expression of genes encoding nuclear factor erythroid 2 (*NRF2*), heme oxygenase-1 (*HMOX1*), B-cell lymphoma 2 (*BCL2*), P53 (*P53*), BAX (*BAX*), BAK (*BAK1*), cytochrome *c* (*CYC*), caspase-9 (*CASP9*), and caspase-3 (*CASP3*) was analyzed via SYBR Green I real-time fluorescent quantitative PCR (relative quantification). The primer sequences of the genes are shown in **Table 1**. All PCR reactions were run at least in quadruplicate using the TransStart Green qPCR SuperMix kit (TransGen Biotech, Beijing, China) in a 20-μl reaction volume consisting of 2 μl cDNA, specific forward and reverse primers (0.5 μl each), and 10 μl Green qPCR Super Mix. The following thermal cycling parameters were used: 94°C for 30 s, 40 amplification cycles at 94°C for 5 s, 61°C for 35 s, and 72°C for 30 s. Relative quantification of each gene was performed using the comparative $2^{-\Delta\Delta CT}$ method (24, 25).

**TABLE 1** | Primers for quantitative real-time PCR.

| Target gene | Primer sequence (5′-3′) | Product length (bp) |
|---|---|---|
| Nrf-2 | F: GCATTTTGCAGCCAGACGAC | 20 |
| | R: TTGTTCCTGTGTCACCGTCC | 20 |
| HO-1 | F: CAACGCCACCAAGTTCAAACA | 21 |
| | R: CAGCGCCTCAAACACCTGTA | 20 |
| Bcl-2 | F: CTGGATCCAGGACAACGGA | 19 |
| | R: GATGCAAGCTCCCACCAGAA | 20 |
| P53 | F: GTCCCATCCACGGAGGATTAT | 21 |
| | R: CCAGGCGGCAATAGACCTTA | 20 |
| Bax | F: CAGATTGGAGAGGCCCTCTT | 20 |
| | R: AATCTGGTCCTGGCTGTTGC | 20 |
| Bak | F: GGCCATCACGAGAGATCAATG | 21 |
| | R: TCCTGTTGGTAGCGGTAGAAG | 21 |
| Cyt-c | F:CCCAGTGCCATACGGTTGAA | 20 |
| | R:GCTTGTCCTGTTTTGCGTCC | 20 |
| Caspase-9 | F: CCGGAGGGATTTATGGAACAG | 21 |
| | R: CAGGCCTGGATGAAGAAGAGT | 21 |
| Caspase-3 | F: GAAGATCACAGCAAGCGAAGC | 21 |
| | R: CAAGAGGGCCATCTGTACCAT | 21 |
| GAPDH | F: CAGAACATCATCCCAGCGTC | 20 |
| | R: GGCAGGTCAGGTCAACAAC | 19 |

## Statistical Analysis

Experimental data were analyzed by one-way ANOVA using SPSS 20.0.0 (IBM, Armonk, NY, USA) software. Results were presented as mean ± SD. The significant difference among treatments was determined using Duncan's multiple-range test. Graph Pad Prism version 8.0.1 (Graph Pad Software, San Diego, CA, USA) was used to generate graphs with error bars.

# RESULTS

## Effect of PCPC Treatment on Weight Gain and Growth Performance

The effect of PCPC treatment on weekly growth performance (days 7, 14, 21, and 28) is summarized in **Figure 1**. The average body weight of each group increased within the first 7 days; however, the difference between the groups was not significant ($p > 0.05$). The group of chickens (age, 2–4 weeks) fed AFB1 showed a lower average weekly weight gain than that of other groups. Supplementation with PCPC and positive drug alleviated this adverse effect, with a significant increase in weekly weight gain and performance of broilers compared to that of the AFB1-fed group (**Figure 1**).

## Biochemical Analysis of Serum Urea and UA Levels, and Kidney Index

To evaluate the effect of AFB1 and PCPC treatment on kidney function, serum urea and UA levels and the kidney index were analyzed on the 28th day of the experiment. AFB1 treatment resulted in increased the kidney index and serum urea and UA levels compared to those in the control group ($p < 0.05$). PCPC and positive drug supplementation significantly ameliorated these adverse effects by decreasing the kidney index and serum urea and UA levels compared to those in the AFB1 group (**Figure 2**).

## Histopathological Analysis of Kidney Tissues

To further explore the effects of PCPC and AFB1 treatment on kidney tissues, H&E staining was performed. Results showed that AFB1 supplementation resulted in kidney tissue injury compared to that in the control group; tissue sections of the AFB1-treated group showed edema and inflammatory cells with glomerulus atrophy, glomerular epithelial cell proliferation, renal tubular lumen stenosis and obscurity, and renal tubular epithelial cell shedding. However, PCPC and positive drug supplementation significantly reduced the development of abnormal histological signs, renal injuries, and structural deterioration in the kidney tissues compared to those in the AFB1 group (**Figure 3**).

## Serum Antioxidant Parameters

The effect of PCPC treatment on serum antioxidant indices of broiler kidneys was evaluated. We found that the SOD level decreased and MDA level increased significantly in the AFB1 group ($p < 0.01$) compared to those in the control group. Administration of PCPC and positive drug to AFB1-treated

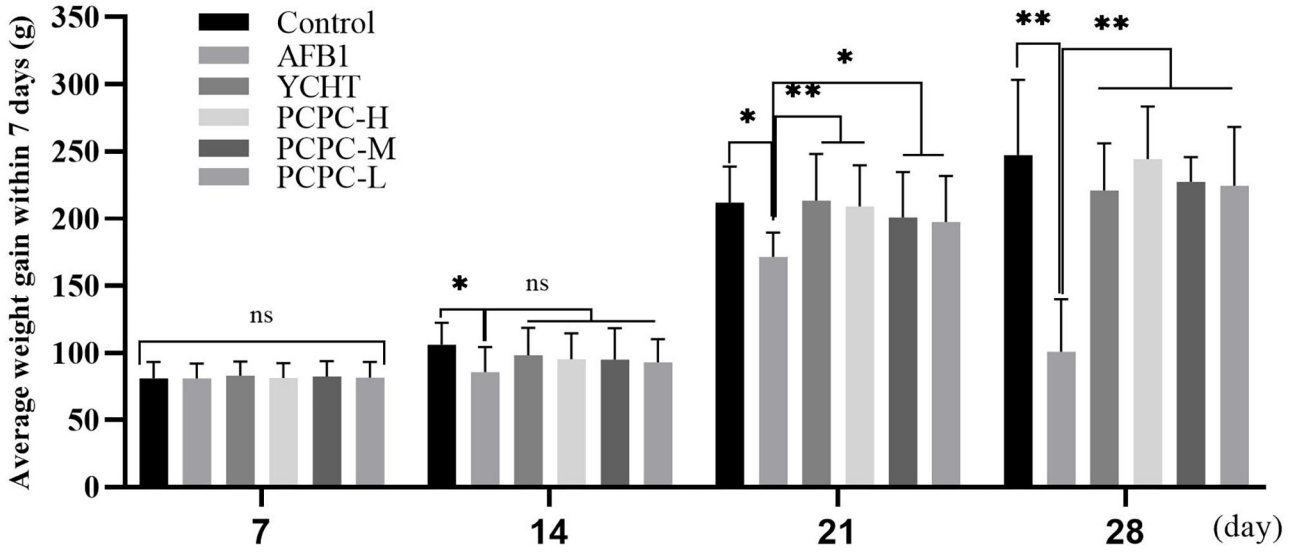


**FIGURE 1 |** Effect of PCPC on weight gain and growth performance of broilers fed diet containing AFB1. The average weekly body weight of each group. Asterisk means values within columns are significantly different ($p < 0.05$) (ns, non-significant). *$p < 0.05$ and **$p < 0.01$.

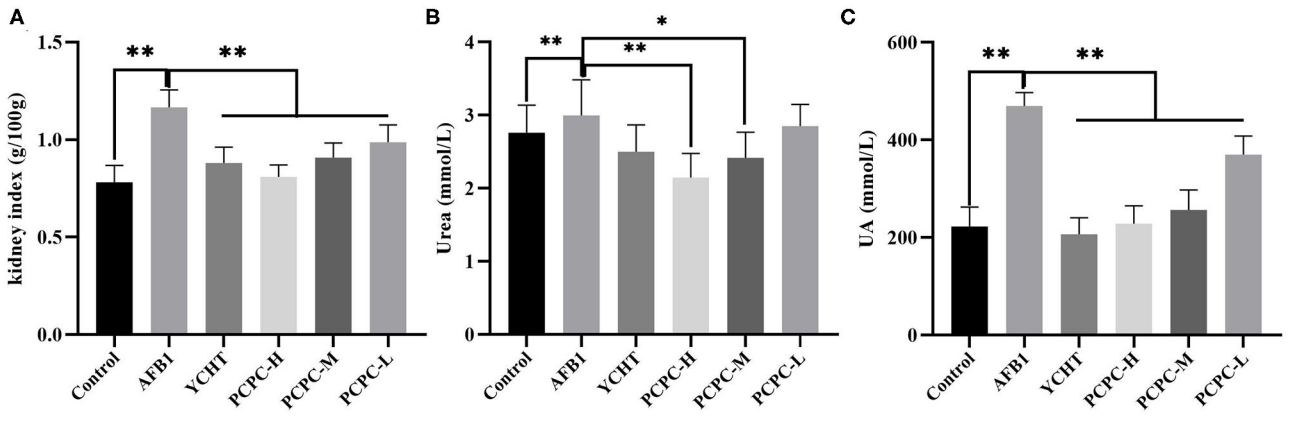


**FIGURE 2 |** Biochemical analysis of serum urea and UA levels and the kidney index analyzed on the 28th day of the experiment. **(A)** Kidney index; **(B)** Urea; **(C)** UA. Asterisk means values within columns are significantly different. *$p < 0.05$ and **$p < 0.01$.

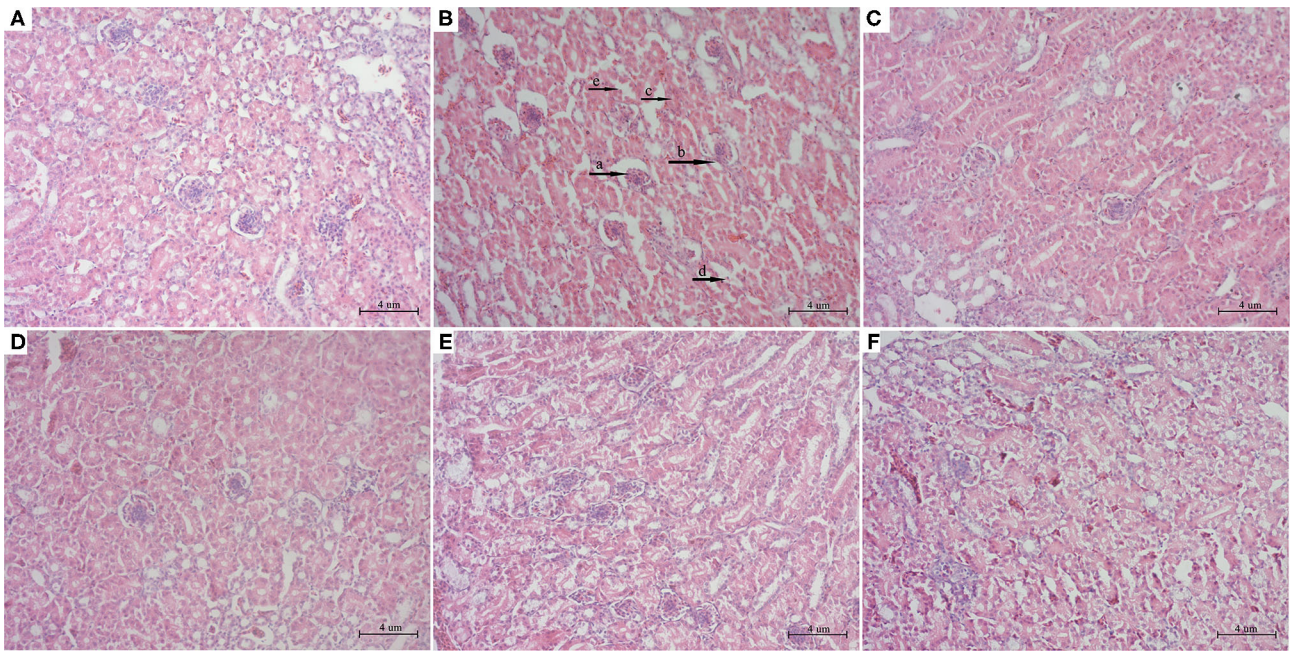


**FIGURE 3 |** Histopathological analysis of kidney from different groups. The kidney tissues were stained with H&E stain. **(A)** Control; **(B)** AFB1; **(C)** YCHT; **(D)** PCPC high dose; **(E)** PCPC medium dose; **(F)** PCPC low dose. (a) glomerulus atrophy, (b) glomerular epithelial cell proliferation, (c) renal tubular lumen stenosis and obscurity, (d) renal tubular epithelial cell shedding.

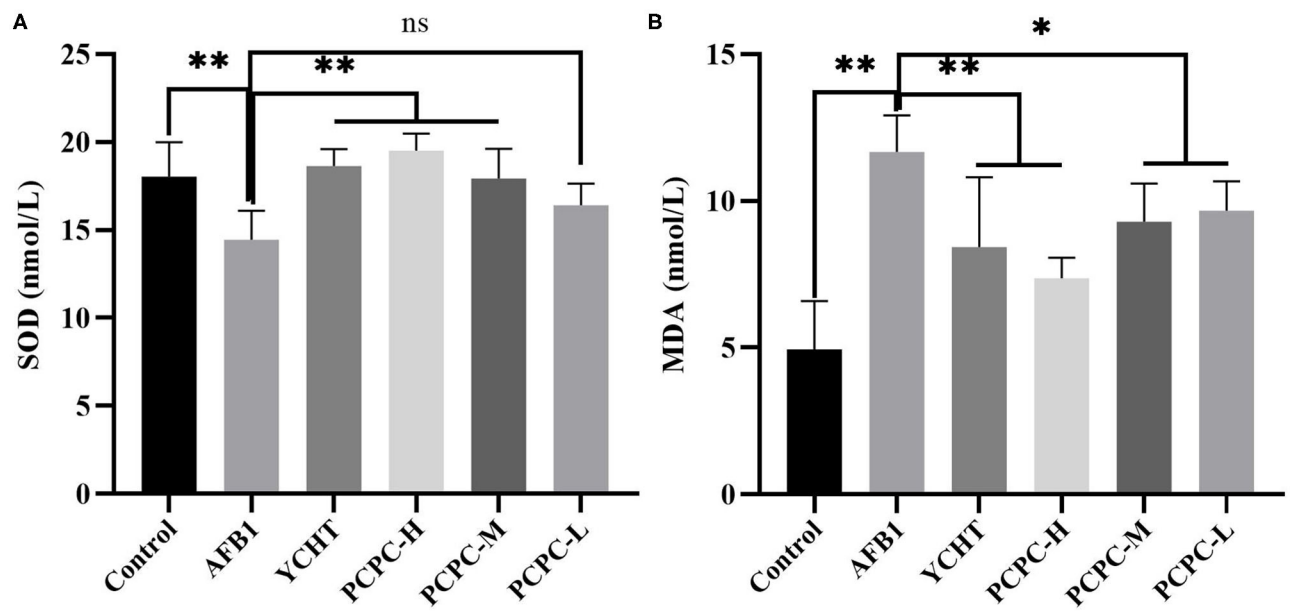


**FIGURE 4 |** Effect of PCPC on serum antioxidant parameters of broiler fed diet containing AFB1. Values are represented as the mean ± SD. **(A)** SOD; **(B)** MDA. Mean values within a column are significantly different ($p < 0.05$). *$p < 0.05$ and **$p < 0.01$, ns, non-significant.

groups significantly enhanced the antioxidant enzyme activities in a dose-dependent manner by increasing SOD levels and decreasing MDA levels compared to those in AFB1-treated birds (**Figure 4**).

## Expression Levels of *NRF2* and *HMOX1* in Kidneys

The mRNA expression levels of *NRF2* and *HMOX1* in the kidneys of broilers in the AFB1 group were significantly reduced ($p <$

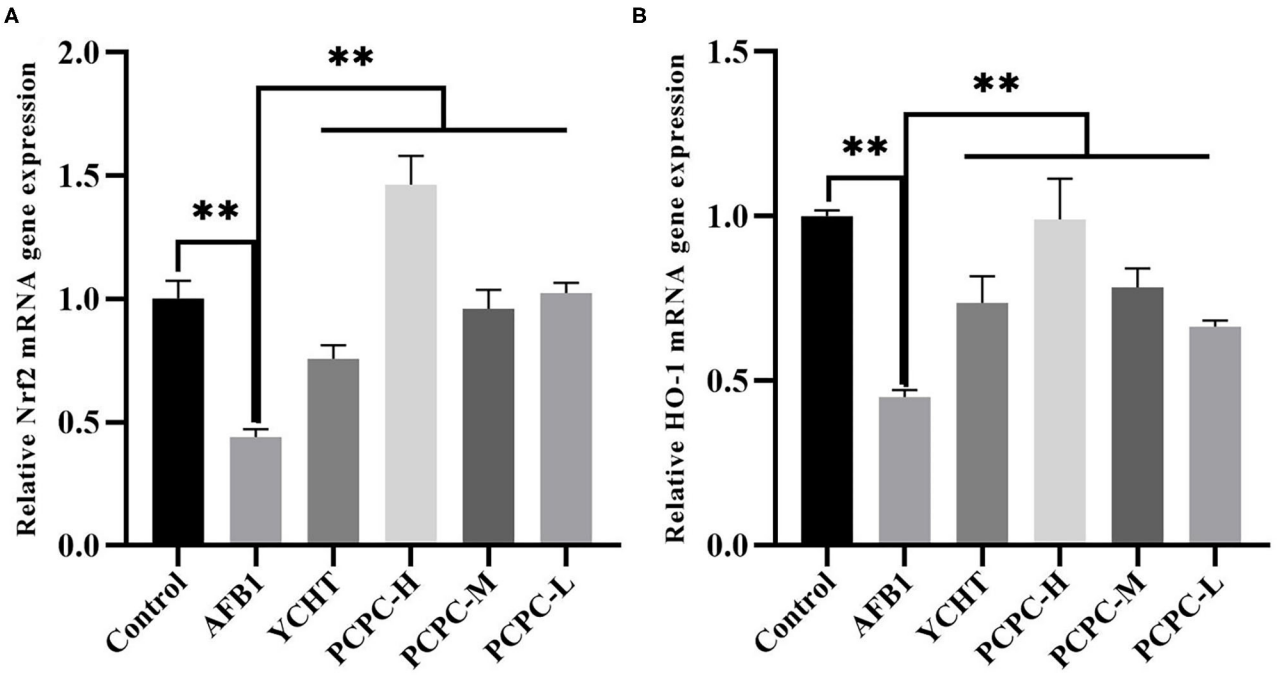


**FIGURE 5 |** Effect of PCPC on expression levels of Nrf2 and HO-1 in kidney of broilers. The mRNA expression of Nrf2 and HO-1 was identified by quantitative real-time PCR. All data are expressed as means ± SD. **(A)** Nrf2 expression; **(B)** HO-1 expression. Asterisk indicates significant difference ($p < 0.05$) compared to the control group and AFB1 group.

0.01) compared to those in the control group. In contrast, the *NRF2* and *HMOX1* mRNA levels in the PCPC and positive drug treatment groups were significantly increased ($p < 0.01$; **Figure 5**).

## Effect of PCPC and AFB1 Treatment on Apoptosis in the Kidney Tissues

The mRNA levels of mitochondrial apoptosis-related genes were analyzed in the kidney tissues of chickens to evaluate the ameliorative effects of PCPC against AFB1-mediated injuries and pathogenesis. The mRNA expression level of *BCL2* decreased and the levels of *BAX*, *BAK1*, *CYC*, *CASP9*, and *CASP3* increased in the AFB1-treated groups compared to those in the control group ($p < 0.01$). However, the change in expression levels of these mitochondrial apoptosis-related genes was significantly ($p < 0.01$) reversed in the PCPC and positive drug treatment groups compared to the trend in the AFB1-treated group (**Figure 6**).

## Effect of PCPC and AFB1 Treatment on Autophagy in Kidney Tissues

AFB1 treatment downregulated Beclin1, LC3-I, and LC3-II, and upregulated p53 compared to those in the control group. PCPC and positive drug treatment significantly reversed these changes in mRNA levels of autophagy-related genes compared to those in the AFB1-treated group ($p < 0.05$; **Figure 7**).

# DISCUSSION

Birds are susceptible to AFB1-mediated toxicity (26). Exposure to AFB1 can cause oxidative stress, immunosuppression, inflammation, and cell apoptosis, and it affects many physiological processes in birds (27). Moreover, due to the ubiquity of AFB1 in the environment, it represents a significant threat to the aquaculture industry and animal product safety (26). The present study evaluated the protective effect of PCPC against AFB1-induced kidney toxicity in broilers and determined the mitochondrial apoptosis-related pathways associated with PCPC and AFB1 treatments.

AFB1 can reduce the growth rate of broilers, leading to higher morbidity and mortality (28, 29). In the current study, we similarly found that the growth performance of broilers significantly decreased with the continuous intake of AFB1, whereas the growth performance of broilers was improved after adding PCPC to the feed. The kidneys are the main organ associated with the excretion and accumulation of AFB1; therefore, AFB1 can disrupt the structure of the kidney and cause organ damage (30). Urea and UA levels in the blood represent major indicators of pathological changes and kidney function (31). The organ index is an indicator of organ toxicity (32). Our findings showed an abnormal increase in kidney index and urea and UA levels; however, these alterations reversed upon PCPC supplementation. The glomerulus and tubules constitute the functional unit (nephron) of the kidney. The glomerulus is

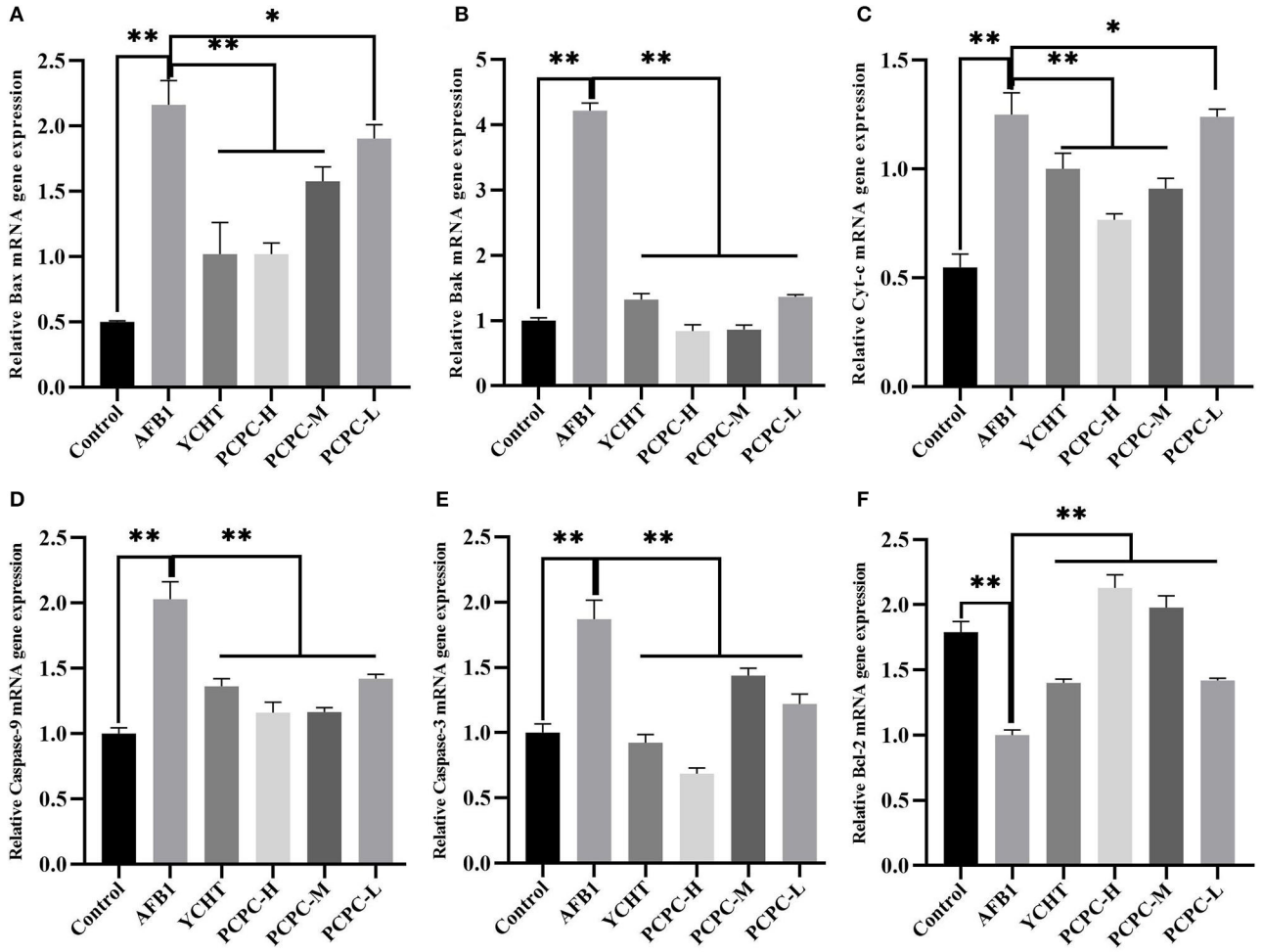


**FIGURE 6 |** Effect of PCPC and $AFB_1$ on apoptosis-related genes in the kidney of broilers. The mRNA expression of apoptosis-related genes were identified by quantitative real-time PCR. All data are expressed as means ± SD. **(A)** Bax; **(B)** Bak; **(C)** Cyt-c; **(D)** Caspase-9; **(E)** Caspase-3; **(F)** Bcl-2. Asterisk indicates significant difference ($p < 0.05$) compared to the control group and AFB1 group. *$p < 0.05$ and **$p < 0.01$.

a spheroid composed of capillaries which filter the blood (33). The glomerular basement membrane is crucial to the glomerular capillaries and is a necessary structure required for the kidneys to perform filtration (34). The renal tubules are responsible for a variety of transport processes and they secrete or reabsorb electrolytes and metabolites in urine (35). We observed glomeruli atrophy in kidney tissue sections; the glomerular basement membrane proliferated and the renal tubules fell off owing to AFB1-mediated injury, indicating that the kidney filtration functions were impaired; however, kidney function significantly improved with PCPC treatment.

Oxidative stress represents one of the main pathogenesis mechanisms of several diseases (36). It promotes the development of diseases by affecting redox homeostasis in the body. Renal insufficiency is generally believed to be related to an imbalance in redox homeostasis (37). AFB1 can induce the generation of high levels of free radicals and promote lipid peroxidation, thereby increasing oxidative stress in the kidneys (38). SOD and MDA are the most important elements related to oxidative stress. SOD is an antioxidant enzyme that plays a vital role in removing $O^{2-}$ (39). MDA is an oxidized lipid metabolite that serves as an indicator of cellular damage and lipid peroxidation status (40). In the present study, the addition of AFB1 to the feed induced a significant increase in MDA levels and decreased SOD levels in the kidneys of broilers; therefore, AFB1 treatment induced oxidative stress generation in the kidneys of broilers. PCPC treatment inhibited the accumulation of MDA and increased the level of SOD, indicating that PCPC can alleviate oxidative stress production in the kidneys induced by AFB1. *Penthorum chinense* Pursh, usually used as a traditional medicine, is studied for its therapeutic effects in diuresis, detoxification, and blood circulation promotion. In addition, the study concluded that PCP herb demonstrated optimistic effects in anti-oxidation, anti-hepatitis, and anti-tumor efficacy (41). Our results are consistent with those of previous studies which

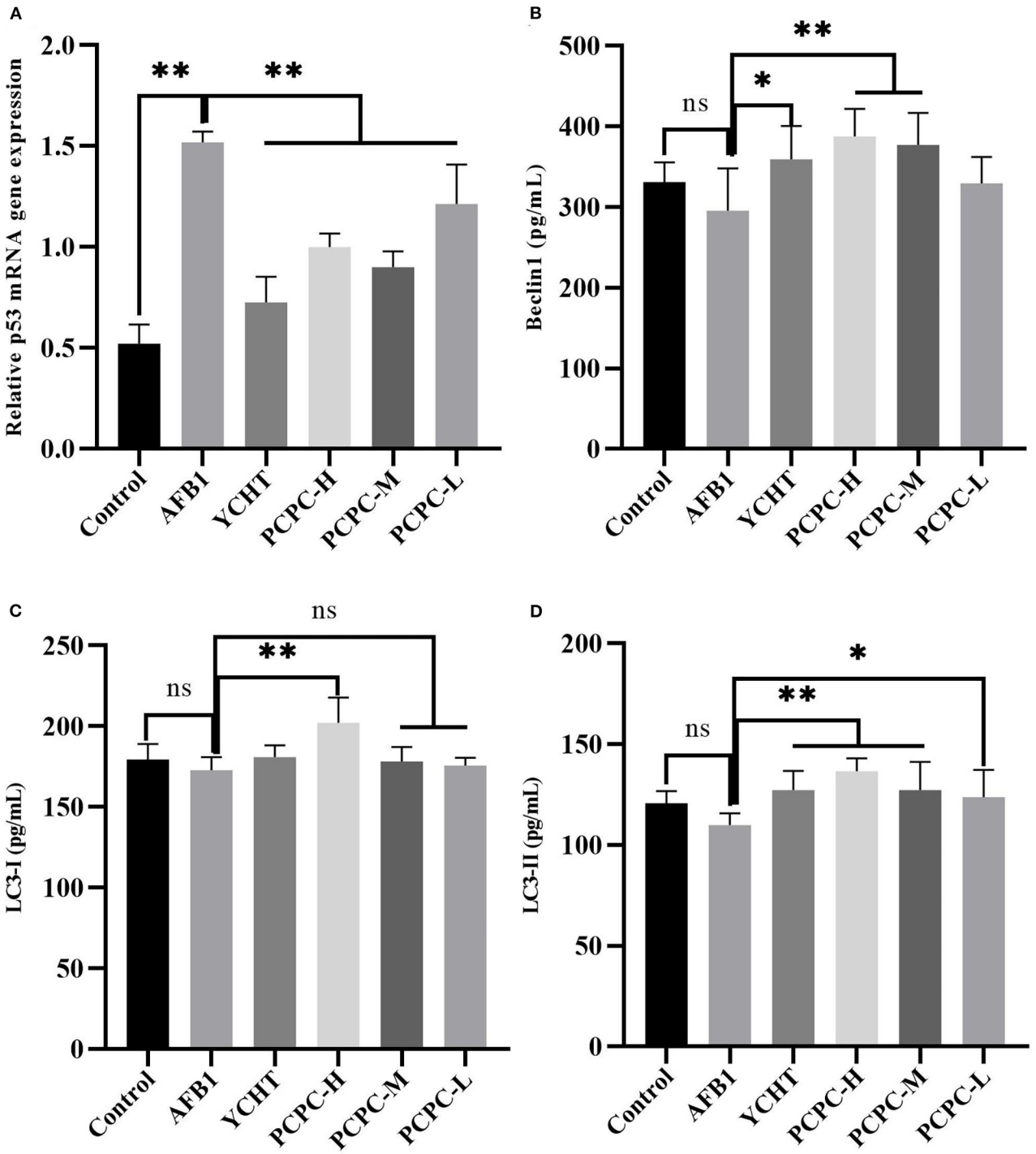


**FIGURE 7 |** Effect of PCPC and $AFB_1$ on autophagy-related genes (Beclin1, LC3-I and LC3-II, and p53) in kidneys. All data are expressed as mean ± SD. **(A)** p53; **(B)** Beclin1; **(C)** LC3-I; **(D)** LC3-II. Asterisk indicates significant difference ($p < 0.05$) compared to the control and AFB1 group. *$p < 0.05$ and **$p < 0.01$, ns, non-significant.

revealed that AFB1 can induce oxidative stress in the kidneys of broilers (26).

NRF2 functions as a regulator of the intracellular redox state, and it directly regulates the antioxidant defense system via various mechanisms (42). HMOX1, an important downstream antioxidant enzyme in the NRF2 signaling pathway, has the ability to enhance antioxidant activity (43, 44). In this study, we investigated the mechanism by which AFB1 induces oxidative

stress by measuring the mRNA expression levels of *NRF2* and *HMOX1* in the NRF2 signaling pathway. The findings revealed that *NRF2* and *HMOX1* were downregulated in the kidney tissues of the AFB1-treated group, and PCPC treatment upregulated these genes and regulated the NRF2 signaling pathway to protect the kidney from oxidative stress, thereby treating kidney damage caused by AFB1 (45).

Apoptosis involves programmed cell death that can effectively remove damaged cells and is essential for animal development (46, 47). However, excessive apoptosis can cause organ damage and is considered to be one of the mechanisms of AFB1-induced toxicity (48–50). Apoptosis may occur via two different apoptotic pathways, the extrinsic and intrinsic apoptotic pathways, which are triggered by internal mitochondria-mediated signal transduction or external receptor-dependent stimuli (46, 51). Mitochondria are essential organelles required for maintaining the viability of eukaryotic cells, and the role of mitochondria in apoptosis has been established (52, 53). The tumor suppressor P53 interacts with members of the BCL2 family present on the mitochondrial outer membrane; P53 can bind to BAK and catalyze BAK activation, and promote transcription-independent activation of BAX. Subsequently, the activated BAK and BAX oligomerize in the mitochondrial outer membrane to induce permeabilization. Proapoptotic factors (such as CYC) are released from the mitochondria into the cytosol to activate the caspase cascade via this pathway (54, 55). Therefore, internal mitochondria-mediated signal transduction activates caspase-9 and leads to the activation of caspase-3 to promote apoptosis. In contrast, BCL2 inhibits the activation of BAX and BAK, thus inhibiting apoptosis (56). In our study, we mainly explored the effect of AFB1 and PCPC on the mitochondria-mediated apoptosis pathway. AFB1 inhibited the transcription of *BCL2* in the kidney tissues of broilers and promoted the transcription of *P53*, *BAX*, *BAK1*, *CYC*, *CASP9*, and *CASP3*, and induced kidney cell apoptosis via the mitochondrial pathway. These findings indicate that AFB1 may activate the mitochondria-mediated apoptosis pathway (57). However, PCPC treatment inhibited the overexpression of P53, BAX, BAK, CYC, CASP9, and CASP3 induced by AFB1, whereas upregulation of BCL2 was observed. Therefore, PCPC treatment protected kidney cells from excessive apoptosis by inhibiting the mitochondrial apoptosis pathway activated by AFB1.

Autophagy is a highly conserved catabolic process that maintains homeostasis under adverse conditions (58, 59). It is generally agreed that autophagy is closely related to apoptosis, and induction of autophagy increases the threshold for cell death and inhibits apoptosis to reduce cytotoxicity (60). Unc-51-like autophagy activating kinase 1 (ULK1) and class III phosphatidylinositol 3-kinase complex I (PI3KC3-C1) are important proteins that initiate autophagy (61). Beclin1 is a part of PI3KC3-C1 and mediates the formation of a phagophore and functions as an autophagy initiation factor via interaction with PtdIns(3)-kinase (62). In the dynamic process of autophagosome formation, ubiquitin-like enzymatic cascades function after ULK1 and PI3KC3-C1 activity; thus, cytosolic LC3-I conjugates to phosphatidyl ethanol amine to form the autophagic marker LC3 (63). In this study, the expression levels of autophagy-associated genes were decreased in the AFB1 group, thereby inhibiting autophagy. Our findings showed that mitochondrial function damage and autophagy-related indicators were related to chicken kidney damage, oxidative injury, and pathogenesis induced by AFB1.

## CONCLUSION

The addition of PCPC to an AFB1-contaminated diet had a positive effect on growth and performance and reduced AFB1 pathogenesis and degenerative changes in the kidneys; PCPC treatment activated autophagy and regulated abnormal kidney function and the imbalance in mitochondrial dynamics. Therefore, PCPC effectively prevented oxidative stress and apoptosis in infected broiler chickens supplemented with AFB1. PCPC represents a natural and safe agent for treating avian mycotoxin-mediated toxicity.

## DATA AVAILABILITY STATEMENT

The original contributions presented in the study are included in the article/supplementary files, further inquiries can be directed to the corresponding author/s.

## ETHICS STATEMENT

The experimental protocols were performed in accordance with animal ethics guidelines and reviewed and approved by the Institutional Animal Care and Use Committee (IACUC) of Southwest University (IACUC-20201203).

## AUTHOR CONTRIBUTIONS

WT, FN, and JL conception and designed of the study. WT and JL analyzed and interpretation for the data. WT, ZL, YH, and ZH performed the experiment. WT and FN wrote the first draft of manuscript. All authors contributed to manuscript revision and read and approved the submitted version.

## FUNDING

This research was funded by Special Project for Fundamental Work of Science and Technology; Grant No. 2013FY110600-03 and special funding for Chongqing Post-Doctoral Research project 2020 number 7820100603.

## ACKNOWLEDGMENTS

The authors thank the Special Project for Fundamental Work of Science and Technology (No. 2013FY110600-03) and special funding for Chongqing Post-Doctoral Research project 2020 number 7820100603 for supporting this study.

## REFERENCES


1. Cheng L, Qin Y, Hu X, Ren L, Zhang C, Wang X, et al. Melatonin protects *in vitro* matured porcine oocytes from toxicity of aflatoxin B1. *J Pineal Res.* (2019) 66:e12543. doi: 10.1111/jpi.12543
2. Rushing BR, Selim MI. Aflatoxin B1: A review on metabolism, toxicity, occurrence in food, occupational exposure, and detoxification methods. *Food Chem Toxicol.* (2019) 124:81–100. doi: 10.1016/j.fct.2018.11.047
3. Galarza-Seeber R, Latorre JD, Bielke LR, Kuttappan VA, Wolfenden AD, Hernandez-Velasco X, et al. Leaky gut and mycotoxins: aflatoxin B1 does not increase gut permeability in broiler chickens. *Front Vet Sci.* (2016) 3:10. doi: 10.3389/fvets.2016.00010
4. Taranu I, Hermenean A, Bulgaru C, Pistol GC, Ciceu A, Grosu IA, et al. Diet containing grape seed meal by-product counteracts AFB1 toxicity in liver of pig after weaning. *Ecotoxicol Environ Saf.* (2020) 203:110899. doi: 10.1016/j.ecoenv.2020.110899
5. Abdel-Daim MM, Abdeen A, Jalouli M, Abdelkader A, Megahed A, Alkahtane A, et al. Fucoidan supplementation modulates hepato-renal oxidative stress and DNA damage induced by aflatoxin B1 intoxication in rats. *Sci Total Environ.* (2021) 768:144781. doi: 10.1016/j.scitotenv.2020.144781
6. Hussain Z, Khan MZ, Khan A, Javed I, Saleemi MK, Mahmood S, et al. Residues of aflatoxin B1 in broiler meat: effect of age and dietary aflatoxin B1 levels. *Food Chem Toxicol.* (2010) 48:3304–7. doi: 10.1016/j.fct.2010.08.016
7. Boyden LM, Choi M, Choate KA, Nelson-Williams CJ, Farhi A, Toka HR, et al. Mutations in kelch-like 3 and cullin 3 cause hypertension and electrolyte abnormalities. *Nature.* (2012) 482:98–102. doi: 10.1038/nature10814
8. Levey AS, Becker C, Inker LA. Glomerular filtration rate and albuminuria for detection and staging of acute and chronic kidney disease in adults: a systematic review. *JAMA.* (2015) 313:837–46. doi: 10.1001/jama.2015.0602
9. Park J, Shrestha R, Qiu C, Kondo A, Huang S, Werth M, et al. Single-cell transcriptomics of the mouse kidney reveals potential cellular targets of kidney disease. *Science.* (2018) 360:758–63. doi: 10.1126/science.aar2131
10. Poston JT, Koyner JL. Sepsis associated acute kidney injury. *BMJ.* (2019) 364:k4891. doi: 10.1136/bmj.k4891
11. Long XD, Yao JG, Zeng Z, Ma Y, Huang XY, Wei ZH, et al. Polymorphisms in the coding region of X-ray repair complementing group 4 and aflatoxin B1-related hepatocellular carcinoma. *Hepatology.* (2013) 58:171–81. doi: 10.1002/hep.26311
12. Li S, Muhammad I, Yu H, Sun X, Zhang X. Detection of Aflatoxin adducts as potential markers and the role of curcumin in alleviating AFB1-induced liver damage in chickens. *Ecotoxicol Environ Saf.* (2019) 176:137–45. doi: 10.1016/j.ecoenv.2019.03.089
13. Cui X, Muhammad I, Li R, Jin H, Guo Z, Yang Y, et al. Development of a UPLC-FLD method for detection of aflatoxin B1 and M1 in animal tissue to study the effect of curcumin on mycotoxin clearance rates. *Front Pharmacol.* (2017) 8:650. doi: 10.3389/fphar.2017.00650
14. Xu F, Wang P, Yao Q, Shao B, Yu H, Yu K, et al. Lycopene alleviates AFB(1)-induced immunosuppression by inhibiting oxidative stress and apoptosis in the spleen of mice. *Food Funct.* (2019) 10:3868–79. doi: 10.1039/c8fo02300j
15. Nagata S, Tanaka M. Programmed cell death and the immune system. *Nat Rev Immunol.* (2017) 17:333–40. doi: 10.1038/nri.2016.153
16. Li H, Li S, Yang H, Wang Y, Wang J, Zheng N. l-Proline alleviates kidney injury caused by AFB1 and AFM1 through regulating excessive apoptosis of kidney cells. *Toxins.* (2019) 11:226. doi: 10.3390/toxins11040226
17. Galluzzi L, Bravo-San Pedro JM, Levine B, Green DR, Kroemer G. Pharmacological modulation of autophagy: therapeutic potential and persisting obstacles. *Nat Rev Drug Discov.* (2017) 16:487–511. doi: 10.1038/nrd.2017.22
18. Lu Q, Jiang MH, Jiang JG, Zhang RF, Zhang MW. Isolation and identification of compounds from *Penthorum chinense* Pursh with antioxidant and antihepatocarcinoma properties. *J Agric Food Chem.* (2012) 60:11097–103. doi: 10.1021/jf303755w
19. Saeed M, Babazadeh D, Arif M, Arain M, Bhutto Z, Shar A, et al. Silymarin: a potent hepatoprotective agent in poultry industry. *Worlds Poul Sci J.* (2017) 73:483–92. doi: 10.1017/S0043933917000538
20. Saeed M, Babazadeh D, Naveed M, Arain MA, Hassan FU, Chao S. Reconsidering betaine as a natural anti-heat stress agent in poultry industry: a review. *Trop Anim Health Prod.* (2017) 49:1329–38. doi: 10.1007/s11250-017-1355-z
21. Arain MA, Mei Z, Hassan F, Saeed M, Alagawany M, Shar A, et al. Lycopene: a natural antioxidant for prevention of heat-induced oxidative stress in poultry. *Worlds Poul Sci J.* (2018) 74:89–100. doi: 10.1017/S0043933917001040
22. Han Y, Sun H, Zhang A, Yan G, Wang X-J. Chinmedomics, a new strategy for evaluating the therapeutic efficacy of herbal medicines. *Pharmacol Therap.* (2020) 216:107680. doi: 10.1016/j.pharmthera.2020.107680
23. Tian X, Liu H, Qiao S, Yin H, Chen M, Hu P, et al. Exploration of the hepatoprotective chemical base of an orally administered herbal formulation (YCHT) in normal and CCl4-intoxicated liver injury rats. Part 2: hepatic disposition *in vivo* and hepatoprotective activity *in vitro*. *J Ethnopharmacol.* (2019) 236:161–72. doi: 10.1016/j.jep.2019.02.022
24. Livak KJ, Schmittgen TD. Analysis of relative gene expression data using real-time quantitative PCR and the 2(-Delta Delta C(T)) method. *Methods.* (2001) 25:402–8. doi: 10.1006/meth.2001.1262
25. Nabi F, Shahzad M, Liu J, Li K, Han Z, Zhang D, et al. Hsp90 inhibitor celastrol reinstates growth plate angiogenesis in thiram-induced tibial dyschondroplasia. *Avian Pathol.* (2016) 45:187–93. doi: 10.1080/03079457.2016.1141170
26. Ali Rajput S, Sun L, Zhang N, Mohamed Khalil M, Gao X, Ling Z, et al. Ameliorative effects of grape seed proanthocyanidin extract on growth performance, immune function, antioxidant capacity, biochemical constituents, liver histopathology and aflatoxin residues in broilers exposed to aflatoxin B1. *Toxins.* (2017) 9:371. doi: 10.3390/toxins9110371
27. Wang Q, Zhang Y, Zheng N, Guo L, Song X, Zhao S, et al. Biological system responses of dairy cows to aflatoxin B1 exposure revealed with metabolomic changes in multiple biofluids. *Toxins.* (2019) 11:77. doi: 10.3390/toxins11020077
28. Slizewska K, Cukrowska B, Smulikowska S, Cielecka-Kuszyk J. The effect of probiotic supplementation on performance and the histopathological changes in liver and kidneys in broiler chickens fed diets with aflatoxin B1*Toxins.* (2019) 11:112. doi: 10.3390/toxins11020112
29. Wang XH, Li W, Wang XH, Han MY, Muhammad I, Zhang XY, et al. Water-soluble substances of wheat: a potential preventer of aflatoxin B1-induced liver damage in broilers. *Poult Sci.* (2019) 98:136–49. doi: 10.3382/ps/pey358
30. Corcuera LA, Vettorazzi A, Arbillaga L, González-Peñas E, López de Cerain A. An approach to the toxicity and toxicokinetics of aflatoxin B1 and ochratoxin A after simultaneous oral administration to fasted F344 rats. *Food Chem Toxicol.* (2012) 50:3440–6. doi: 10.1016/j.fct.2012.06.048
31. Chen Y, Li C, Duan S, Yuan X, Liang J, Hou S. Curcumin attenuates potassium oxonate-induced hyperuricemia and kidney inflammation in mice. *Biomed Pharmacother.* (2019) 118:109195. doi: 10.1016/j.biopha.2019.109195
32. Vaijayanthimala V, Cheng PY, Yeh SH, Liu KK, Hsiao CH, Chao JI, et al. The long-term stability and biocompatibility of fluorescent nanodiamond as an *in vivo* contrast agent. *Biomaterials.* (2012) 33:7794–802. doi: 10.1016/j.biomaterials.2012.06.084
33. Vallon V, Thomson SC. The tubular hypothesis of nephron filtration and diabetic kidney disease. *Nat Rev Nephrol.* (2020) 16:317–36. doi: 10.1038/s41581-020-0256-y
34. Naylor RW, Morais M, Lennon R. Complexities of the glomerular basement membrane. *Nat Rev Nephrol.* (2021) 17:112–27. doi: 10.1038/s41581-020-0329-y
35. Rinschen MM, Limbutara K, Knepper MA, Payne DM, Pisitkun T. From molecules to mechanisms: functional proteomics and its application to renal tubule physiology. *Physiol Rev.* (2018) 98:2571–606. doi: 10.1152/physrev.00057.2017
36. Singh A, Kukreti R, Saso L, Kukreti S. Oxidative stress: role and response of short guanine tracts at genomic locations. *Int J Mol Sci.* (2019) 20:4258. doi: 10.3390/ijms20174258
37. Tamma G, Valenti G. Evaluating the oxidative stress in renal diseases: what is the role for S-glutathionylation? *Antioxid Redox Signal.* (2016) 25:147–64. doi: 10.1089/ars.2016.6656
38. Kanbur M, Eraslan G, Sarica ZS, Aslan O. The effects of evening primrose oil on lipid peroxidation induced by subacute aflatoxin exposure in mice. *Food Chem Toxicol.* (2011) 49:1960–4. doi: 10.1016/j.fct.2011.05.006

39. Miao L, St Clair DK. Regulation of superoxide dismutase genes: implications in disease. *Free Radic Biol Med.* (2009) 47:344–56. doi: 10.1016/j.freeradbiomed.2009.05.018
40. Ayala A, Muñoz MF, Argüelles S. Lipid peroxidation: production, metabolism, and signaling mechanisms of malondialdehyde and 4-hydroxy-2-nonenal. *Oxid Med Cell Longev.* (2014) 2014:360438. doi: 10.1155/2014/360438
41. Sun X, Wu A, Kwan Law BY, Liu C, Zeng W, Ling Qiu AC, et al. The active components derived from *Penthorum chinense* Pursh protect against oxidative-stress-induced vascular injury via autophagy induction. *Free Radic Biol Med.* (2020) 146:160–80. doi: 10.1016/j.freeradbiomed.2019.10.417
42. Hybertson BM, Gao B, Bose SK, McCord JM. Oxidative stress in health and disease: the therapeutic potential of Nrf2 activation. *Mol Aspects Med.* (2011) 32:234–46. doi: 10.1016/j.mam.2011.10.006
43. Liang L, Gao C, Luo M, Wang W, Zhao C, Zu Y, et al. Dihydroquercetin (DHQ) induced HO-1 and NQO1 expression against oxidative stress through the Nrf2-dependent antioxidant pathway. *J Agric Food Chem.* (2013) 61:2755–61. doi: 10.1021/jf304768p
44. Sun Y, Wu Y, Wang Z, Chen J, Yang Y, Dong G. Dandelion extract alleviated lipopolysaccharide-induced oxidative stress through the Nrf2 pathway in bovine mammary epithelial cells. *Toxins.* (2020) 12:496. doi: 10.3390/toxins12080496
45. Noel S, Hamad AR, Rabb H. Reviving the promise of transcription factor Nrf2-based therapeutics for kidney diseases. *Kidney Int.* (2015) 88:1217–8. doi: 10.1038/ki.2015.328
46. Cheng X, Ferrell JEJr. Apoptosis propagates through the cytoplasm as trigger waves. *Science.* (2018) 361:607–12. doi: 10.1126/science.aah4065
47. Nagata S. Apoptosis and clearance of apoptotic cells. *Annu Rev Immunol.* (2018) 36:489–517. doi: 10.1146/annurev-immunol-042617-053010
48. Chen Y, Feng X, Hu X, Sha J, Li B, Zhang H, et al. Dexmedetomidine ameliorates acute stress-induced kidney injury by attenuating oxidative stress and apoptosis through inhibition of the ROS/JNK signaling pathway. *Oxid Med Cell Longev.* (2018) 2018:4035310. doi: 10.1155/2018/4035310
49. Zhu L, Huang C, Yang X, Zhang B, He X, Xu W, et al. Proteomics reveals the alleviation of zinc towards aflatoxin B1-induced cytotoxicity in human hepatocyes (HepG2 cells). *Ecotoxicol Environ Saf.* (2020) 198:110596. doi: 10.1016/j.ecoenv.2020.110596
50. Frenette C, Kayali Z, Mena E, Mantry PS, Lucas KJ, Neff G, et al. Emricasan to prevent new decompensation in patients with NASH-related decompensated cirrhosis. *J Hepatol.* (2021) 74:274–82. doi: 10.1016/j.jhep.2020.09.029
51. Zhu S, Liu Y, Li Y, Yi J, Yang B, Li Y, et al. The potential risks of herbicide butachlor to immunotoxicity via induction of autophagy and apoptosis in the spleen. *Chemosphere.* (2022) 286:131683. doi: 10.1016/j.chemosphere.2021.131683
52. Pfanner N, Warscheid B, Wiedemann N. Mitochondrial proteins: from biogenesis to functional networks. *Nat Rev Mol Cell Biol.* (2019) 20:267–84. doi: 10.1038/s41580-018-0092-0
53. Abate M, Festa A, Falco M, Lombardi A, Luce A, Grimaldi A, et al. Mitochondria as playmakers of apoptosis, autophagy and senescence. *Semin Cell Dev Biol.* (2020) 98:139–53. doi: 10.1016/j.semcdb.2019.05.022
54. Estaquier J, Vallette F, Vayssiere JL, Mignotte B. The mitochondrial pathways of apoptosis. *Adv Exp Med Biol.* (2012) 942:157–83. doi: 10.1007/978-94-007-2869-1_7
55. Bock FJ, Tait SWG. Mitochondria as multifaceted regulators of cell death. *Nat Rev Mol Cell Biol.* (2020) 21:85–100. doi: 10.1038/s41580-019-0173-8
56. Ouyang Z, Yang B, Yi J, Zhu S, Lu S, Liu Y, et al. Exposure to Fluoride induces apoptosis in liver of ducks by regulating Cyt-C/Caspase 3/9 signaling pathway. *Ecotoxicol Environ Saf.* (2021) 224:112662. doi: 10.1016/j.ecoenv.2021.112662
57. Rajput SA, Zhang C, Feng Y, Wei XT, Khalil MM, Rajput IR, et al. Proanthocyanidins alleviates aflatoxin B1-induced oxidative stress and apoptosis through mitochondrial pathway in the bursa of fabricius of broilers. *Toxins.* (2019) 11:157. doi: 10.3390/toxins11030157
58. Dikic I, Elazar Z. Mechanism and medical implications of mammalian autophagy. *Nat Rev Mol Cell Biol.* (2018) 19:349–64. doi: 10.1038/s41580-018-0003-4
59. Wang Y, Li A, Mehmood K, Hussain R, Abbas RZ, Javed MT, et al. Long-term exposure to the fluoride blocks the development of chondrocytes in the ducks: the molecular mechanism of fluoride regulating autophagy and apoptosis. *Ecotoxicol Environ Saf.* (2021) 217:112225. doi: 10.1016/j.ecoenv.2021.112225
60. Maiuri MC, Zalckvar E, Kimchi A, Kroemer G. Self-eating and self-killing: crosstalk between autophagy and apoptosis. *Nat Rev Mol Cell Biol.* (2007) 8:741–52. doi: 10.1038/nrm2239
61. Hurley JH, Young LN. Mechanisms of autophagy initiation. *Annu Rev Biochem.* (2017) 86:225–44. doi: 10.1146/annurev-biochem-061516-044820
62. Sun Y, Cai Y, Zang QS. Cardiac autophagy in sepsis. *Cells.* (2019) 8:141. doi: 10.3390/cells8020141
63. Brier LW, Ge L, Stjepanovic G, Thelen AM, Hurley JH, Schekman R. Regulation of LC3 lipidation by the autophagy-specific class III phosphatidylinositol-3 kinase complex. *Mol Biol Cell.* (2019) 30:1098–107. doi: 10.1091/mbc.E18-11-0743


**Conflict of Interest:** The authors declare that the research was conducted in the absence of any commercial or financial relationships that could be construed as a potential conflict of interest.

The handling editor declared a past co-authorship with one of the authors, FN.

**Publisher's Note:** All claims expressed in this article are solely those of the authors and do not necessarily represent those of their affiliated organizations, or those of the publisher, the editors and the reviewers. Any product that may be evaluated in this article, or claim that may be made by its manufacturer, is not guaranteed or endorsed by the publisher.

frontiers in Veterinary Science

ORIGINAL RESEARCH
published: 26 October 2021
doi: 10.3389/fvets.2021.765623

# Severe Inhibition of Long-Chain Acyl-CoA Enoylhydratase (EC 4.2.1.74) in a Newborn Foal Suffering From Atypical Myopathy

*Johannes Sander*[1,2]*, *Michael Terhardt*[1] *and Nils Janzen*[1,2]

[1] Screening-Labor Hannover, Hanover, Germany, [2] Hanover Medical School, Hanover, Germany

In horses, congenital defects of energy production from long-chain fatty acids have not been described so far. In contrast, inhibition of fatty acid degradation caused by the toxins hypoglycin A and methylenecyclopropylglycine from various maple species are observed frequently. These non-proteinogenic aminoacids are passed on placentally to fetuses or with collostrum or milk to newborn foals. Nevertheless, newborn foals become very rarely symptomatic. Vertical transmission apparently is not sufficient to induce clinical disease without a particular genetic constellation being present. One of these rare cases was investigated here using samples from a mare and her foal. Intoxication by hypoglycin A and methylenecyclopropylglycine is also of interest to human pathology, because these toxins have caused fatal poisonings after consumption of certain fruits many times, especially in children. Maple toxins, their metabolites and some short-chain acyl compounds were quantified by ultrahigh-pressure liquid chromatography/tandem mass spectrometry. An comprehensive spectrum of long-chain acylcarnitines was prepared using electrospray ionization tandem mass spectrometry. Organic acids and acylglycines were determined by gas chromatography mass spectrometry. For evaluation, results of other horses poisoned by maple material as well as unaffected control animals were used. In the serum of the foal, hypoglycin A was detected at a low concentration only. Toxin metabolites reached <3.5% of the mean of a comparison group of horses suffering from atypical myopathy. The spectrum of acylcarnitines indicated enzyme inhibition in short-chain and medium-chain regions typical of acer poisoning, but the measured concentrations did not exceed those previously found in clinically healthy animals after maple consumption. The values were not sufficient to explain the clinical symptoms. In contrast, a remarkably strong enrichment of tetradecenoylcarnitine and hexadecenoylcarnitine was observed. This proves a blockade of the long-chain enoyl-CoA hydratase (EC 4.2.1.74). Vertical transfer of maple toxins to a newborn foal is sufficient for induction of clinical disease only if there is an additional specific reactivity to the active toxins. This was found here in an inhibition of long-chain enoyl-CoA hydratase. Isolated dysfunction of this enzyme has not yet been reported in any species. Further studies are necessary to prove a specific genetic defect.

**Keywords: long-chain enoyl-CoA hydratase (EC 4.2.1.74), vertical toxin transmission, hypoglycin A (HGA), methylenecyclopropylglycine (MCPG), atypical myopathy, newborn foal**

OPEN ACCESS

***Edited by:***
*Hui Zhang,*
*South China Agricultural University, China*

***Reviewed by:***
*Houqiang Luo,*
*Wenzhou Vocational College of Science and Technology, China*
*Qingyue Han,*
*South China Agricultural University, China*

***Correspondence:**
*Johannes Sander*
*j.sander@metabscreen.de*
*orcid.org/0000-0003-1645-8967*

***Specialty section:***
*This article was submitted to Animal Nutrition and Metabolism, a section of the journal Frontiers in Veterinary Science*

***Received:*** *27 August 2021*
***Accepted:*** *27 September 2021*
***Published:*** *26 October 2021*

***Citation:***
*Sander J, Terhardt M and Janzen N (2021) Severe Inhibition of Long-Chain Acyl-CoA Enoylhydratase (EC 4.2.1.74) in a Newborn Foal Suffering From Atypical Myopathy. Front. Vet. Sci. 8:765623. doi: 10.3389/fvets.2021.765623*

## INTRODUCTION

Several thousands of severe, often letal cases of atypical myopathy (AM) caused by the ingestion of seeds and seedlings of some *Acer* species have been observed in horses and other equids, occurring in all age groups from the very young to the very old animals [for review see Votion et al. (1)]. Hypoglycin A (HGA) and methylenecyclopropylglycine (MCPG) are the constituents responsible for this. Newborn foals, however, that do not yet consume green forage themselves and therefore can receive *Acer* toxins prenatally only via the placenta or postnatally with the milk are apparently very rarely affected by AM.

MCPA-CoA and MCPF-CoA, the active toxins formed from HGA and MCPG, are known to interrupt the energy production from fatty acids and certain amino acids. They inhibit mitochondrial acyl-CoA dehydrogenases and enoyl-CoA hydratases involved in the ß-oxidation of fatty acids (2–4). In view of the high postpartum requirement for products of the ß-oxidation of fatty acids and amino acid catabolism, one might assume that newborn foals are particularly vulnerable to maple toxins. However, so far, only one case of AM in a foal has been described in the literature (5).

The maple toxins HGA and MCPG have the structure of amino acids. Thus, they can pass through the placenta and enter the fetus like other amino acids. They are also secreted into the milk (6–8). Transplacental transport and secretion of amino acids into the milk, on the other hand are not primarily achieved by passive diffusion but are the results of active transport. And, in order to trigger toxic effects, HGA, and MCPG must be converted into the active toxins in the foal's organism after vertical transfer.

Based on the above facts, it must be assumed that placental passage of the toxins into the fetal circulation as well as secretion into the milk are limited. Concentrations sufficient to affect metabolism will therefore not be reached frequently. Furthermore, there is the possibility that the activity of the enzymes necessary for metabolizing maple toxins to MCPA-CoA and MCPF-CoA, cytosolic aminotransferase, and mitochondrial branched-chain dehydrogenase, is comparatively low in the tissues at the end of the fetal period or in the early neonatal period. This would mean that only a small proportion of the toxic amino acids entering the newborn foal's organism would be converted into active toxins.

On the basis of these considerations, we hypothesize that the low concentrations of active maple toxins to be expected in a foal fed with collostrum or milk will only lead to acute disease if there is a special, possibly genetically determined sensitivity.

Test material received by our laboratory from a mare/foal pair suffering from AM allowed us to investigate some aspects of this hypothesis and to draw tentative conclusions.

**Abbreviations:** AM, atypical myopathy; ECH, enoyl-CoA hydratase; Fi-MS/MS, flow injection-tandem mass spectrometry; HGA, hypoglycin A; MCPA, methylenecyclopropyl acetic acid; MCPF, methylenecyclopropyl formic acid; UPLC-MS/MS, ultra high pressure liquid chromatography-tandem mass spectrometry.

## MATERIALS AND METHODS

### Anamnestic Details

A male foal weighing 50 kg had been nursed by his dam (Iceland pony, 5 years old) until the 7th day of life in a pasture in the neighborhood of *Acer pseudoplatanus*. When depression, insecure gait, weakness, and finally recumbency were detected in the foal on the 7th day postpartum, in view of the fact that cases of AM had already been confirmed in this pasture, the owner expressed the suspicion that it could be AM. Dam and foal were seen by a veterinarian at the 8th day postpartum. At this time, the dam was described as being weak and stiff but she did not appear to be in acute distress. The foal on the other hand was moribund. Enzyme activities in serum were 45,305 U/L for creatine kinase (CK) in the foal and 19,515 U/L in the dam (ref. <200). Lactate dehydrogenase (LDH) activity in the serum was 2,254 U/L for the foal and 12,833 U/L for the dam (ref. <250). Levels of aspartate aminotransferase (AST) activity in the serum were also greatly elevated (foal 2,656 U/L, dam 16,999 U/L, ref. < 50). High concentrations of myoglobin were detected in the urine of the foal (3,990 μg/L) and the dam (1,060 μg/L, ref. <25). The results obtained are compatible with the diagnosis of AM.

The dam recovered within 3 days on a maple free diet of hay and oats. The foal was euthanized because of the severity of symptoms and obviously poor chance of survival. The veterinarian collected samples for diagnostic purposes and requested the toxicological analyses described below.

### Materials and Data Available

- Foal: Serum, collected before euthanasia on the 8th day postpartum, urine collected immediately after death
- Dam: Serum and urine, collected on the 8th day postpartum
- Data for comparison were available from the diagnostic workup of our laboratory of 34 AM positive horses and 19 negative controls.

Data of all the horses were used for scientific purposes with owner-informed consent.

### Ultrahigh-Performance Liquid Chromatography/Tandem Mass Spectrometry (UPLC-MS/MS)

The quantification of HGA and MCPG plus their metabolites in serum and urine was carried out by UPLC-MS/MS as described in detail earlier (9–12). For all analyses, 25 μL of material were extracted with 300 μL of methanol containing the internal standards. Analysis was performed after butylation. For chromatographic separation 5 μL of the final extracts were injected onto an Acquity UPLC BEH C18 1.7 μm, 2.1 × 50 mm column (Waters). Gradient chromatography was performed using acetonitrile/water modified by 0.1% formic acid and 0.01% trifluoroacetic acid. Quantifications were done on a Xevo TQMS UPLC-MS/MS system (Waters, Eschborn, Germany), calculation of concentrations was conducted with single-point calibration. Concentrations of C4 to C10 acyl conjugates were also determined by this method in order to differentiate branched and unbranched C4 and C5 metabolites. The isomers of 2-MBC

**TABLE 1 |** Hypoglycin A and toxin metabolites in serum and urine of the foal and his mare.

| | Serum | | | | Urine | | | |
|---|---|---|---|---|---|---|---|---|
| | Foal | | Mare | | Foal | | Mare | |
| | nmol/L | % of mean of 34 AM horses | nmol/L | % of mean of 34 AM horses | nmol/mmol creatinine | % mean of 14 AM horses | nmol/mmol creatinine | % mean of 14 AM horses |
| HGA | 438 | 24.3 | 813 | 45.3 | 68 | 125 | 4.4 | 8.1 |
| MCPA-G | 6.2 | 3.3 | 48.0 | 25.3 | 969 | 8.4 | 2,550 | 22.2 |
| MCPA-C | 2.8 | 3.2 | 8.2 | 9.5 | 20.5 | 3.0 | 3.4 | 0.5 |
| MCPF-G | 1.2 | 1.6 | 30.2 | 39.2 | 57.0 | 1.8 | 1,567 | 49.3 |
| MCPF-C | 14.5 | 1.2 | 122 | 10.3 | 110 | 1.0 | 194 | 1.8 |

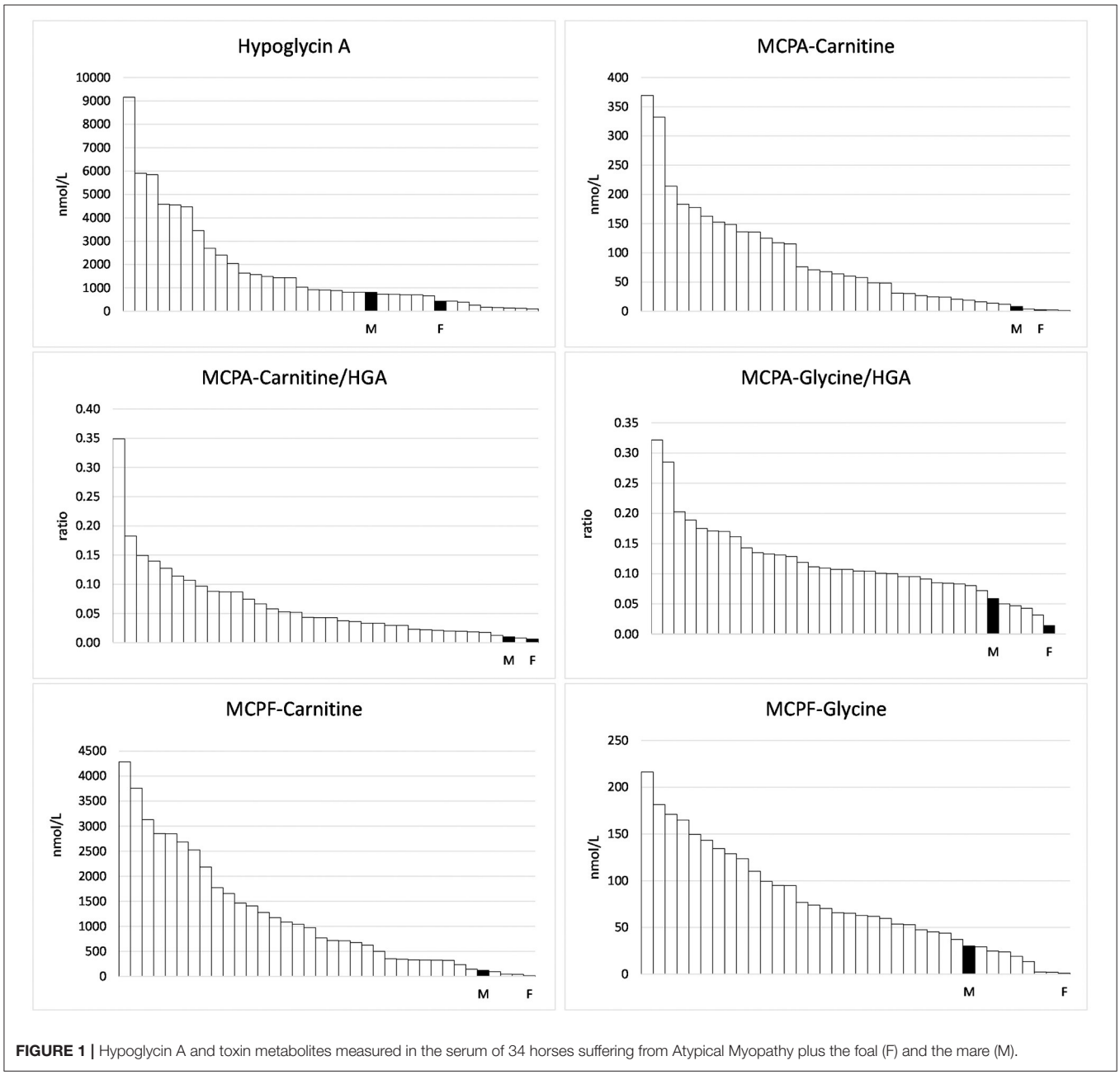


**FIGURE 1 |** Hypoglycin A and toxin metabolites measured in the serum of 34 horses suffering from Atypical Myopathy plus the foal (F) and the mare (M).

appeared in two separate peaks, the values of both isomers were added for quantification.

## Flow Injection-Tandem Mass Spectrometry (FI-MS/MS)

A comprehensive range of long-chain acylcarnitines (C12-C18) was quantified using a method originally developed for the study of infant blood (13, 14). This method has been adapted in our laboratory for the analysis of horse serum samples (15). For the study presented here, the serum was spotted onto filter paper (Ahlstrom-Munskjö, Germany). After air-drying, disks of 3.2 mm diameter were punched out (corresponding to 3.5 µl serum) and extracted with 100 µl methanol. After butylation with 50 µL HCl-butanol, drying and resolving the extracts were analyzed using flow injection tandem mass spectrometry without chromatographic separation. Analysis was done on a Waters TQD instrument (Waters, Eschborn, Germany) with an electrospray interface. The instrument was run in the ESI positive mode. Capillary voltage was 2.5 kV. Collision gas (argon) pressure was $2.4 \times 10^{-3}$ mbar. The analysis was done as parent scan, the long chain hydroxylated AC, however, were measured in positive MRM mode because of their very low intensities. MS/MS results were calculated using the Neolynx software 4.1 (Waters), quantifications were done by comparing peak height to the respective d3- carnitine derivatives (C12-C18).

## Gas Chromatography Mass Spectrometry (GC-MS)

Organic acids and acylglycines were measured as commissioned service by a commercial human medical laboratory (MVZ Dr. Eberhard & Partner, Dortmund, Germany) who established a spectrum using gas chromatography mass spectrometry as

**TABLE 2 |** Concentrations of acylcarnitines found in serum and urine of the foal and the mare.

| Acyl carnitines | Serum | | | | | Urine | | | | |
|---|---|---|---|---|---|---|---|---|---|---|
| | Foal | | Mare | | | Foal | | Mare | | |
| | µmol/L | % of mean of 34 AM horses | µmol/L | % of mean of 34 AM horses | Mean of 19 neg. controls | µmol/ mmol crea | % mean of 14 AM horses | µmol/ mmol crea | % of mean of 14 AM horses | Mean of 11 neg. controls |
| Butyryl | 23 | 40.4 | 4.9 | 8.5 | 0.98 | 82.9 | 31.4 | 4.1 | 1.6 | 0.65 |
| Hexanoyl | 3.3 | 45.4 | 2.0 | 27.3 | 0.24 | 3.6 | 6.2 | 0.41 | 0.70 | 0.04 |
| Octanoyl | 0.4 | 32.4 | 0.37 | 30.0 | 0.02 | 1.0 | 13.7 | 0.17 | 2.22 | 0.01 |
| Decenoyl | 0.09 | 11.8 | 0.14 | 18.3 | 0.01 | 0.79 | 11.4 | 0.07 | 0.99 | n.d. |
| Isobutyryl | 8.3 | 129 | 1.3 | 19.8 | 1.5 | 138 | 181 | 7.4 | 9.7 | 2.3 |
| Isovaleryl | 7.0 | 42.8 | 1.1 | 6.5 | 0.31 | 41.8 | 64.8 | 2.7 | 4.2 | 0.28 |
| Methylbutyryl | 4.3 | 31.6 | 1.3 | 9.6 | 0.31 | 47.8 | 58.7 | 6.9 | 8.5 | 0.37 |

**TABLE 3 |** Long-chain acylcarnitines, measured by flow-injection MS/MS.

| Acyl-Carnitines | 21 neg. controls | Foal | | Mare | |
|---|---|---|---|---|---|
| | Mean nmol/L | Level nmol/L | % of mean of 34 AM horses | Level nmol/L | % of mean of 34 AM horses |
| Dodecanoyl, C12 | 99.8 | 114 | 86.9 | 132 | 101 |
| Dodecenoyl, C12:1 | 15.7 | 75 | 93.5 | 14 | 175 |
| Myristoyl, C 14 | 27.6 | 52.8 | 103 | 30.4 | 59.6 |
| Hydroxymyristoyl, C14-OH | 4.7 | 2.8 | 17.0 | 5.8 | 35.2 |
| Tetradecenoyl C14:1 | 14.1 | 155 | 262 | 13 | 22.1 |
| Tertradecadienoyl C14:2 | 6.2 | 16 | 111 | 6.4 | 44.6 |
| Palmitoyl, C 16 | 43.3 | 61.9 | 33.5 | 42.4 | 22.9 |
| Hydroxypalmitoyl, C 16-OH | 3.6 | 4.3 | 23.0 | 4.9 | 26.1 |
| Palmitoleoy, C 16:1 | 17.7 | 103 | 133 | 12 | 15.4 |
| Hydroxypalmitoleyl, C 16:1-OH | 5.7 | 5.4 | 23.4 | 5.2 | 22.5 |
| Stearyl, C 18 | 24.0 | 34.8 | 49.5 | 23.7 | 33.8 |
| Hydroxy-octadecenoyl, C 18-OH | 4.4 | 11.3 | 164 | 9 | 130 |
| Oleoyl, C 18:1 | 37.1 | 68.5 | 42.0 | 31.7 | 19.4 |
| Hydroxyoleyl, C 18:1-OH | 4.4 | 6.9 | 41.3 | 6.4 | 38.3 |
| Linoleyl, C 18:2 | 10.2 | 7.3 | 19.3 | 11.5 | 30.4 |
| C 18:2-OH | 6.5 | 10 | 64.3 | 17 | 109 |

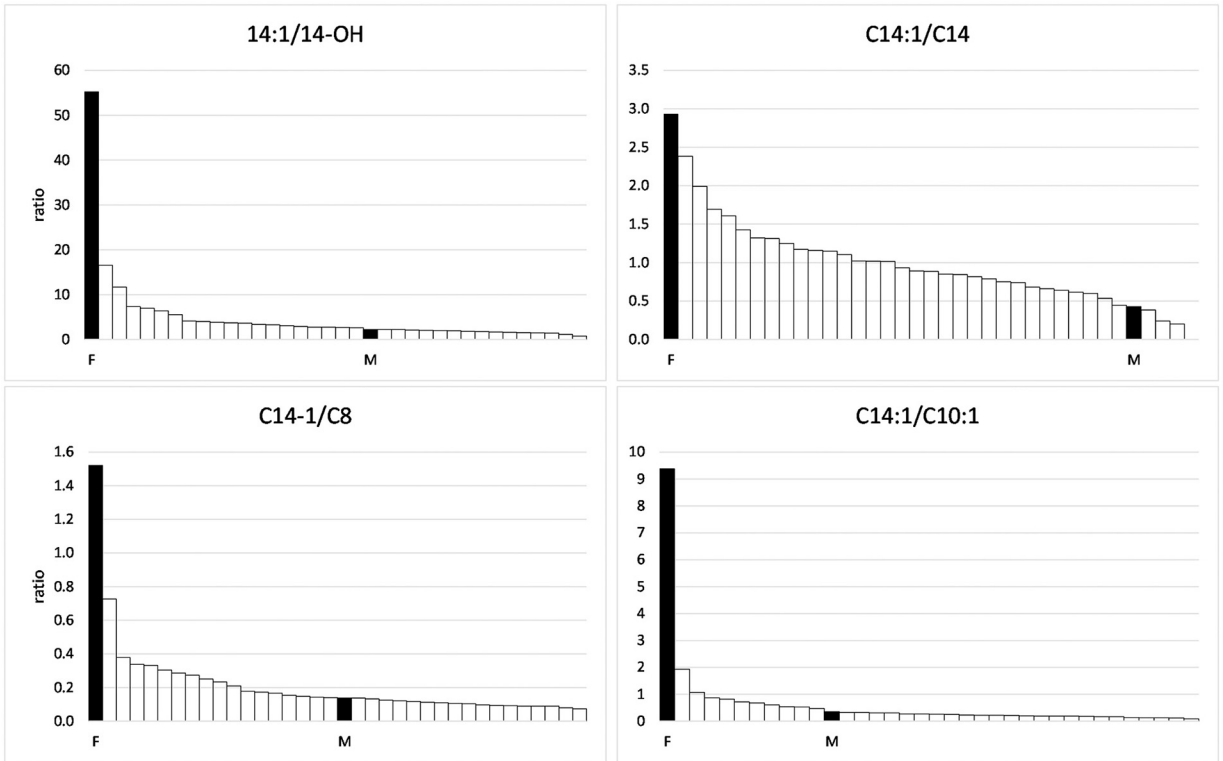


**FIGURE 2 |** Ratios of C14:1 to other acylcarnitines in the group of horses suffering from Atypical Myopathy including the foal (F) and the mare (M).

described by Hoffmann et al. (16). The methods are used there as quality-controlled routine diagnostic procedures in human medicine.

# RESULTS

## Toxins and Toxin Metabolites

Concentrations of HGA and toxin metabolites are shown in **Table 1**. In the serum of the foal, HGA, not present in body fluids of unaffected horses, reached only 53.3% of the level of the mare. However, the foal excreted unmetabolized HGA to a considerably higher extent than the mare. With 68 nmol HGA/mmol creatinine, the foal reached 125% of the mean of positive controls. Non-metabolized MCPG, which we had confirmed in other cases of maple poisoning of horses (17) was not detected in quantifiable concentrations. In serum, the metabolites MCPA-glycine and MCPA-carnitine derived from HGA as well as MCPF-carnitine and -glycine derived from MCPG, not detectable in unaffected horses, reached only a few percent of the mean of the group. This is clearly visible in **Figure 1**. The low levels corresponded to a very low excretion of toxin metabolites as compared to other AM horses (**Table 1**).

## Medium-Chain Acyl Carnitines in Serum and Urine

A high accumulation in the serum of the mare and the foal of butyrylcarnitine, a derivative of butyryl-CoA, which is metabolized by both medium-chain acyl-CoA dehydrogenase (MCAD, OMIM 607008) and short-chain acyl-CoA dehydrogenase (SCAD, OMIM 606885) was found (**Table 2**). The high concentrations indicate a pronounced inhibition of both enzymes especially in the foal. Increased concentrations in the serum of the foal and the mare alike of octanoylcarnitine and decenoylcarnitine are further indicators of inhibition of the MCAD enzyme. The branched-chain isobutyrylcarnitine, however, which indicates dysfunction of the isobutyryl-CoA dehydrogenase (OMIM 611283), was measured in increased concentrations in the serum of the foal only.

In the group of acylcarnitines with five carbon atoms high values for isovalerylcarnitine and 2-methylbutyrylcarnitine were measured especially in the serum of the foal indicating that he had a particularly pronounced inhibition of isovaleryl-CoA dehydrogenase (OMIM 607036) and 2-methylbutyryl-CoA dehydrogenase (OMIM 610006), which have functions in the degradation of leucine and isoleucine, respectively. Values for the unbranched valerylcarnitine were within the normal range in both animals.

## Long-Chain Acylcarnitines in the Serum

In the range of long-chain acylcarnitines with chain lengths of 12–18 C-atoms, again, the values measured in the foal and the mare exceeded those of the negative controls (**Table 3**). This was true for both the saturated compounds that are products of the first step of the ß-oxidation spiral as well as for the products of

the second step, the monounsaturated acylcarnitines. However, while values close to or below the mean of the comparison group were found for the saturated compounds, values for the unsaturated compounds C 14:1 and C16:1 were particularly high in the serum of the foal, amounting to 262 and 133% of the means of the comparison group, respectively. The particularly strong inhibition of the second reaction step of ß-oxidation in the foal becomes clear when the concentrations of C14:1 are put in relation to that of C14-OH as shown in **Figure 2**. While a ratio of 51.7/1 is calculated for the foal, the ratio for the mare is only 2.2/1.

## Organic Acids and Acylglycines in Urine

The analysis of the urine for organic acids provided results that confirmed and expanded those obtained by serum samples. In their entirety, they are a sign for a massively disturbed energy production from fatty acids and amino acids, a fact that is also underlined by the extremely high excretion of lactate in the foal. The results of the urine tests not only confirmed the impairment of the dehydrogenases and enoylhydratases shown for serum but also revealed various secondary metabolic disorders e.g., the accumulation of pyroglutamic acid as a sign of malfunction of the glutamyl cycle (**Table 4**).

While inhibition of the SCAD enzyme (OMIM 201470) in the mare as well as in the foal is indicated by high values obtained for ethylmalonic acid and 2-ethyl-3-hydroxypropionic acid, inhibition of the short/branched-chain acyl-CoA dehydrogenase enzyme (OMIM 600301), also called 2-methylbutyryl-CoA dehydrogenase, is proven by elevated excretion of 2-ethylhydracrylic acid (2-ethyl-3-hydroxypropionic acid) (18, 19). The pronounced excretion of the saturated dicarboxylic acids adipic and suberic acids and the ketone body 3-hydroxybutyric acid are clear indicators for the inhibition of the MCAD enzyme. Metabolites such as methylsuccinic acid or glutaric acid are typical markers of disorders in the metabolism of various amino acids.

Metabolic inhibition also led, as expected, to a greatly increased excretion of the corresponding acylglycines. The excretion of the acylglycines exceeded that of the corresponding carnitine compounds by two to three powers of ten. As a consequence of a nutrition from vegetable food, a large excretion of hippuric acid and phenylpropionyglycine (**Table 5**) was observed in the dam but not in the foal who did not eat plant material.

**TABLE 4 |** Excretion of organic acids in urine showing organaciduria which is severe in the foal, less pronounced in the mare, values in mg/g creatinine.

| Acid | Foal | Mare | Control |
|---|---|---|---|
| lactic | 3,800 | 17.5 | 4.9 |
| glycolic | 41 | 11.6 | 5.6 |
| 3-hydroxypropionic | 1.8 | 0 | 0.6 |
| 3-hydroxybutyric | 128 | 18 | 1.6 |
| 3-hydroxyisovaleric | 66 | 1.2 | 0.3 |
| 2-methyl-3-hydroxybutyric | 9.5 | 14.5 | 10.8 |
| 3-hydroxy-isovaleric | 6.4 | 8.4 | 7.5 |
| metylmalonic | 0.4 | 0.9 | 1.6 |
| 2-ethyl-3-hydroxypropionic | 33 | 41 | 1.4 |
| 4-Hydroxybutyric | 7.8 | 2 | 0.5 |
| ethylmalonic | 47 | 36 | 1 |
| methylsuccinic | 33 | 30 | 7.6 |
| glyceric | 53 | 2.8 | 2.2 |
| fumaric | 2.5 | 0.5 | 0.6 |
| mevalonic | 0 | 0 | 1 |
| glutaric | 13.5 | 2 | 0.3 |
| 3-methylglutaric | 0 | 0 | 0.2 |
| 3-methylglutaconic | 1.6 | 3 | 0 |
| adipic | 106 | 9.7 | 0.4 |
| pyroglutamic | 131 | 8.6 | 17 |
| 2-hydroxy glutaric | 114 | 31 | 3.4 |
| 3-hydroxy glutaric | 6.2 | 3.4 | 1.6 |
| 3-hydroxy-3-methylglutaric | 3.1 | 0 | 4.8 |
| 2-ketoglutaric | 4.6 | 3.2 | 0 |
| N-acetylaspartic | 2.1 | 4.4 | 0.2 |
| suberic | 76 | 4.7 | 1 |
| sebacic | 0 | 1.3 | 0.4 |

**TABLE 5 |** Renal excretion of acylglycines and hippuric acid.

| Excretion[a] | Foal | Dam | Control |
|---|---|---|---|
| Isovalerylglycine | 25.7 | 40.6 | 0.3 |
| Hexanoylglycine | 23.6 | 29.5 | 0.1 |
| Methylcrotonylglycine | 2.1 | 8.3 | 0.1 |
| Tiglylglycine | 0.2 | 1.2 | <0.1 |
| Phenylpropionylglycine | 0.5 | 15 | <0.1 |
| Hippuric acid | 2.8 | 44.3 | 0.5 |

[a] *Excretion measured in μmol/mmol creatinine.*

# DISCUSSION

The foal developed the full clinical picture of AM. The diagnosis is supported by strongly elevated values for muscle enzymes such as CK, LDH and by the excretion of myoglobin. Nevertheless, the biochemical findings suggest marked differences from other cases of AM. First, the very low serum level of HGA measured at the peak of clinical disease is noteworthy. It reached only 24.3% of the mean of the values found in the horses with AM used for comparison. The low level of HGA is further demonstrated by comparison with samples obtained from clinically healthy individuals. In a previous study (19), we found HGA levels that were higher than in the foal in 9 out of 12 clinically unsuspicious horses who had shared pasture with horses suffering from AM. A mean HGA level of 771 nmol (range: 268–2,327) was found in this group. The value of 438 nmol/L measured in the foal examined here represents only 56.8% of this mean. This corresponds in magnitude to values in 2 clinically healthy co-grazing horses observed by Baise et al. (20). Also noteworthy are the very low values found for MCPA and MCPF conjugates, as shown in **Table 1**. The concentrations of MCPA carnitine and

MCPA glycine were only 0.63 and 1.4% of those of the parent compound HGA.

The fact that the foal developed the characteristic picture of AM despite only small amounts of vertically transferred toxins suggests a special readiness to react or, better, a special vulnerability of the biochemical processes of cellular energy production. An indication of a special point of attack comes from the analysis of the acylcarnitine concentrations. Very striking is the strong accumulation of the unsaturated long-chain acylcarnitines, especially of C14:1, the concentration of which was higher than in all compared AM horses. In contrast, the backlog of fatty acid degradation in the medium chain length region, although evident, was not very pronounced as compared to other AM horses. Hexanoyl-, octanoyl- and decenoylcarnitines reached only 45.4, 32.4, and 11.8% of the mean of the positive cases.

The strong accumulation of tetradecenoyl and hexadecenoyl carnitines makes it evident that the ß-oxidation of the long-chain fatty acids was blocked at the stage of hydration to the C14-OH and C16-OH compounds. This indicates an extensive loss of function of the enzyme responsible for this hydration step, long-chain enoyl-CoA hydratase (OMIM 609015, EC 4.2.1.74). The enzyme is, at least in humans, integrated into the mitochondrial trifunctional protein which also harbors the ß-hydroxy-acyl-CoA dehydrogenase and long-chain thiolase. However, there was no indication that these activities were negatively affected neither in the mare nor the foal.

An isolated defect of the long-chain ECH as a congenital disease has not yet been described for any species. Whether a genetic defect could underlie the present case would have had to be proven by appropriate genetic studies. Unfortunately, no suitable tissue was available. Thus, it must be left to the investigation of further cases to confirm this speculation.

In horses, congenital defects of the trifunctional protein have not been described yet, in humans they are rare (21). In newborn screening, an incidence of about 1:100 000 was found (22). As a differential diagnosis, a defect in very long-chain acyl-CoA dehydrogenase (OMIM #201475, EC 1.3.99.13) must also be considered. This disorder leads to an accumulation of C14:1 and other long-chain acylcarnitines. A genetic defect of the enzyme is known for humans [for review see van Calcar et al. (23)] and for dogs (24). However, this has not yet been observed in horses.

A risk of vertically transmitted HGA or MCPG might also exist for newborn babies because consumption of HGA and MCPG-containing fruits is widespread and increasingly popular. Based on the observations made here in a foal, one would have to conclude that newborns with a congenital defect of an enzyme of the ß-oxidation of fatty acids would be particularly at hazard. Further studies are needed to clarify a possible synergism of *Sapindaceae* toxins and special congenital defects.

## DATA AVAILABILITY STATEMENT

The raw data supporting the conclusions of this article will be made available by the authors, without undue reservation.

## AUTHOR CONTRIBUTIONS

JS was the principal investigator and conducted the conceptualization and experimental design. MT performed the analyses and was responsible for quality control. NJ supervised the interpretation of the study results and reviewed the draft. All authors contributed to the article and approved the submitted version.

## REFERENCES


1. Votion DM, François AC, Kruse C, Renaud B, Farinelle A, Bouquieaux MC, et al. Answers to the frequently asked questions regarding horse feeding and management practices to reduce the risk of atypical myopathy. *Animals.* (2020) 10:365. doi: 10.3390/ani10020365
2. Kean EA. Selective inhibition of acyl-CoA dehydrogenases by a metabolite of hypoglycin. *Biochim Biophys Acta.* (1976) 422:8–14. doi: 10.1016/0005-2744(76)90003-6
3. Li D, Agnihotri G, Dakoji S, Zhou HQ, Liu HW. The toxicity of methylenecyclopropylglycine: studies of the inhibitory effects of (methylenecyclopropyl)formyl-CoA on enzymes involved in fatty acid metabolism and the molecular basis of its inactivation of enoyl-CoA hydratases. *J Am Chem Soc.* (1999) 121:9034–42. doi: 10.1021/ja991908w
4. Westermann CM, de Sain-van der Velden MG, van der Kolk JH, Berger R, Wijnberg ID, Koeman JP, et al. Equine biochemical multiple acyl-CoA dehydrogenase deficiency (MADD) as a cause of rhabdomyolysis. *Mol Genet Metab.* (2007) 91:362–9. doi: 10.1016/j.ymgme.2007.04.010
5. Karlíková R, Široká J, Mech M, Friedecký D, Janečková H, Mádrová L, et al. Newborn foal with atypical myopathy. *J Vet Intern Med.* (2018) 32:1768–72. PMID: 30216546. doi: 10.1111/jvim.15236
6. Sander J, Terhardt M, Janzen N. Detection of maple toxins in mare's milk. *J Vet Intern Med.* (2020) 35:606–9. doi: 10.1111/jvim.16004
7. Renaud B, François AC, Boemer F, Kruse C, Stern D, Piot A, et al. Grazing mares on pasture with sycamore maples: a potential threat to suckling foals and food safety through milk contamination. *Animals.* (2021) 11:87. doi: 10.3390/ani11010087
8. González-Medina S, Bevin W, AlzolaDomingo R, Chang Y-M, Piercy RJ. Hypoglycin A absorption in sheep without concurrent clinical or biochemical evidence of disease. *J Vet Intern Med.* (2021) 35:1170–6. doi: 10.1111/jvim.16077
9. Sander J, Terhardt M, Sander S, Aboling S, Janzen N. A new method for quantifying causative and diagnostic markers of methylenecyclopropylglycine poisoning. *Toxicol Rep.* (2019) 6:803–8. doi: 10.1016/j.toxrep.2019.08.002
10. Sander J, Terhardt M, Sander S, Janzen N. Quantification of methylenecyclopropyl compounds and acyl conjugates by UPLC-MS/MS in the study of the biochemical effects of the ingestion of canned ackee (Blighia sapida) and lychee (Litchi chinensis). *J Agric Food Chem.* (2017) 65:2603–8. doi: 10.1021/acs.jafc.7b00224
11. Sander J, Cavalleri JM, Terhardt M, Bochnia M, Zeyner A, Zuraw A, et al. Rapid diagnosis of hypoglycin A intoxication in atypical myopathy of horses. *J Vet Diagn Invest.* (2016) 28:98–104. doi: 10.1177/1040638715624736
12. Sander J, Terhardt M, Sander S, Janzen N. Quantification of hypoglycin A as butyl ester. *J Chromatogr B Analyt Technol Biomed Life Sci.* (2016) 1029-1030:169–73. doi: 10.1016/j.jchromb.2016.07.005
13. Chace DH, DiPerna JC, Naylor EW. Laboratory integration and utilization of tandem mass spectrometry in neonatal screening: a model for clinical mass spectrometry in the next millennium. *Acta Paediatr Suppl.* (1999) 88:45–7. doi: 10.1111/j.1651-2227.1999.tb01156.x

14. Rashed MS, Rahbeeni Z, Ozand PT. Application of electrospray tandem mass spectrometry to neonatal screening. *Semin Perinatol.* (1999) 23:183–93. doi: 10.1016/S0146-0005(99)80050-0
15. Sander J, Terhardt M, Sander S, Janzen N. Use of a standard newborn screening test for the rapid diagnosis of inhibited ß-Oxidation in atypical myopathy in horses. *J Equine Vet Sci.* (2018) 67:71–4. doi: 10.1016/j.jevs.2018.03.010
16. Hoffmann G, Aramaki S, Blum-Hoffmann E, Nyhan WL, Sweetman L. Quantitative analysis for organic acids in biological samples: batch isolation followed by gas chromatographic-mass spectrometric analysis. *Clin Chem.* (1989) 35:587–95. doi: 10.1093/clinchem/35.4.587
17. Bochnia M, Ziegler J, Sander J, Uhlig A, Schaefer S, Vollstedt S, et al. Hypoglycin A content in blood and urine discriminates horses with atypical myopathy from clinically normal horses grazing on the same pasture. *PLoS One.* (2015) 10:e0136785. doi: 10.1371/journal.pone.0136785
18. Korman SH, Andresen BS, Zeharia A, Gutman A, Boneh A, Pitt JJ. 2-ethylhydracrylic aciduria in short/branched-chain acyl-CoA dehydrogenase deficiency: application to diagnosis and implications for the R-pathway of isoleucine oxidation. *Clin Chem.* (2005) 51:610–7. doi: 10.1373/clinchem.2004.043265
19. Sass JO, Ensenauer R, Röschinger RW, Reich H, Steuerwald U, Schirrmacher O, et al. 2-Methylbutyryl-coenzyme A dehydrogenase deficiency: functional and molecular studies on a defect in isoleucine catabolism. *Mol Genet Metab.* (2007) 93:30–5. doi: 10.1016/j.ymgme.2007.09.002
20. Baise E, Habyarimana JA, Amory H, Boemer F, Douny C, Gustin P, et al. Samaras and seedlings of Acer pseudoplatanus are potential sources of hypoglycin A intoxication in atypical myopathy without necessarily inducing clinical signs. *Equine Vet J.* (2016) 48:414–7. doi: 10.1111/evj.12499
21. Boutron A, Acquaviva C, Vianey-Saban C. Comprehensive cDNA study and quantitative analysis of mutant HADHA and HADHB transcripts in a French cohort of 52 patients with mitochondrial trifunctional protein deficiency. *Mol Genet Metab.* (2011) 103:341–8. doi: 10.1016/j.ymgme.2011.04.006
22. Sander J, Sander S, Steuerwald U, Janzen N, Peter M, Wanders RJA, et al. Neonatal screening for defects of the mitochondrial trifunctional protein. *Mol Genet Metab.* (2005) 85:108–14. doi: 10.1016/j.ymgme.2005.02.002
23. Van Calcar SC, Sowa M, Rohr F, Beazer J, Setlock T, Weihe TU, et al. Nutrition management guideline for very-long chain acyl-CoA dehydrogenase deficiency (VLCAD): an evidence- and consensus-based approach. *Mol Genet Metab.* (2020) 131:23–37. doi: 10.1016/j.ymgme.2020.10.001
24. Lepori V Mühlhause F, Sewell AC, Jagannathan V, Janzen N, Rosati M, et al. Nonsense variant in the ACADVL gene in german hunting terriers with exercise induced metabolic myopathy. *G3 (Bethesda).* (2018) 8:1545–54. doi: 10.1534/g3.118.200084

**Conflict of Interest:** The authors declare that the research was conducted in the absence of any commercial or financial relationships that could be construed as a potential conflict of interest.

**Publisher's Note:** All claims expressed in this article are solely those of the authors and do not necessarily represent those of their affiliated organizations, or those of the publisher, the editors and the reviewers. Any product that may be evaluated in this article, or claim that may be made by its manufacturer, is not guaranteed or endorsed by the publisher.

frontiers in Veterinary Science

ORIGINAL RESEARCH
published: 26 October 2021
doi: 10.3389/fvets.2021.756534

# Vanadium Induces Oxidative Stress and Mitochondrial Quality Control Disorder in the Heart of Ducks

*Zhiwei Xiong[1†], Chenghong Xing[1†], Tianfang Xu[2†], Yan Yang[2], Guohui Liu[3], Guoliang Hu[1], Huabin Cao[1], Caiying Zhang[1], Xiaoquan Guo[1] and Fan Yang[1*]*

[1] Jiangxi Provincial Key Laboratory for Animal Health, Institute of Animal Population Health, College of Animal Science and Technology, Jiangxi Agricultural University, Nanchang, China, [2] Jiangxi Agricultural Technology Extension Center, Nanchang, China, [3] Ganzhou Agriculture and Rural Affairs, Ganzhou, China

Vanadium (V) is an ultra-trace element presenting in humans and animals, but excessive V can cause toxic effects. Mitochondrial quality control (MQC) is an essential process for maintaining mitochondrial functions, but the relationship between V toxicity and MQC is unclear. To investigate the effects of excessive V on oxidative stress and MQC in duck hearts, 72 ducks were randomly divided into two groups, including the control group and the V group (30 mg of V/kg dry matter). The cardiac tissues were collected for the histomorphology observation and oxidative stress status evaluation at 22 and 44 days. In addition, the mRNA and protein levels of MQC-related factors were also analyzed. The results showed that excessive V could trigger vacuolar degeneration, granular degeneration, as well as mitochondrial vacuolization and swelling in myocardial cells. In addition, CAT activity was elevated in two time points, while T-SOD activity was increased in 22 days but decreased in 44 days after V treatment. Meanwhile, excessive V intake could also increase the number of Drp1 puncta, the mRNA levels of mitochondrial fission–related factors (Drp1and MFF), and protein (MFF) level, but decrease the number of Parkin puncta and the mitochondrial biogenesis (PGC-1α, NRF-1, and TFAM), mitochondrial fusion (OPA1, Mfn1, and Mfn2), and mitophagy (Parkin, PINK1, P62, and LC3B) related mRNA levels and protein (PGC-1α, Mfn1, Mfn2, PINK1) levels. Collectively, our results suggested that excessive V could induce oxidative stress and MQC disorder in the heart of ducks.

**Keywords: vanadium, oxidative stress, mitochondrial quality control, heart, duck**

OPEN ACCESS

***Edited by:***
*Hui Zhang,*
*South China Agricultural University, China*

***Reviewed by:***
*Xiaolong Gu,*
*China Agricultural University, China*
*Fazul Nabi,*
*Lasbela University of Agriculture, Water and Marine Sciences, Pakistan*

***Correspondence:**
*Fan Yang*
*yfan@jxau.edu.cn*

*†These authors have contributed equally to this work*

***Specialty section:***
*This article was submitted to Animal Nutrition and Metabolism, a section of the journal Frontiers in Veterinary Science*

***Received:*** *10 August 2021*
***Accepted:*** *03 September 2021*
***Published:*** *26 October 2021*

***Citation:***
*Xiong Z, Xing C, Xu T, Yang Y, Liu G, Hu G, Cao H, Zhang C, Guo X and Yang F (2021) Vanadium Induces Oxidative Stress and Mitochondrial Quality Control Disorder in the Heart of Ducks. Front. Vet. Sci. 8:756534. doi: 10.3389/fvets.2021.756534*

## INTRODUCTION

Vanadium (V) is an ultra-trace element that can affect the activities of intracellular enzymes and acts a crucial role in metabolism and normal cell function and development (1). Moreover, most studies indicated that the concentration of V below $1\times10^{-5}$ M could be used as a potential therapeutic agent for the treatments of cancer or diabetes (2–4). However, due to the extensive use of V in industry, excessive V pollutes the environmental ecosystems and is enriched in the humans and animals via the food chain, subsequently causing various tissue and organ injuries, such as heart, kidney, and lung. The heart, one of the target organs of V's toxicity, and excessive V entering the body could cause serious damage to it (5). Moreover, many studies demonstrated

that excessive V could cause the injury of cardiac tissues via promoting the generation of reactive oxygen species (ROS) (6, 7), which in turn leads to mitochondrial dysfunction by complex signaling mechanisms.

Mitochondria are highly dynamic double-membraned organelles, especially abundant in cardiac tissue, which takes part in numerous cellular processes, such as ATP production, bioenergetics, metabolism, redox balance, and cell death (8). They also can produce ROS via transferring electrons in the mitochondrial respiratory chain to the oxygen atoms (9). Meanwhile, efficient antioxidant systems neutralize the extra ROS to resist oxidative stress and protect mitochondria (10, 11). Most of the studies suggested that V induced the generation of excess ROS and impaired antioxidant defense systems, eventually causing oxidative stress and mitochondrial dysfunction (12, 13). However, the maintenance of mitochondrial function depends on the normal operation of the mitochondrial quality control (MQC) system.

MQC, a self-functioning security mechanism, maintains the functional integrity of mitochondria, including mitochondrial biogenesis, mitochondrial fission, mitochondrial fusion, and mitophagy. Mitochondrial biogenesis coordinates energy homeostasis and cell growth by generating new mitochondria from existing mitochondria through crosstalk between nuclear and mitochondrial genomes (14). In addition, mitochondrial fission and fusion are the critical processes to maintain the health of mitochondria and cells for keeping the steady-state morphology of the mitochondrial network, which were related to the changes in metabolic states and diseases (15). In addition, mitophagy participates in a course of mitochondrial repairment, in the process of which damaged portions of mitochondria were removed from the healthy parts by division, subsequently degraded via a specific mode of autophagy (16). Based on the aforementioned, these specific mechanisms of MQC are effective ways to promote mitochondria renewal to maintain cell homeostasis. As shown in a recent study, cadmium could cause necroptosis and tissue damage by promoting mitochondrial fission leads to MQC disorder (17). Manganese has been verified to induce mitochondrial dysfunction by enhancing the activation of mitophagy (18). Therefore, we realized that MQC plays an important role in the toxic mechanism of heavy metals. A previous study has indicated that excessive V could induce mitochondrial dysfunction (19), but the specific mechanism should be further explored.

Emerging evidence suggested that the toxicity mechanism of V is mainly manifested in the damage of high levels of ROS to mitochondria, leading to oxidative stress and mitochondrial dysfunction (20). However, the role of MQC in the mechanism is unclear. Therefore, we explored the impacts of V exposure on oxidative stress and MQC in the heart of ducks in this study via histomorphometry observation, transmission electron microscope observation, immunofluorescence detection analysis, antioxidant-related indicator detection, and MQC-related mRNA and protein level detection further to enrich the theory of the V-induced cardiac toxicity mechanism.

# MATERIALS AND METHODS

## Experiment Animals and Management

The study was conducted according to ethical guidelines and approved by the animal ethics committee of Jiangxi Agricultural University (Approval ID: JXAULL-2020-32). All ducks have received the standard rations according to the National Research Council (NRC), which referred to Ren et al. (21). Dietary composition and nutrient levels are shown in **Table 1**. Before the formal experiment, all ducks' health were assessed by the clinical examination. All ducks were reared under duck feeding conditions with a light/dark cycle for 12 h, a relative humidity of 65%, a relative temperature of 25°C, and had *ad libitum* feeding and drinking in 44 days.

## Determination of Lethal Dose 50 ($LD_{50}$)

The ammonium metavanadate ($NH_4VO_3$) was used as the source of V. Fifty-four 1-day-old ducks were randomly divided into nine groups for the determination of $LD_{50}$. Different doses of V, i.e., 10, 50, 100, 500, 1000, 1500, 2000, 2500, and 3000 mg/kg V dry matter (DM), were given to these groups, respectively. The dose-dependent effects of mortality were observed daily. Ultimately, 125.35 mg/kg V DM was assessed to be the $LD_{50}$ of $NH_4VO_3$.

## Toxicity Trials

Seventy-two healthy 1-day-old Peking ducks were randomly assigned to two groups: the control group (basal diet) and the V group (30 mg/kg V DM), which followed the principle of the half male and half female. According to the $LD_{50}$ of V in the ducks and the previous study (22), we chose a more conservative dose of 30 mg of V/kg DM. Cardiac tissues of the ducks were collected on 22 and 44 days.

## Sample Collection

On days 22 and 44, cardiac tissues were collected after ducks were anesthetized with an overdose of the intravenous injection of sodium pentobarbital anesthesia. Subsequently, the cardiac tissues were flushed with normal saline (0.9% NaCl; Gemeiyan, China) and removed the surface fluid with filter paper. Finally, the parts of the cardiac tissues were put into cryotubes and stored at −80°C, and the rest were applied to histomorphology observation and immunofluorescence detection analysis (23).

## Histomorphology Observation

The cardiac tissue specimens with a volume of $2 \times 2 \times 0.3$ $cm^3$ ($n = 6$) on 44 days were fixed with 4% paraformaldehyde at room temperature for 48 h, and the specific method was described in Zhang's publication (24). Afterward, the slides were stained with H&E and the pathological changes in the heart were evaluated under a light microscope (Olympus, Japan) (25).

## Transmission Electron Microscope Observation

The experimental procedures referred to the method of description in Shi et al.'s (26) paper. In brief, the samples were fixed in 2.5% glutaraldehyde and 0.1 M sodium phosphate mixed buffer (pH 7.2), respectively, and then post set with 1% osmium tetroxide in sodium phosphate buffer. Subsequently,

**TABLE 1 |** The component and nutritional levels of the basal diet.

| Item (%, unless noted) | Content |
|---|---|
| Corn | 47 |
| Wheat bran | 13 |
| Rice bran | 9 |
| Soybean meal, 43% | 9 |
| Rapeseed meal | 9 |
| Cottonseed meal | 6 |
| Rapeseed oil | 2.88 |
| Calcium carbonate | 0.96 |
| Dicalcium phosphate, $2H_2O$ | 1.275 |
| l-Lysine-HCl | 0.37 |
| d, l-Methionine | 0.226 |
| Threonine, 98.5% | 0.044 |
| Tryptophan, 98.5% | 0.032 |
| Sodium chloride | 0.4 |
| Choline chloride, 50% | 0.2 |
| Bentonite | 0.913 |
| Mineral premix[1] | 0.4 |
| Vitamin premix[2] | 0.2 |
| **Analyzed nutrient content** | |
| ME (kcal/kg, calculated) | 2,914 |
| CP (analyzed) | 17.12 |
| Calcium (analyzed) | 0.94 |
| Total phosphorus (analyzed) | 0.84 |
| Nonphytate phosphorus (calculated) | 0.478 |

[1]*Dietary supply per kilogram: copper, 8 mg; iron, 80 mg; zinc, 90 mg; manganese, 70 mg; selenium, 0.3 mg; iodine, 0.4 mg.* [2]*Dietary supply per kilogram: vitamin A, 15,000 IU; vitamin $D_3$, 5,000 IU; vitamin $K_3$, 5 mg; vitamin E, 80 mg; vitamin $B_1$, 3 mg; vitamin $B_2$, 9 mg; vitamin $B_6$, 7 mg; vitamin $B_{12}$, 0.04 mg; nicotine acid, 80 mg; pantothenic acid, 15 mg; biotin, 0.15 mg; folic acid, 2 mg; vitamin C, 200 mg; 25-hydroxycholecalciferol, 0.069 mg.*

the specimens were graded, dehydrated with 50% ethanol, and treated twice with propylene oxide. Finally, the specimens were embedded in araldite to slice and stain. The pathological changes of the myocardial cell were observed under microscope transmission electron microscopy Zeiss 900 microscope (Zeiss, Germany) (27).

## Oxidative Stress Indices Determination

The levels of total superoxide dismutase (T-SOD), catalase (CAT), malonaldehyde (MDA), and hydrogen peroxide ($H_2O_2$) were measured using commercial kits (Nanjing Jiancheng Bioengineering Institute, China) according to the manufacturer's instructions.

## Immunofluorescence Detection Analysis

Immunofluorescence staining observation was carried out by Zhang et al. (23) as reference. In short, the sections were incubated with antibodies against Drp1 (1:100; Wanleibio, China) or Parkin (1:400; Proteintech, USA) at 4°C overnight, and incubated the fluorescein (FITC) conjugated goat anti-rabbit or anti-mouse immunoglobulin (Ig)G (1:1,000, diluted) after washing off excess antibody with phosphate-buffered saline (PBS). Finally, the sections were washed by PBS and strained with 4′,6-diamidino-2-phenylindole (DAPI). The fluorescence intensities of Drp1 and Parkin were observed under the fluorescence microscope (Nikon Eclipse C1, Tokyo, Japan) (28).

**TABLE 2 |** Premier sequences used for real-time PCR.

| Gene | 5′-Primer (F) | 3′-Primer (R) |
|---|---|---|
| PGC-1α | GTCTGCCTCTGCGCGAC | CCAGAGCAGCACACTCGAT |
| NRF-1 | AGACGCGTTTGCTACGGAAG | TGTGCCTGGGTCATCTTGTC |
| TFAM | GGAGTTTCACCTGTGGCAAA | TCCACGTAGTGGAGCTTTGG |
| OPA1 | GGATCTGCTGTAGGTGGTGG | TCACTAACCAAATTGTAACCAGGA |
| Mfn1 | GCTGTGTACGAGGCAGCTAT | GTTCCTGTATGTTGCTTCCACG |
| Mfn2 | GGAAGGGAGGAAAGCGCAATG | CCAGTACCTGCTCTTCTGTGG |
| Drp1 | AAGTGGCCTGAGGTGGATGA | CGGGTTCTCCACAGTTTCACT |
| MFF | TCGACTAAGGATTGCACTGTGA | TGGTAAGCCCTACGAGTGGA |
| PINK1 | GCTGTGTACGAGGCAGCTAT | CGAAGAACCAGCCGAGATGT |
| Parkin | CGCCGCCATGATAGTGTTTGTT | TTCTGCAGCGTCAAGTCGTT |
| P62 | TCCCTTCTTGGTTCAACGGG | GAAGGGGCACCAAGTGAGAG |
| LC3B | ACAGTACAGACGAGCACCTC | CCAGAAAACTGTCACACGCA |
| GAPDH | TGATGCTCCCATGTTCGTGA | CTTTTCCCACAGCCTTAGCAG |

*F, forward, R, reverse.*

## Real-Time Quantitative Polymerase Chain Reaction (RT-qPCR) Analysis

The primers and sequences used for RT-qPCR are shown in **Table 2**. According to the manufacturer's protocol, approximately total RNA of 40 μg ($n = 6$) was isolated from cardiac tissue by applying a Trizol reagent (Vazyme, China) and then using GeneQuant 1,300 spectrophotometer determined the RNA concentration. The RNA of 1,000 ng was reverse-transcribed into cDNA using the TransScript Uni All-in-One First-Strand cDNA Synthesis Super Mix (Trans, China) according to the manufacturer's instructions. Then RT-qPCR reaction was performed using 2× SYBR Green qPCR Master Mix (Servicebio, China) and carried out using QuantStudio7 Flex Real-Time PCR Systems (ABI 7900HT; Applied Biosystems, USA). The changes of the relative mRNA levels were assessed using the $2^{-\Delta\Delta CT}$ method and standardized by GAPDH (29).

## Western Blot Analysis

According to the manufacturer's protocol, the total protein was isolated from the 44-day cardiac tissue using RIPA lysis buffer (Solarbio, China), which contains protease inhibitors (PMSF) (Servicebio, China) (30). Subsequently, we measured the protein concentrations by using the bicinchoninic acid protein assay kit (Solarbio, China). Equal protein samples (10 μg) were boiled for 10 min after mixing with the 6 × SDS-PAGE loading buffer (TransGen Biotech, China), and run on 12% SDS-polyacrylamide denaturing gels and transferred onto polyvinylidene fluoride (PVDF) membranes (Biosharp, China) (31). After blocking with tris buffered saline tween (TBST) containing 5% non-fat milk powder for 2 h at room temperature, the membrane was

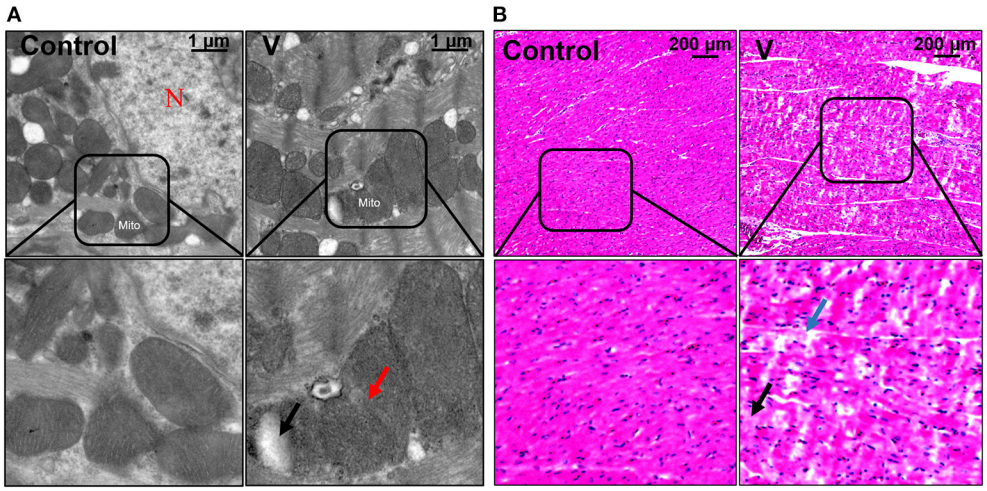


**FIGURE 1 |** The changes of histomorphology in the heart of ducks on 44 days. **(A)** TEM observation. The scale bar is 1 μm. The red arrow refers to mitochondrial swelling. The black arrow refers to mitochondrial vacuolization. N, nucleus; Mito, mitochondria. **(B)** Pathological observation of the hearts in ducks. Scale bar, 200 μm. The black row indicates granular degeneration of cardiomyocytes. The blue row indicates the vacuolar degeneration of cardiomyocytes.

incubated overnight with diluted primary antibodies against PGC-1α (1:5,000; Proteintech, USA), Mfn1 (1:2,000; Proteintech, USA), Mfn2 (1:2,000; Wanleibio, China), Drp1 (1:1,500; Wanleibio, China), PINK1 (1:500; Bioss, China), and GAPDH (1:5,000; Proteintech, USA) at 4°C for 12 h. Subsequently, these membranes were washed by PBS adding tween-20 and incubated with corresponding second antibodies for 2 h. The bands were visualized by using enhanced chemiluminescence (ECL) reagents (Vazyme Biotech, USA). The signal was detected with Image Lab Software (Bio-Rad, USA), and protein levels were analyzed by ImageJ software. The quantitative analysis of each band was normalized in its respective loading control (GAPDH).

## Statistical Analysis

The data were expressed as the mean ± SD. All data were calculated by Microsoft Excel 2016 and homogenous data were analyzed by one-way ANOVA using SPSS 25.0 (SPSS Inc., Chicago, IL, USA), in which the significances of intergroup differences were analyzed via least-significant difference analysis. All bar graphs were drawn using the GraphPad Prism 8.0 (GraphPad Inc., La Jolla, CA, USA). The $p$-value $< 0.05$ was considered statistically significant unless otherwise stated.

# RESULTS

## The Effects of V on Histopathology in the Heart of Ducks

The ultrastructural and pathological changes of heart in ducks on 44 days are shown in **Figure 1**. According to the results of the histopathological examination in the heart, the cardiomyocytes were arranged neatly and orderly in the control group, but V exposure induced vacuolization and granular degeneration in the myocardial cells on 44 days (**Figure 1B**). In addition, the ultrastructural observation of the myocardial cells showed that the structure of organelles and nucleus were clear in the control group, and mitochondrial swelling and vacuolization were observed under ultrastructure in the V group on 44 days (**Figure 1A**).

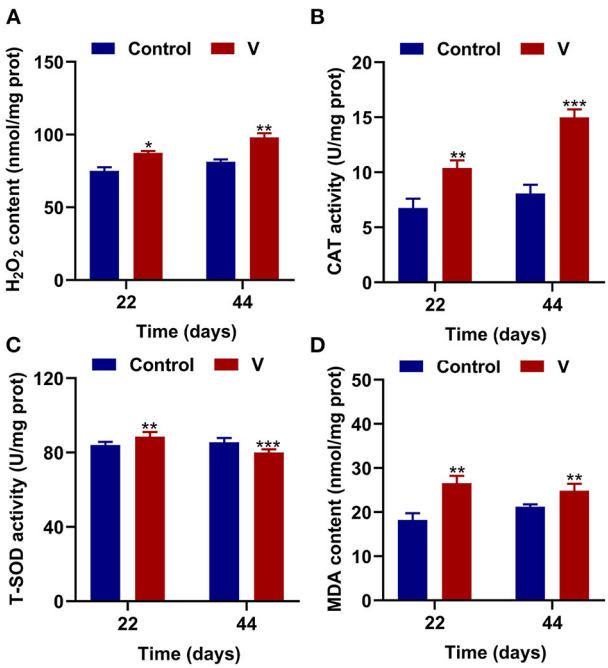


**FIGURE 2 |** V induced oxidative stress in the heart of ducks. **(A)** $H_2O_2$ content. **(B)** The activity of CAT. **(C)** The activity of T-SOD. **(D)** MDA content. Data are represented as mean ± SD ($n = 6$ per group). "*" Indicates significant difference compared with the corresponding control (*$p < 0.05$, **$p < 0.01$, and ***$p < 0.001$).

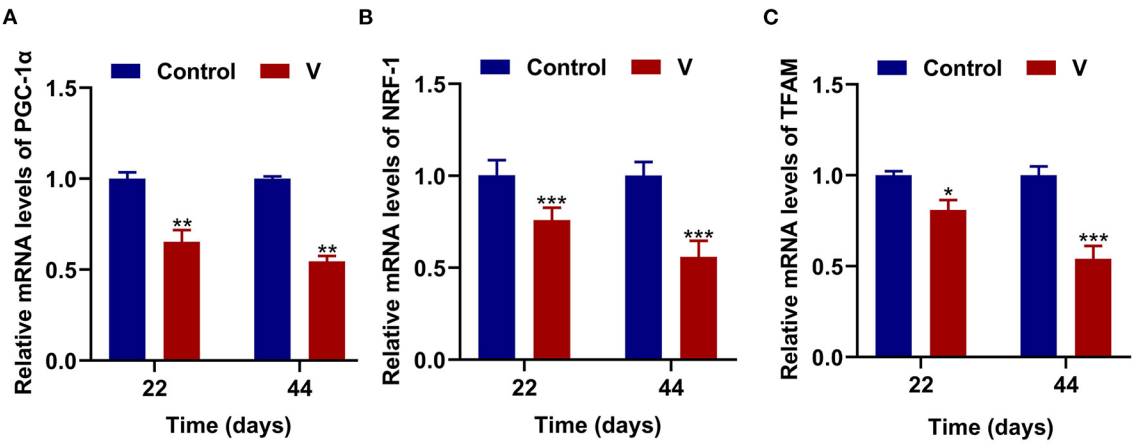


**FIGURE 3 |** The effects of V on mitochondrial biogenesis in the heart of ducks. **(A)** The mRNA levels of PGC-1α. **(B)** The mRNA levels of NRF-1. **(C)** The mRNA levels of TFAM. *$p < 0.05$, **$p < 0.01$, and ***$p < 0.001$.

## The Effects of V on Oxidative Stress Status in the Heart of Ducks

The results showed that excessive V significantly ($p < 0.05$, $p < 0.01$, or $p < 0.001$) increased the levels of $H_2O_2$, MDA, and CAT on 22 and 44 days (**Figures 2A,B,D**). However, T-SOD activity was observably ($p < 0.01$ or $p < 0.001$) increased on 22 days but decreased on 44 days in the V group compared with the control group (**Figure 2C**).

## The Effects of V on Mitochondrial Biogenesis in the Heart of Ducks

As shown in **Figure 3**, V exposure dramatically ($p < 0.05$, $p < 0.01$, or $p < 0.001$) decreased the mRNA levels of mitochondrial biogenesis (PGC-1α, NRF-1, and TFAM) on 22 and 44 days. Moreover, the PGC-1α protein level in the V group was also reduced significantly ($p < 0.001$) in comparison with the control group on 22 and 44 days (**Figures 6A,B**).

## The Effects of V on Mitochondrial Fission and Fusion Related Factors in the Heart of Ducks

The mRNA levels of OPA1, Mfn1, and Mfn2 were markedly ($p < 0.05$, $p < 0.01$, or $p < 0.001$) lower in the V group than the control group on 22 and 44 days (**Figures 4A–C**). However, the mRNA levels of Drp1 and MFF were decreased remarkably ($p < 0.05$, $p < 0.01$, or $p < 0.001$) in the V group compared with the control group on 22 and 44 days (**Figures 4D,E**). The results of heatmap analysis was consistent with the variation of mRNA levels (**Figure 4F**). Meanwhile, on days 22 and 44, excessive V significantly ($p < 0.001$) elevated the protein levels of Mfn1 and Mfn2 (**Figures 6A,C,D**), but markedly ($p < 0.01$) descended the protein level of MFF (**Figures 6A,E**). In addition, V exposure enhanced the fluorescent localization signal of Drp1 in the myocardial cells on day 44 (**Figure 4G**).

## The Effects of V on Mitophagy in the Heart of Ducks

The mRNA levels of PINK1, Parkin, P62, and LC3B were reduced conspicuously ($p < 0.05$, $p < 0.01$, or $p < 0.001$) in the V group compared with the control group on 22 and 44 days (**Figures 5A–D**), and protein level of PINK1 was markedly ($p < 0.001$) lower in the V group than the control group on days 22 and 44 (**Figures 6A,F**). As shown in **Figure 5E**, the numbers of fluorescent spots of Parkin in the V group were decreased in comparison with the control group on 44 days.

# DISCUSSION

V is an essential substance to support biological activities, but it also can cause organ injury when its concentration exceeds the body's tolerance. The heart with lots of mitochondria is one of V toxicity's main target organs, and mitochondria in which could be damaged by V toxicity leading to heart disorders. Previous studies have shown that V induced the impairment of mitochondrial electron transport by interacting with cysteine thiol, which in turn led to oxidative stress and mitochondrial dysfunction (32, 33). Simultaneously, MQC, as an important way to maintain mitochondrial function, can also be destroyed by the toxicity of heavy metal and its obstacle is usually accompanied by the occurrence of oxidative stress (34). Therefore, we speculate that V toxicity also causes damage to the MQC system, but the specific regulation mechanism of excessive V on oxidative stress and MQC deserves further exploration. Herein, this study was to explore the main events of V-induced cardiotoxicity via observing the variations of the antioxidant capacity and MQC-related factors in the heart of ducks.

V plays a key part in the growth and development of the body, but V exposure can cause functional and organic damage to many organs or systems. Previous studies have shown that V exposure could cause vacuolar degeneration

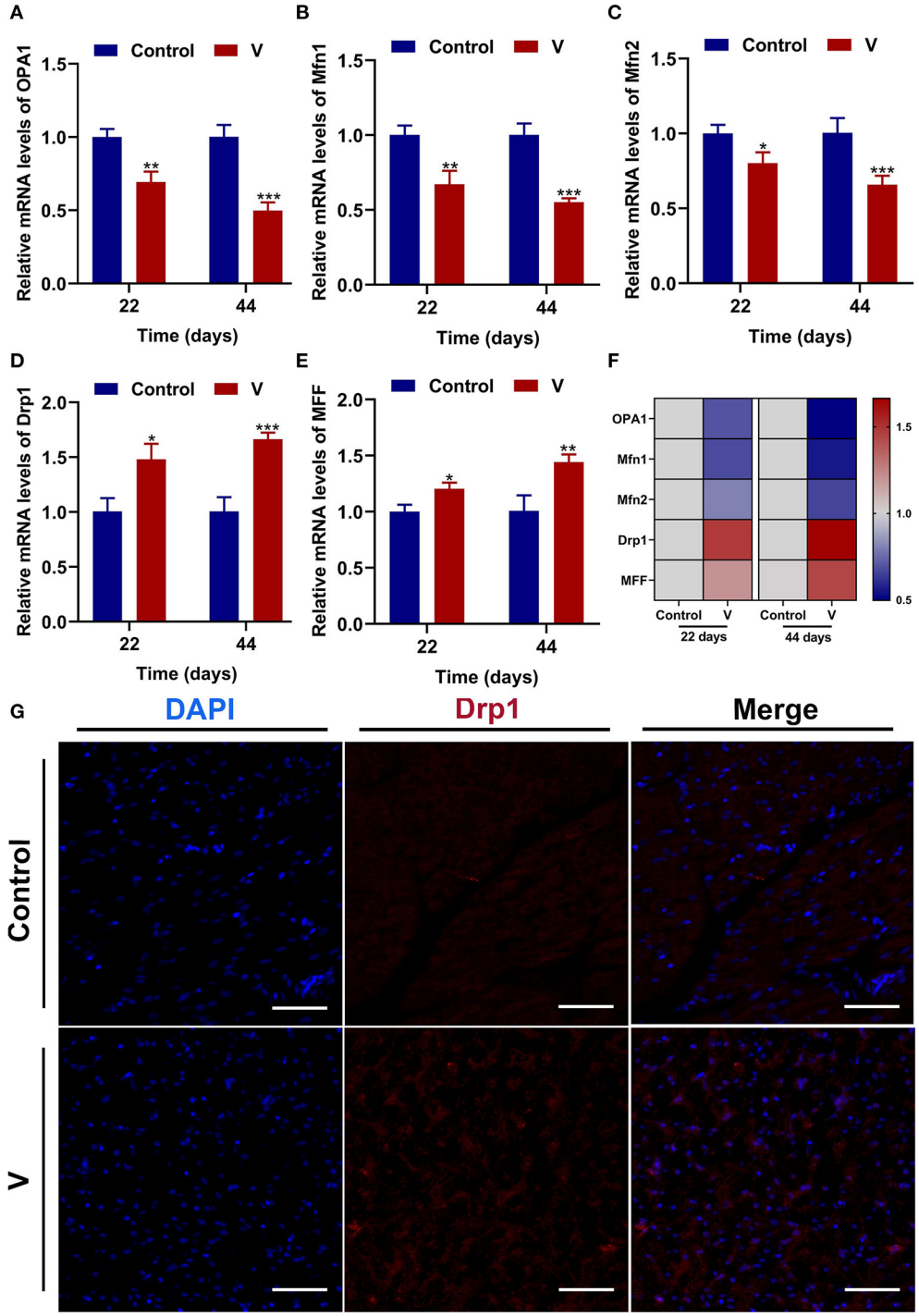


**FIGURE 4 |** The effects of V on mitochondrial fission and fusion in the heart of ducks. **(A–E)** OPA1, Mfn1, Mfn2, Drp1, and MFF mRNA expression levels. **(F)** Heatmap analysis of mitochondrial fission and fusion-related mRNA levels. **(G)** Fluorescence microscope analysis of mitochondrial fission. In this picture, the nucleus straining is shown in blue, Drp1 straining is shown in red, and the bright red light is the fluorescent spot (×400 total magnification). Scale bar: 20 μm. $^{*}p < 0.05$, $^{**}p < 0.01$, and $^{***}p < 0.001$.

and granular degeneration in hepatocytes, and it could also cause pathological changes in brain and kidney tissues (35, 36). In the present study, the sections of cardiac tissue from the V-treated group showed vacuolar and granular degeneration in cardiomyocytes. In addition, the results of the ultrastructure observed by the electron microscope

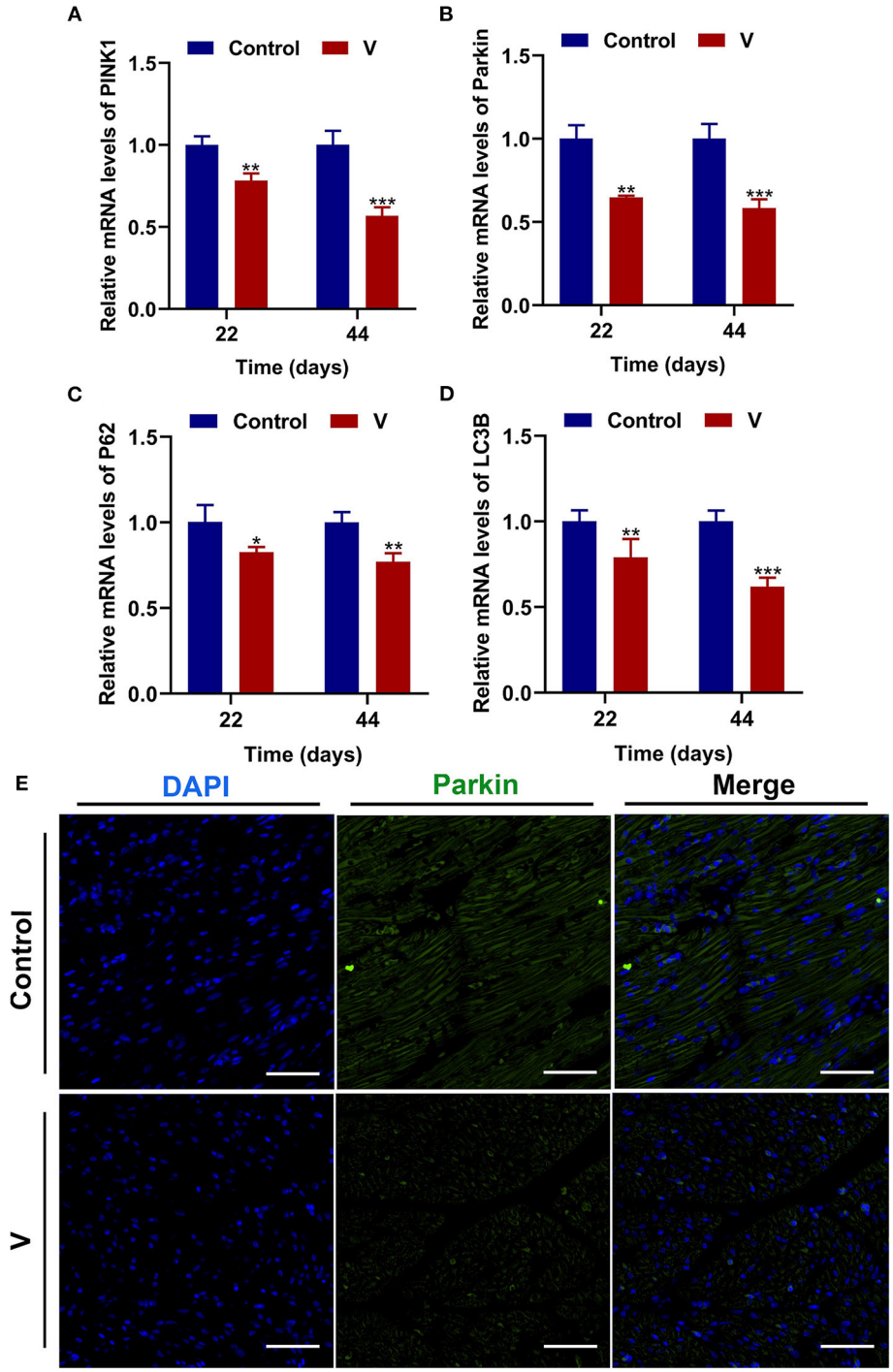


**FIGURE 5 |** V exposure caused the inhibition of mitophagy in the heart of ducks. **(A–D)** PINK1, Parkin, P62, and LC3B mRNA levels. **(E)** Fluorescence microscope analysis of mitophagy. In this image, the nucleus straining is shown in blue, Parkin straining is shown in green, the bright green light is the fluorescent spot (×400 total magnification). The scale bar is 20 μm. *$p < 0.05$, **$p < 0.01$, and ***$p < 0.001$.

showed that excessive V could trigger mitochondrial swelling and vacuolization in cardiomyocytes. These results strongly demonstrated that excessive V intake could induce cell damage in duck hearts.

V, a transition metal, participates in redox behavior and induces the production of ROS. Many scholars have pointed out that V induced cells to produce excessive amounts of ROS, leading to oxidative stress, which in turn triggered mitochondrial

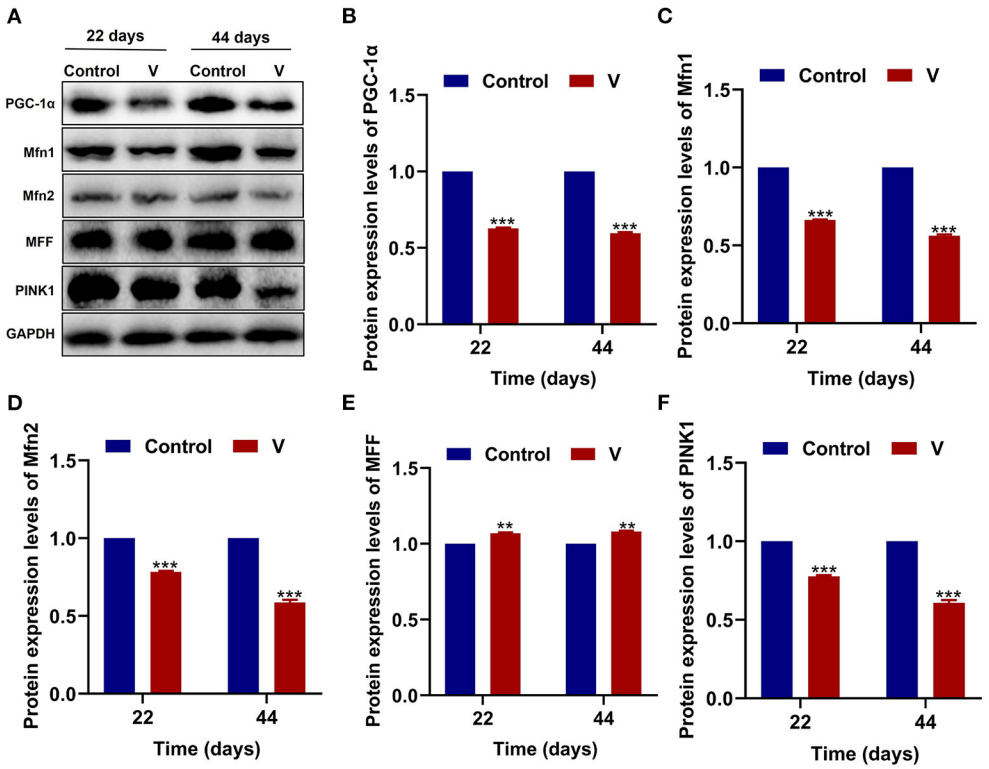


**FIGURE 6 |** The effects of V on MQC-related proteins in the heart of ducks. **(A)** Protein band graph. **(B–F)** Protein levels of PGC-1α, Mfn1, Mfn2, MFF, and PINK1. $^{**}p < 0.01$ and $^{***}p < 0.001$.

dysfunction (37, 38). Meanwhile, the antioxidative system can scavenge ROS through free radical scavenging antioxidant enzymes and non-enzymatic antioxidants (39). Notably, the antioxidant enzymes (SOD and CAT) play central roles in the antioxidant processes (40). Among them, $O_2^{\bullet-}$ converts to $H_2O_2$ via the catalysis of SOD, then CAT catalyzes $H_2O_2$ into $H_2O$ and oxygen (41). MDA, the product of lipid peroxidation, the content of which reflects the injury degree of the oxidative damage. Thus, these antioxidant indexes are usually used as the basis to judge the degree of oxidative damage. In our study, excessive V elevated the levels of $H_2O_2$, MDA, and CAT, but increased T-SOD activity at 22 days and decreased at 44 days. According to the previous study, the antioxidant enzyme activities were enhanced but decreased after a while when the body suffered different degrees of oxidative damage (42, 43). Therefore, the changes of T-SOD activity might be related to the oxidative damage's intensity and time, which is higher at slight or transitory damage, opposite lower. Simultaneously, we speculated that V at a concentration of 30 mg/kg might cause severe damage to the heart of ducks, but the specific mechanism of the variations of T-SOD level deserves further study. Accordingly, these results indicated that excessive V could induce oxidative stress in the heart of ducks.

Oxidative stress is often accompanied by mitochondrial damage and then leads to mitochondrial dysfunction. Picca et al.'s study demonstrated that mitochondrial damage was induced by oxidative stress, MQC disorder, and the transfer of mitochondrial constituents (e.g., mitochondrial DNA, mtDNA) (44). However, MQC is a key mechanism for maintaining the mitochondrial function, and its regulatory mechanism under V exposure is unclear. Therefore, we investigated the regulatory mechanism of MQC under V exposure in duck hearts by measuring the levels of MQC-related mRNA and protein and their location in cardiomyocytes (45). PGC-1α, NRF-1, and TFAM are the key regulators of mitochondrial biogenesis (46). TFAM is activated by the combination of PGC-1α and NRF-1 to regulate the mitochondrial biogenesis transcription process for mitochondrial homeostasis. Herein, high dietary V decreased the mRNA levels of PGC-1α, NRF-1, and TFAM, as well as the protein level of PGC-1α in the heart of ducks, suggesting that excessive V could induce the impairment of mitochondrial biogenesis in the heart of ducks. In addition, mitochondrial fission and fusion are regarded as critical processes to determine the mitochondrial shape (47). Drp1 is recruited to the mitochondrial outer membrane and interacts with multiple receptor proteins like mitochondrial fission factor (MFF) to achieve the segregation of damaged mitochondria (48, 49). However, mitochondrial fusion is a mechanism that mediates OPA1, Mfn1, and Mfn2 to form OPA1 and Mfn1/2 protein complexes to achieve stable mitochondrial membrane fusion (50). In this paper, excessive V upregulated the mRNA and protein levels of Drp1 and MFF in the heart of ducks, and downregulated

the mRNA and protein levels of OPA1, Mfn1, and Mfn2, which indicated that V promoted mitochondrial fission in the heart of ducks but inhibited mitochondrial fusion. In addition, there are mainly PINK1/Parkin, Bnip3/Nix, and FUNDC1 pathways to regulate mitophagy, and PINK1/Parkin pathway is closely related to the regulation of mitochondrial function (51, 52). In this pathway, PINK1 selectively acts on the upstream of Parkin when mitochondria depolarize and accumulate on the damaged mitochondria to activate Parkin's translocation to the mitochondria, which then triggers mitophagy (53). Meanwhile, LC3B binds to P62 accumulated in the ubiquitinated mitochondrial matrix to initiate mitochondrial autophagy by mediating the entry of ubiquitinated substrates into autophagosomes (52). In our study, excessive V could reduce the mRNA levels of Parkin, PINK1, P62, LC3B, and the protein level of PINK1 leading to defective mitophagy in cardiomyocytes. Yu et al.'s (54) research showed that the high dose of heavy metal could cause serious damage to cells and mitochondria by inhibiting the mitophagy pathway. Therefore, we speculated that excessive V could damage cardiomyocytes severely, and mediated the defects of mitophagy by inhibiting the PINK1/Parkin signaling pathway, but the effects on other mitophagy pathways need to be further studied. Collectively, we found that V could induce MQC disorder in the heart of ducks. However, the interrelationship of multiple mechanisms within MQC needs further study.

Taken together, we found that excessive V could induce oxidative stress and MQC disorder in the heart of ducks, which provides a basis for exploring the toxicological mechanisms of V in the heart.

## DATA AVAILABILITY STATEMENT

The original contributions presented in the study are included in the article/supplementary material, further inquiries can be directed to the corresponding authors.

## ETHICS STATEMENT

The animal study was reviewed and approved by the Animal Ethics Committee of Jiangxi Agricultural University (Approval ID: JXAULL-2020-32).

## AUTHOR CONTRIBUTIONS

ZX, CX, TX, GL, YY, GH, and HC were responsibility for experiment conception, design, and practice. ZX, CX, and TX were involved in the drafting of the article. HC, FY, CZ, and XG revised the article.

## FUNDING

This work was supported by the National Natural Science Foundation of China (No. 31902333) and the Science and Technology Plan of Education Department of Jiangxi Province (GJJ190216).

## REFERENCES

1. Tripathi D, Mani V, Pal RP. Vanadium in biosphere and its role in biological processes. *Biol Trace Elem Res.* (2018) 186:52–67. doi: 10.1007/s12011-018-1289-y
2. Trevino S, Diaz A, Sanchez-Lara E, Sanchez-Gaytan BL, Perez-Aguilar JM, Gonzalez-Vergara E. Vanadium in biological action: chemical, pharmacological aspects, and metabolic implications in diabetes mellitus. *Biol Trace Elem Res.* (2019) 188:68–98. doi: 10.1007/s12011-018-1540-6
3. Crans DC, Henry L, Cardiff G, Posner BI. Developing vanadium as an antidiabetic or anticancer drug: a clinical and historical perspective. *Met Ions Life Sci.* (2019) 19:203–30. doi: 10.1515/9783110527872-014
4. Trevino S, Diaz A. Vanadium and insulin: partners in metabolic regulation. *J Inorg Biochem.* (2020) 208:111094. doi: 10.1016/j.jinorgbio.2020.111094
5. Andres-Delgado L, Mercader N. Interplay between cardiac function and heart development. *Biochim Biophys Acta.* (2016) 1863:1707–16. doi: 10.1016/j.bbamcr.2016.03.004
6. Eun-Jung P, Gwang-Hee L, Cheolho Y, Dong-Wan K. Comparison of distribution and toxicity following repeated oral dosing of different vanadium oxide nanoparticles in mice. *Environ Res.* (2016) 150:154–65. doi: 10.1016/j.envres.2016.05.036
7. Hadjiadamou I, Vlasiou M, Spanou S, Simos Y, Papanastasiou G, Kontargiris E, et al. Synthesis of vitamin E and aliphatic lipid vanadium(IV) and (V) complexes, and their cytotoxic properties. *J Inorg Biochem.* (2020) 208:111074. doi: 10.1016/j.jinorgbio.2020.111074
8. Jadiya P, Tomar D. Mitochondrial protein quality control mechanisms. *Genes.* (2020) 11:563. doi: 10.3390/genes11050563
9. Sarniak A, Lipińska J, Tytman K, Lipińska S. Endogenous mechanisms of reactive oxygen species (ROS) generation. *Postepy higieny i medycyny doswiadczalnej.* (2016) 70:1150–65. doi: 10.5604/17322693.1224259
10. Plamena RA, Andrey YA. Role of mitochondrial ROS in the brain: from physiology to neurodegeneration. *FEBS Lett.* (2018) 592:692–702. doi: 10.1002/1873-3468.12964
11. Long H, Ting H, Shabnam F, Linbao J, Tianyi L, Xi M. Antioxidants maintain cellular redox homeostasis by elimination of reactive oxygen species. *Cell Physiol Biochem.* (2017) 44:532–53. doi: 10.1159/000485089
12. Folarin OR, Adaramoye OA, Akanni OO, Olopade JO. Changes in the brain antioxidant profile after chronic vanadium administration in mice. *Metab Brain Dis.* (2018) 33:377–85. doi: 10.1007/s11011-017-0070-9
13. Scibior A, Kurus J. Vanadium and oxidative stress markers - in vivo model: a review. *Curr Med Chem.* (2019) 26:5456–500. doi: 10.2174/0929867326666190108112255
14. Bouchez C, Devin A. Mitochondrial biogenesis and mitochondrial reactive oxygen species (ROS): a complex relationship regulated by the cAMP/PKA signaling pathway. *Cells-Basel.* (2019) 8:287. doi: 10.3390/cells8040287
15. Abrisch RG, Gumbin SC, Wisniewski BT, Lackner LL, Voeltz GK. Fission and fusion machineries converge at ER contact sites to regulate mitochondrial morphology. *J Cell Biol.* (2020) 219:e201911122. doi: 10.1083/jcb.201911122
16. Tagaya M, Arasaki K. Regulation of mitochondrial dynamics and autophagy by the mitochondria-associated membrane. *Adv Exp Med Biol.* (2017) 997:33–47. doi: 10.1007/978-981-10-4567-7_3
17. Shili Z, Lin C, Chengyong H, Jing H, Nijun G, Jiazhang S, et al. Drp1 and RB interaction to mediate mitochondria-dependent necroptosis induced by cadmium in hepatocytes. *Cell Death Dis.* (2019) 10:1428–47.

18. Liu K, Jing MJ, Liu C, Yan DY, Ma Z, Wang C, et al. Effect of trehalose on manganese-induced mitochondrial dysfunction and neuronal cell damage in mice. *Basic Clin Pharmacol Toxicol.* (2019) 125:536–47. doi: 10.1111/bcpt.13316
19. Giuseppa V, Maria PB, Isa P, Pasquale S, Angela DP. Mitochondrial dysfunction by pro-oxidant vanadium: ex vivo assessment of individual susceptibility. *Environ Toxicol Phar.* (2015) 39:93–101. doi: 10.1016/j.etap.2014.11.008
20. Rizwan H, Pal S, Sabnam S, Pal A. High glucose augments ROS generation regulates mitochondrial dysfunction and apoptosis via stress signalling cascades in keratinocytes. *Life Sci.* (2020) 241:117148. doi: 10.1016/j.lfs.2019.117148
21. Ren ZZ, Zeng QF, Wang JP, Ding XM, Bai SP, Su ZW, et al. Effects of maternal dietary canthaxanthin and 25-hydroxycholecalciferol supplementation on antioxidant status and calcium-phosphate metabolism of progeny ducks. *Poult Sci.* (2018) 97:1361–7. doi: 10.3382/ps/pex402
22. Cui W, Guo H, Cui H. Vanadium toxicity in the thymic development. *Oncotarget.* (2015) 6:28661–77. doi: 10.18632/oncotarget.5798
23. Zhang L, Yang F, Li Y, Cao H, Huang A, Zhuang Y, et al. The protection of selenium against cadmium-induced mitophagy via modulating nuclear xenobiotic receptors response and oxidative stress in the liver of rabbits. *Environ Pollut.* (2021) 285:117301. doi: 10.1016/j.envpol.2021.117301
24. Zhang WX, He BM, Wu Y, Qiao JF, Peng ZY. Melatonin protects against sepsis-induced cardiac dysfunction by regulating apoptosis and autophagy via activation of SIRT1 in mice. *Life Sci.* (2019) 217:8–15. doi: 10.1016/j.lfs.2018.11.055
25. Li Q, Liao J, Lei C, Shi J, Zhang H, Han Q, et al. Metabolomics analysis reveals the effect of copper on autophagy in myocardia of pigs. *Ecotoxicol Environ Saf.* (2021) 213:112040. doi: 10.1016/j.ecoenv.2021.112040
26. Shi Q, Jin X, Fan R, Xing M, Guo J, Zhang Z, et al. Cadmium-mediated miR-30a-GRP78 leads to JNK-dependent autophagy in chicken kidney. *Chemosphere.* (2019) 215:710–5. doi: 10.1016/j.chemosphere.2018.10.019
27. Xue H, Cao H, Xing C, Feng J, Zhang L, Zhang C, et al. Selenium triggers Nrf2-AMPK crosstalk to alleviate cadmium-induced autophagy in rabbit cerebrum. *Toxicology.* (2021) 459:152855. doi: 10.1016/j.tox.2021.152855
28. Liu F, Wang XY, Zhou XP, Liu ZP, Song XB, Wang ZY, et al. Cadmium disrupts autophagic flux by inhibiting cytosolic Ca(2+)-dependent autophagosome-lysosome fusion in primary rat proximal tubular cells. *Toxicology.* (2017) 383:13–23. doi: 10.1016/j.tox.2017.03.016
29. Zhu S, Liu Y, Li Y, Yi J, Yang B, Li Y, et al. The potential risks of herbicide butachlor to immunotoxicity via induction of autophagy and apoptosis in the spleen. *Chemosphere.* (2021) 286:131683. doi: 10.1016/j.chemosphere.2021.131683
30. Song XB, Liu G, Liu F, Yan ZG, Wang ZY, Liu ZP, et al. Autophagy blockade and lysosomal membrane permeabilization contribute to lead-induced nephrotoxicity in primary rat proximal tubular cells. *Cell Death Dis.* (2017) 8:e2863. doi: 10.1038/cddis.2017.262
31. Ouyang Z, Yang B, Yi J, Zhu S, Lu S, Liu Y, et al. Exposure to fluoride induces apoptosis in liver of ducks by regulating Cyt-C/Caspase 3/9 signaling pathway. *Ecotoxicol Environ Saf.* (2021) 224:112662. doi: 10.1016/j.ecoenv.2021.112662
32. James MS, Hao C, Edward RP, Philip AB. Non-redox cycling mechanisms of oxidative stress induced by PM metals. *Free Radical Bio Med.* (2020) 151:26–37. doi: 10.1016/j.freeradbiomed.2019.12.027
33. Usende IL, Olopade JO, Emikpe BO, Oyagbemi AA, Adedapo AA. Oxidative stress changes observed in selected organs of African giant rats (Cricetomys gambianus) exposed to sodium metavanadate. *Int J Vet Sci Med.* (2018) 6:80–9. doi: 10.1016/j.ijvsm.2018.03.004
34. Zhang S, Che L, He C, Huang J, Guo N, Shi J, et al. Drp1 and RB interaction to mediate mitochondria-dependent necroptosis induced by cadmium in hepatocytes. *Cell Death Dis.* (2019) 10:523. doi: 10.1038/s41419-019-1730-y
35. Folarin OR, Snyder AM, Peters DG, Olopade F, Connor JR, Olopade JO. Brain metal distribution and neuro-inflammatory profiles after chronic vanadium administration and withdrawal in mice. *Front Neuroanat.* (2017) 11:58. doi: 10.3389/fnana.2017.00058
36. Liu J, Cui H, Liu X, Peng X, Deng J, Zuo Z, et al. Dietary high vanadium causes oxidative damage-induced renal and hepatic toxicity in broilers. *Biol Trace Elem Res.* (2012) 145:189–200. doi: 10.1007/s12011-011-9185-8
37. Hasnaa AE, Biswadeep D. Crosstalk between mitochondrial dysfunction, oxidative stress, and age related neurodegenerative disease: etiologies and therapeutic strategies. *Life Sci.* (2019) 218:165–84. doi: 10.1016/j.lfs.2018.12.029
38. Suma PR, Padmanabhan RA, Telukutla SR, Ravindran R, Velikkakath AKG, Dekiwadia CD, et al. Vanadium pentoxide nanoparticle mediated perturbations in cellular redox balance and the paradigm of autophagy to apoptosis. *Free Radical Bio Med.* (2020) 161:198–211. doi: 10.1016/j.freeradbiomed.2020.10.008
39. Zhao XJ, Li ZP, Wang JH, Xing XM, Wang ZY, Wang L, et al. Effects of chelated Zn/Cu/Mn on redox status, immune responses and hoof health in lactating Holstein cows. *J Vet Sci.* (2015) 16:439–46. doi: 10.4142/jvs.2015.16.4.439
40. Zhang C, Ge J, Lv M, Zhang Q, Talukder M, Li JL. Selenium prevent cadmium-induced hepatotoxicity through modulation of endoplasmic reticulum-resident selenoproteins and attenuation of endoplasmic reticulum stress. *Environ Pollut.* (2020) 260:113873. doi: 10.1016/j.envpol.2019.113873
41. Fan Y, Ruonan P, Zhuowei Z, Jianzhao L, Wenlan Y, Na Q, et al. Copper induces oxidative stress and apoptosis through mitochondria-mediated pathway in chicken hepatocytes. *Toxicol in Vitro.* (2019) 54:310–6. doi: 10.1016/j.tiv.2018.10.017
42. Yang S, Li P, Yu L, Li L, Long M, Liu M, et al. Sulforaphane protect against cadmium-induced oxidative damage in mouse Leydig cells by activating Nrf2/ARE signaling pathway. *Int J Mol Sci.* (2019) 20:630. doi: 10.3390/ijms20030630
43. Lang W, Qiuguo Y, Guo Z, Feili W, Yingying Z, Cong Y, et al. Single and combined exposures of waterborne Cu and Cd induced oxidative stress responses and tissue injury in female rare minnow (Gobiocypris rarus). *Comp Biochem Physiol C Toxicol Pharmacol.* (2019) 222:90–9. doi: 10.1016/j.cbpc.2019.04.013
44. Picca A, Calvani R, Coelho-Junior HJ, Landi F, Bernabei R, Marzetti E. Mitochondrial dysfunction, oxidative stress, and neuroinflammation: intertwined roads to neurodegeneration. *Antioxidants.* (2020) 9:647. doi: 10.3390/antiox9080647
45. Ferver A, Greene E, Wideman R, Dridi S. Evidence of mitochondrial dysfunction in bacterial chondronecrosis with osteomyelitis-affected broilers. *Front Vet Sci.* (2021) 8:640901. doi: 10.3389/fvets.2021.640901
46. Ai G, Kai L, Qian X. Fibroblast growth factor 19 alleviates palmitic acid-induced mitochondrial dysfunction and oxidative stress via the AMPK/PGC-1α pathway in skeletal muscle. *Biochem Bioph Res Co.* (2020) 526:1069–76. doi: 10.1016/j.bbrc.2020.04.002
47. Ge J, Zhang C, Sun YC, Zhang Q, Lv MW, Guo K, et al. Cadmium exposure triggers mitochondrial dysfunction and oxidative stress in chicken (Gallus gallus) kidney via mitochondrial UPR inhibition and Nrf2-mediated antioxidant defense activation. *Sci Total Environ.* (2019) 689:1160–71. doi: 10.1016/j.scitotenv.2019.06.405
48. Verónica E, Martin P, György H. Mitochondrial dynamics in adaptive and maladaptive cellular stress responses. *Nat Cell Biol.* (2018) 20:755–65. doi: 10.1038/s41556-018-0133-0
49. Murata D, Arai K, Iijima M, Sesaki H. Mitochondrial division, fusion and degradation. *J Biochem.* (2020) 167:233–41.
50. Hoppins S, Edlich F, Cleland MM, Banerjee S, McCaffery JM, Youle R, et al. The soluble form of bax regulates mitochondrial fusion via MFN2 homotypic complexes. *Mol Cell.* (2011) 41:150–60. doi: 10.1016/j.molcel.2010.11.030
51. Chen J, Su Y, Lin R, Lin F, Shang P, Hussain R, et al. Effects of acute diquat poisoning on liver mitochondrial apoptosis and autophagy in ducks. *Front Vet Sci.* (2021) 8:727766. doi: 10.3389/fvets.2021.727766
52. Yang F, Liao J, Yu W, Qiao N, Guo J, Han Q, et al. Exposure to copper induces mitochondria-mediated apoptosis by inhibiting mitophagy and the PINK1/parkin pathway in chicken (Gallus gallus) livers. *J Hazard Mater.* (2021) 408:124888. doi: 10.1016/j.jhazmat.2020.124888

53. Zhang Q, Zhang C, Ge J, Lv MW, Talukder M, Guo K, et al. Ameliorative effects of resveratrol against cadmium-induced nephrotoxicity via modulating nuclear xenobiotic receptor response and PINK1/Parkin-mediated mitophagy. *Food Funct.* (2020) 11:1856–68. doi: 10.1039/C9FO02287B
54. Yu W, Liao J, Yang F, Zhang H, Chang X, Yang Y, et al. Chronic tribasic copper chloride exposure induces rat liver damage by disrupting the mitophagy and apoptosis pathways. *Ecotoxicol Environ Saf.* (2021) 212:111968. doi: 10.1016/j.ecoenv.2021.111968

**Conflict of Interest:** The authors declare that the research was conducted in the absence of any commercial or financial relationships that could be construed as a potential conflict of interest.

**Publisher's Note:** All claims expressed in this article are solely those of the authors and do not necessarily represent those of their affiliated organizations, or those of the publisher, the editors and the reviewers. Any product that may be evaluated in this article, or claim that may be made by its manufacturer, is not guaranteed or endorsed by the publisher.

frontiers in Veterinary Science

ORIGINAL RESEARCH
published: 07 January 2022
doi: 10.3389/fvets.2021.819293

# *ABCC9* Is Downregulated and Prone to Microsatellite Instability on ABCC9tetra in Canine Breast Cancer

*Pan Hao, Kai-yue Song, Si-qi Wang, Xiao-jun Huang, Da-wei Yao* and De-ji Yang**

*College of Veterinary Medicine, Nanjing Agricultural University, Nanjing, China*

Tumorigenesis is associated with metabolic abnormalities and genomic instability. Microsatellite mutations, including microsatellite instability (MSI) and loss of heterozygosity (LOH), are associated with the functional impairment of some tumor-related genes. To investigate the role of MSI and LOH in sporadic breast tumors in canines, 22 tumors DNA samples and their adjacent normal tissues were evaluated using polyacrylamide gel electrophoresis and silver staining for 58 microsatellites. Quantitative real-time polymerase chain reaction, promoter methylation analysis and immunohistochemical staining were used to quantify gene expression. The results revealed that a total of 14 tumors (6 benign tumors and 8 breast cancers) exhibited instability as MSI-Low tumors. Most of the microsatellite loci possessed a single occurrence of mutations. The maximum number of MSI mutations on loci was observed in tumors with a lower degree of differentiation. Among the unstable markers, FH2060 (4/22), ABCC9tetra (4/22) and SCN11A (6/22) were high-frequency mutation sites, whereas FH2060 was a high-frequency LOH site (4/22). The ABCC9tetra locus was mutated only in cancerous tissue, although it was excluded by transcription. The corresponding genes and proteins were significantly downregulated in malignant tissues, particularly in tumors with MSI. Furthermore, the promoter methylation results of the adenosine triphosphate binding cassette subfamily C member 9 (ABCC9) showed that there was a high level of methylation in breast tissues, but only one case showed a significant elevation compared with the control. In conclusion, MSI-Low or MSI-Stable is characteristic of most sporadic mammary tumors. Genes associated with tumorigenesis are more likely to develop MSI. ABCC9 protein and transcription abnormalities may be associated with ABCC9tetra instability.

**Keywords: microsatellite instability, canine breast cancer, oncogenesis, the adenosine triphosphate binding cassette subfamily C member 9, loss of heterozygosity**

OPEN ACCESS

***Edited by:***
*Hui Zhang,*
*South China Agricultural University, China*

***Reviewed by:***
*Meng-yao Guo,*
*Northeast Agricultural University, China*
*Xiaobing Li,*
*Yunnan Agricultural University, China*

****Correspondence:***
*Da-wei Yao*
*yaodawei@njau.edu.cn*
*De-ji Yang*
*djyang@njau.edu.cn*

***Specialty section:***
*This article was submitted to Animal Nutrition and Metabolism, a section of the journal Frontiers in Veterinary Science*

***Received:*** *21 November 2021*
***Accepted:*** *06 December 2021*
***Published:*** *07 January 2022*

***Citation:***
*Hao P, Song KY, Wang SQ, Huang XJ, Yao DW and Yang DJ (2022) ABCC9 Is Downregulated and Prone to Microsatellite Instability on ABCC9tetra in Canine Breast Cancer. Front. Vet. Sci. 8:819293. doi: 10.3389/fvets.2021.819293*

## INTRODUCTION

Tumorigenesis is a complex multistep process associated with metabolic abnormalities and genomic instability (1). Studies have shown that tumor cells differ significantly from normal cells in terms of ion channel expression activity and membrane potential (2, 3). Through electrochemical synapse ionic coupling networks, tumor cells can induce or inhibit the occurrence and metastasis of tumors (4). The adenosine triphosphate (ATP)-binding cassette subfamily C, member 9 (ABCC9) can be matched with potassium channel proteins Kir6.1 (KCNJ8) or Kir6.2 (KCNJ11) to assemble

ATP sensitive $K^+$ channels ($K_{ATP}$) in the heart, pancreaticislets, skeletal muscle and smooth muscle (5). The $K_{ATP}$ channel is controlled by G proteins and allows potassium to flow into the cell. Previous studies have found that blocking the activity of $K_{ATP}$ channels can significantly inhibit the proliferation of glioma and xenografted cells, inhibit the cell cycle at the G0/G1 phase, and induce apoptosis (6, 7). In contrast, the opening of $K_{ATP}$ located on the mitochondrial membrane can attenuate cell apoptosis by maintaining the mitochondrial membrane potential (8).

As short tandem repeat DNA motifs (1–6 bp), microsatellites (MS) are ubiquitous in the eukaryotic genome, and the mutational rate of insertions/deletions in MS sequences is 10–100 times higher than that of traditional gene coding sequences. In 1993, cancer geneticists first discovered loss of heterozygosity (LOH) and microsatellite instability (MSI) in colorectal tumor tissues as a result of DNA mismatch-repair pathway obstruction, revealing a new pathway for oncogenesis (9). A previous study revealed that MSI is associated with clinical and pathological features in tumor tissues (10). Patients with the MSI-positive phenotype have a more robust T lymphocyte response than microsatellite-stable (MSS) cancer patients (11, 12). In addition, recent studies have shown that the diagnosis of MSI is tissue-specific, with varying frequency and prognostic values across multiple cancer types (13–15).

Mammary tumors as the common disease in female dogs. The MSI in canine mammary tumors (CMTs) has not been well-studied. Therefore, the aim of this trial was to investigated the relationship between MSI and tumor formation by screening MS loci in CMTs.

# METHODS

## Material Collection and Histopathology Examinations

Twenty-two CMTs from different breeds of female dogs were provided by the Teaching Hospital of Nanjing Agricultural University. Procedures were approved by the Animal Ethics Committee of Nanjing Agricultural University (NJAU - 20171019, 10 October 2017). Experiment operates were performed under the Guidelines for Care and Use of Laboratory Animals of Jiangsu province (SYXK2017 - 0027). The mean age of the 22 canine patients was 9.77 ± 0.50 years, and the main breed was poodles (7/22, 31.8%). The adjacent normal and mammary gland tumors were excised; half of the samples were fixed in 10% formalin solution, and the remaining samples were stored at −80°C for further DNA and RNA extraction. The fixed samples were processed in a series of graded ethanol solutions and cleared with xylene. The samples were then embedded in paraffin, sectioned at 4 μm thickness, and stained with hematoxylin and eosin. Each stained tumor and its matched non-neoplastic tissue were examined using light microscopy.

## DNA Extraction and Microsatellite Locus Identification

DNA was isolated using the Animal Tissues/Cells Genomic DNA Extraction Kit (Solarbio Science & Technology Co., Beijing, China). Based on the instructions, 25 mg of tissue sample was used. The concentration and purity were estimated using a NanoDrop 2000 (Thermo Fisher Scientific, Waltham, MA, USA). The polymerase chain reaction (PCR) was performed using 500 ng of total DNA and TaKaRa Premix Taq™ according to the manufacturer's recommendations (Takara Co., Otsu, Japan). Genomic microsatellite loci were identified as described in our previous study (16), **Table 1** shows the 58 pairs of primers used in this research. The cycle conditions were as follows: an initial incubation of 94°C for 5 min followed by 30 cycles of 30 s at 94°C, 30 s at their Tm (56–60°C), 30 s at 72°C, and finally extension at 72°C for 10 min. PCR amplified fragments were separated by 10% denatured polyacrylamide gel electrophoresis for 8 h at 100 V; mutations were observed by silver staining.

MSI was defined as addition or deletion of fragments to one or both tumor DNA alleles compared with normal tissues; LOH was defined as a reduction in the DNA signal intensity of tumor allele at least 50% (17). Positive cases were repeated three times to confirm the results. For MSI identification, mutation products were purified and cloned into the pMD19-T vector (Takara Co., Otsu, Japan) and sequencing. Sequence alignments were conducted using DNAMAN software v9.0.1.

## RNA Extraction and mRNA Analysis

Total RNA was isolated using the Total RNA Extraction Kit (Solarbio Science & Technology Co., Beijing, China). Based on the instructions, 100 mg of tissue sample was used. The size of the RNA samples was estimated using a NanoDrop 2000 (Thermo Fisher Scientific, Waltham, MA, United States). Reverse transcription was performed using 800 ng of total RNA treated with DNase I and PrimeScript RT Master Mix Perfect Real Time according to the manufacturer's instructions (Takara Co., Otsu, Japan).

The mRNA levels of MSI-mutated adjacent genes were detected by quantitative real-time PCR (QRT-PCR). Target sequences were amplified using Green Fast qPCR Mix (Takara Co., Otsu, Japan) and analyzed with an ABI 7300 instrument (Applied Biosystems, Foster City, CA, USA). The primer information is presented in **Table 1**. The cycle conditions were as follows: 95°C for 15 s followed by 95°C for 5 s and 60°C for 31 s for 40 cycles. The specific of each gene primer was confirmed by melting curve performance and gel electrophoresis. Results were presented as CT mean values of three technique replicates.

Reference genes were evaluated using geNorm v3.5 and NormFinder v0.953. Finally, the geometric means of *A5B*, *RPL8*, *GAPDH*, *RPL32*, *RPS5*, *β-actin*, and *HRPT* were used for normalization.

## DNA Methylation Analysis

DNA methylation was measured using next-generation sequencing based bisulfite sequencing PCR (18). First, DNA modification with sodium bisulfite of 6 canine breast cancers and matched samples was performed using an EZ DNA

**TABLE 1 |** Primer informations.

| Type | Primers | Genomic location | Amplicon size (bp) |
|---|---|---|---|
| **Microsatellites** | | | |
| FH2305 | F:TCATTGTCTCCCTTTCCCAG | CFA 30 | 208 |
| | R:AAGCAGGACATTCATAGCAGTG | | |
| CDK6B | F:TTGGGGCCAGATGTTGTTAG | CFA 14 | 285 |
| | R:GAAGGAAAAGAGAAACAAGGCAA | | |
| AHTK209 | F:AGTGGTAGGTGTTCCAGCCG | CFA 20 | 91 |
| | R:TCGACCTCTTGAGATAACAA | | |
| C22.763 | F:CAGCCCACTTCCTGGAAATA | CFA 22 | 206 |
| | R:GACCAGTGTGCATTAAGCC | | |
| AHT117 | F:GCCTGCGTGGTACACACACA | CFA 1 | 84 |
| | R:GTTTACCTGCCATCATCTCA | | |
| REN287B11 | F:CAGATTCCAGGTTGGGAAGA | CFA 5 | 348 |
| | R:AGCTGTAGGATACGCCGAGA | | |
| REN122J03 | F:GTGCGAGTCATCAACAAAT | CFA 5 | 197 |
| | R:ACTAAAGCCCATAAATCGTG | | |
| FH3837 | F:GGCCTCGTAGAATACATTTGG | CFA 5 | 325 |
| | R:AGCAAGGAAGGCATCTGG | | |
| CDK6A | F:TAACTTTTATTTATTTATGATA | CFA 6 | 163 |
| | R:GGCGCCTGCCTTTGGCCCAG | | |
| ABCC9ca | F:TCCAAGGTTTGTGTAAGGGT | CFA 27 | 240 |
| | R:GGATTCAAGGTATATGCCCA | | |
| HIVEP3 | F:ACAGTCAAGGGTGCAAGAA | CFA 15 | 264 |
| | R:ATGGCTCAGCGGTTTAGTGT | | |
| TBC1D5 | F:TGCCAGGCAATTACAAAAGA | CFA 23 | 291 |
| | R:GCAGAAATCCTTGAAGCCAG | | |
| ORF133 | F:TACTTCTGTGTTCATCATCC | CFA 12 | 333 |
| | R:GCTTTATTCAAGTATGCTTA | | |
| REN49F22b | F:GGGGCTCTGTTATTAGGTG | CFA 22 | 154 |
| | R:TCATAAGGCAAAGAAAACC | | |
| 15F11 | F:TCTGGCTAGAGGTTTATCCA | CFA 6 | 234 |
| | R:ACACAGGCCTAACTCAAGAA | | |
| REN41F10 | F:TACCCCAATGTTTACTGC | CFA 2 | 221 |
| | R:TATTTGTCTATTTTGCTCTGA | | |
| SLCA4 | F:TATGCCTTGAGACTTCATCC | CFA 13 | 168 |
| | R:CCAGAAAGAATCTAATCCCAC | | |
| DKFZ | F:CTGGATCCTTTTCCTGTGGA | CFA 34 | 132 |
| | R:AGGACACCTGTTGTTCTTGG | | |
| FLJ32685 | F:CTGCCTCAGCTGGGAAAATA | CFA 23 | 436 |
| | R:CACTACAGCTGGGATCAGCA | | |
| LRFN2A | F:TGGTTCAGTTCGTTGAGTGC | CFA 12 | 316 |
| | R:ATGTCTGTGGTGACGCAAAA | | |
| WNT2B | F:TGATACTGCCAGTCAGCAGG | CFA 17 | 277 |
| | R:GAGGGAGGAGAACCTTGGTC | | |
| LPP | F:TCAGTGAGGCAGATTTGGTG | CFA 34 | 415 |
| | R:CAAACGCCTTGCTTCTTGTC | | |
| MLH1 | F:GGTTTAGTGCCGCCTTCAC | CFA 1 | 297 |
| | R:GAGAAATGCTATGTGGCAAA | | |
| REN47D17 | F:GGCACTTGAGCTCTAATCCTA | CFA 1 | 346 |
| | R:TGCTAATGAATCCACAGAATG | | |
| REN47J11b | F:TCTCCTCGCGTGTTTCTG | CFA 18 | 170 |
| | R:GGGGACACTCAGAAGGACG | | |

*(Continued)*

**TABLE 1 |** Continued

| Type | Primers | Genomic location | Amplicon size (bp) |
|---|---|---|---|
| C26.733 | F:CCCTCTACTTATGTCTCGGCC | CFA 26 | 255 |
| | R:GAGAGGAGAAACAACCAACACC | | |
| CXX.279 | F:TGCTCAATGAAATAAGCCAGG | CFA 22 | 128 |
| | R:GGCGACCTTCATTCTCTGAC | | |
| C08.410 | F:GAGGAAAACCAAGTGATTTTGG | CFA 8 | 114 |
| | R:ACCTGCAAGTGACCCTCTCT | | |
| FH2516 | F:AATGGATGGAACTTAGGGCA | CFA 36 | 190 |
| | R:CTGCATCTGGTAACCATCGA | | |
| TRERFI | F:TTTGACCCCCCAAATGATAAA | CFA 12 | 164 |
| | R:CAACCGCTAAGCCACTCAG | | |
| MAML1 | F:GTGATCCTGGAGTCCCGGAA | CFA 11 | 212 |
| | R:CACACAATGTCACGGAGGAGG | | |
| TPK1 | F:AAACATACTTTTCTACATGGTT | CFA 16 | 167 |
| | R:TTGTAATTGTGACAGATCATAG | | |
| RYR3 | F:CATGCAGATGCCCCTAATCT | CFA 30 | 165 |
| | R:GGTGACAGGTGATTCTTGGA | | |
| CXX873 | F:CTGGCAGATTACAGGTAGC | CFA 11 | 145 |
| | R:GTTCTCCAAAGCACTCAT | | |
| C01.424 | F:AGCTTAGCTTACTGCCCTGG | CFA 1 | 176 |
| | R:TCCTTTGGTTTTTAGCAGGG | | |
| HLA | F:ATCAACAATGCATGCCACAT | CFA 7 | 407 |
| | R:GAGGAGGTGGGGAGATTGGC | | |
| CPH14 | F:GAAAGACAATCCCTGAAATGC | CFA 5 | 193 |
| | R:ACCCCATTTATGAGAATCATGT | | |
| ABCC9tetra | F:GCATTAAGGAGGGCACTTGA | CFA 27 | 219 |
| | R:TAAGACCCAGCCTTGA | | |
| FH2060 | F:GTTTTGAGGAAGCCTTGCTG | CFA 14 | 222 |
| | R:GAAGGAAGGGGCCAGTATTC | | |
| SCN10A | F:TCCAAGCATCCTCTTATCCA | CFA 23 | 196 |
| | R:CCACGTTGGTCTCCCTACTTA | | |
| ANGPT1 | F:GTTTTCCTGCTGTCCCAGTG | CFA 13 | 390 |
| | R:TTCCCTTTTGTGAATCCTGC | | |
| SCN11A | F:GCAGTTTGGGGACTGCTAAA | CFA 23 | 260 |
| | R:AGAATGGAATCTTGCCCAGA | | |
| IGHE | F:CAAGACTGGCTCTGCTCTG | CFA 8 | 141 |
| | R:CCACTGAAAACAAGCCCATC | | |
| CDH4 | F:AAGTCAACAAGCTCCATCCC | CFA 24 | 136 |
| | R:AGGATTTTCCCCTAAGAGCTG | | |
| PPP1R9A | F:TAAAGATCCAAGTGGCGAGG | CFA 14 | 189 |
| | R:AACCACTCCCTTCACCACAG | | |
| 9A5 | F:GTCTGCTTTCAACTCAGGTC | CFA 4 | 266 |
| | R:CTCTAAACTGGACTTCGTGG | | |
| FH2401 | F:CTGATTCTGCCCATTGGG | CFA 12 | 224 |
| | R:ATGTAAGCTCTACTGGGGTACTGG | | |
| FH2377 | F:TCCCTTGGGGAAGTAGAGTG | CFA 34 | 312 |
| | R:TAGCTAATGTGGTTAACGGTTACC | | |
| REN198P23 | F:TTGTACATTATCTGTTCTACCTCGG | CFA 9 | 132 |
| | R:TCTTCAGCAGGCCTTTTCTC | | |
| AHT137 | F:TACAGAGCTCTTAACTGGGTCC | CFA 11 | 137 |
| | R:CCTTGCAAAGTGTCATTGCT | | |
| FH3113 | F:CTGAATTATGGGAAAACATGG | CFA 5 | 207 |

*(Continued)*

**TABLE 1** | Continued

| Type | Primers | Genomic location | Amplicon size (bp) |
|---|---|---|---|
| | R:CAGGGAAGGAAGAAAACAGC | | |
| FH2594 | F:TTTAAGGAGCTGCTCATGCA | CFA 5 | 311 |
| | R:CTGAAATTCCTGGCCCAGTA | | |
| FH2561 | F:TGCTCAAGGTTGAATAAATATGC | CFA 6 | 364 |
| | R:TTTATGGCCTGTGGGCTC | | |
| FH2175 | F:TTCATTGATTTCTCCATTGGC | CFA 16 | 253 |
| | R:AGGACTCTAAAAACTTGCCTCC | | |
| FH2495 | F:ATTTCATATGTGAGGCTGAGATTG | CFA 24 | 132 |
| | R:CAGTGGGAGAAAGATGCCAT | | |
| BTN1A1 | F:CTGCCATGTAGGGTGTTT | CFA 12 | 240 |
| | R:ACCCTTTGACAAGAGCTC | | |
| CPH5 | F:TCCATAACAAGACCCCAAAC | CFA 17 | 114 |
| | R:GGAGGTAGGGGTCAAAAGTT | | |
| C13.900 | F:TTGGACTTCTAATTTTTCATT | CFA 13 | 128 |
| | R:CAACTGACTAAATCTCCTAATG | | |
| **Genes** | | | |
| *GAPDH* | F:ACCACAGTCCATGCCATCAC | U94889 | 268 |
| | R:CCTGCTTCACCACCTTCTTGA | | |
| *A5B* | F:GCACGGAAAATACAGCGTTT | NM_001686 | 187 |
| | R:TTGCCACAGCTTCTTCAATG | | |
| *HPRT* | F:TGCTCGAGATGTGATGAAGG | NM_000194 | 192 |
| | R:TCCCCTGTTGACTGGTCATT | | |
| *β-actin* | F:GATATCGCCGCGCTCGTCGTC | U39357 | 384 |
| | R:GGCTGGGGTGTTGAAGGTCTC | | |
| *RPS5* | F:GGATGACCGAGTGGGAGA | XM_022427163 | 122 |
| | R:TGCAATGTAGTCCTGCAAAGA | | |
| *RPL8* | F:AGGTCATTTCTTCCGCCAA | XM_853403 | 164 |
| | R:AGGATGCTCCACAGGATTCA | | |
| *RPL32* | F:ATGCCCAACATTGGTTATGG | XM_540107 | 181 |
| | R:CTCTTTCCACGATGGCTTTG | | |
| *ABCC9* | F:TGTGCATCATCTGTTTTTGTGCT | NC_006609 | 183 |
| | R:TTAGGGCCTGCTATGGGCTA | | |
| **BSP analysis** | | | |
| ABCC9-1 | F:AGAGTGGAGGAGGGAGAAGTAGGTTTTATG | | 265 |
| | R:CAAACAATCCCCRAACACACACCTAAATATC | | |
| ABCC9-2 | F:GTGATAAATAGTTTYGGGGGGTAGTTGG | | 228 |
| | R:ACCTAAAAAAACTAAAACCRACCCCCCC | | |

Methylation Kit (Zymo Research, Irvine, CA, USA) according to the manufacturer's protocol. The sequence included 2,000 bp upstream of the *ABCC9* transcription start site and 1,000 bp downstream (a total of 3 kb). Elution products were then used as templates for PCR amplification with 35 cycles using the KAPA 2G Robust HotStart PCR Kit (Kapa Biosystems, Wilmington, MA, USA). The primers for BSP were designed using online MethPrimer software (**Table 1**). The bisulfite sequencing PCR products of each sample were pooled equally, 5'-phosphorylated, 3'-dA-tailed and ligated to a barcoded adapter using T4 DNA ligase (Thermo Fisher Scientific, Foster city, CA, USA). The barcoded libraries were then prepared and sequenced on an Illumina platform. Using the clean sequencing reads directly aligned to the target sequences, Bsmap v2.73 software was used with the default parameters. Methylation level was defined as the fraction of "C" read counts in the total read counts of both "C" and "T" for each covered C site. According to the method of Lister (19), each methylation context calculates the probability mass function, and only those CGs covered by at least 200 reads in one sample were considered for testing.

## Immunohistochemical Analysis

Tissue sections were taken from 22 CMTs along with adjacent controls after fixation in 4% paraformaldehyde, dehydration, and embedding in paraffin. The expression of ABCC9 (1:200, Affinity Biosciences Cat# DF9255) in the breast was examined

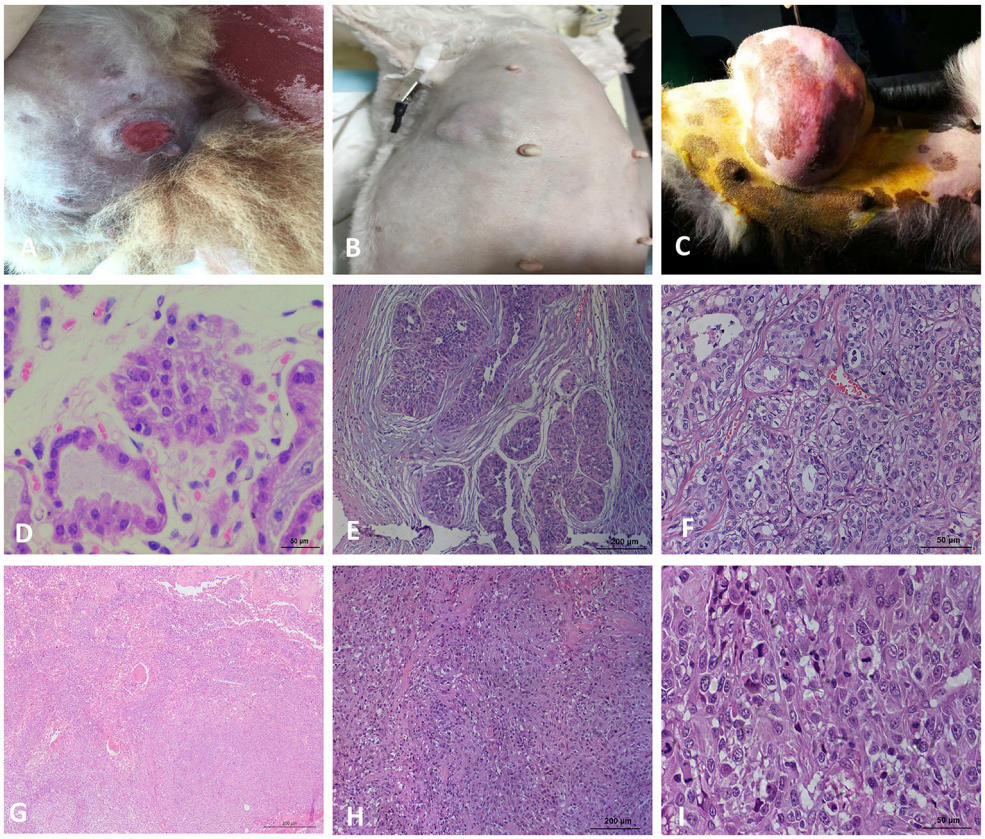


**FIGURE 1 |** Macroscopic observation and HE staining of CMTs. **(A)** Macroscopic observation of CMT, the skin surface of the tumor ruptured. **(B)** Macroscopic observation of CMT, a cauliflow-like mass in mammary gland with obviously boundary and hard texture. **(C)** Macroscopic observation of CMT, the tumor located on the mammary tissue with a great size. **(D)** HE staining of the breast lobules in a normal dog (400×). **(E)** HE staining of mammary gland adenoma (200×), the capsule is intact and tumor cells grow in the enlarged lumen. **(F)** HE staining of mammary gland adenoma (400×), Adenoma arising in the glandular tissue, myoepithelial cells are inconspicuous, the islands of neoplastic cells are separated by a fine fibrovascular connective. **(G)** HE staining of solid carcinoma (200×). **(H)** HE staining for ductal carcinoma (200×), tumor cells invaded the connective tissue, glandular ducts were disappeared. **(I)** HE staining for ductal carcinoma (400×), tumor cells are pleomorphic and mitotic.

using an SP immunohistochemistry kit (Sangon Biotech Co., Shanghai, China) according to the manufacturer's instructions. A semiquantitative determination was conducted with Image J software to detect protein expression. The immunohistochemical staining intensity was expressed in average optical density (AOD) units, AOD = integrated optical density (IOD)/Area; five fields were randomly selected in a blinded manner, counted for the signal density of tissue areas, and then statistically analyzed.

## Data Analysis and Statistics

The statistical analyses were conducted with GraphPad Prism software version 8.0 and SPSS version 21.0. A genome map of microsatellite loci was constructed using the MapChart program. The comparison of results between MSI/LOH and tumor type and methylation data were performed using Fisher's exact test. The Mann–Whitney *U*-test was used to analyze vs. benign and breast cancer groups. The relative mRNA expression levels of *ABCC9* in tumors and matched normal tissues were calculated using the $2^{-\Delta\Delta Ct}$ method. The *t*-test was performed to compare the relative mRNA level and protein expression between the two groups. The results are presented as the mean ± SD. The statistical significance was set at $p < 0.05$ for all analyses.

# RESULTS

## The Pathological Identification of CMTs

The 22 CMTs were classified as either benign (8/22, 36.4%) or malignant (14/22, 63.6%) (**Figure 1**). Based on the predominant cell type, the benign tumors were subclassified as fibroadenoma (4/8, 50%), complex adenoma (1/8, 12.5%), adenoma (1/8, 12.5%), or intraductal papilloma (2/8, 25%). The malignant tumors were subclassified into invasive ductal carcinoma (7/14, 50%), situ carcinoma (1/14, 7.1%), ductal carcinoma (1/14, 7.1%), complex carcinoma (2/14, 14.3%), intraductal papillary carcinoma (2/14, 14.3%), or solid carcinoma (1/14, 7.1%).

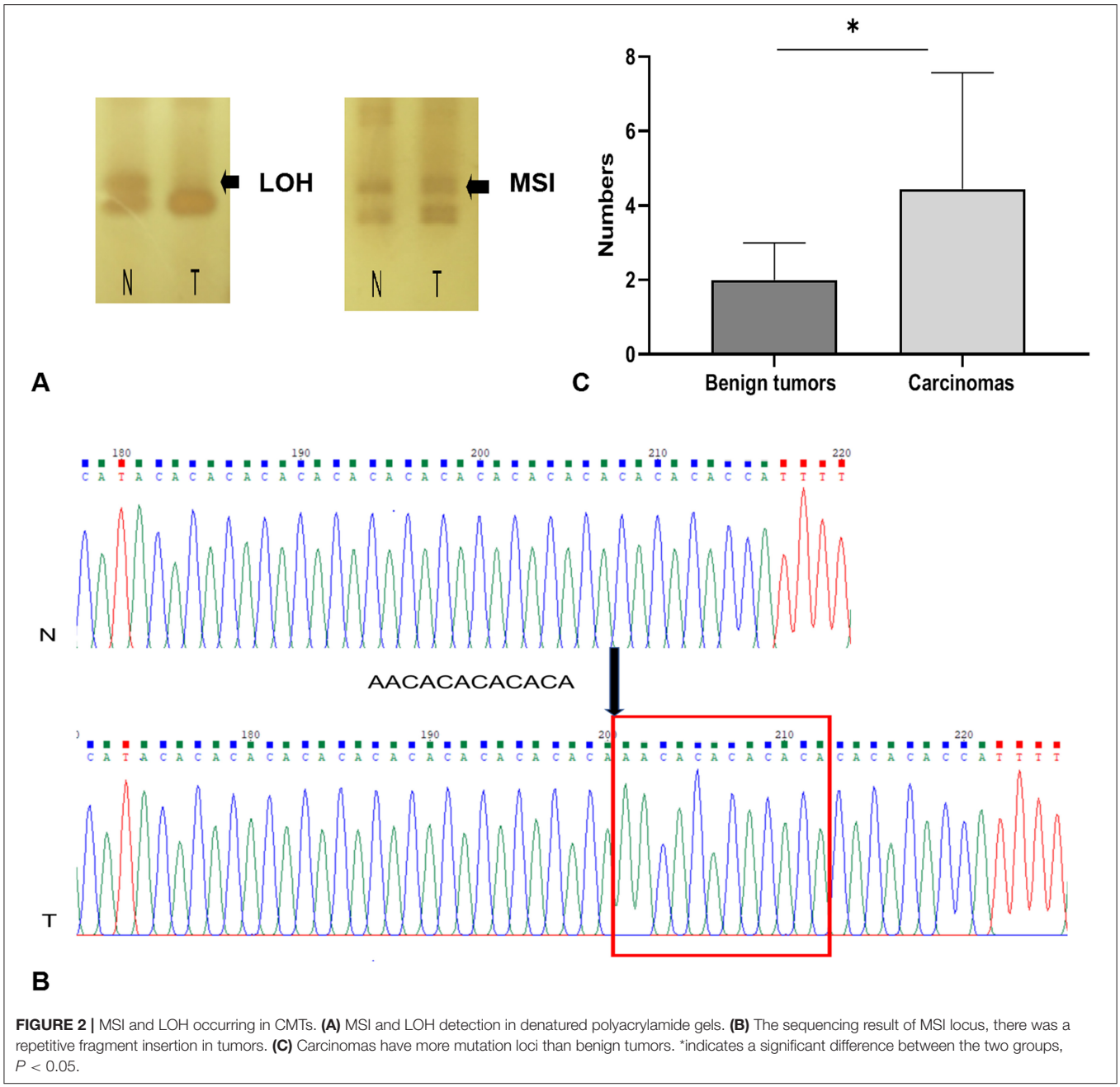


**FIGURE 2 |** MSI and LOH occurring in CMTs. **(A)** MSI and LOH detection in denatured polyacrylamide gels. **(B)** The sequencing result of MSI locus, there was a repetitive fragment insertion in tumors. **(C)** Carcinomas have more mutation loci than benign tumors. *indicates a significant difference between the two groups, $P < 0.05$.

## Malignant Tumors Have More MS Mutation Loci Than Benign Tumors

Using the panel of 58 MS markers, a LOH/MSI analysis between tumor tissues and their matched non-neoplastic tissues was carry out, the variation in the electropherogram of MS makers was described in **Figure 2A**. Differential bands were extracted and sequenced (**Figure 2B**). The sequencing result verified that the mutation form of MS in CMTs mainly included the insertion or deletion of nucleic acid fragments in repeated sequences. In addition, point mutations were also discovered in flank conserved sequences of MSI loci. Based on the National Cancer Institute guidelines (20), 14 tumors (14/22, 63.6%) were defined as MSI-L (MSI-Low), and 8 tumors were defined as MSS (MSI-Stable) (**Table 2**). Of the MSI-L tumors, 5 were diagnosed as benign tumors, and 9 were diagnosed as breast cancers. In addition, we found that the phenomenon of LOH was present in 6 MSI-L tumors (6/14, 42.9%), of which 2 tumors were benign and 4 tumors were malignant. There was no evidence of a difference in mutation rates between MSI and LOH in benign or malignant tumors (Fisher's test, $P > 0.05$). However, the histological type was significantly correlated with the number of MSI loci. Malignant tumors had more MS mutation loci than

**TABLE 2 |** Information of canine mammary tumors.

| Case no. | Age | Breed | Tumor Histo-type | MSI/LOH mutation | Tumor type |
|---|---|---|---|---|---|
| 1 | 8 | Pomeranian | Intraductal papilloma | | MSS |
| 2 | 9 | Golden retriever | Invasive ductal carcinoma | MSI | MSI-L |
| 3 | 13 | Mongrel dog | Invasive ductal carcinoma | MSI | MSI-L |
| 4 | 8 | Poodle | Situ carcinoma | MSI/LOH | MSI-L |
| 5 | 12 | Pomeranian | Complex adenoma | | MSS |
| 6 | 11 | Poodle | Adenoma | MSI/LOH | MSI-L |
| 7 | 11 | Mongrel dog | Ductal carcinoma | MSI | MSI-L |
| 8 | 5 | Poodle | Fibroadenoma | | MSS |
| 9 | 9 | Schnauzer | Complex carcinoma | | MSS |
| 10 | 8 | Bichon Frise | Intraductal papillary carcinoma | MSI | MSI-L |
| 11 | 11 | Rottweiler | Complex carcinoma | MSI/LOH | MSI-L |
| 12 | 9 | Samoyed | Fibroadenoma | MSI | MSI-L |
| 13 | 12 | Border Collie | Solid carcinoma | MSI/LOH | MSI-L |
| 14 | 10 | Poodle | Invasive ductal carcinoma | MSI/LOH | MSI-L |
| 15 | 7 | Poodle | Fibroadenoma | MSI | MSI-L |
| 16 | 9 | Poodle | Intraductal papillary carcinoma | | MSS |
| 17 | 13 | Mongrel dog | Invasive ductal carcinoma | MSI | MSI-L |
| 18 | 10 | Samoyed | Invasive ductal carcinoma | | MSS |
| 19 | 5 | Poodle | Invasive ductal carcinoma | | MSS |
| 20 | 13 | Mongrel dog | Intraductal papilloma | MSI/LOH | MSI-L |
| 21 | 10 | Yorkshire | Invasive ductal carcinoma | | MSS |
| 22 | 12 | Mongrel dog | Fibroadenoma | MSI | MSI-L |

benign tumors ($P < 0.05$) (**Figure 2C**). Case 13 had the highest frequency of MSI (10/58, 17.2%) in this study, which was defined by pathological grading as grade III.

## Tetranucleotide Microsatellites Are Prone to Instability in CMTs

A total of 44 aberrations of MSI were found at 27 MS loci (27/58, 46.5%), which were distributed across 17 chromosomes (**Figure 3**). The classification of mutated MS markers in this study was shown in **Table 3**. In addition to dinucleotide [CA]n, tetranucleotide [CTTT]n and more complex types of microsatellite loci also has a high mutation frequency in this research. Among them, most of MS loci were only mutated once (1/14, 7.1%). The interrupted marker SCN11A (6/14, 42.9%) and tetranucleotide markers FH2060 (4/14, 28.6%) and ABCC9tetra (4/14, 28.6%) were loci with high mutation rate from the result. Moreover, the phenomenon of LOH was also observed on FH2060 (4/6, 66.75%), SCN11A (2/6, 33.3%), ABCC9tetra (1/6, 16.7%) and PPP1RA (1/6, 16.7%). **Table 4** shows the mutation results for ABCC9tetra, FH2060 and SCN11A markers in CMTs. There were five tumor cases had at least two loci mutated as MSI or LOH for ABCC9tetra, FH2060 and SCN11A. Because of the locus of ABCC9tetra was only mutated in malignant group, the relationship between ABCC9tetra and breast cancer were studied.

## ABCC9 Is Downregulated in Canine Breast Cancer

NCBI revealed that ABCC9tetra was located in the intron region of *ABCC9*, and the mutation in this locus did not cause a frameshift mutation in open reading frame. But the result of QRT–PCR showed that the mRNA level of *ABCC9* was significantly downregulated in the malignant group ($P < 0.05$) (**Figure 4A**). And the result of immunohistochemistry was similar to it. The AOD value showed that the expression of ABCC9 protein in malignant tumors was significantly lower than that in para-cancer tissues and benign tumors ($P < 0.05$) (**Figure 4B**). Strongly positive cells can be observed in normal and para-cancer tissues (**Figure 4C**) and even in benign tumors (**Figure 4D**). However, the number of ABCC9 positive cells was significant decreased in malignant tumors (**Figure 4E**). Moreover, the expression of ABCC9 protein may be related to the cellular composition and pathological grading. In the tumor sample of grade III, ABCC9 strongly positive cells almost disappeared, and were only weakly or micro-expressed in cells (**Figure 4F**). In addition, ABCC9 protein expression and mRNA levels were significantly reduced

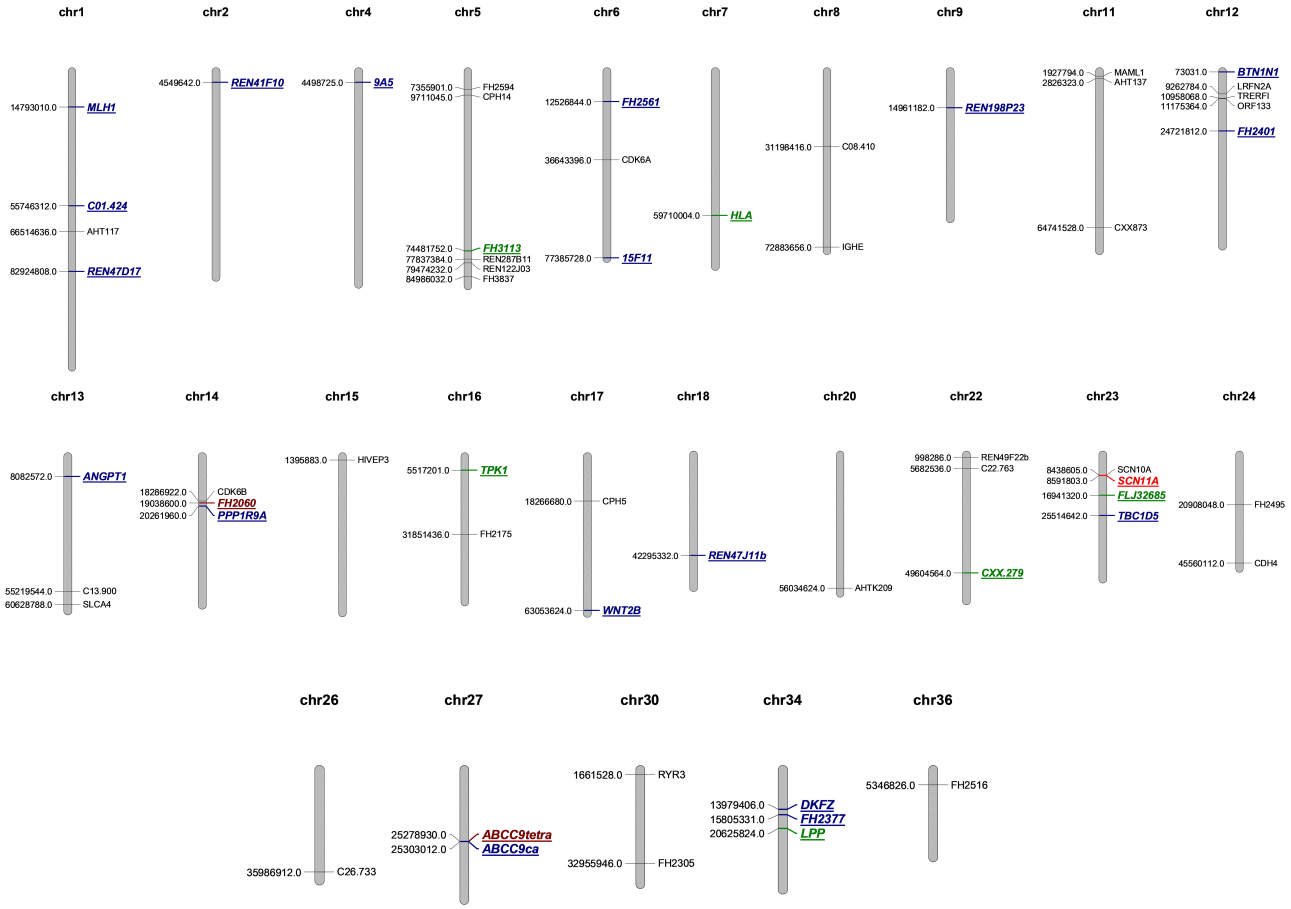


**FIGURE 3 |** Genome map of microsatellite loci in this study. MSS are depicted in black, the single mutation of microsatellite loci is labeled blue, twice mutation is green, four times mutation is brown, and six is marked in red.

in tumor samples with ABCC9tetra locus instability ($P < 0.05$).

Total of 6 tumor sample with *ABCC9* mRNA levels significantly reduced were tested by methylation analysis. MathPrimer software detected a 703 bp CpG island in *ABCC9* 5′UTR (GC = 65.4%, and Obs/Exp ratio = 0.92). The methylation results of *ABCC9* promoter CpG island revealed that high levels of methylation occurred at multiple sites in cancer tissues, but no new methylation sites were formed (**Figure 5A**). There was no significant difference in methylation level of each site (**Figure 5C**). And only one cancer sample showed significantly higher promoter methylation level than the control tissue ($P < 0.05$), with both MSI and LOH (**Figure 5B**).

## DISCUSSION

Genomic instability is a hallmark of tumors, and tumor tissue has a higher mutation rate than non-tumor tissue. Study showed that the sensitivity of MSI detection is not limited by tumor heterogeneity or normal tissue contamination when large resection tissues are used (21). The most endorsed explanation of MS mutagenesis is the slip strand mispairing model, and repeated numbers of motifs are highly polymorphic among individuals. A previous study of an MS mutation model showed that deletion is produced by the misalignment loop in the template chain, and insertion is subsequently produced in the nascent chain (22, 23). According to the sequence alignment analysis, we found that MS mutations mainly included the insertion or deletion of repeat sequences and point mutations of flanking conserved sequences. In addition, in the same MS locus, the forms of the mutations were differed among the samples. This phenomenon may be due to the mutation of MS occurring at different stages of tumor cell replication, whereas the point mutation may be caused by the suppression of mismatch repair genes. The length and unit type of MS and DNA shape are the main factors influencing DNA fragility and have the greatest influence on the mutation rate (24). In addition to dinucleotides, tetranucleotides and interrupted MS also showed frequent mutations in our research, which confirmed the susceptibility of the DNA structure to mutation.

The guidelines of the National Cancer Institute suggest that MS that display instability at $\geq$ 2 loci or instability at $\geq$ 30–40%

**TABLE 3 |** Classification of mutated microsatellite DNA markers.

| Motif | Marker | Sequence | Number |
|---|---|---|---|
| Pure Di | TBC1D5 | $[CT]_{21}$ | 1 |
| | TPK1 | $[CA]_{20}$ | 2 |
| | C01.424 | $[CA]_{13}$ | 1 |
| | MLH1 | $[CT]_{21}$ | 1 |
| | ABCC9ca | $[CA]_{19}$ | 1 |
| | REN47D17 | $[CA]_{16}$ | 1 |
| | 15F11 | $[CA]_{10}$ | 1 |
| | CXX.279 | $[CA]_{17}$ | 2 |
| | REN47J11b | $[CA]_{11}$ | 1 |
| | WNT2B | $[CA]_{21}$ | 1 |
| | REN198P23 | $[CA]_{15}$ | 1 |
| | DKFZ | $[CT]_{20}$ | 1 |
| | Ren41F10 | $[CA]_{20}$ | 1 |
| Pure Tetra | FH2060 | $[AATG]_5$ | 4 |
| | FH2377 | $[CTTT]_4$ | 1 |
| | PPP1R9A | $[GTTT]_9$ | 1 |
| | 9A5 | $[CTTT]_{18}$ | 1 |
| | FH2401 | $[CTTT]_{11}$ | 1 |
| | FH2561 | $[CTTT]_{21}$ | 1 |
| | HLA | $[CTTT]_{13}$ | 2 |
| | ABCC9tetra | $[CTTT]_8$ | 4 |
| Pure Penta | BTN1A1 | $[CTTTT]_3$ | 1 |
| Compound Tetra | LPP | $[TTCC]_5[CTTT]_{15}$ | 2 |
| | FLJ32685 | $[CTTT]_{14}[CTTTT]_{14}$ | 2 |
| Interrupted | SCN11A | $[CAAT]_3[CTAT]_4$ $CATC[TATC]_5$ | 6 |
| | FH3113 | $[TG]_7$ $A[GT]_3[ACGC]_2$ | 2 |
| | ANGPT1 | $[CCTT]_{12}T[CTTT]_{11}$ | 1 |

**TABLE 4 |** Frequency of ABCC9tetra, FH2060, and SCN11A in MS mutation tumors.

| Type | Cases | ABCC9tetra | FH2060 | SCN11A |
|---|---|---|---|---|
| Benign | 6 | I | LOH | MSI/LOH |
| | 12 | I | I | I |
| | 15 | I | I | I |
| | 20 | I | LOH | MSI |
| | 22 | I | I | MSI |
| | Mutation frequency (%) | 0 | 40 | 60 |
| Cancer | 2 | I | I | I |
| | 3 | I | MSI | MSI |
| | 4 | MSI | MSI/LOH | I |
| | 7 | MSI | I | I |
| | 10 | I | I | MSI |
| | 11 | MSI | MSI | MSI/LOH |
| | 13 | I | MSI/LOH | I |
| | 14 | MSI/LOH | I | I |
| | 17 | I | I | I |
| | Mutation frequency (%) | 44.44 | 44.44 | 33.33 |

*I indicated that LOH or MSI does not occur at this site, and LOH/MSI indicates that both LOH and MSI occur at this site.*

of loci (more than five loci) be defined as MSI-High (MSI-H). If all tumor MS loci are comparable to their normal specimen, the tumor is classified as MSS. The range between MSS and MSI-H is defined as MSI-L (20). To date, tumors with an MSI-H frequency of 0% and tumors with MSI mutations all exhibited the MSI-L type, which is consistent with studies by Eldama'ria and Ando (17, 25). Work by Dustin showed that 800 loci are required to achieve diagnostic sensitivity and specificity for HBC, and diagnosis using predefined microsatellite locus panels is challenging (26). Overall, 31 MS loci were stable, and 27 MS loci exhibited MSI. Different cancer types exhibited distinct patterns of MS mutations. It appears that for breast tumors, the instability event may have a more neutral fitness effect, resulting in fewer recurrent mutation loci.

Although there was no significant difference in the frequency of MSI or LOH between benign and malignant tumors, malignant tumors had more MSI mutation loci than benign tumors. Of the 23 that we previously reported (4 benign and 19 malignant tumors), ABCC9tetra, FLJ32685, SCN11A and 9A5 loci showed a higher incidence of instability events in most canine breast cancers (16). In the present work, ABCC9tetra (4/22, 18.2%) and SCN11A (6/22, 27.3%) loci also exhibited higher mutation rates in CMTs. Our newly discovered high-frequency MSI locus, FH2060 (4/22, 18.2%), also had the highest LOH frequency (4/22, 18.2%). This phenomenon is potentially caused by selective pressures in tumor evolution (14). Biological pressures are involved in the selection of MS mutations, and some specific MS may be subject to positive or negative selection through changes in gene expression or function that result in more malignant transformation such as proliferation and metastasis (27, 28). Furthermore, a previous study showed that LOH can confer a growth advantage in tumor cells, and the tumor suppressor genes *BRCA1* and *BRCA2* loci are frequently altered due to allelic imbalance during carcinogenesis in the breast (29). Therefore, we suspected that the MSI locus was involved in the formation of breast tumors and began to explore the genes adjacent to the MSI locus.

Cancer genome sequencing has revealed that regional autosomal differential mutation rates at megabase resolution are related to changes in the timing of DNA replication or in gene expression and are less correlated with cancer type (30). The effect of DNA damage on highly expressed genes is limited to the MS within a specific gene in a specific tissue. In our results, ABCC9tetra, an MS locus, was mutated only in malignant tumors. The expression of adjacent gene *ABCC9* was significantly decreased in the malignant tumor group. It is worth noting that the ABCC9 protein is involved in bioelectric control. ABCC9 can couples with potassium channel proteins KCNJ8 or KCNJ11 to form the $K_{ATP}$ channel. The $K_{ATP}$ channels were located on cell membranes and mitochondrial membranes. Past studies have shown that the channels formed by different combinations of KCNJ8, KCNJ11, ABCC8, and ABCC9 vary based on tissue localization (31). Immunohistochemistry reflected that ABCC9

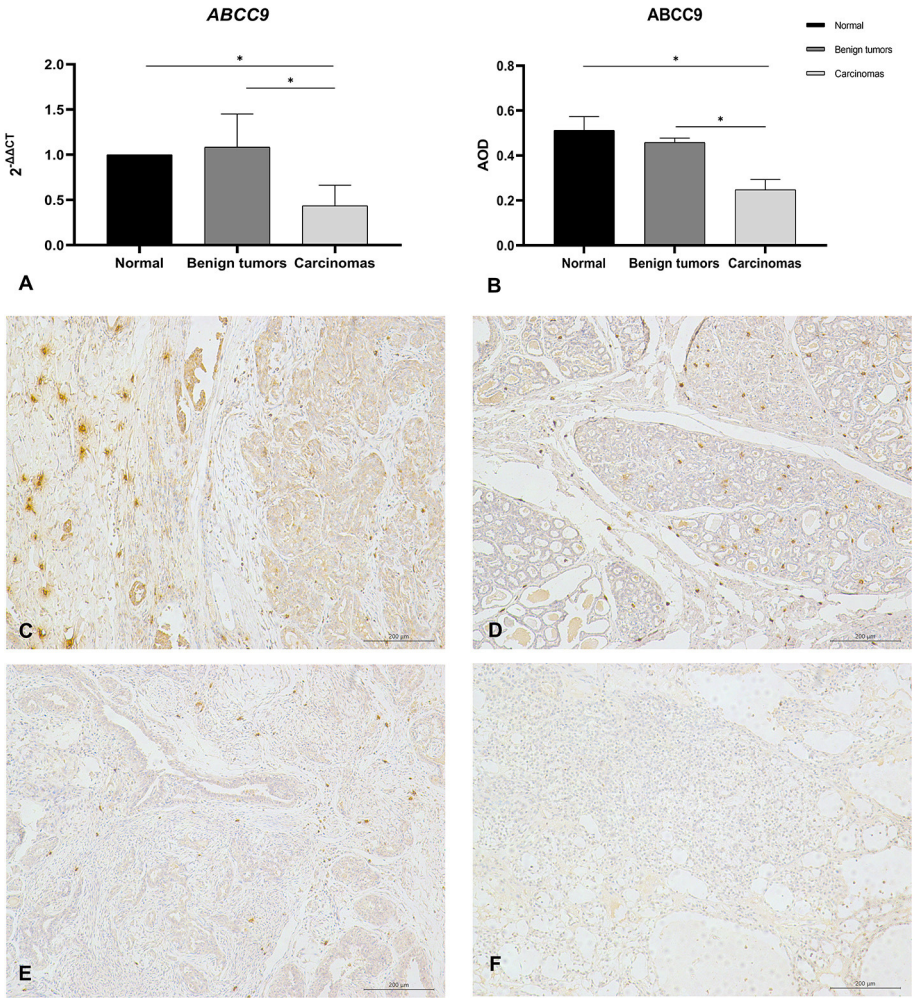


**FIGURE 4 |** The mRNA level and protein expression of ABCC9. **(A)** The mRNA level of *ABCC9,* the mRNA level was expression by $2^{-\Delta\Delta Ct}$. **(B)** Average optical density values of ABCC9 protein in CMTs. AOD = IOD/Area, all of data are shown as means ± SD, $^{*}$indicates that there is significant difference between two groups ($P < 0.05$). **(C)** IHC staining of ABCC9 in paracancer tissue (200×). **(D)** IHC staining of ABCC9 in benign tumor (200×). **(E)** IHC staining of ABCC9 in complex breast cancer (200×). **(F)** No strong positive staining of ABCC9 in higher malignancy cells (200×). Strongly positive cells can be observed in para-cancer tissues and benign tumors, but was significant decreased in malignant tumors.

was overexpressed in both normal and paracancerous tissues and in benign tumors, indicating that it is involved in the assembly of the $K_{ATP}$ channel in the breast.

The ionic concentrations of $Na^+$, $K^+$, $Ca^{2+}$, and $Cl^-$ are regulated by ion channels. In this study, ABCC9 on cell membranes and the mRNA level of *ABCC9* were significantly decreased in malignant tissues. Furthermore, a negative correlation was observed between ABCC9 expression and cancer grading, with positive cells basically disappearing in cancer samples of grade III. This relationship may be due to the inhibition of the $K_{ATP}$ channel in cancer tissue. The cytoplasm of depolarized cells is more positively charged relative to the extracellular space and has a less negative $V_{mem}$ (32). Inhibition of potassium influx can lead to continuous depolarization of cells, which can induce mitosis and promote the proliferation of cancer cells (33, 34). Furthermore, a study of cardiac ischemia-reperfusion injuries revealed that the opening of mitoKATP channels could inhibit the depolarization of the mitochondrial membrane and protect against apoptosis in its early stages (35).

In addition, many studies have shown that ABCC9 can be used as a biomarker for cancers. The enrichment analysis of gastric cancer found that ABCC9 was involved in ATPase activity, transmembrane transport, and ABC transporters (36). Another study on the methylation pattern of breast cancer revealed that ABCC9 is a potential grade III biomarker of breast cancer in white individuals. However, in our study, only one case of cancer showed a significant increase in promoter CpG islands, which could not explain the reduced gene expression.

In conclusion, CMT is a highly heterogeneous disease with multiple genetic and epigenetic alterations. Malignant tumors have more unstable loci than benign tumors,

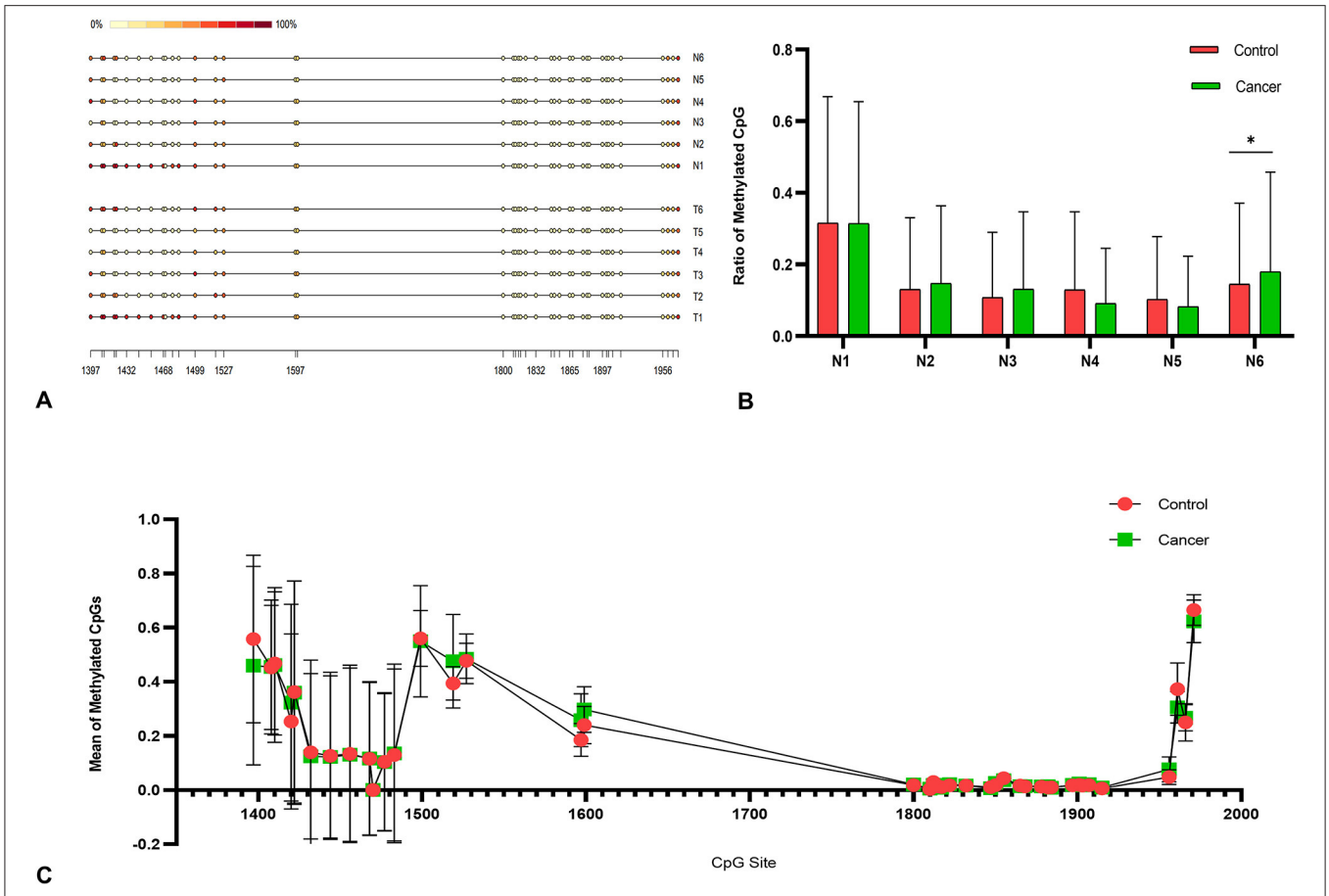


**FIGURE 5 |** Methylation analysis of ABCC9 promoter. **(A)** Methylation analysis of ABCC9 CpG island. **(B)** Methylation CpG levels of six samples. **(C)** Methylation levels in average CpG sites. *indicates a significant difference between the two groups, $P < 0.05$.

which may be related to altered gene expression. ABCC9 is significantly downregulated in breast cancer and ABCC9tetra is particularly prone to mutation. In the future, additional studies on the regulation of ABCC9 protein in cancer cells are needed.

## DATA AVAILABILITY STATEMENT

The datasets presented in this study can be found in online repositories. The names of the repository/repositories and accession number(s) can be found in the article/**Supplementary Material**.

## ETHICS STATEMENT

The animal study was reviewed and approved by the Animal Ethics Committee of Nanjing Agricultural University (NJAU-20171019, 10 October 2017). Experiment operates were performed under the Guidelines for Care and Use of Laboratory Animals of Jiangsu province (SYXK2017-0027). Written informed consent was obtained from the owners for the participation of their animals in this study.

## AUTHOR CONTRIBUTIONS

PH and DWY: conceptualization. PH: methodology, software, formal analysis, resources, data curation, and writing-original draft preparation. SQW and XJH: validation. KYS: investigation. DWY: writing-review, editing and visualization. DJY: supervision, project administration, and funding acquisition. All authors contributed to the article and approved the submitted version.

## FUNDING

Natural Science Foundation of Jiangsu Province (BK20130686), National Natural Science Foundation of China (30871847), and Priority Academic Program Development of Jiangsu Higher Education Institutions (PAPD).

## SUPPLEMENTARY MATERIAL

The Supplementary Material for this article can be found online at: https://www.frontiersin.org/articles/10.3389/fvets.2021.819293/full#supplementary-material

## REFERENCES


1. Hanahan D, Weinberg RA. Hallmarks of cancer: the next generation. *Cell.* (2011) 144:646–74. doi: 10.1016/j.cell.2011.02.013
2. Ko JH, Ko EA, Gu W, Lim I, Bang H, Zhou T. Expression profiling of ion channel genes predicts clinical outcome in breast cancer. *Mol Cancer.* (2013) 12:106. doi: 10.1186/1476-4598-12-106
3. Prevarskaya N, Skryma R, Shuba Y. Ion channels and the hallmarks of cancer. *Trends Mol Med.* (2010) 16:107–21. doi: 10.1016/j.molmed.2010.01.005
4. Tuszynski J, Tilli TM, Levin M. Ion channel and neurotransmitter modulators as electroceutical approaches to the control of cancer. *Curr Pharm Des.* (2017) 23:4827–41. doi: 10.2174/1381612823666170530105837
5. Olson TM, Terzic A. Human K(ATP) channelopathies: diseases of metabolic homeostasis. *Pflugers Arch.* (2010) 460:295–306. doi: 10.1007/s00424-009-0771-y
6. Ru Q, Tian X, Wu YX, Wu RH, Pi MS, Li CY. Voltage-gated and ATP-sensitive K+ channels are associated with cell proliferation and tumorigenesis of human glioma. *Oncol Rep.* (2014) 31:842–8. doi: 10.3892/or.2013.2875
7. Huang L, Li B, Li W, Guo H, Zou F. ATP-sensitive potassium channels control glioma cells proliferation by regulating ERK activity. *Carcinogenesis.* (2009) 30:737–44. doi: 10.1093/carcin/bgp034
8. Liu X, Sun K, Song A, Zhang X, Zhang X, He X. Curcumin inhibits proliferation of gastric cancer cells by impairing ATP-sensitive potassium channel opening. *World J Surg Oncol.* (2014) 12:389. doi: 10.1186/1477-7819-12-389
9. Thibodeau SN, Bren G, Schaid D. Microsatellite instability in cancer of the proximal colon. *Science.* (1993) 260:816–9. doi: 10.1126/science.8484122
10. Patino GA, Isom LL. Electrophysiology and beyond: multiple roles of Na+ channel β subunits in development and disease. *Neurosci Lett.* (2010) 486:53–9. doi: 10.1016/j.neulet.2010.06.050
11. Mandal R, Samstein RM, Lee KW, Havel JJ, Wang H, Krishna C, et al. Genetic diversity of tumors with mismatch repair deficiency influences anti-PD-1 immunotherapy response. *Science.* (2019) 364:485–91. doi: 10.1126/science.aau0447
12. Łuksza M, Riaz N, Makarov V, Balachandran VP, Hellmann MD, Solovyov A, et al. A neoantigen fitness model predicts tumour response to checkpoint blockade immunotherapy. *Nature.* (2017) 551:517–20. doi: 10.1038/nature24473
13. Baudrin LG, Deleuze JF, How-Kit A. Molecular and computational methods for the detection of microsatellite instability in cancer. *Front Oncol.* (2018) 8:621. doi: 10.3389/fonc.2018.00621
14. Hause RJ, Pritchard CC, Shendure J, Salipante SJ. Classification and characterization of microsatellite instability across 18 cancer types. *Nat Med.* (2016) 22:1342–50. doi: 10.1038/nm.4191
15. Murphy KM, Zhang S, Geiger T, Hafez MJ, Bacher J, Berg KD, et al. Comparison of the microsatellite instability analysis system and the Bethesda panel for the determination of microsatellite instability in colorectal cancers. *J Mol Diagn.* (2006) 8:305–11. doi: 10.2353/jmoldx.2006.050092
16. Khand FM, Yao DW, Hao P, Wu XQ, Kamboh AA, Yang DJ. Microsatellite instability and MMR genes abnormalities in canine mammary gland tumors. *Diagnostics (Basel).* (2020) 10:104. doi: 10.3390/diagnostics10020104
17. de Vargas Wolfgramm E, Alves LN, Stur E, Tovar TT, De Nadai Sartori MP, de Castro Neto AK, et al. Analysis of genome instability in breast cancer. *Mol Biol Rep.* (2013) 40:2139–44. doi: 10.1007/s11033-012-2272-x
18. Pan X, Gong D, Nguyen DN, Zhang X, Hu Q, Lu H, et al. Early microbial colonization affects DNA methylation of genes related to intestinal immunity and metabolism in preterm pigs. *DNA Res.* (2018) 25:287–96. doi: 10.1093/dnares/dsy001
19. Lister R, Pelizzola M, Dowen RH, Hawkins RD, Hon G, Tonti-Filippini J, et al. Human DNA methylomes at base resolution show widespread epigenomic differences. *Nature.* (2009) 462:315–22. doi: 10.1038/nature08514
20. Boland CR, Thibodeau SN, Hamilton SR, Sidransky D, Eshleman JR, Burt RW, et al. A national cancer institute workshop on microsatellite instability for cancer detection and familial predisposition: development of international criteria for the determination of microsatellite instability in colorectal cancer. *Cancer Res.* (1998) 58:5248–57.
21. Danjoux M, Guimbaud R, Al Saati T, Meggetto F, Carrère N, Portier G, et al. Contribution of microdissection for the detection of microsatellite instability in colorectal cancer. *Hum Pathol.* (2006) 37:361–8. doi: 10.1016/j.humpath.2005.06.022
22. Ellegren H. Microsatellites: simple sequences with complex evolution. *Nat Rev Genet.* (2004) 5:435–45. doi: 10.1038/nrg1348
23. Maruvka YE, Mouw KW, Karlic R, Parasuraman P, Kamburov A, Polak P, et al. Analysis of somatic microsatellite indels identifies driver events in human tumors. *Nat Biotechnol.* (2017) 35:951–9. doi: 10.1038/nbt.3966
24. Fujimoto A, Fujita M, Hasegawa T, Wong JH, Maejima K, Oku-Sasaki A, et al. Comprehensive analysis of indels in whole-genome microsatellite regions and microsatellite instability across 21 cancer types. *Genome Res.* (2020) 30:334–46. doi: 10.1101/gr.255026.119
25. Ando Y, Iwase H, Ichihara S, Toyoshima S, Nakamura T, Yamashita H, et al. Loss of heterozygosity and microsatellite instability in ductal carcinoma *in situ* of the breast. *Cancer Letters.* (2000) 156:207–14. doi: 10.1016/s0304-3835(00)00467-5
26. Long DR, Waalkes A, Panicker VP, Hause RJ, Salipante SJ. Identifying optimal loci for the molecular diagnosis of microsatellite instability. *Clin Chem.* (2020) 66:1310–8. doi: 10.1093/clinchem/hvaa177
27. Chen H, Maxwell C, Connell M. The generation, detection, and prevention of genomic instability during cancer progression and metastasis. *Cancer Metastasis.* (2015) 20:15–38.
28. Charames GS, Bapat B. Genomic instability and cancer. *Curr Mol Med.* (2003) 3:589–96. doi: 10.2174/1566524033479456
29. Maxwell KN, Wubbenhorst B, Wenz BM, De Sloover D, Pluta J, Emery L, et al. BRCA locus-specific loss of heterozygosity in germline BRCA1 and BRCA2 carriers. *Nat Commun.* (2017) 8:319. doi: 10.1038/s41467-017-00388-9
30. Supek F, Lehner B. Differential DNA mismatch repair underlies mutation rate variation across the human genome. *Nature.* (2015) 521:81–4. doi: 10.1038/nature14173
31. Akrouh A, Halcomb SE, Nichols CG, Sala-Rabanal M. Molecular biology of K(ATP) channels and implications for health and disease. *IUBMB Life.* (2009) 61:971–8. doi: 10.1002/iub.246
32. Blackiston DJ, McLaughlin KA, Levin M. Bioelectric controls of cell proliferation: ion channels, membrane voltage and the cell cycle. *Cell Cycle.* (2009) 8:3527–36. doi: 10.4161/cc.8.21.9888
33. Fukushiro-Lopes DF, Hegel AD, Rao V, Wyatt D, Baker A, Breuer EK, et al. Preclinical study of a Kv11.1 potassium channel activator as antineoplastic approach for breast cancer. *Oncotarget.* (2018) 9:3321–37. doi: 10.18632/oncotarget.22925
34. Zhang P, Yang X, Yin Q, Yi J, Shen W, Zhao L, et al. Inhibition of SK4 potassium channels suppresses cell proliferation, migration and the epithelial-mesenchymal transition in triple-negative breast cancer cells. *PLoS ONE.* (2016) 11:e0154471. doi: 10.1371/journal.pone.0154471
35. Jia D. The protective effect of mitochondrial ATP-sensitive $K^+$ channel opener, nicorandil, combined with $Na^+/Ca^{2+}$ exchange blocker KB-R7943 on myocardial ischemia-reperfusion injury in rat. *Cell Biochem Biophys.* (2011) 60:219–24. doi: 10.1007/s12013-010-9142-8
36. Mao X, He Z, Zhou F, Huang Y, Zhu G. Prognostic significance and molecular mechanisms of adenosine triphosphate-binding cassette subfamily C members in gastric cancer. *Medicine.* (2019) 98:e18347. doi: 10.1097/MD.0000000000018347


**Conflict of Interest:** The authors declare that the research was conducted in the absence of any commercial or financial relationships that could be construed as a potential conflict of interest.

frontiers in Veterinary Science

ORIGINAL RESEARCH
published: 14 January 2022
doi: 10.3389/fvets.2021.808863

# Acute Succinate Administration Increases Oxidative Phosphorylation and Skeletal Muscle Explosive Strength via SUCNR1

*Guli Xu, Yexian Yuan, Pei Luo, Jinping Yang, Jingjing Zhou, Canjun Zhu, Qingyan Jiang and Gang Shu**

*Guangdong Laboratory for Lingnan Modern Agriculture and Guangdong Province Key Laboratory of Animal Nutritional Regulation, National Engineering Research Center for Breeding Swine Industry, College of Animal Science, South China Agricultural University, Guangzhou, China*

OPEN ACCESS

**Edited by:**
*Jianzhu Liu,*
*Shandong Agricultural University, China*

**Reviewed by:**
*Natalia Belosludtseva, Institute of Theoretical and Experimental Biophysics (RAS), Russia*
*Kun Li, Nanjing Agricultural University, China*

***Correspondence:**
*Gang Shu*
*shugang@scau.edu.cn*

**Specialty section:**
*This article was submitted to Animal Nutrition and Metabolism, a section of the journal Frontiers in Veterinary Science*

**Received:** *04 November 2021*
**Accepted:** *30 November 2021*
**Published:** *14 January 2022*

**Citation:**
*Xu G, Yuan Y, Luo P, Yang J, Zhou J, Zhu C, Jiang Q and Shu G (2022) Acute Succinate Administration Increases Oxidative Phosphorylation and Skeletal Muscle Explosive Strength via SUCNR1. Front. Vet. Sci. 8:808863. doi: 10.3389/fvets.2021.808863*

Endurance training and explosive strength training, with different contraction protein and energy metabolism adaptation in skeletal muscle, are both beneficial for physical function and quality of life. Our previous study found that chronic succinate feeding enhanced the endurance exercise of mice by inducing skeletal muscle fiber-type transformation. The purpose of this study is to investigate the effect of acute succinate administration on skeletal muscle explosive strength and its potential mechanism. Succinate was injected to mature mice to explore the acute effect of succinate on skeletal muscle explosive strength. And C2C12 cells were used to verify the short-term effect of succinate on oxidative phosphorylation. Then the cells interfered with succinate receptor 1 (SUCNR1) siRNA, and the SUCNR1-GKO mouse model was used for verifying the role of SUCNR1 in succinate-induced muscle metabolism and expression and explosive strength. The results showed that acute injection of succinate remarkably improved the explosive strength in mice and also decreased the ratio of nicotinamide adenine dinucleotide (NADH) to $NAD^+$ and increased the mitochondrial complex enzyme activity and creatine kinase (CK) activity in skeletal muscle tissue. Similarly, treatment of C2C12 cells with succinate revealed that succinate significantly enhanced oxidative phosphorylation with increased adenosine triphosphate (ATP) content, CK, and the activities of mitochondrial complex I and complex II, but with decreased lactate content, reactive oxygen species (ROS) content, and NADH/$NAD^+$ ratio. Moreover, the succinate's effects on oxidative phosphorylation were blocked in SUCNR1-KD cells and SUCNR1-KO mice. In addition, succinate-induced explosive strength was also abolished by SUCNR1 knockout. All the results indicate that acute succinate administration increases oxidative phosphorylation and skeletal muscle explosive strength in a SUCNR1-dependent manner.

**Keywords: succinate, SUCNR1, oxidative phosphorylation, muscle explosive strength, mitochondrion**

## INTRODUCTION

Skeletal muscle function is a crucial prerequisite to ensure quality of life, in physical exercise, and in athletic sports. Based on muscle contraction intensity and time, endurance exercise, and resistance exercise require different contraction units and energy metabolism patterns (1). Endurance exercises are mainly dependent on the aerobic metabolism of glucose and fatty acid (2). Acetyl-CoA produced from glycolysis of glucose, oxidation of pyruvate, and β-oxidation of fatty acid produces nicotinamide adenine dinucleotide (NADH) by tricarboxylic acid (TCA) cycle to generate adenosine triphosphate (ATP) (3). The latter relies on the glycolysis of glucose and glycogen to produce ATP rapidly with a byproduct-lactate accumulation (4). Therefore, individuals with stronger endurance exercise usually have weaker explosive power, and vice versa.

In recent years, a series of studies have shown that a variety of energy metabolism intermediates, such as α-ketoglutarate (AKG) and fumarate, can be used as important molecule signals to regulate cell metabolism by inducing autocrine or paracrine (5–7). As an intermediate of the TCA cycle, chronic treatment of cardiomyocytes with 1 mM succinate (SUC) will activate the hypertrophic signaling pathway through SUC receptor 1 (SUCNR1) (8). And short-term treatment with extracellular SUC leads to mitochondrial fission by SUCNR1 in the membrane of cardiomyocytes (9). Previous studies also demonstrated that long-term administration of SUC could convert fast muscle fiber into slow muscle fiber, which improves endurance exercise ability (10, 11). However, whether SUC has any effect on short-term explosive strength is not clear.

SUC has been considered as an important metabolic signal molecule with diverse potential mechanisms. Similarly, mitochondrial SUC is the substrate of complex II and produces fumarate with its oxidation (12). Extracellular SUC could not be permeated across mammalian cell membranes (11, 13, 14) but could be recognized by SUCNR1, which has been revealed to mediate the effects of extracellular SUC on several biological processes, such as adipose tissue thermogenesis (15), mitochondrial biogenesis (11), and mitophagy (16). However, there is still controversy about whether this receptor is expressed in the cell membrane of skeletal muscle myotube (17, 18). And the role of SUCNR1 in regulating the energy metabolism of skeletal muscle remains unclear.

In this study, we conducted both *in vivo* and *in vitro* experiments and revealed that acute SUC administration increased the explosive strength of muscle and energy production increased by oxidative phosphorylation. We also found SUCNR1 mRNA and protein are expressed in skeletal muscle and C2C12 myotube. Both SUCNR1-KD cell models and SUCNR1-knockdown mouse models confirmed that SUCNR1 mediated the effects of SUC on oxidative phosphorylation and skeletal muscle explosive strength.

## MATERIALS AND METHODS

### Animal Experiments

All animal breeding and experiments comply with 'the instructive notions with respect to caring for laboratory animals' issued by the Ministry of Science and Technology of the People's Republic of China; the ethics number of our experiment is 2021b121. C57BL/6J mice (3 weeks old) from the Medical Experimental Animal Center of Guangdong Province (Guangzhou, Guangdong, China) were housed in a 12-h light–dark cycle room under conditions of controlled room temperature (23°C ± 3°C) and humidity (70 ± 10%). After 6 weeks of age, healthy male mice weighing 22–26 g were randomly divided into different groups according to their body weight. All mice were fasted for 1 h, and muscle force was detected as standard; after 0.5 h to rest, the muscle force was tested again at a different time of acute injection to varying concentrations of SUC. After injection, mice were sacrificed and their eyeballs collected to get blood samples. Then the serum, biceps, gastrocnemius, soleus, tibialis anterior, and extensor digitorum were collected. The SUCNR1-knockout mouse in this study was designed by the Shanghai Model Organisms Center (Shanghai, China), and the details have been introduced in a previous study (10). Briefly, sgRNAs of SUCNR1 were knocked into zygotes *in vitro* to delete exon 2 of SUCNR1 by clustering regularly, interspaced short palindromic repeats CRISPR-associated proteins 9 (CRISPR-Cas9) systems, and the embryo was transferred to pseudo-pregnant recipients to obtain F0 generation. Male and female heterozygous mice were mated to produce the homozygous SUCNR1 mice and the wild-type (WT) mice in the same cages. The gene types of next-generation mice were identified by PCR.

### Cell Culture

The C2C12 cell line (ATCC) was cultured in a growth medium (high-glucose DME/F-12 medium with 10% fetal bovine serum) in a Thermo Scientific $CO_2$ incubator (37°C, 95% humidity, 5% $CO_2$). When cells grew to 80%, they were inoculated into plates uniformly. The density of these C2C12 cells was $3 \times 10^4/cm^2$. The culture medium was switched to the differentiated medium (high-glucose DME/F-12 medium with 2% horse serum) after cells reached 90% to induce differentiation. After being induced for 4–6 days, the mature muscle fibers were observed, and the differentiated cells were treated with SUA for 1 h and then collected for further detection.

### SUCNR1 siRNA Transfection

When C2C12 cells were grown to 60%, instructions for the use of Lipofectamine 2000 (Invitrogen, Carlsbad, CA, USA) were followed to transfect SUCNR1 siRNA to cells. Suzhou GenePharma Co., Ltd (Suzhou, China) designed the siRNA sequences: 5′-GCUUCUACUACAAGAUTT-3′ and 5′-AUCUUGUAGUAGAAGCTT-3′. After transfected cells were grown to 80%, cells were inoculated and treated as mentioned before.

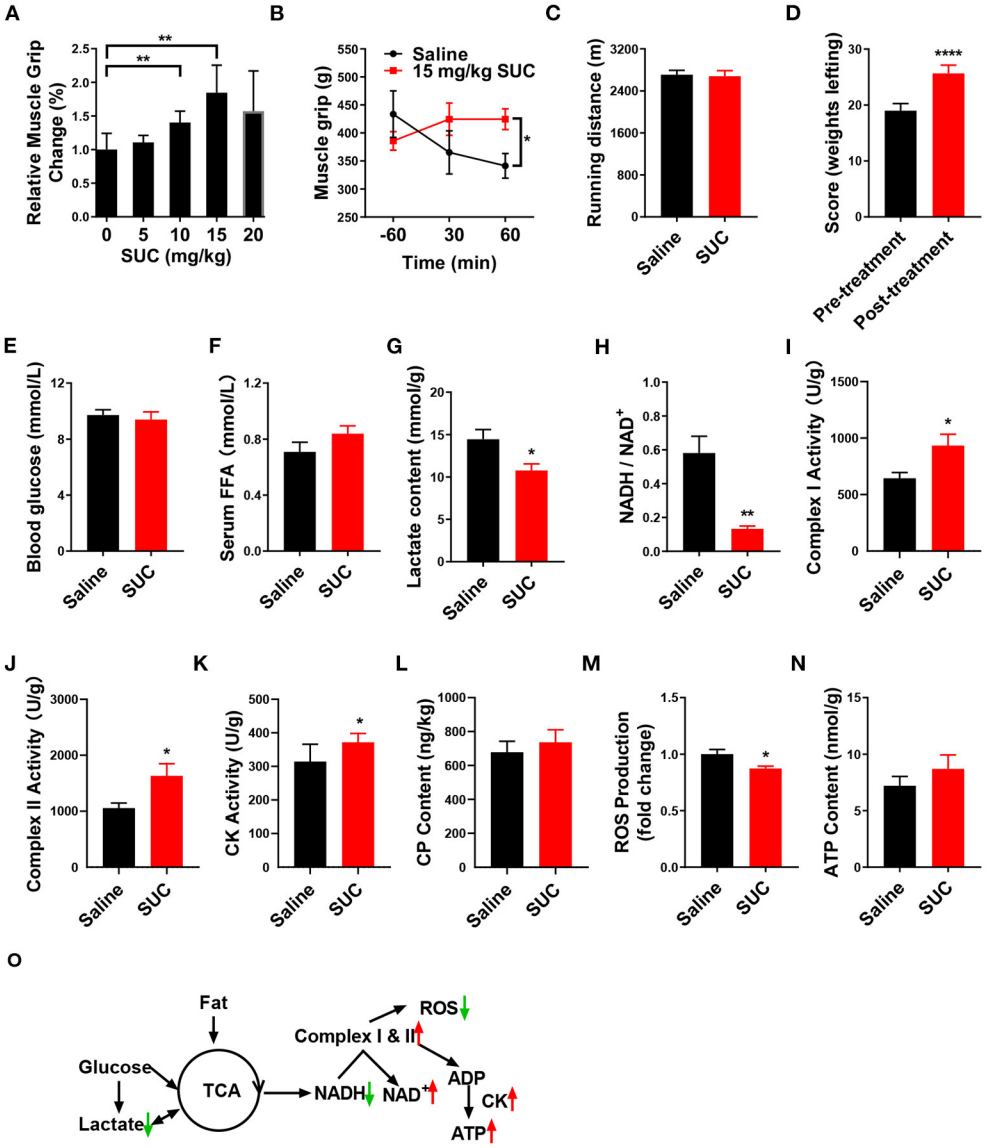


**FIGURE 1 |** SUC increases explosive strength and mitochondrial oxidative phosphorylation in mice. **(A)** Relative muscle grip of the mice injected with different doses of SUC or saline for 1 h. **(B)** Muscle grip change at different times after injection of 15 mg/kg SUC. **(C)** Running distance of the mice after injecting with saline and SUC for 1 h. **(D)** Weight lifting of the mice after being injected with saline and SUC for 1 h again. Blood and gastrocnemius were collected after the muscle grip test for **(E–N)** results to detect. **(E)** Blood glucose content. **(F)** FFA level in serum. **(G)** Lactate content in muscle. **(H)** NADH/$NAD^+$ ratio change in muscle. **(I)** Complex I activity in muscle. **(J)** Complex II activity in muscle. **(K)** Muscle CK activity in muscle. **(L)** Muscle phosphocreatine (CP) content. **(M)** Muscle ROS content. **(N)** Muscle ATP content. **(O)** Schematic diagram of energy production pathway in normal conditions. In the normal process of energy production, acetyl-CoA from glycolysis of glucose and subsequent oxidation of pyruvate and β-oxidation of fatty acid produces NADH by TCA cycle (3). The electrons from NADH pass through the mitochondrial electron transport chain and synthesize ATP by CK in the mitochondrial outer compartment (23). Premature leakage of electrons in the electron transport chain will lead to generating ROS. Lactate, a byproduct of acute exercise, could be used as an energy substrate (24), $n = 6$ mice per group. Each value is shown as the mean ± SEM. *, **, and *** indicate $P < 0.05$, 0.01, and 0.001, respectively.

## Immunofluorescence

Muscles were sliced into 10 μm by a cryostat (CM1850, Leica), after fixing in Tissue-Tek OCT. Muscle slices were fixed with 4% paraformaldehyde for 10 min, washed three times per 5 min by PBS, and permeabilized with Triton X-100 (0.5%, 10 min), washed three times per 5 min by PBS. Obtained sections were blocked with blocking buffer (5% BSA and 5% normal goat serum) for 30 min and then incubated with primary antibodies overnight. Primary antibodies were mouse anti-MyHC I (BA-D5-S, 1:200, DSHB) and rabbit anti-SUCNR1 (NBP1-00861, 1:1,000, Novus). Sections were washed in PBS three times per 10 min and incubated with Cy3-AffiniPure Goat-Anti-Rabbit IgG (H+L) (111-165-045, UNIV) and Alexa Fluor 488-AffiniPure Goat-Anti-Rabbit IgG (H+L) (115-545-003, UNIV), followed by

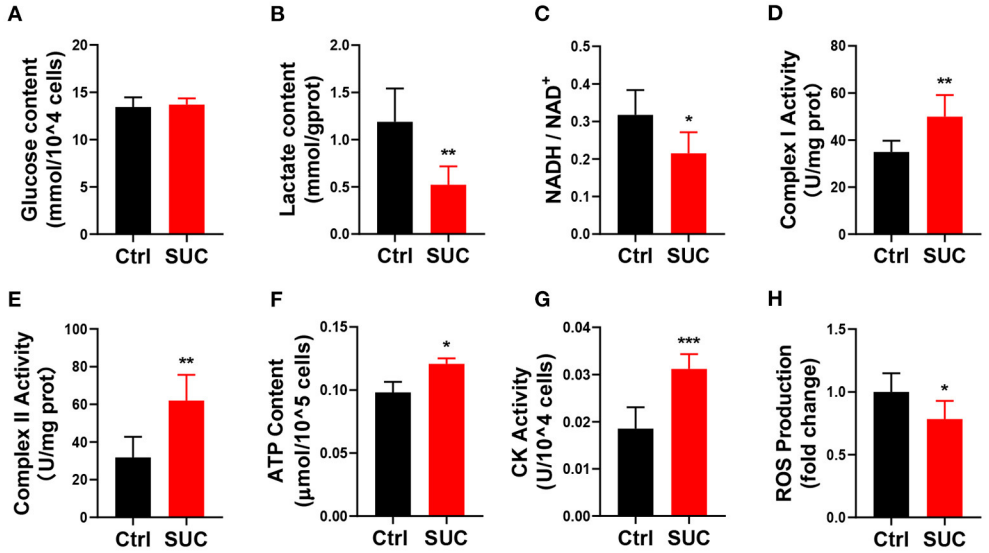


**FIGURE 2 |** SUC promotes oxidative phosphorylation in C2C12 cells. C2C12 cells could be observed in mature fibers after induced differentiation for 4–6 days, and then cells were treated with 1 mM SUC for 1 h to detect oxidative phosphorylation. **(A)** Glucose content in cells. **(B)** Lactate content. **(C)** NADH/$NAD^+$ ratio change. **(D)** Complex I activity. **(E)** Complex II activity. **(F)** ATP content. **(G)** CK activity. **(H)** ROS fold change compared to the control group. $n = 6$ for each group. Each value is shown as the mean ± SEM. *, **, and *** indicate $P < 0.05$, 0.01, and 0.001, respectively.

secondary antibodies (1:2,000, 1 h) and then washed (three times, 10 min/time). The slides were observed with a Nikon ECLIPSE Ti microscope.

## Protein Expression Analysis

Protein was extracted from C2C12 cells with RIPA lysis buffer (P0013B, Beyotime), and the concentration of protein was detected by a BCA protein assay kit (23227, Thermo Scientific). The concentration of all proteins was adjusted to 1 μg/μl and denatured with a protein sample loading buffer (LT 101, Epizyme). Western blotting (WB) was performed as described in the previous study (19). Primary antibodies anti-SUCNR1 (NBP1-00861, 1:1,000, Novus) and tubulin (AP0064, 1:5,000, BioWord) were used. Protein signals were visualized by Protein Simple (Santa Clara, CA, USA) after being incubated on a PVDF membrane with protein as per the Super ECL Enhanced Pico Light Chemiluminescence Kit (SQ 101, Epizyme). The protein expression level was analyzed by ImageJ (National Institutes of Health, USA).

## Absolute Real-Time PCR

RNA isolation and reverse transcription were performed as per the previous study (20). Kidney cDNAs were chosen to prepare SUCNR1 and tubulin standard samples by PCR. After the concentration was detected, the copies per microliter were calculated, and the calibration was set after dilution by 10 multiple gradients. Real-time PCR was carried out via the Applied Biosystems QuantStudio 3 (Thermo Fisher Scientific) to calculate SUCNR1 copies compared with tubulin copies. The primers for SUCNR1 and tubulin were as follows: mouse SUCNR1, 5′-CGAGACAGAAGCCGACAGCA-3′ (sense) and 5′-TAGCCAAACACCACAGTGACAT-3′ (anti-sense); mouse tubulin, 5′-GATCTTCTGGAGCAGTGCGA-3′ (sense) and 5′-GGAGAGATTGACTTACTGGATTGC-3′ (anti-sense); and they were prepared in Tsingke Biotechnology Co., Ltd.

## Biochemical Analysis

Creatine phosphate (CP) and acetyl Co-A concentrations were detected by an enzyme-linked immunosorbent assay (ELISA) kit according to the manufacturer's instructions (Shanghai Ruifan Biological Technology Co., Ltd, Shanghai, China). Similarly, creatine kinase (CK) activity, complex I activity, and complex II activity were quantified by a commercial product of Solarbio Life Science Beijing, China. The NADH/$NAD^+$ ratio and ATP content were computed according to Beyotime (China). And the glucose content and reactive oxygen species (ROS) content were detected by kits from Rsbio. All the quantification was performed as per the instructions of the company.

## Muscle Force Measurement

Maximum muscle force was tested by a grip strength meter (YLS-13A, Jinan Yiyan Technology Development Co., Ltd). Briefly, the mouse's tail was grabbed, and the mouse was put on the grip strength meter; after all limbs of the mouse caught the grip strength meter, the mouse was gently pulled to make it resist, and the resist force value was read to analyze.

Weight lifting is another method to measure the muscular strength of mice, and the method was followed as described in the previous study (21). In brief, the middle part of the tail of each mouse was grabbed, and the mouse was then lowered to be able to grasp the different weights. After grasping the weight, the mouse was raised until the weight was also fully raised. If the mouse could hold the weight for 3 s, then it meets the criteria. If not, the time until the weight was dropped was noted, and the

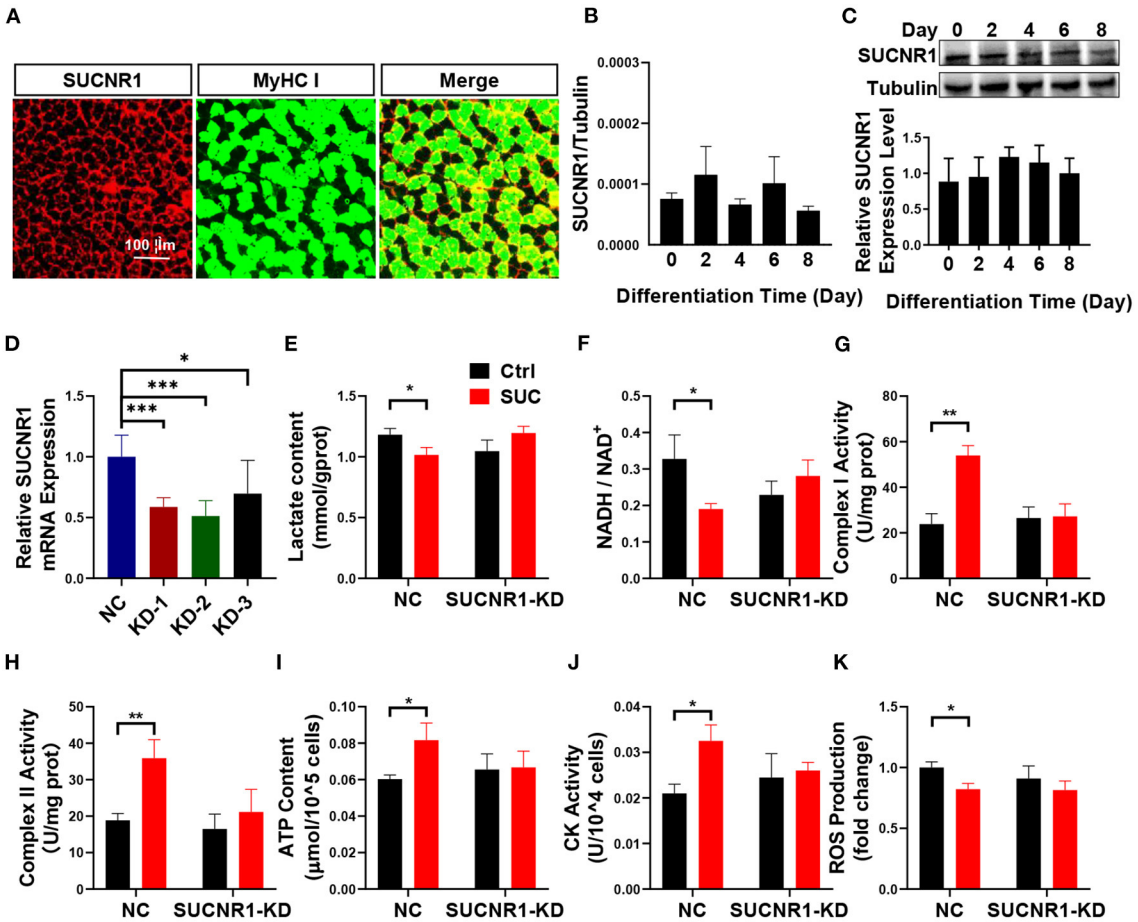


**FIGURE 3 |** SUCNR1 is required for the short-term effects of SUC in C2C12 cells. **(A)** Immunofluorescence staining; red for SUCNR1 and green for MyHC I. **(B)** Absolute quantitative detection of SUCNR1 mRNA expression level compared to tubulin. **(C)** WB to detect the SUCNR1 protein expression level in a different induced day. **(D)** SUCNR1 relative mRNA expression level after being treated with three different SUCNR1 siRNAs for 24 h. The cells in **(E–K)** SUCNR1 knockdown by SUCNR1 siRNA and were then induced to differentiate for 4–6 days; 1 mM SUC cells were treated for 1 h to detect related factors. **(E)** Lactate content. **(F)** NADH/$NAD^+$ ratio change. **(G)** Complex I activity. **(H)** Complex II activity. **(I)** ATP content. **(J)** CK activity. **(K)** ROS fold change compared to ctrl group. $n = 6$ per group. Each value is showed as the mean ± SEM. *, **, and *** indicate $P < 0.05$, 0.01, and 0.001, respectively.

trial was repeated after a 10 s rest. Before being able to successfully hold the weight for 3 s, each mouse was allowed to undergo the trial five times. Once the mouse is able to successfully hold the weight for 3 s, it was allowed to try the next heavier weight. The device comprised seven weights, the weights being 26, 36, 46, 66, 86, 106, and 126 g, corresponding to scores of 1, 2, 3, 4, 5, 6, and 7, respectively. The sum of all the scores held by the mouse represents the score of each mouse.

Similarly, the mice performed the treadmill-running test on the FT-200 animal treadmill at an initial speed of 10 m/min for 10 min until mice adaptation. Then, the speed was raised by 1 m/min every 3 min in low-speed running tests.

## Statistical Analysis

All data are presented as means ± the standard error of the mean (SEM). The difference between standard and treated groups was determined by paired *t*-tests; other differences between control and treated groups were determined by unpaired *t*-tests (GraphPad Prism 8.0.1). In the figures, $P < 0.05$ was considered statistically significant ($^*P < 0.05$, $^{**}P < 0.01$, $^{***}P < 0.001$).

# RESULTS

## SUC Increases Explosive Strength and Oxidative Phosphorylation in Mice

Our previous study showed that chronic SUC treatment enhanced mice endurance exercise (10). Here, we also found that acute SUC administration could dose-dependently increase muscle grip strength, which was in line with our previous observations. Besides, 15 mg/kg SUC enhanced mice grip strength to the maximum, suggesting that this dose is probably optimal to improve mice explosive strength (**Figure 1A**). Subsequently, we detected mice grip strength at different time points after 15 mg/kg SUC administration or saline. The result showed that SUC effectively increases this index for 60 min (**Figure 1B**). Interestingly, our previous evidence confirmed

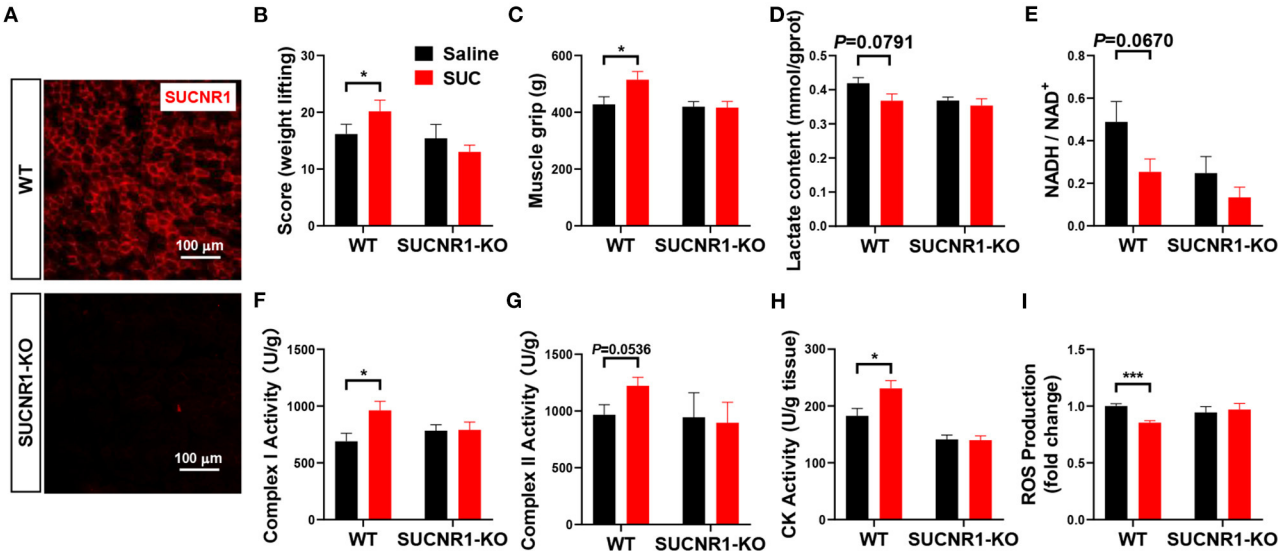


**FIGURE 4 |** SUCNR1 knockout reversed the effect of SUC on explosive strength. Mice were injected with saline or 15 mg/kg SUC for 1 h to detect the muscle force, and then gastrocnemius were collected for the following detection. **(A)** IF stains red for SUCNR1. **(B)** Weight lifting and **(C)** muscle grip to detect the mouse explosive strength. **(D)** Lactate content. **(E)** NADH/NAD$^+$ ratio change. **(F)** Complex I activity. **(G)** Complex II activity. **(H)** CK activity in muscle. **(I)** ROS production fold change. Each group $n = 6$ mice. Each value is shown as the mean ± SEM. *Indicate $P < 0.05$, ***Indicate $P < 0.001$.

that chronic SUC supplementation significantly increases mice running time and further improves endurance (22), while acute SUC treatment enhanced mice's explosive strength rather than endurance. And so, 15 mg/kg SUC obviously increased mouse weight lifting scores (**Figure 1D**), but not running distance (**Figure 1C**).

It is well-established that the body utilizes glucose and fatty acid to provide the energy required for muscle contraction and further maintenance of homeostasis in response to exercise (25, 26). During endurance exercise, the body utilizes fat to produce free fatty acids (FFAs) (27). Here, we found that SUC treatment failed to elevate the serum FFA level (**Figure 1F**), which indicates that β-oxidation of fatty acid probably does not provide the energy for the enhanced muscle explosive strength by SUC. Oxidative metabolism of glucose produces a large amount of energy under endurance exercise conditions, while glycolysis produces energy rapidly under resistance exercise conditions (28). However, our result showed that 15 mg/kg SUC administration failed to affect mice's blood glucose (**Figure 1E**), which suggests that increased explosive strength by SUC is independent of glucose metabolism. Notably, SUC treatment markedly decreased the serum lactate level (**Figure 1G**), indicating that lactate is consumed in resistance exercise after SUC treatment. Importantly, the decreased ratio of NADH/NAD$^+$ and the increased activities of mitochondrial complexes I and II indicate that the electron transfer in the mitochondrial respiratory chain was accelerated by short-term SUC treatment (**Figures 1H–J**). Moreover, SUC treatment failed to affect phosphocreatine (CP) content in the gastrocnemius but increased the CK enzyme activity, which implies that SUC probably could increase energy production (**Figures 1K,L**).

SUC did not increase the ATP content significantly in skeletal muscle, which prompts us to speculate that ATP produced by SUC probably had been utilized by muscles (**Figure 1N**). Once oxidative phosphorylation efficiency is reduced, the production of ROS is increased in the mitochondria (29). Decreased ROS content in the SUC group might relate to the enhanced ATP production efficiency (**Figure 1M**). Taken together, these results indicate that the stimulatory effect of SUC on muscle explosive strength probably requires energy supplement by oxidative phosphorylation rather than fatty acid or glucose energy substrates.

## SUC Promotes Oxidative Phosphorylation in C2C12 Cells

We next examined if *in vitro* SUC treatment would produce similar oxidative phosphorylation effects, as we observed in mice receiving acute SUC administration. Here, we characterized SUC's effects on C2C12 cells by following the previous study (30). Consistent with observations *in vivo*, 1 mM SUC treatment effectively decreased the lactate content, NADH/NAD$^+$ ratio, and ROS content (**Figures 2B,C,H**) and increased the mitochondrial complex I and II activity, ATP content, CK activity (**Figures 2D–G**). However, it failed to affect glucose content in C2C12 cells (**Figure 2A**). These data support the view that SUC enhances oxidative phosphorylation in C2C12 cells.

## SUCNR1 Is Required for the Short-Term Effects of SUC in C2C12 Cells

To explore the mechanism in which SUC increased oxidative phosphorylation in skeletal muscle, we characterized the

effect of the SUC membrane receptor SUCNR1 on SUC-induced oxidative phosphorylation. SUC exhibits many functions through SUCNR1, but the existence of SUCNR1 in muscles cells is controversial (18). The IF result showed that SUCNR1 is enriched around the muscle fiber membrane (**Figure 3A**). Similarly, absolutely quantitative PCR proved the existence of SUCNR1 mRNA in differentiated C2C12 cells (**Figure 3B**). Furthermore, the results of WB showed that the SUCNR1 protein was expressed in differentiated C2C12 cells (**Figure 3C**).

These results suggest a possible role of SUCNR1 in stimulatory effects of SUC on oxidative phosphorylation. To test this point, we first generated a loss-of-function C2C12 cell model by using siRNA to target SUCNR1 specifically. We found that SUCNR1 siRNA-treated C2C12 cells showed significantly less mRNA expression of SUCNR1 compared to control siRNA-treated cells (**Figure 3D**), which validated our SUCNR1-knockdown C2C12 cell model. By using this model, we showed that the knockdown of SUCNR1 abolished the stimulatory effects of SUC on the mitochondrial complex I and II activity, ATP content, and CK activity (**Figures 3G–J**) and reversed the inhibitory effects of SUC on the lactate content, NADH/$NAD^+$ ratio, and ROS content (**Figures 3E,F,K**). These results supported an intermedia role of SUCNR1 in SUC-induced oxidative phosphorylation.

## SUCNR1 Knockout Reversed the Effect of SUC on Explosive Strength

To further determine the role of SUCNR1 in SUC metabolic effect *in vivo*, we generated the SUCNR1 global knockout mouse model (SUCNR1-KO) by using the Clustered Regularly Interspaced Short Palindromic Repeats (CRISPR) method (10). We found that SUCNR1-KO mice completely abolished SUCNR1 expression compared to WT mice (**Figure 4A**), which validates that our knockout model could be used in the following experiments. Consistent with the *in vitro* C2C12 cell model, SUCNR1 knockout abolished SUC-induced effects, indicated by increasing weight lifting, muscle grip, complex I and II activity, and CK activity (**Figures 4B,C,F,G,H**). Additionally, SUCNR1 deletion also eliminated SUC-induced inhibitory effects on the lactate content, NADH/$NAD^+$ ratio, and ROS content (**Figures 4D,E,I**). These results illustrated that SUC accelerated electron transfer in the respiratory chain through SUCNR1. The enhancement of the CK activity effect indicates that the SUC promoted oxidative phosphorylation by SUCNR1. Thus, the results from both loss-of-function models demonstrate that SUCNR1 mediates the SUC administration-induced increase of explosive strength and oxidative phosphorylation.

# DISCUSSION

Explosive strength and endurance training play an important role in animal exercise capacity and body health (31), distinguished by different physical performance characteristics, energy resources, and energy production processes (32). In general, the regents enhance explosive power with lower endurance exercise, and vice versa. SUC is an intermediate in the TCA cycle, and a previous study has found that long-term feeding of SUC can transform the fast muscle fiber types to slow muscle fiber types and enhance the endurance exercise of mice (10). Interestingly, we found that the acute administration of SUC enhanced the explosive strength of mice. Many factors could influence explosive strength, such as the distribution of nerve synapses, the ratio of muscle fiber types, blood flow, and metabolism (33–36). Acute effects make it hard to increase the distribution of nerve synapses or the proportion of fast muscle fibers, and the change in blood flow is often accompanied by the consumption of blood glucose (37). However, the treatment of SUC did not affect the blood glucose. Therefore, acute administration of SUC is more likely to change energy metabolism to enhance explosive strength in skeletal muscle. In normal conditions, the energy source of explosive strength is mainly produced through glycolysis and β-hydrolysis of fatty acid to produce ATP rapidly, with a large amount of lactate generation simultaneously (38). Our results exhibited that the blood glucose and serum FFA content did not change by acute SUC administration, but the lactate content in skeletal muscle was significantly reduced. Therefore, these results demonstrated that the enhanced explosive power of SUC does not rely on glycolysis and β-oxidation of fatty acids.

With the treatment of SUC, ATP was increased by enhancing electron transfer efficiency and oxidative phosphorylation. In physiological conditions, the mitochondrial electron transport chain transits electrons through systematic electron transfer reactions and generates ATP for energy supply through the coupling effect (24, 39). ROS is produced by the premature leak of electrons from the mitochondrial electron transport chain, which will lead to the decrease in the potential energy of electrons used to synthesize ATP (40, 41). Therefore, the accumulation of ROS is often accompanied by inefficient ATP synthesis (42). Our results found that acute SUC treatment notably decreased mice ROS content in skeletal muscle and C2C12 cells, which suggested that the energy metabolism efficiency induced by SUC is increased. Here, our results revealed that SUC intervention decreased the NADH/$NAD^+$ ratio, enhanced mitochondrial complex enzymes, increased CK activity, and increased skeletal muscle strength caused by increased ATP production. These results indicate that oxidative phosphorylation was increased by SUC acute treatment (23).

SUC has many biological functions with various mechanisms. Intracellular SUC can be oxidized to fumarate under the catalysis of mitochondrial complex II, which participates in energy metabolism (43, 44) and affects epigenetics through SUC dehydrogenase (45). Even though SUC is not permeable to mammalian cell membranes (11, 13, 14), it can activate calcium ion signals via the membrane receptor SUCNR1 (22). Some people held the opinion that SUCNR1 was not expressed in skeletal muscle cells (18), but we found that SUCNR1 mRNA and protein were expressed on C2C12 cells, and the fluorescence of SUCNR1 presented around the skeletal muscle fibers, which is consistent with some research findings (17). The mitochondrial calcium level strictly controls mitochondrial ATP production (46), which could stimulate complex III and ATP synthase on the electron transport chain to accelerate oxidative phosphorylation (47). We have proved that SUC can activate calcium signals after activating SUCNR1 in our previous study (10). Consequently,

we conjectured that SUC could increase energy production due to the effect of SUC on the mitochondrial calcium signal by increasing intracellular calcium.

Altogether SUC enhances the energy production efficiency by consuming lactate consumption and accelerating oxidative phosphorylation via SUCNR1 under the condition of rapid exercise.

## CONCLUSION

In conclusion, the acute administration of SUC enhanced mitochondrial oxidative phosphorylation, accelerated electron transfer in the mitochondrial oxidative respiratory chain, greatly increased energy for acute exercise, and consumed lactate. The interaction mechanism of SUCNR1 activation with mitochondrial oxidative phosphorylation should be further developed.

## DATA AVAILABILITY STATEMENT

The original contributions presented in the study are included in the article/supplementary material, further inquiries can be directed to the corresponding authors.

## ETHICS STATEMENT

The animal study was reviewed and approved by Animal Subjects Committee of South China Agricultural University.

## AUTHOR CONTRIBUTIONS

Data acquisition and methodology were completed by GX and GS was the main contributor to the study conceptualization, article reviewing, and editing. GX, YY, and PL contributed to the manuscript writing. JY and JZ supported mice feeding. All authors were involved in data analysis and data interpretation.

## FUNDING

This study was supported by the research project of Guangdong Laboratory for Lingnan Modern Agriculture (NZ2021028); the local innovative and research team project of Guangdong province (2019BT02N630); Guangdong Key Research and Development Program (2019B020218001).

## REFERENCES

1. Consitt LA, Dudley C, Saxena G. Impact of endurance and resistance training on skeletal muscle glucose metabolism in older adults. *Nutrients*. (2019) 11:E2636. doi: 10.3390/nu11112636
2. Holloszy JO, Coyle EF. Adaptations of skeletal muscle to endurance exercise and their metabolic consequences. *J Appl Physiol*. (1984) 4:831–8. doi: 10.1152/jappl.1984.56.4.831
3. Martinez-Reyes I, Chandel NS. Mitochondrial TCA cycle metabolites control physiology and disease. *Nat Commun*. (2020) 1:102. doi: 10.1038/s41467-019-13668-3
4. Pascoe DD, Gladden LB. Muscle glycogen resynthesis after short term, high intensity exercise and resistance exercise. *Sports Med*. (1996) 2:98–118. doi: 10.2165/00007256-199621020-00003
5. Chin RM, Fu X, Pai MY, Vergnes L, Hwang H, Deng G, et al. The metabolite α-ketoglutarate extends lifespan by inhibiting ATP synthase and TOR. *Nature*. (2014) 7505:397–401. doi: 10.1038/nature13264
6. An D, Zeng Q, Zhang P, Ma Z, Zhang H, Liu Z, et al. Alpha-ketoglutarate ameliorates pressure overload-induced chronic cardiac dysfunction in mice. *Redox Biol*. (2021) 46:102088. doi: 10.1016/j.redox.2021.102088
7. Herrmann AK, Wüllner V, Moos S, Graf J, Chen J, Kieseier B, et al. Dimethyl fumarate alters intracellular Ca(2+) handling in immune cells by redox-mediated pleiotropic effects. *Free Radical Biol Med*. (2019) 141:338–47. doi: 10.1016/j.freeradbiomed.2019.07.005
8. Aguiar CJ, Rocha-Franco JA, Sousa PA, Santos AK, Ladeira M, Rocha-Resende C, et al. Succinate causes pathological cardiomyocyte hypertrophy through GPR91 activation. *Cell Commun Signal*. (2014) 12:78. doi: 10.1186/s12964-014-0078-2
9. Lu YT, Li LZ, Yang YL, Yin X, Liu Q, Zhang L, et al. Succinate induces aberrant mitochondrial fission in cardiomyocytes through GPR91 signaling. *Cell Death Dis*. (2018) 6:672. doi: 10.1038/s41419-018-0708-5
10. Wang T, Xu YQ, Yuan YX, Xu PW, Zhang C, Li F, et al. Succinate induces skeletal muscle fiber remodeling via SUNCR1 signaling pathway. *EMBO Rep*. (2019) 20:e47892. doi: 10.15252/embr.201947892
11. Mills EL, Pierce KA, Jedrychowski MP, Garrity R, Winther S, Vidoni S, et al. Accumulation of succinate controls activation of adipose tissue thermogenesis. *Nature*. (2018) 7716:102–6. doi: 10.1038/s41586-018-0353-2
12. Tomasiak TM, Cecchini G, Iverson TM. Succinate as donor; fumarate as acceptor. *EcoSal Plus*. (2007) 2:1–24. doi: 10.1128/ecosal.3.2.6
13. Hems R, Stubbs M, Krebs HA. Restricted permeability of rat liver for glutamate and succinate. *Biochem J*. (1968) 6:807–15. doi: 10.1042/bj1070807
14. Ehinger JK, Piel S, Ford R, Karlsson M, Sjövall F, Frostner E, et al. Cell-permeable succinate prodrugs bypass mitochondrial complex I deficiency. *Nat Commun*. (2016) 7:12317. doi: 10.1038/ncomms12317
15. McCreath KJ, Espada S, Galvez BG, Benito M, de Molina A, Sepulveda P, et al. Targeted disruption of the SUCNR1 metabolic receptor leads to dichotomous effects on obesity. *Diabetes*. (2015) 4:1154–67. doi: 10.2337/db14-0346
16. Kirova YI, Shakova FM, Germanova EL, Romanova GA, Voronina TA. The effect of Mexidol on cerebral mitochondriogenesis at a young age and during aging. *Zhurnal nevrologii i psikhiatrii imeni S.S. Korsakova*. (2020) 1:62–9. doi: 10.17116/jnevro202012001162
17. Guo Y, Cho SW, Saxena D, Li X. multifaceted actions of succinate as a signaling transmitter vary with its cellular locations. *Endocrinol Metabol*. (2020) 1:36–43. doi: 10.3803/EnM.2020.35.1.36
18. Reddy A, Bozi LHM, Yaghi OK, Mills EL, Xiao H, Nicholson HE, et al. pH-Gated succinate secretion regulates muscle remodeling in response to exercise. *Cell*. (2020) 1:62–75.e17. doi: 10.1016/j.cell.2020.08.039
19. Zhu CJ, Xu PW, He YL, Yuan YX, Wang T, Cai XC, et al. Heparin increases food intake through AgRP neurons. *Cell Rep*. (2017) 10:2455–67. doi: 10.1016/j.celrep.2017.08.049
20. Yuan Y, Xu P, Jiang Q, Cai X, Wang T, Peng W, et al. Exercise-induced alpha-ketoglutaric acid stimulates muscle hypertrophy and fat loss through OXGR1-dependent adrenal activation. *EMBO J*. (2020) 39:e103304. doi: 10.1101/796037
21. Lahiri S, Kim H, Garcia-Perez I, Reza MM, Martin KA, Kundu P, et al. The gut microbiota influences skeletal muscle mass and function in mice. *Sci Transl Med*. (2019) 502:1–15. doi: 10.1126/scitranslmed.aan5662
22. Wang T, Xu YQ, Yuan YX, Xu PW, Zhang C, Li F, et al. Succinate induces skeletal muscle fiber remodeling via SUCNR1 signaling. *EMBO Rep*. (2021) 6:e53027. doi: 10.15252/embr.202153027
23. Nolfi-Donegan D, Braganza A, Shiva S. Mitochondrial electron transport chain: oxidative phosphorylation, oxidant

production, and methods of measurement. *Redox biology*. (2020) 37:101674. doi: 10.1016/j.redox.2020.101674
24. Hui S, Ghergurovich JM, Morscher RJ, Jang C, Teng X, Lu W, et al. Glucose feeds the TCA cycle via circulating lactate. *Nature*. (2017) 7678:115–8. doi: 10.1038/nature24057
25. Moghetti P, Bacchi E, Brangani C, Donà S, Negri C. Metabolic effects of exercise. *Front Hormone Res*. (2016):44–57. doi: 10.1159/000445156
26. Hunter GR, Fisher G, Neumeier WH, Carter SJ, Plaisance EP. Exercise training and energy expenditure following weight loss. *Med Sci Sports Exercise*. (2015) 9:1950–7. doi: 10.1249/MSS.0000000000000622
27. Ranallo RF, Rhodes EC. Lipid metabolism during exercise. *Sports Med*. (1998) 1:29–42. doi: 10.2165/00007256-199826010-00003
28. Van Proeyen K, Szlufcik K, Nielens H, Ramaekers M, Hespel P. Beneficial metabolic adaptations due to endurance exercise training in the fasted state. *J Appl Physiol*. (2011) 1:236–45. doi: 10.1152/japplphysiol.00907.2010
29. Cadenas S. Mitochondrial uncoupling, ROS generation and cardioprotection. *Biochimica et Biophysica Acta. Bioenergetics*. (2018) 9:940–50. doi: 10.1016/j.bbabio.2018.05.019
30. Yuan Y, Xu Y, Xu J, Liang B, Cai X, Zhu C, et al. Succinate promotes skeletal muscle protein synthesis via Erk1/2 signaling pathway. *Mol Med Rep*. (2017) 5:7361–6. doi: 10.3892/mmr.2017.7554
31. Ruegsegger GN, Booth FW. Health benefits of exercise. *Cold Spring Harbor Perspect Med*. (2018) 7:11. doi: 10.1101/cshperspect.a029694
32. Paavolainen L, Häkkinen K, Hämäläinen I, Nummela A, Rusko H. Explosive-strength training improves 5-km running time by improving running economy and muscle power. *J Appl Physiol*. (1999) 5:1527–33. doi: 10.1152/jappl.1999.86.5.1527
33. Linnamo V, Häkkinen K, Komi PV. Neuromuscular fatigue and recovery in maximal compared to explosive strength loading. *Eur J Appl Physiol Occup Physiol*. (1998) 1–2:176–81. doi: 10.1007/s004210050317
34. Beattie K, Carson BP, Lyons M, Kenny IC. The effect of maximal- and explosive-strength training on performance indicators in cyclists. *Int J Sports Physiol Performance*. (2017) 4:470–80. doi: 10.1123/ijspp.2016-0015
35. Berryman N, Maurel DB, Bosquet L. Effect of plyometric vs. dynamic weight training on the energy cost of running. *J Strength Cond Res*. (2010) 7:1818–25. doi: 10.1519/JSC.0b013e3181def1f5
36. Häkkinen K, Kraemer WJ, Newton RU, Alen M. Changes in electromyographic activity, muscle fibre and force production characteristics during heavy resistance/power strength training in middle-aged and older men and women. *Acta Physiol Scand*. (2001) 1:51–62. doi: 10.1046/j.1365-201X.2001.00781.x
37. Jansson L, Andersson A, Bodin B, Kallskog O. Pancreatic islet blood flow during euglycaemic, hyperinsulinaemic clamp in anaesthetized rats. *Acta Physiol*. (2007) 4:319–24. doi: 10.1111/j.1748-1716.2006.01666.x
38. Giovanelli N, Taboga P, Rejc E, Lazzer S. Effects of strength, explosive and plyometric training on energy cost of running in ultra-endurance athletes. *Eur J Sport Sci*. (2017) 7:805–13. doi: 10.1080/17461391.2017.1305454
39. Morioka S, Perry JSA, Raymond MH, Medina CB, Zhu Y, Zhao L, et al. Efferocytosis induces a novel SLC program to promote glucose uptake and lactate release. *Nature*. (2018) 100:14–31. doi: 10.1038/s41586-018-0735-5
40. Brand MD. Mitochondrial generation of superoxide and hydrogen peroxide as the source of mitochondrial redox signaling. *Free Radical Bio Med*. (2016) 100:14–31. doi: 10.1016/j.freeradbiomed.2016.04.001
41. Kim J, Kim J, Bae JS. ROS homeostasis and metabolism: a critical liaison for cancer therapy. *Exp Mol Med*. (2016) 11:e269. doi: 10.1038/emm.2016.119
42. Bottje WG. Oxidative metabolism and efficiency: the delicate balancing act of mitochondria. *Poultry Sci*. (2019) 10:4223–30. doi: 10.3382/ps/pey405
43. Her YF, Maher LJ III. Succinate dehydrogenase loss in familial paraganglioma: biochemistry, genetics, and epigenetics. *Int J Endocrinol*. (2015) 2015:296167. doi: 10.1155/2015/296167
44. Tretter L, Patocs A, Chinopoulos C. Succinate, an intermediate in metabolism, signal transduction, ROS, hypoxia, and tumorigenesis. *Biochim et Biophys Acta*. (2016) 8:1086–101. doi: 10.1016/j.bbabio.2016.03.012
45. Dalla Pozza E, Dando I, Pacchiana R, Liboi E, Scupoli MT, Donadelli M, et al. Regulation of succinate dehydrogenase and role of succinate in cancer. *Semin Cell Dev Biol*. (2020) 98:4–14. doi: 10.1016/j.semcdb.2019.04.013
46. Pathak T, Trebak M. Mitochondrial Ca(2+) signaling. *Pharmacol Therapeut*. (2018) 192:112–23. doi: 10.1016/j.pharmthera.2018.07.001
47. Bertero E, Maack C. Calcium signaling and reactive oxygen species in mitochondria. *Circ Res*. (2018) 10:1460–78. doi: 10.1161/CIRCRESAHA.118.310082

**Conflict of Interest:** The authors declare that the research was conducted in the absence of any commercial or financial relationships that could be construed as a potential conflict of interest.

frontiers in Veterinary Science

ORIGINAL RESEARCH
published: 28 January 2022
doi: 10.3389/fvets.2021.815878

# Mitochondrial and Glycolytic Capacity of Peripheral Blood Mononuclear Cells Isolated From Diverse Poultry Genetic Lines: Optimization and Assessment

*Meaghan M. Meyer, Susan J. Lamont and Elizabeth A. Bobeck**

*Department of Animal Science, Iowa State University, Ames, IA, United States*

Cellular metabolic preference is a culmination of environment, nutrition, genetics, and individual variation in poultry. The Seahorse XFe24 analyzer was used to generate foundational immune cellular metabolic data in layer, broiler, and legacy genetic strains using fresh chicken peripheral blood mononuclear cells (PBMCs). Baseline mitochondrial respiration [oxygen consumption rate (OCR)] and glycolytic activity [extracellular acidification rate (ECAR)] were determined in modern commercial laying hen (Bovans White) and broiler (Ross 308) lines, as well as the highly inbred lines of Iowa State University (L8, Fayoumi M-15.2, Spanish, Ghs-6), partially inbred broiler line, and advanced intercrosses of broiler by Fayoumi M-15.2 and broiler by Leghorn lines. Commercial broiler vs. Bovans layer and unvaccinated vs. vaccinated Bovans layer immune cell metabolic potential were compared following an in-assay pathway inhibitor challenge. Titrations consistently showed that optimal PBMC density in laying hens and broilers was 3 million cells per well monolayer. Assay media substrate titrations identified 25 mM glucose, 1 mM glutamine, and 1 mM sodium pyruvate as the optimal concentration for layer PBMCs. Pathway inhibitor injection titrations in Bovans layers and broilers showed that 0.5 μM carbonyl cyanide-4 phenylhydrazone (FCCP) and 1 μM oligomycin were optimal. Baseline OCR and ECAR were significantly affected by genetic line of bird ($p < 0.05$), with the dual-purpose, L8 inbred line showing the highest OCR (mean 680 pmol/min) and the partially inbred broiler line showing the greatest ECAR (mean 74 mpH/min). ECAR metabolic potential tended to be greater in modern layers than broilers ($p < 0.10$), indicating increased ability to utilize the glycolytic pathway to produce energy. OCR was significantly higher in vaccinated than unvaccinated hens ($p < 0.05$), while baseline ECAR values were significantly lower in vaccinated Bovans laying hens, showing increased oxidative capacity in activated immune cells. These baseline data indicate that different genetic strains of birds utilized the mitochondrial respiration pathway differently and that modern commercial lines may have reduced immune cell metabolic capacity compared with legacy lines due to intense selection for production traits. Furthermore, the Seahorse assay demonstrated the ability to detect differences in cellular metabolism between genetic lines and immune status of chickens.

**Keywords: PBMC, cellular metabolism, glycolysis, mitochondrial respiration, genetic selection**

OPEN ACCESS

***Edited by:***
*Hui Zhang,*
*South China Agricultural University, China*

***Reviewed by:***
*Zhenlei Zhou,*
*Nanjing Agricultural University, China*
*Xiaolong Gu,*
*China Agricultural University, China*

****Correspondence:***
*Elizabeth A. Bobeck*
*eabobeck@iastate.edu*

***Specialty section:***
*This article was submitted to Animal Nutrition and Metabolism, a section of the journal Frontiers in Veterinary Science*

***Received:*** *16 November 2021*
***Accepted:*** *10 December 2021*
***Published:*** *28 January 2022*

***Citation:***
*Meyer MM, Lamont SJ and Bobeck EA (2022) Mitochondrial and Glycolytic Capacity of Peripheral Blood Mononuclear Cells Isolated From Diverse Poultry Genetic Lines: Optimization and Assessment. Front. Vet. Sci. 8:815878. doi: 10.3389/fvets.2021.815878*

## INTRODUCTION

Environmental and disease challenges alter feed intake, caloric requirements, and thus downstream energy metabolism in livestock. The impact of challenges on the immune system can be measured by isolating a population of cells and monitoring changes in cellular metabolism. Baseline cellular metabolic preference can be determined as impacted by disease status, nutrition, genetics, and individual variation in poultry. However, past research modeling energy usage in avian species has largely utilized immortal cell lines rather than heterogeneous cells isolated from whole blood collected from the animal itself. Hence, the objectives of the current study were to use the chicken as a model: fresh chicken peripheral blood mononuclear cells (PBMC) were used in an advanced metabolic assay to measure the effects of genetics and vaccination on baseline immune cell mitochondrial respiration and glycolysis. Furthermore, we aimed to quantify differences in the ability of cells isolated from two vastly divergent production strains (meat-type vs. egg-laying birds) to respond to an in-assay metabolic pathway inhibitor challenge. Before metabolic analysis, a series of titration experiments were conducted to ensure optimal plating conditions for cells assayed immediately post-isolation from whole blood because of the novelty of the cell types and treatments used.

Peripheral blood mononuclear cells (PBMCs) in chickens contain leukocytes, thrombocytes, and a small percentage of erythrocytes and monocytes (1) and are considered to be high-quality immune cells once isolated for use in further assays (2). Chicken cell culture lines have been used previously in the Seahorse metabolic assay, including immortal chicken macrophage-like cells (3), chicken embryo fibroblast cells (4), and cultured chicken primary brain cells (5), but to the knowledge of the authors, there is no published work using freshly isolated immune cells analyzed the same day. However, previous metabolic work has highlighted the functionality of immune cells as models for cellular metabolism (6, 7), hence, the relevance in using these cells directly after isolation. Chicken immune cells make for a particularly interesting model, as chicken populations in the last 60–70 years have been genetically selected from what were once multipurpose birds to two divergent, highly feed-efficient commercial lines: fast-growing broilers (8) or egg-producing layers (9). Ultimately, stringent artificial genetic selection for production traits of muscle accretion or egg production comes at the cost of other natural, biological functions that are also energetically expensive, i.e., the immune system (10). Baseline metabolic rates and immune cell pathway preferences between modern broiler and layer lines vs. legacy lines of chickens are, thus, of interest but have not been evaluated using an advanced metabolic assay. Furthermore, immune system activation, such as that induced by vaccination, has been shown to come at a cost in terms of redirecting energy from metabolism, nutrient partitioning, behavior, thermoregulation, etc. (11).

The Seahorse Extracellular Flux Analyzer (Agilent, CA, USA) is considered the "gold standard" for quantifying mitochondrial function and bioenergetics in cells. It measures two key outcomes: oxygen consumption rate (OCR) and extracellular acidification rate (ECAR), and includes assays specifically designed to stress cells and measure metabolic potential (Agilent). Mitochondria are organelles containing a double membrane, termed the outer and inner mitochondrial membranes, which, in turn, give rise to two components called the intermembrane space and the matrix (12). Passage of electrons through the electron transport chain creates energy, and the energy created by the electron transport chain establishes the proton motive force (12). In the Seahorse assay environment, without limited substrate availability, mitochondrial oxygen consumption is driven solely by proton motive force. Proton motive force is potential energy in the form of an electrochemical proton gradient that exists across the inner mitochondrial membrane and drives ATP production from ADP (13), and is increasingly used with increasing energy demands of the cell, hence, increasing the rate of oxygen consumption. When all ADP available has been converted into ATP by ATP synthase, oxygen consumption slows and is driven by proton leak. Mitochondrial proton leak is the process through which protons return to the mitochondrial matrix in the absence of ADP (14).

Oligomycin is an ATP synthase inhibitor that prevents phosphorylation of ADP, hence, slowing OCR and leaving only proton leak or non-mitochondrial respiration (14, 15). Glycolysis is then stimulated to meet the need of the cell for energy production (15). Glycolytic rate is measured through increased proton concentration/decreased pH, termed ECAR in-assay (Agilent). Carbonyl cyanide-4 phenylhydrazone (FCCP) is a mitochondrial uncoupler that depolarizes mitochondria, maximizing proton leak and, hence, oxygen consumption. After FCCP addition, the electron transport chain is no longer reliant on maintenance of a membrane potential, effectively speeding the passage of electrons to the maximum, limited only by substrate and oxygen availability (15). The Cell Energy Phenotype Assay (Agilent, CA, USA) allows assessment of the relative use of each energy-producing metabolic pathway and a unique comparison of the preference of the cells or more utilized pathway. After measuring baseline OCR and ECAR a pathway inhibitor challenge is introduced through simultaneous injection of FCCP and oligomycin. As described, FCCP is an uncoupler that disrupts mitochondrial membrane potential and drives oxygen consumption, while oligomycin inhibits ATP synthase and reduces mitochondrial respiration, hence, driving compensatory glycolysis. The effect of both stressors injected together is an increased glycolytic rate due to inhibited mitochondrial ATP production (Oligomycin) and increased oxygen consumption as the depolarized mitochondrial membranes drive the mitochondria to work to re-establish membrane potential (FCCP). Assay output includes baseline and stressed rates, metabolic rates, used together to calculate metabolic potential. In other words, "the cells' ability to meet an energy demand *via* respiration and glycolysis" (Agilent).

Therefore, the current work aimed to conduct titration experiments utilizing chicken PBMCs isolated from whole blood collections for same-day analysis in the Seahorse Xfe24 Analyzer in order to compare baseline metabolic phenotype between modern commercial broiler and layer lines as well as multiple

inbred lines of chickens, some dating back to 1925. Additionally, the study aimed to determine metabolic response to in-assay pathway inhibitors between the two commercial lines, and to determine the effects of an *in vivo* immune system challenge in the form of a vaccine on laying hen PBMC metabolism, both baseline and following an in-assay pathway inhibitor injection.

## MATERIALS AND METHODS

All live bird procedures were approved by the Iowa State University Institutional Animal Care and Use Committee (IACUC #8-16-8294-GM).

### Animals

Nine different chicken genetic lines from an existing colony at the Iowa State University Research and Teaching Farm (Ames, IA, USA) were used as the animal model, including two modern commercially available lines (laying hen and broiler) as well as seven additional genetic bird lines unique to Iowa State University. Birds were selected at random for blood draws, with the exception of a subset of recently vaccinated Bovans layers (IL-4 peptide vaccine; $n = 15$ hens) utilized for a bird-level immune challenge comparison. The commercial laying hen line used was Bovans White (Hendrix Genetics). Bovans layers were singly housed in 10 by 16-in. hanging cages (18 in. height) and were aged ∼40 weeks at the time of the experiment. Approximately 140 Bovans laying hens were available for blood collections throughout this experiment. The commercial line of broilers (meat-type chickens) utilized were mixed sex Ross 308 (Aviagen), aged 5–7 weeks. Broilers were group housed in 4 by 4-ft pens of 10 (100 total broilers). The remaining genetic lines used for metabolic comparison were ∼32 weeks of age and were singly housed hens kept in the same-sized cages as Bovans White hens, with the exception of the larger inbred broiler line, which were individually housed in 23 by 16-in. cages (21 in. height). There was a total of seven birds per genetic line available for blood draws. These lines are maintained by the Iowa State University for genetics research and include highly inbred lines (L8, Ghs-6, Spanish, Fayoumi M-15.2), a partially inbred broiler line, and two advanced intercrosses (broiler x inbred Ghs-6; broiler x inbred Fayoumi M-15.2). Brief genetic descriptions are provided in **Table 1**.

### Blood Collection and Peripheral Blood Mononuclear Cell Isolation

Approximately 3 ml of blood/bird was collected from the brachial wing vein into a 3-ml syringe and transferred into sterile heparinized tubes (BD Vacutainer, NJ, USA). Peripheral blood mononuclear cells (PBMC) were isolated from whole blood using Histopaque 1077 and 1119 (Sigma-Aldrich, MO, USA). Live cells were resuspended in Seahorse assay media (pH 7.4, 37°C) and counted using a hemocytometer and trypan blue staining.

### Metabolic Analysis

Metabolic analyses were conducted on live primary peripheral blood mononuclear immune cells using the Cell Energy Phenotype Test within the Seahorse XFe24 Analyzer (Agilent, CA, USA). The Cell Energy Phenotype Test measures both mitochondrial respiration through oxygen consumption rate (OCR; pmol/min) and glycolysis through lactic acid production/extracellular acidification rate (ECAR; mpH/min) before and after a metabolic pathway inhibitor challenge. Assay preparation and procedure as outlined by Agilent (Seahorse XF Cell Energy Phenotype Test Kit User Guide) were followed to carry out titrations and metabolic tests using Xfe 24-well plates. Sensor cartridges were hydrated using Seahorse XF Calibrant, pH 7.4 (Agilent) the day before assay and placed in a 37°C incubator overnight. On the day of the run, assay media were prepared according to Agilent protocols and media optimization (described under *Titrations*) at pH 7.4 and placed in 37°C incubator prior to use. FCCP and oligomycin were resuspended in assay media and loaded into the Seahorse Sensor Cartidge Port A at a volume of 56 μl/port. Seahorse cell culture plates were prepared in advance with Cell-Tak solution (Corning, NY, USA) to better adhere cells to the plate. After live PBMCs were counted and resuspended in assay media, they were seeded in the Seahorse cell culture plate in duplicate at a volume of 100 μl/well and centrifuged at 200 × g for 1 min. Following centrifugation, fresh assay media were added to each well for a total volume of 500 μl/well. Four blanks/plate were filled with 500 μl of assay media alone. Cell culture plates were incubated at 37°C for 1 h prior to assay. Raw OCR and ECAR values are presented without an assay inhibitor challenge (baseline readings), and in the presence of an assay inhibitor challenge, the metabolic potential (%) is calculated by dividing the stressed (post-injection) values by the baseline values (pre-injection) × 100.

### Titrations

Due to the novelty of using fresh chicken cells isolated from whole blood within the Seahorse assay, prior to assessing challenges or differences between strains, a titration experiment was carried out using laying hen (Bovans white) and broiler (Ross 308) PBMCs to determine optimal cell seeding density, concentration of substrates in the assay media, and FCCP injection concentration. Each set of titrations were conducted using cells isolated from the same bird to allow comparison without inter-bird variation.

#### Cell Seeding Density

Cell seeding densities of 2, 3, 4, and 5 million cells per well were assessed using both laying hen and broiler PBMCs. Visual analysis of cells under a microscope for distribution in a monolayer as well as mean baseline OCR and ECAR values were used to determine ideal plating density.

#### Assay Media

Working media for this assay include Agilent Seahorse XF Base Media, pH 7.4, (Agilent, CA, USA) with the addition of sodium pyruvate (Sigma-Aldrich, MO, USA), L-glutamine (Sigma-Aldrich), and glucose (Sigma-Aldrich). Therefore, consecutive titration experiments were conducted using laying hen PBMCs to determine the optimal concentration of each substrate added to base media. Bovans laying hen cells alone were initially used for substrate optimization to provide optimal, identical assay

**TABLE 1 |** Name and description of each of the genetic lines utilized for metabolic comparison with modern commercial layer and broiler lines.

| Line name | Description |
|---|---|
| Line-8 | Inbred since 1925. Laying hen body size |
| Spanish | Inbred since 1954. Originated in Spain |
| Fayoumi M-15.2 | Inbred since 1954. Originated from Fayoum, Egypt |
| Ghs-6 | Inbred since 1954. Originated from two US commercial Leghorn layer lines |
| Broiler (partially inbred) | Closed breeding population for 30 generations; accumulated inbreeding ∼50%. Originated from commercial broiler parent line |
| Broiler x Ghs-6 advanced intercross | Advanced intercross line established from single broiler male and inbred Ghs-6 females |
| Broiler x Fayoumi M-15.2 advanced intercross | Advanced intercross line established from single broiler male and inbred Fayoumi M-15.2 females |

media. Analyses between genetic lines were verified to behave similarly, and therefore, assays were conducted using the same media compositions for metabolic comparison so outcomes were not impacted by differences in substrate availability. Agilent recommends a concentration of 1 mM sodium pyruvate, 2 mM l-glutamine, and 10 mM glucose in the assay; hence, these concentrations were used as a starting point. Glucose was titrated first, testing 5.5, 10, 25, and 50 mM glucose in combination with the recommended concentrations of sodium pyruvate (1 mM) and l-glutamine (2 mM). Sodium pyruvate was optimized second, using 0.5, 1, 2, and 4 mM sodium pyruvate in combination with the recommended concentration of l-glutamine (2 mM) and 25 mM glucose, the optimized concentration from the glucose titration. Last, 1, 2, 4, and 8 mM l-glutamine were tested using the optimized concentration of sodium pyruvate, 1 mM pyruvate, and 25 mM glucose. Optimal concentration of each substrate was determined by peak baseline OCR and ECAR values.

### Drug Injection

FCCP injection concentration was optimized using ideal cell seeding density and assay media concentrations determined in previous titrations in laying hen and broiler PBMCs. FCCP was titrated independently at 0.125, 0.25, 0.5, 1, and 2 μM. Following FCCP optimization, FCCP was titrated in laying hen cells only in combination with oligomycin (kept constant at 1 μM) to ensure that ideal concentration did not change. Optimal FCCP concentration was determined by response post-injection challenge, hence, using peak stressed OCR and ECAR values.

## Baseline Metabolism

Following assay optimization for chicken PBMCs, comparison of baseline metabolic performance with no pathway inhibitor challenge was compared across the nine genetic lines of birds previously described. Baseline OCR and ECAR values were measured using the Cell Energy Phenotype Test without pathway inhibitor (FCCP and oligomycin) injections. This allowed for an unchallenged comparison of inherent differences between immune cells isolated from different strains of birds under identical conditions.

## Metabolic Challenges

### Pathway Inhibitor (*In vitro*)

Following baseline comparisons, mitochondrial respiration and glycolytic rate were analyzed within the Cell Energy Phenotype Test following simultaneous FCCP and oligomycin pathway inhibitor injection. The stressed (post-injection) OCR and ECAR were divided by baseline (pre-injection) OCR and ECAR and multiplied by 100 to calculate metabolic potential (%) of the cells. Metabolic potential, hence, measures the capacity of the immune cells to rise to an increased energy demand. These values were compared between the two common commercial lines of birds (broiler vs. layer) to determine genetic effect on the use of mitochondrial respiration and glycolysis when the immune cells are presented with a metabolic challenge. Seven distinct legacy genetic lines maintained at Iowa State University were also compared in separate assays.

### Vaccination Status (*In vivo*)

A subset of vaccinated Bovans laying hens ($n = 15$) were compared against 15 unvaccinated hens to study the effects of a practical immune challenge on both baseline OCR and ECAR as well as metabolic potential (mitochondrial and glycolytic). The vaccine administered contained IL-4 peptides conjugated to bovine gamma globulin. The first dose used Fruend's complete adjuvant and a booster, 3 weeks later, used Freud's incomplete adjuvant. Hens received 1 ml of oil emulsion vaccine subcutaneously across four sites (breast and legs). Blood was collected for Seahorse metabolic assay approximately 12 weeks following vaccination booster.

## Statistical Analysis

Immune cell metabolic data generated using the Cell Energy Phenotype Test (Seahorse XFe24 Analyzer) were analyzed using Proc Mixed, a mixed linear model, following assessment of data distribution and normality using Proc Univariate in SAS Version 9.4 (NC, USA). Titration data (compared within Bovans laying hen and Ross 308 broiler genetic lines only) were analyzed with the fixed effect of cell seeding density, media substrate concentration, and pathway inhibitor concentration alone. Following titration for optimal assay conditions, baseline ECAR and OCR values (nine genetic lines compared) and metabolic potential (%; commercial broiler and Bovans layer lines compared) were analyzed with the fixed effect of bird genetic line and using a *post-hoc* Tukey–Kramer adjustment for all pairwise comparisons. To study the effects of an *in vivo* bird challenge within the commercial Bovans layer line only, OCR, ECAR, and metabolic potential data were analyzed with the fixed effect of vaccination status (unvaccinated vs. vaccinated). For all measures, least square means (LSMeans) and standard

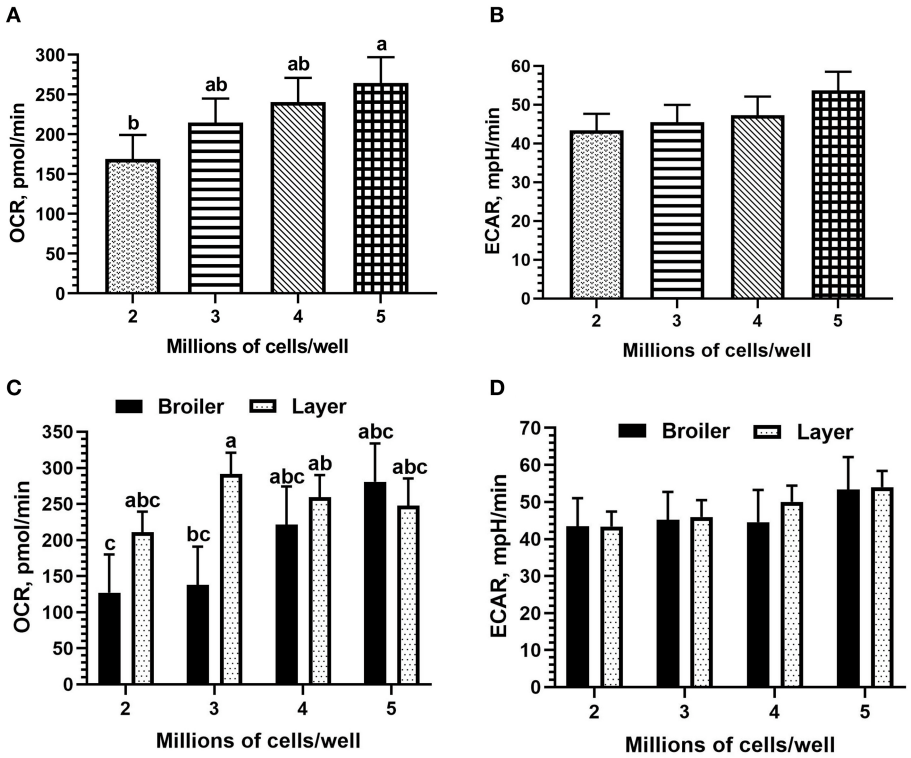


**FIGURE 1 |** Cell seeding density titrations for optimal results using fresh chicken peripheral blood mononuclear cells (PBMCs) (Ross 308 broiler and Bovans layer) in the Seahorse Xfe24 Analyzer (Agilent) by main effect of cell seeding density on **(A)** oxygen consumption rate (OCR) and **(B)** extracellular acidification rate (ECAR), and by the cell seeding density x line of bird interaction on **(C)** OCR and **(D)** ECAR. All data are presented as least square means (LSMeans[1]) (SEM). [1]Bars that do not share letters indicate means that are significantly different ($p \leq 0.05$).

error (SEM) are reported; a value of $p \leq 0.05$ was considered statistically significant.

# RESULTS

## Titrations

### Cell Seeding Density

Cell seeding density did not affect mean OCR nor ECAR, but all titration values fell within an optimal range (OCR: 40–450 pmol/min; ECAR: 20–120 mpH/min). However, both OCR and ECAR values increased with increasing density as expected (**Figures 1A,B**); OCR was significantly increased between 2 and 5 million cells per well (mean 168.97 vs. 264.38 pmol/min). When including the effect of bird line (both broiler and layer PBMCs were used for seeding density titrations), line of bird significantly affected OCR ($p = 0.05$), broiler mean of 191.8 pmol/min vs. 252.39 pmol/min in layer, but not ECAR. Resulting bird type x seeding density interactions were not significant, but differences existed between broiler and layer seeding densities in mean OCR (**Figures 1C,D**). The peak OCR was observed at 3 million cells/well in Bovans layers (mean 291.43 pmol/min) and at 5 million cells/well in broilers (mean 280.87 pmol/min). Peak ECAR was observed at 5 million cells/well in both broilers and Bovans layers (broiler mean 53.35 pmol/min; layer mean 53.97 pmol/min). However, a key requirement of an accurate Seahorse assay is the maintenance of a monolayer of cells, visualized under microscope post-plating. Due to this requirement and the physical limitations of the 24-plate well size, 3 million chicken PBMCs per well were determined as the maximum without inducing overlapping cells. Taking this into consideration, along with the optimal OCR in layers observed at 3 million cells per well, 3 million cells were plated, moving forward, for all titrations and metabolic assays using chicken immune cells.

### Assay Media

The main effect of glucose concentration in the assay media was not statistically significant on OCR nor ECAR, but peak OCR (mean 389.38 pmol/min) and ECAR (mean 57.82 mpH/min) were each observed at 50 mM glucose concentration (**Figures 2A,B**). Due to lack of statistical significance, physiological limits, and the similarity between 25 and 50 mM in ECAR results (53.07 vs. 57.82 mpH/min), 25 mM glucose was determined adequate and used for the remaining titrations and metabolic assays. Sodium pyruvate concentration did not affect OCR but approached significance for ECAR ($p = 0.08$), with a peak of both values occurring at 1 mM pyruvate (mean 243.1 pmol/min and 57.65 mpH/min, respectively, **Figures 2C,D**). Hence, 1 mM was determined optimal for this substrate. The effect of L-glutamine concentration in the assay media was not significant on OCR or ECAR. Numerically,

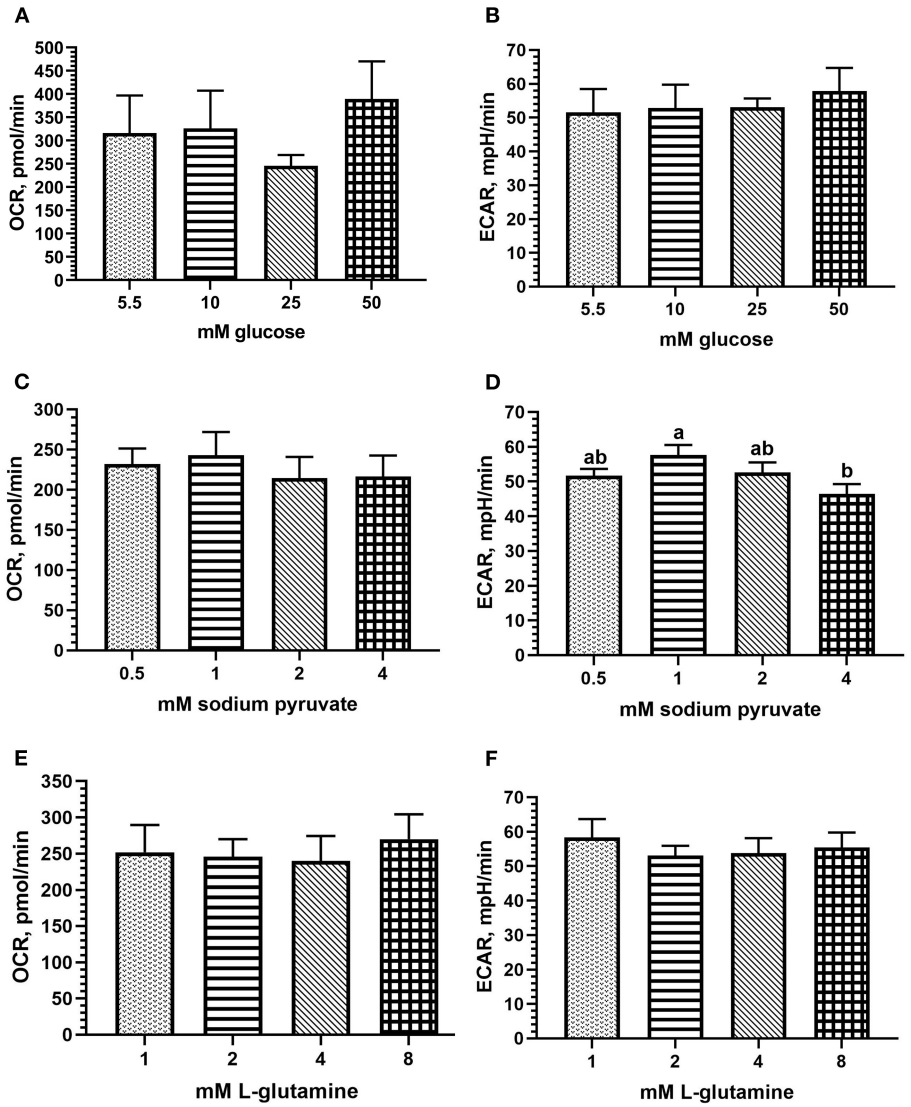


**FIGURE 2 |** Assay media substrate titrations for optimal results using fresh chicken PBMCs in the Seahorse Xfe24 Analyzer (Agilent) by main effect of substrate concentration, including **(A)** glucose; OCR, **(B)** glucose; ECAR, **(C)** sodium pyruvate; OCR; **(D)** sodium pyruvate; ECAR; **(E)** l-glutamine; OCR; and **(F)** l-glutamine; ECAR. All data are presented as LSMeans[1] (SEM). [1]Bars that do not share letters indicate means that are significantly different ($p \leq 0.05$).

peak OCR was observed at 8 mM L-glutamine (mean 269.93 pmol/min; **Figure 2E**), and peak ECAR occurred at 1 mM L-glutamine (mean 58.32 mpH/min; **Figure 2F**). As 8 mM may exceed physiological relevance, and 1 mM followed in OCR peak (mean 251.82 pmol/min), 1 mM L-glutamine was determined optimal for the assay.

## Drug Injection

FCCP was optimized in both Bovans layer and broiler PBMCs. FCCP titration is based off of maximal OCR response and is established to reach a plateau following maximal respiration (**Figure 3**). The effect of FCCP concentration injection was not significant for OCR nor ECAR in the current study. Peak OCR occurred at 0.5 mM FCCP (mean 314.58 pmol/min; **Figure 4A**), and peak ECAR was nearly equivalent between 0.125 and 1 μM FCCP (**Figure 4B**). The bird line x FCCP concentration interaction was not significant for OCR nor ECAR. Peak OCR occurred at 1 μM FCCP in broiler cells (mean 313.78 pmol/min) and at 0.5 μM FCCP in layer cells (mean 337.01 pmol/min; **Figure 4C**). Peak ECAR occurred at 0.25 μM FCCP in broilers (mean 54.76 mpH/min) and at 0.5 μM FCCP in Bovans layers (mean 39.62 mpH/min; **Figure 4D**). When including oligomycin in the titration at a constant concentration of 1 μM in layer cells alone, 0.5 μM FCCP induced peak OCR (363.84 pmol/min; **Figure 4E**) and ECAR (43.58; **Figure 4F**). Due to consistency in 0.5 μM FCCP inducing optimal response in layer cells with and without oligomycin, and to the variability in the results from broiler cells,

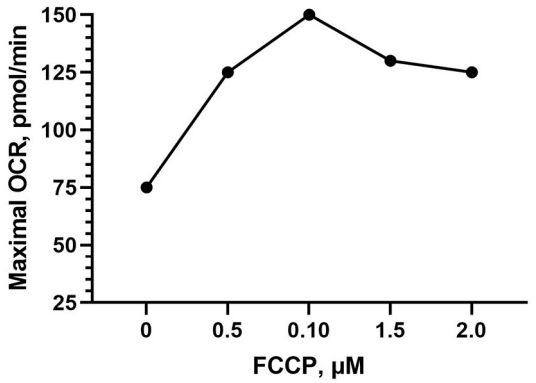


**FIGURE 3 |** Example carbonyl cyanide-4 phenylhydrazone (FCCP) titration within the Seahorse Cell Energy Phenotype test showing the established effect of a plateau in OCR following peak respiration stimulation.

0.5 µM was determined ideal and used moving forward in the metabolic assay.

## Baseline Metabolism

Baseline OCR and ECAR values were compared within nine genetic lines of chickens using optimized conditions determined in laying hen and broiler PBMCs. The effect of genetic line was significant for baseline OCR ($p < 0.01$) and baseline ECAR ($p = 0.01$). Greater OCR was consistently observed in the L8 genetic line (inbred legacy line; mean 679.39 pmol/min) compared with all other lines (**Figure 5A**), representing a 428-pmol/min difference with the modern layer line, and a 404-pmol/min difference with the modern broiler line used here. Peak ECAR was observed in the partially inbred broiler line (mean 74.06 mpH/min), representing a 14-mpH/min difference with the modern Ross 308 broiler line, and a 33 mpH/min difference compared with the modern layer line (Bovan's white; **Figure 5B**).

## Metabolic Challenges

### Pathway Inhibitor

Differences in metabolic potential (%) between broiler and layer PBMCs were examined using the combination of FCCP and oligomycin injection within the Cell Energy Phenotype Test. The effect of bird line was not significant on OCR metabolic potential, but Bovans layer cells (mean of 257.7%) showed a numerical increase of 50% using this mitochondrial pathway compared with broilers (mean 207.4%) when faced with the pathway inhibitor challenge. The effect of genetic line on ECAR metabolic potential approached significance ($p = 0.08$), with a 32.4% difference between layer (mean 207%) and broiler cells (mean 174.5%).

### Vaccination Status

Vaccinated and unvaccinated layer PBMCs were first compared at the baseline to determine differences in resting metabolic rate due to a bird-level immune challenge. Vaccination did not affect OCR, but vaccinated Bovans laying hens (mean 247.72 pmol/min) showed a numerical 15.7 pmol/min increase compared with unvaccinated hens (mean 232.05 pmol/min). ECAR was also unaffected by vaccination, but in contrast to OCR, vaccinated Bovans laying hens (mean 44.77 mpH/min) showed a decrease of 8 mpH/min compared with unvaccinated hens (mean 52.81 mpH/min). In the in-assay pathway inhibitor challenge, OCR metabolic potential was unaffected by vaccination, but vaccinated hens (mean 281.1%) showed an increased response of 14.6% compared with their unvaccinated counterparts (mean 266.6%). ECAR metabolic potential was likewise unaffected by vaccination, but unvaccinated hens (mean 222.2%) showed a 4.4% increase compared with the vaccinated Bovans layers (mean 217.83%).

# DISCUSSION

The Seahorse Analyzer provides a unique opportunity to measure metabolic activity in living cells, but due to variation in cell/cell lines used, titrations are critical to ensure optimal conditions. Multiple authors have performed titration experiments and published protocols in order to provide guidance to assay a wide variety of cells, including human cell lines (HK2) (16), isolated mitochondria from mouse liver (17), mouse skeletal muscle (18), and human skeletal muscle (19), as well as immune cells, including mice lymphocytes (20), mice T cells (21), and human T cells, and B cells (22). Studies using poultry cells, specifically, has included immortal cell culture lines, such as chicken macrophage-like cells (3), embryo fibroblast cells (4), and primary brain cells (5). More recent Seahorse optimization and disease research has been published using PBMCs isolated from humans (23, 24) and human cell lines (25), and research using laying hen PBMCs within the Seahorse assay has been recently published by the current lab group (26), but no optimization of chicken PBMCs has been published. Peripheral blood mononuclear cells are, however, suitable and well-published cells to use in immune cell metabolic and disease research (25), and are an ideal option for Seahorse analysis. Hence, the cell-seeding density (3 million cells/well), assay media substrate concentrations (25 mM glucose, 1 mM sodium pyruvate, and 1 mM l-glutamine) and FCCP injection concentration (0.5 µM) determined here are a suitable guide for future use of chicken PBMCs in the Seahorse Xfe24 Analyzer to maximize the quality of OCR and ECAR. It is well-established that there is an optimal FCCP injection unique to cells used in the assay to stimulate peak or maximal respiration (OCR) before a drop or a plateau in response (Agilent; example visualized in **Figure 3**). In our assays utilizing chicken PBMCs, 0.5 µM FCCP produced the maximal response OCR most consistently (**Figures 4A–F**).

Genetic influence on metabolism is evident at a whole-animal level when selecting for specific traits. For example, in chickens selected for divergence in abdominal fat pad by Dupont et al. (27), changes in liver metabolism were observed to favor lipogenesis and ultimately greater abdominal fat deposition. Meat quality-focused work in broilers has shown that divergent selection for breast ultimate pH at harvest resulted in differences in carbohydrate and protein metabolism, specifically by altering glucose storage and key enzymes in both the mitochondrial respiration and glycolytic pathways (28).

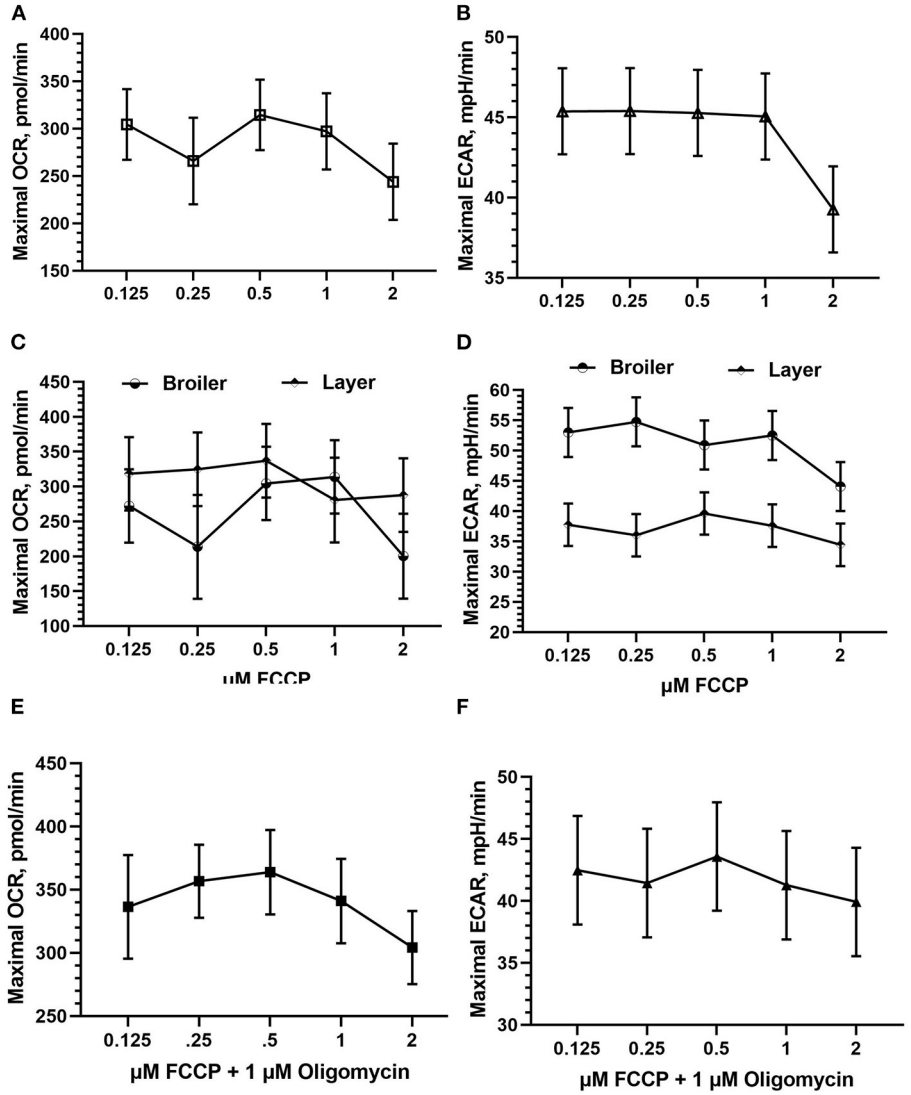


**FIGURE 4 |** FCCP injection optimization using fresh chicken PBMCs in the Seahorse Xfe24 Analyzer (Agilent) by main effect of FCCP concentration on **(A)** OCR, **(B)** ECAR, and the interaction of FCCP concentration x bird line (Ross 308 broiler vs. Bovans layer) on **(C)** OCR and **(D)** ECAR. Last, FCCP was titrated in Bovans white layer cells in combination with 1 µM oligomycin on **(E)** OCR and **(F)** ECAR. All data presented are LSMeans (SEM).

Additionally, lipid metabolism is shown to be dysregulated in broilers affected by the woody breast myopathy, an unintended consequence of selection for increased breast yield (29). Genetic selection for egg-producing traits has profoundly impacted bone metabolism in layers (30). Environmental conditions have been shown to affect metabolism in caged vs. free-range layers by Zhang et al. (31), where meat quality-focused inosine monophosphate metabolism genes were differentially expressed based on housing. Environmental heat stress in chickens has a clear impact on metabolism, inducing uncoupling of oxidative phosphorylation in the mitochondria and resulting heat production (32). Therefore, the differences in baseline PBMC mitochondrial respiration and glycolysis due to genetic variation in chickens observed in the current study are not unexpected but have not been previously studied at the cellular level.

A novel feature of the current work was the comparison between two modern lines with seven unselected, inbred, or intercrossed lines of chickens, the earliest dating back to 1925. The significantly increased OCR, a measure of mitochondrial respiration, observed in the L8, dual-purpose line (inbred line since 1925) compared with modern commercial layer and broiler lines was an unanticipated outcome (**Figure 5A**) that may provide insight into consequences of intense genetic selection in modern commercial breeds. It has been established that selection for economic-focused traits in broilers has reduced diversity of immune system genetics (33) and that laying hens selected for feed efficiency show reduced antibody response to Newcastle

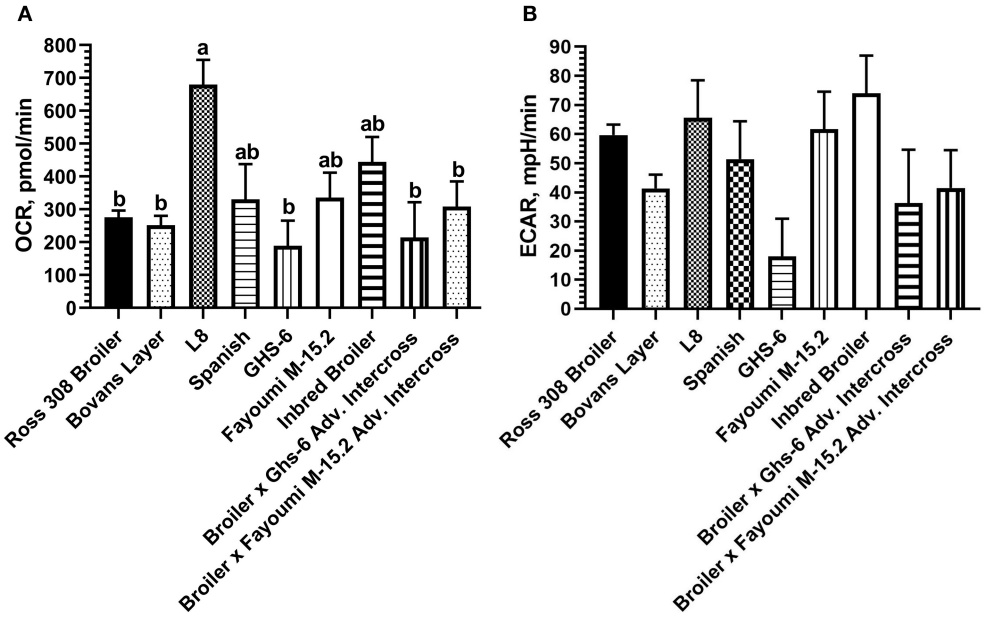


**FIGURE 5 |** Baseline metabolic **(A)** OCR and **(B)** ECAR observed across nine strains of chickens using PBMCs within the Seahorse Xfe24 Analyzer with the main effect of bird genetic line. All data are presented as LSMeans[1] (SEM). [1]Bars that do not share letters indicate means that are significantly different ($p \leq 0.05$).

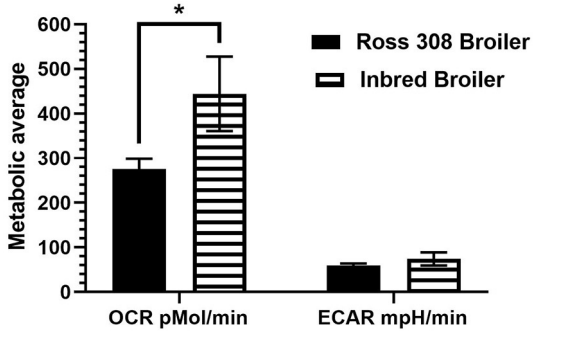


**FIGURE 6 |** Baseline metabolic comparison of OCR and ECAR analyzed between two broiler genetic lines of different ages: Ross 308 broilers (aged 5–7 weeks) and inbred broilers (aged 32 weeks) using PBMCs within the Seahorse Xfe24 Analyzer with the main effect of bird age/genetic line. All data are presented as LSMeans[1] (SEM). [1]Asterisk indicates a difference in LSMeans approaching statistical significance ($p < 0.10$).

disease virus (10). However, given that the L8 is highly inbred, its genetics is expected to be primarily fixed at the alleles in highest frequency at its founding. Overall, production traits are negatively correlated with disease resistance in poultry (34), so we may hypothesize that the unselected, dual-purpose L8 line has maintained more robust baseline immune cell energy production through mitochondrial respiration compared with the two modern day, high-producing strains. Interestingly, the inbred layer strain compared here (Ghs-6, inbred since 1954) was not different in baseline oxygen consumption compared with broilers and Bovans layers, which may be due to the specific genetic line (Leghorn). In terms of baseline glycolytic rate (measured by ECAR), no differences were detected between all nine genetic lines (**Figure 5B**). Regarding the effect of age of chickens on baseline metabolic capacity, the baseline OCR and ECAR were compared between the 5- and 7-week-old Ross 308 broilers and the aged, partially inbred broiler line (∼32 weeks of age; closest genetic age comparison available). The effect of age between these two lines approached significance for OCR ($p = 0.06$) and did not affect ECAR (comparison in **Figure 6**). The lack of difference observed between ECAR in these lines indicate that the age of birds may not be a factor significantly impacting the glycolytic outcomes of this assay. However, OCR was increased in the aged line of inbred broiler, indicating a potentially increased capacity for mitochondrial respiration with age using this animal model. A future true metabolic comparison of the same genetic line of birds from different ages would be necessary to validate this point, as in the current study age and genetics of the bird were statistically confounded. Furthermore, the influence of sex has not been analyzed in this study, as the majority of the birds/genetic lines available for sampling were hens with the exception of mixed sex Ross 308 broilers. Future work comparing male and female cell populations within the same genetic line could explore or rule out this effect.

Glycolysis is considerably less efficient in terms of ATP production compared with mitochondrial respiration, producing only 2 vs. 36 molecules of ATP per molecule of glucose (35). Immune cells in a quiescent state generally rely on mitochondrial oxidative phosphorylation, while activated cells tend to transition to a glycolytic state to swiftly meet increased energy demands (36). Therefore, as the baseline comparison in the current work occurred in birds that were not disease challenged, it is likely

that the glycolytic pathway was less preferred across all cell lines despite varying genetics. Notably, the partially inbred legacy broiler line showed numerically increased glycolytic rate, and the inbred Leghorn line (Ghs-6) showed a numerically decreased ECAR compared with all other lines. This variation may be due to reduced productive efficiency in the partly inbred broiler line, which appears to devote more resources to baseline immune cell metabolism, compared with the inbred layer line, which displayed consistently decreased OCR and ECAR. Interestingly, in the advanced intercross of these two lines (broiler x Ghs-6), both mitochondrial respiration and glycolysis were diminished compared with the inbred broiler line and seemed to be more influenced by the Ghs-6 immune cell metabolic phenotype. Overall, these data provide an interesting perspective in the shift of resource allocation away from the immune system toward performance characteristics with genetic selection over time.

This study also included introducing challenges, either applied to the bird itself or to immune cells within the metabolic assay. When commercial broiler and layer PBMCs were metabolically challenged using FCCP and oligomycin, no statistical differences were found in OCR metabolic potential, or the ability of the cell to rise to the inhibitor challenge using mitochondrial respiration. However, layer cells showed a numerically increased response of 50%, indicating a potentially biologically relevant change. In terms of glycolysis, Bovans layer PBMCs tended to show greater ECAR than broiler PBMCs, with a 32.4% increase. Broiler selection for weight gain has decreased immune system resources, an established phenomenon (10), likely to a greater extent than selection for high egg production has affected the immune response of the hen. Animal behavior may provide confirmation of this: broiler locomotion decreases over development; this is believed to be due in part to energy allocation toward significant weight gain that takes away from metabolic costs of standing, walking, perching, etc. (37). Laying hens, on the other hand, maintain significant physical activity throughout production (38). Additionally, antibody response in laying-type birds has been shown to be stronger and longer lasting than in broilers, making layers more suited for long-term humoral immune response (39). Therefore, a difference in metabolic potential of immune cells between these lines likely reflects their vastly different production traits and the resulting effects on immune system resources.

Due to the relatively more robust metabolic response in layer PBMCs, Bovans laying hens were used for a vaccine response experiment. Vaccines in poultry serve to activate a humoral immune response through antigen introduction (40). Vaccines stimulate B cells to produce antibodies specific to microorganisms of concern to prevent the spread of infection (41), hence, stimulating the immune system. The vaccine administered in the current study did not affect baseline OCR or ECAR, nor metabolic potential of either pathway. However, baseline and metabolic potential of mitochondrial respiration were numerically increased in vaccinated hens compared with unvaccinated hens, and baseline and metabolic potential of the glycolytic pathway in vaccinated Bovans laying hens were slightly numerically decreased in vaccinated hens. Stimulation of B cells has been shown to increase oxygen consumption and mitochondrial respiration (42), explaining the increased OCR in vaccinated hen cells both at the baseline and when challenged in-assay. This outcome also validates efficacy of the vaccine applied to hens in stimulating a humoral immune response. Additionally, the decrease in ECAR reflects the preference of the activated immune cells in the vaccinated model to use oxidative phosphorylation to produce energy rather than glycolysis, as stimulated B cells are not reported to induce glycolysis (42). These data indicate the ability of the Cell Energy Phenotype Test to detect differences in chicken PBMC as induced by a bird-level change in immune status.

In summary, the current work has established optimal assay parameters for use of fresh chicken PBMCs in the Seahorse Xfe24 Analyzer (Agilent) as well as validated use of the assay in determining metabolic differences among various genetic lines and vaccination status of the animal. A novel comparison of immune cell metabolism among modern commercial lines and inbred and intercrossed lines, one dating back to 1925, demonstrated shifts in immune system resources, showing a marked decrease in the baseline capacity of cells isolated from modern production broiler and layer lines. Finally, a vaccinated subset of Bovans layers demonstrated increased use of the mitochondrial respiration pathway, an indication of humoral immune response, compared with their unvaccinated counterparts. This optimized assay provides opportunity for future work using fresh poultry immune cells.

## DATA AVAILABILITY STATEMENT

The raw data supporting the conclusions of this article will be made available by the authors, without undue reservation.

## ETHICS STATEMENT

The animal study was reviewed and approved by Iowa State University Institutional Animal Care and Use Committee (IACUC #8-16-8294-GM).

## AUTHOR CONTRIBUTIONS

EB contributed to conception and design of the study. MM and EB contributed to on-farm sample collection, laboratory metabolic analysis, statistical analysis, and manuscript drafts. SL supplied birds and contributed to the manuscript content. All authors contributed to manuscript revision, read, and approved the submitted version.

## ACKNOWLEDGMENTS

The authors wish to acknowledge Cameron Hall, Jeff Tjelta, Bill Rodgers, the Iowa State Poultry Farm for ongoing animal care, and Julianna Jespersen for experiment support.

## REFERENCES


1. Désert C, Merlot E, Zerjal T, Bed'hom B, Härtle S, Cam AL. Transcriptomes of whole blood and PBMC in chickens. *Comparat Biochem Physiol D Genom Proteomics*. (2016) 20:1–9. doi: 10.1016/j.cbd.2016.06.008
2. Suklek A, Kayan A, Rattanasrisomporn J. Boonkaewwan1 C. Isolation of peripheral blood mononuclear cells and the expression of toll-like receptors in Betong chickens. *Vet World*. (2020) 13:7. doi: 10.14202/vetworld.2020.1372-1375
3. Perry F, Aylward CJ, Arsenault RJ. *The Differential Phosphorylation-Dependent Signaling and Glucose Immunometabolic Responses Induced during Infection by Salmonella Enteritidis and Salmonella Heidelberg in Chicken Macrophage-like cells Microorganisms*. (2020) 8:1041. doi: 10.3390/microorganisms8071041
4. Kong M, Xiang H, Wang J, Liu J, Zhang X, Zhao X. Mitochondrial DNA haplotypes influence energy metabolism across chicken transmitochondrial cybrids. *Genes*. (2020) 11:1. doi: 10.3390/genes11010100
5. Tang Q, Ding C, Xu Q, Bai Y, Xu Q, Wang K, et al. Mitochondrial fusion potentially regulates a metabolic change in Tibetan chicken embryonic brain during hypoxia. *Front Cell Dev Biol*. (2021) 9:585166. doi: 10.3389/fcell.2021.585166
6. Geltink RIK, Kyle RL, Pearce EL. Unraveling the complex interplay between T Cell metabolism and function. *Annu Rev Immunol*. (2019) 36:461–88. doi: 10.1146/annurev-immunol-042617-053019
7. Jung J, Zeng H, Horng T. Metabolism as a guiding force for immunity. *Nat Cell Biol*. (2019) 21:85–93. doi: 10.1038/s41556-018-0217-x
8. Tallentire CW, Leinonen I, Kyriazakis I. Breeding for efficiency in the broiler chicken: a review. (2016) 36:4. doi: 10.1007/s13593-016-0398-2
9. Kidd MT, Anderson KE. Laying hens in the U.S. market: an appraisal of trends from the beginning of the 20th century to present. *J Appl Poult Res*. (2019) 28:771–84. doi: 10.3382/japr/pfz043
10. Zerjal T, Härtle S, Gourichon D, Guillory V, Bruneau N, Laloë D. Assessment of trade-offs between feed efficiency, growth-related traits, and immune activity in experimental lines of layer chickens. *Genet Select Evolut*. (2021) 53:44. doi: 10.1186/s12711-021-00636-z
11. Colditz IG. Effects of the immune system on metabolism: implications for production and disease resistance in livestock. *Livestock Product Sci*. (2002) 75:257–68. doi: 10.1016/S0301-6226(01)00320-7
12. Cheng J, Nanayakkara G, Shao Y, Cueto R, Wang L, Yang WY, et al. Mitochondrial proton leak plays a critical role in pathogenesis of cardiovascular diseases. *Adv Exp Med Biol*. (2017) 982:359–70. doi: 10.1007/978-3-319-55330-6_20
13. Berry BJ, Trewin AJ, Amitrano AM, Kim M, Wojtovich AP. Use the protonmotive force: mitochondrial uncoupling and reactive oxygen species. *J Mol Biol*. (2019) 430:3873–91. doi: 10.1016/j.jmb.2018.03.025
14. Martin Jastroch, ASD, Mookerjee S, Treberg JR, Brand MD. Mitochondrial proton and electron leaks. *Essays Biochem*. (2011) 47:53–67. doi: 10.1042/bse0470053
15. Chacko BK, Kramer PA, Ravi S, Benavides GA, Mitchell T, Dranka BP. The bioenergetic health index: a new concept in mitochondrial translational research. *Clin Sci*. (2014) 127:367–73. doi: 10.1042/CS20140101
16. Gu X, Ma Y, Liu Y, Wan Q. Measurement of mitochondrial respiration in adherent cells by Seahorse XF96 Cell Mito Stress Test. *Star Protoc*. (2021) 2:1. doi: 10.1016/j.xpro.2020.100245
17. Rogers GW, Brand MD, Petrosyan S, Ashok D, Elorza AA, Ferrick DA. High Throughput Microplate Respiratory Measurements Using Minimal Quantities Of Isolated Mitochondria. *PLoS ONE*. (2011) 6:e.21746. doi: 10.1371/journal.pone.0021746
18. Boutagy NE, Pyne E, Rogers GW, Ali M, Hulver MW, Frisard MI. Isolation of mitochondria from minimal quantities of mouse skeletal muscle for high throughput microplate respiratory measurements. *J Vis Exp*. (2015) 105:e53217. doi: 10.3791/53217
19. Bharadwaj MS, Tyrrell DJ, Lyles MF, Demons JL, Rogers GW, Molina AJA. Preparation and respirometric assessment of mitochondria isolated from skeletal muscle tissue obtained by percutaneous needle biopsy. *J Vis Exp*. (2015) 96:e52350. doi: 10.3791/52350
20. Traba J, Miozzo P, Akkaya B, Pierce SK, Akkaya M. An optimized protocol to analyze glycolysis and mitochondrial respiration in lymphocytes. *J Vis Exp*. (2016) 117:54918. doi: 10.3791/54918
21. Windt GJW, Windt vd, Chang C-H, Pearce EL. Measuring bioenergetics in T cells using a seahorse extracellular flux analyzer. *Curr Protoc Immunol*. (2016) 113:3.16B. 11-13.16B.14. doi: 10.1002/0471142735.im0316bs113
22. Nicholas D, Proctor EA, Raval FM, Ip BC, Habib C, Ritou E, et al. Advances in the quantification of mitochondrial function in primary human immune cells through extracellular flux analysis. *PLoS ONE*. (2017) 12:e0170975. doi: 10.1371/journal.pone.0170975
23. Smith AM, Depp C, Ryan BJ, Johnston GI, Alegre-Abarrategui J, Evetts S. Mitochondrial dysfunction and increased glycolysis in prodromal and early Parkinson's blood cells. *Mov Disord*. (2018) 33:1580–90. doi: 10.1002/mds.104
24. Altintas MM, DiBartolo S, Tadros L, Samelko B, Wasse H. Metabolic changes in peripheral blood mononuclear cells isolated from patients with end stage renal disease. *Front Endocrinol*. (2021) 12:629239. doi: 10.3389/fendo.2021.629239
25. Janssen JJE, Lagerwaard B, Bunschoten A, Savelkoul HFJ, van Neerven RJJ, Kiejer J. Novel standardized method for extracellular flux analysis of oxidative and glycolytic metabolism in peripheral blood mononuclear cells. *Nature*. (2021) 11:1662. doi: 10.1038/s41598-021-81217-4
26. Fries-Craft K, Meyer MM, Sato Y, El-Gazzar M, Bobeck EAge A. *Staphylococcus aureus* inoculation route differentially alter metabolic potential and immune cell populations in laying hens. *Front Vet Sci*. (2021) 8:653129. doi: 10.3389/fvets.2021.653129
27. Dupont J, Chen J, Derouet M, Simon J, Leclercq B, Taouis M. Metabolic differences between genetically lean and fat chickens are partly attributed to the alteration of insulin signaling in liver. *J Nutr*. (1999) 129:1937–44. doi: 10.1093/jn/129.11.1937
28. Métayer-Coustard S, Tesseraud S, Praud C, Royer D, Bordeau T, Coudert E. Early growth and protein-energy metabolism in chicken lines divergently selected on ultimate pH. *Front Physiol*. (2021) 12:643580. doi: 10.3389/fphys.2021.643580
29. Papah MB, Abasht B. *Dysregulation of lipid metabolism and appearance of slow myofiber-specific isoforms accompany the development of Wooden Breast myopathy in modern broiler chickens*. Sci Rep. (2019) 9:17170. doi: 10.1038/s41598-019-53728-8
30. Johnsson M, Jonsson KB, Andersson L, Jensen P, Wright D. Genetic regulation of bone metabolism in the chicken: similarities and differences to mammalian systems. *Plos Genet*. (2015) 11:e1005250. doi: 10.1371/journal.pgen.1005250
31. Zhang T, Lu H, Wang L, Yin M, Yang L. Specific expression pattern of IMP metabolism related-genes in chicken muscle between cage and free range conditions. *PLoS ONE*. (2018) 13:e0201736. doi: 10.1371/journal.pone.0201736
32. Ouchi Y, Chowdhury VS, Cockrem JF, Bungo T. Effects of thermal conditioning on changes in hepatic and muscular tissue associated with reduced heat production and body temperature in young chickens. *Front Vet Sci*. (2021) 7:610319. doi: 10.3389/fvets.2020.610319
33. Borodin AM, Alekseev YI, Gerasimov KE, Konovalova NV, Terentjeva EV, Efimov DN. Chickens productivity selection affects immune system genes. *Vavilovskii Zhurnal Genet Selektsii*. (2020) 24:755–60. doi: 10.18699/VJ20.670
34. Zekarias B, Huurne AAHMT, Landman WJM, Rebel JMJ, Pol JMA, Gruys E. Immunological basis of differences in disease resistance in the chicken. *Vet Res*. (2002) 33:109–25. doi: 10.1051/vetres:2002001
35. Bahar Yetkin-Arik IMCV, Vogles IMC, Nowak-Sliwinska P, Weiss A, Houtkooper RH, Van Noorden CJF, et al. The role of glycolysis and mitochondrial respiration in the formation and functioning of endothelial tip cells during angiogenesis. *Sci Rep*. (2019) 9:12608. doi: 10.1038/s41598-019-48676-2
36. Rambold AS, Pearce EL. Mitochondrial dynamics at the interface of immune cell metabolism and function. *Trends Immunol*. (2018) 39:6–18. doi: 10.1016/j.it.2017.08.006
37. Tickle PG, Hutchinson JR, Codd JR. Energy allocation and behaviour in the growing broiler chicken. *Nature*. (2018) 8:4562. doi: 10.1038/s41598-018-22604-2

38. Kozak M, Tobalske B, Springthorpe D, Szkotnicki B, Harlander-Matauschek A. Development of physical activity levels in laying hens in three-dimensional aviaries. *Appl Anim Behav Sci.* (2016) 185:66–72. doi: 10.1016/j.applanim.2016.10.004
39. Koenen ME, Boonstra-Blom AG, Jeurissen SHM. Immunological differences between layer- and broiler-type chickens. *Vet Immunol Immunopathol.* (2002) 89:47–56. doi: 10.1016/S0165-2427(02)00169-1
40. van Ginkel FW, Padgett J, Martinez-Romero G, Miller MS, Joiner KS, Gulley SL, et al. Age-dependent immune responses and immune protection after avian coronavirus vaccination. *Vaccine.* (2015) 33:2655–61. doi: 10.1016/j.vaccine.2015.04.026
41. Janeway CA Jr, Travers P, Walport M. The humoral immune response. In: *Immunobiology: The Immune System in Health and Disease. 5th edition.* New York, NY: Garland Science (2001).
42. Waters LR, Ahsan FM, Wolf DM, Shirihai O, Teitell MA. Initial B cell activation induces metabolic reprogramming and mitochondrial remodeling. *iScience.* (2018) 5:99–109. doi: 10.1016/j.isci.2018.07.005

**Conflict of Interest:** The authors declare that the research was conducted in the absence of any commercial or financial relationships that could be construed as a potential conflict of interest.

frontiers in Veterinary Science

ORIGINAL RESEARCH
published: 31 January 2022
doi: 10.3389/fvets.2021.814765

# Positive Selection Drives the Adaptive Evolution of Mitochondrial Antiviral Signaling (MAVS) Proteins-Mediating Innate Immunity in Mammals

*Hafiz Ishfaq Ahmad[1], Gulnaz Afzal[2], Muhammad Nouman Iqbal[3], Muhammad Arslan Iqbal[4], Borhan Shokrollahi[5], Muhammad Khalid Mansoor[6] and Jinping Chen[7]**

[1] Department of Animal Breeding and Genetics, University of Veterinary and Animal Sciences, Lahore, Pakistan, [2] Department of Zoology, The Islamia University of Bahawalpur, Bahawalpur, Pakistan, [3] Rural Health Centre Sardar Pur Kabirwala, Khanewal, Pakistan, [4] District Head Quarter Hospital, Muzaffargarh, Pakistan, [5] Department of Animal Science, Sanandaj Branch, Islamic Azad University, Sanandaj, Iran, [6] Department of Microbiology, Faculty of Veterinary and Animal Science, The Islamia University of Bahawalpur, Bahawalpur, Pakistan, [7] Guangdong Key Laboratory of Animal Conservation and Resource Utilization, Guangdong Public Laboratory of Wild Animal Conservation and Utilization, Institute of Zoology, Guangdong Academy of Sciences, Guangzhou, China

OPEN ACCESS

**Edited by:**
Jianzhu Liu,
Shandong Agricultural University, China

**Reviewed by:**
Tian Li,
Southwest University, China
Jaleel A. Miyan,
The University of Manchester, United Kingdom

***Correspondence:**
Jinping Chen
chenjp@giz.gd.cn

**Specialty section:**
This article was submitted to Animal Nutrition and Metabolism, a section of the journal Frontiers in Veterinary Science

**Received:** 14 November 2021
**Accepted:** 24 December 2021
**Published:** 31 January 2022

**Citation:**
Ahmad HI, Afzal G, Iqbal MN, Iqbal MA, Shokrollahi B, Mansoor MK and Chen J (2022) Positive Selection Drives the Adaptive Evolution of Mitochondrial Antiviral Signaling (MAVS) Proteins-Mediating Innate Immunity in Mammals. Front. Vet. Sci. 8:814765. doi: 10.3389/fvets.2021.814765

The regulated production of filamentous protein complexes is essential in many biological processes and provides a new paradigm in signal transmission. The mitochondrial antiviral signaling protein (MAVS) is a critical signaling hub in innate immunity that is activated when a receptor induces a shift in the globular caspase activation and recruitment domain of MAVS into helical superstructures (filaments). It is of interest whether adaptive evolution affects the proteins involved in innate immunity. Here, we explore and confer the role of selection and diversification on mitochondrial antiviral signaling protein in mammalian species. We obtined the MAVS proteins of mammalian species and examined their differences in evolutionary patterns. We discovered evidence for these proteins being subjected to substantial positive selection. We demonstrate that immune system proteins, particularly those encoding recognition proteins, develop under positive selection using codon-based probability methods. Positively chosen regions within recognition proteins cluster in domains involved in microorganism recognition, implying that molecular interactions between hosts and pathogens may promote adaptive evolution in the mammalian immune systems. These significant variations in MAVS development in mammalian species highlights the involvement of MAVS in innate immunity. Our findings highlight the significance of accounting for how non-synonymous alterations affect structure and function when employing sequence-level studies to determine and quantify positive selection.

**Keywords: MAVS, mammals, innate immunity, adaptive evolution, mitochondria, positive selection**

## INTRODUCTION

Immune responses in mammalian cells are dependent on the exposure to conserved molecular patterns present in pathogens, such as bacterial flagellins, lipoproteins, peptidoglycans, and lipopolysaccharides, as well as viral nucleic acids (1). Identification of pathogen-derived nucleic acid is an important process of the host defense cells against invading pathogens. After identifying foreign invaders, the transcription of antiviral genes results in the cellular antiviral state that arms the cells to battle and subdues the infection. The host cells' sensors against pathogen-associated DNA and RNA exist (2). Therefore, mitochondria are important sensors in antiviral immunity through their key role in apoptosis (3). One of the most important defense mechanisms against viral infections is the removal of infected cells through apoptosis. Mitochondria are chief performers in antiviral immunity because of their key role in apoptosis (3).

A new mitochondrial protein called mitochondrial antiviral signaling protein (MAVS), along with mitochondrial DNA acting as a danger-associated molecular pattern (DAMP) and mitochondrial ROS generated from mitochondrial sources, may establish mitochondria as key signaling platforms in antiviral immunity in vertebrates (4). In recent years, a thorough understanding of the emerging and intervening role of mitochondria in toll-like receptor-mediated innate immune responses and the activation of the NLRP3 inflammasome complex has gained clarity, which supports the idea that mitochondria have imposing functions in the context of innate immunity (5).

The identification of Retinoic acid Inducible Gene I-(RIG-I)-Like Receptors (RLRs), which are RNA sensing cytosolic receptors that require mitochondrial antiviral signaling protein adaptors to activate the production of interferons and pro-inflammatory cytokines against invading pathogens, revealed the role of mitochondria in innate antiviral immunity (6). RLRs are a set of germline-encoded Pattern Recognition Receptors (PRRs) that directly activate immune cells against invading organisms (7). Previous research has demonstrated that non-microbial danger signals, also known as danger-associated molecular patterns, are composed of host chemicals released by necrotic cells in response to tissue damage. These signals activate innate immune response (8). One of the most exciting discoveries in the last decade about the specific roles of mitochondria has been their role in cellular innate antiviral immunity in vertebrates, particularly mammals (9, 10). MAVS is located on the outer membrane of the mitochondria and has been associated with peroxisomes, the endoplasmic reticulum, and autophagosomes, where it coordinates signaling processes downstream of RLRs. MAVS has a role in regulating apoptotic and metabolic activities and activating antiviral and inflammatory pathways. The MAVS adaptor and its important role in the innate immune response to RNA viruses are highlighted in this study (11).

According to recent research, activation of MAVS molecules results in the polymerization of the molecules, which results in the formation of functional groups (12). As with prion fibers, these high-molecular-weight aggregates have properties comparable to those of prion fibers. They are resistant to detergent or protease and may self-replicate by encouraging inactive protein to produce functional groups. The CARD domain located at the N-terminus of MAVS is required to form active MAVS aggregates and is adequate in this regard. It is linked to MDA5 and RIG-first I's CARD domains (13). Interspecies genetic diversity study illuminates the broad evolutionary history of genes. It can be used to identify protein sites or domains that interact directly with viral components or provide an explanation for antiviral specificity (14). When a host interacts with a virus, a dynamic arms race occurs. When viruses discover ways to overwhelm the host immune system, the host proteins responsible for pathogen recognition must change in order to avoid or restrict subsequent infections. These mechanisms result in adaptation and counter-adaptation on the side of the host pathogen interaction, culminating in rapid co-evolution of both parties. This fast development on the molecular level is typically reflected in host defense genes, which provide strong evidence of continuous diversifying selection (15). Given the wide variety of serious and fatal diseases caused by viruses and the critical function of RLRs in the mammalian innate immune system, it was expected that the RIG-I, MDA5, and LGP2 genes would have been exposed to strong selective pressures in all mammals. TLRs, another family of mammalian PRRs, have previously been demonstrated to exhibit extraordinary evidence of positive genetic selection in response to pathogen-induced selective pressures (16).

Therefore, we sought to determine whether MAVS exhibits evidence of being subjected to positive selection, as has been demonstrated for other duplicated genes, and whether this signal appears genuine or whether it could be an artifact of sequence level constraints due to the unusual genic organization of the gene family in question. Following sequence level studies to uncover potential positive selection residues, we looked at the structural and functional features of the detected sequence alterations to better understand their biological consequences.

## MATERIALS AND METHODS

The nucleotide and amino acid sequences of MAVS proteins from mammalian species were obtained from the NCBI and KEGG databases (17). They included any protein for which there is direct molecular evidence of an immune role in mammalian species. The nucleotide and amino acid sequences of MAVS proteins from mammalian species were obtained from the NCBI and KEGG databases (**Supplementary Table**) (18). The maximum likelihood technique was used in the phylogenetic analysis carried out in MEGA6. In the bootstrap test, taxa were grouped using the maximum likelihood technique on 1,000 repetitions, and the results were analyzed (19, 20).

### Sequence Analysis

The sequences were modified and organized using the BioEdit program (21). After individual sequences were aligned, CLUSTALW was used to align different species' sequences together (22). It was necessary to confirm sequences similar to previously published sequences from passerine species using the

NCBI BLAST program (23). ClustalW was used to match the sequences of each gene individually using the outgroup taxon *Myotis davidii* and the default automated alignment option. Each consecutive alignment was utilized for MEGA 6's Maximum Likelihood tree inference. A computer programme called MEGA6 was used to compute the average pairwise nucleotide distances (24) and the Poisson-corrected amino acid distances, which were utilized to calculate the distances between amino acids. We estimated standard errors by repeating the data 1,000 times using the bootstrap method (25).

## Inference of Recombination

We investigated recombination first because it can affect the outcomes of selection. In version 4 of the Recombination Detection Program, exon nucleotide alignment studies were implemented (RDP4) (26). Numerous techniques were employed to detect recombination events, including RDP (27), Chimera (28), BootScan (29). The Datamonkey webserver's online GARD tool (30) was utilized to analyze recombination signals. Recombination can provide a significant selective advantage, according to our findings. As allele frequencies at individual loci increase in response to selection, random recombination gradually pieces together chromosomes that contain increasing numbers of favorable alleles, resulting in a significant selective advantage (31).

## Tests for Selection

A variety of methods were used to identify which MAVS locations should be evaluated for selection. Using DnaSP 5.0 (32), it was estimated that the first standard selection test could be considered. For the overall dN/dS of MAVS codons, MEGA6 and the Nei-Gojobori approach (33) was utilized in conjunction with each other. Positive selection was detected in PAML 4.9 by using the maximum likelihood technique developed in codeml to find places that had been subjected to positive selection, as indicated by a ratio of (dN/dS) larger than one (34, 35). The models M7 (beta) and M8 were the two matched models that were investigated. To evaluate whether or not the alternative model (M8) provided a better fit than the M7, we used a distribution two to compare log-likelihood ratios (2lnL) to assess whether or not M8 offered a better fit than the M7. We used the Bayes empirical Bayes approach to find posterior probabilities in the M8 model, and the results were correct. In addition to the methods described above, positively selected sites were independently verified at each codon site using a variety of complementary methods carried out in datamonkey (http://www.datamonkey.org/) (30) using a range of complementary approaches MEME, FEL, SALC, and FUBER carried out in datamonkey (35, 36).

## Phylogenetic Analysis

We build two phylogenies using Bayesian inference (one for the sampled species and another for MAVS sequences from related passerines and sampled species). MrModeltest (37) and the Akaike Information Criterion (AICc) (38) were used to identify the best-fitting GTR+T nucleotide substitution model (39). Two million generations of Bayesian Markov chain Monte Carlo (MCMC) were run with 1,000 generations of sampling to determine whether log Likelihood entered the stationary phase (40). MrBayes v3.1.2 (41) was used to summarize the phylogenetic tree, with the top 25% removed. We utilized MEGA6's maximum likelihood (ML) approach to explore the connection between the sampled and related bird species (42). The data were examined using the T92+G model. Support was assessed using 1,000 bootstrap repeats. Values of more than 75% were seen in the ML phylogenetic trees. The second stage is to ascertain which amino acids have been selected affirmatively and whose existence is confirmed by the probability text. As a result of the Bayes theorem, we may deduce the posterior probability of each site from groups of sites of various kinds (43). Values greater than one are assigned to amino acid residues having a high chance of positive selection under range. It was necessary to test the aligned MAVS protein sequence in the Selecton version 2.2 server (http://selecton.tau.ac.il/), which allows for the different MAVS gene ratios to vary between codons within the aligned structure calculated using Bayesian inference method (34) by using different probability testing methods, to confirm positive codon selection. The Selecton's tests were also shown in a variety of colors, suggesting that they were subjected to a variety of various choosing procedures.

## Conservation Analyses

We examined the conserved synteny of genomic regions adjacent to the MAVS gene in mammalian species and discovered that it was pretty high in most of them. Using the ConSurf library, it was possible to assess the evolutionary distinctiveness of these genes by examining the evolutionary survival of human MAVS proteins across time (consurf.tau.ac.il/) (44), which was explicitly designed to study the evolutionary survival of human MAVS proteins. Changes in conserved amino acid sequences have a more significant negative impact on protein function and structure than polymorphisms in variable regions of the protein. Given that conserved synteny is associated with both gene function and expression (35), we performed an enrichment analysis to determine the biological importance of synteny genes by probing them in a variety of programs, including the enrichment analysis program the EnrichNet (45), to determine their biological significance. In addition to identifying genes in various molecular structures, EnrichNet can estimate the gaps between genes and pathways in a reference database (46) by employing an arbitrary selection technique.

## Protein Modeling and Structural Analysis

In this study, we used the Swiss model (http://swissmodel.expasy.org) online tool (47), I-TESSAR (48), and Phyre2 (http://www.sbg.bio.ic.ac.uk/phyre2/html/page.cgi?id=index) (49) to build the crystal structures of the human MAVS protein. In this study, the structure of proteins was predicted using a technique known as homology modeling. The assembled target proteins were minimized in UCSF Chimera 1.10.1 using the Amber force field and the conjugate gradient technique developed by the University of California San Francisco. Additionally, the ProSA webserver (50) was used to assess the stereo-chemical characteristics of the anticipated structures.

# RESULTS

In this study, the mammalian MAVS have been examined to identify the adaptive selection and evolution in protein sequences. The MAVS protein has been identified as the major protein implicated in innate signaling against bacterial and fungal infections (51). Positive selection signals have been detected in these proteins, as demonstrated by a plethora of genetic markers, including higher non-synonymous exchange rates, large homologous haplotypes, and a lack of genetic diversity. As a result, as indicated by our findings, this signaling protein family has been under intense evolutionary pressure throughout its evolutionary history. We examined a set of 26 MAVS protein-coding orthologs shared by the human, monkey, dog, cat, cow, mouse, and domestic yak genomes to detect positive selection signals (**Supplementary Table**). In MAVS genes with significant signals ($P < 0.05$ corrected), branch site analyses revealed evidence of positive selection along the mammalian lineage (**Supplementary Table**).

## Adaptive Evolution of MAVS Proteins

Using various site models, we were able to identify genes that were under positive selection across mammalian species. We evaluated several models for the genes from the data set that were chosen. Probability analysis was used to evaluate alternative models based on a range of ratios to categorize the codons in the corresponding positively chosen genes. The results were shown in **Table 1**. The positive selection test was carried out with the help of two sets of models: M1a; M2a and M7; M8, respectively. In comparing M0 and M3, the likelihood test value was 2lnL = 114.827712 ($p < 0.05$). Still, the findings were significant in M1a vs. M2a, where the likelihood test value was 2lnL = 31.398468 ($p < 0.05$), and an M7 vs. M8, where the likelihood ratio test value was 2lnL = 32.374384 ($p < 0.05$) (**Table 1**). The HyPhy program was then used to investigate the positive selection evidence. MEME, FEL, and SLAC studies were performed to infer further positive selection signals. In this way, sites found using various strategies (and which were consistent with two or more approaches) were judged to be excellent candidates for positive selection. Our findings offered convincing evidence that natural selection had successfully selected these genes in mammals. By estimating the posterior probability for each codon, we identified the sites under selective strain using the Bayesian method. Sites having a greater probability of occurrence than sites with a lower probability of occurrence are more likely to experience positive selection with either >1 (**Figure 1**). Using BEB analysis, we were able to identify numerous positive selection sites in these proteins, with the bulk of these sites having a high retrospective probability of 95%. We observed that many sites were identified as under selection pressure throughout evolution, which further validated the positive consequences of selection (**Figure 2**). The Selecton technique can anticipate the adaptive selection pressure applied at certain codons. We utilized the ConSurf server (52) to forecast nucleic acid locations and the degree of conservation of amino acids in these two genes across different mammalian species (**Figure 2**). In our study, we discovered that the majority of locations that were favorably

**TABLE 1** | Likelihood Log ratios and PAML site models for positive selection.

| Gene | *N* | *Lc* | *S* | Model | Categories | $2\Delta l$ *M3 vs. M0* | $2\Delta l$ *M2 vs. M1* | $2\Delta l$ *M8 vs. M7* | Parameter estimates | Positively selected sites |
|---|---|---|---|---|---|---|---|---|---|---|
| *MAVS* | 45 | 560 | 2.27 | *M1* | Nearly Neutral (2 categories) | 114.827712 | 31.398468 | 32.374384 | $P1 = 0.34017$; $P2 = 0.65983$ | **14, 45*, 60*, 74, 78, 82*, 90*,** 116*, 126, 149**, 163*, 312**, 438**, 465*, 513* |
| | | | | *M2* | Positive Selection (3 categories) | | | | $\omega1 = 0.06983$; $\omega2 = 1.00000$ P1 = 0.33817; P2 = 0.57824; P3 = 0.08360 | |
| | | | | *M3* | Discrete (3 categories) | | | | $\omega1 = 0.09769$; $\omega2 = 1.00000$; $\omega3 = 3.81373$ P1 = 0.23466; P2 = 0.65644; P3 = 0.10890 | |
| | | | | *M7* | Beta (10 categories) | | | | $\omega1 = 0.00868$; $\omega2 = 0.82550$; $\omega3 = 3.45775$ $P = 0.04076$; $q = 0.01519$ | |
| | | | | *M8* | Betaandw>1 (11 categories) | | | | $P0 = 0.90653$; $p = 0.23986$; $q = 0.13299$ $p1 = 0.09347$; $\omega1 = 3.64677$ | |

*The beta distribution parameters p and q, and the fraction of sites under positive selection (p1). Positive selection parameters are bolded. p: significant at 5%; p: significant at 1%. Positive selection sites found by model M8 are listed by human sequence numbering. Sites with high posterior probability. 0.8–0.9 in bold, and 0.5–0.7 in normal print. In this case, the critical values are 5.99, 9.21, and 13.82, respectively, for a l distribution with 2 degrees of freedom. **significant at 1%; *significant at 5%.*

selected remained stable throughout the evolution of mammalian clades. The neural network algorithm residues of these proteins have been shown to have many conserved amino acids with a positive signal range, which can be found either visible or hidden.

We found an average of 22 MAVS protein locations subjected to positive selection. In all, we found 22 conserved sites under positive selection in the CARD-IPS1 domain. To eliminate PAML false positives, we employed a Selecton server (53) that detects adaptive selection at a specific amino acid position in the protein using the Mechanistic Empirical Combined Model (MEC). The MEC model quantifies variations in amino acid substitution rates. As a result, we discovered adaptive selection in the MAVS protein (**Figure 2**). Our research found that these proteins include Ig-V-like domains that have been implicated in several places. Positively chosen proteins may be retained and subjected to purifying selection throughout adaptive evolution.

In order to generate positive selection signals, a lineage specific selection strategy must be used in conjunction with certain codons that are under selection pressure in a number of distinct lineages. In taxonomy and biological function prediction, biochemical sequences are frequently used to infer phylogenies from which to infer phylogenies. The process of creating a phylogeny often entails matching sequences. We employed an adaptive branch-site random effects likelihood (aBS-REL) model to quantify selection probability and identify lineage-specific selection for each phylogenetic grouping to find lineage-specific selection. This paradigm was developed at the University of California, Berkeley, and is credited with its invention. Following that, each gene was evaluated using the aBS-REL program in order to identify lineages that had undergone positive selection over the course of evolutionary adaptation. The aBS-REL model indicated that the genes identified by BUSTED as being under positive selection in mammalian lineages were also under positive selection, demonstrating that the two models were complementary, as evidenced by our findings (**Figure 3**). The branch-site-REL (BSR) program, which runs on the Data Monkey Web Server and searches for clades with statistically significant positive selection signals ($p < 0.05$) in the avian, mammalian, and reptile lineages, discovered clades with statistically significant positive selection signals ($p < 0.05$) in the avian, mammalian, and reptile lineages.

The width of each color component corresponds to the percentage of sites that fall into the associated class in the classification hierarchy. Using a corrected 0.05, the sequential likelihood ratio test revealed that larger branches had undergone episodic diversifying selection, but thinner branches had not. The Selectome database (https://selectome.unil.ch/) was used to undertake an evolutionary analysis of positive selection. By comparingessentially neutral evolutionary models, we were able to calculate the fraction of preferentially selected gene sites in genes across mammalian species. Non-synonymous substitution rates (*dN/dS*) were greater at the chosen sites than expected when the parameter was set to one. Selectome accepts gene requests for both positive selection outcomes and gene-related principles, which may be seen on the Selectome database. The positively picked findings may be seen in the tree and matching protein sequences. When a gene was selected by Darwinian selection, it was selected for a specific subset of sites in the phylogenetic tree. The Selectome server identified species branching in MAVS genes, which the researchers confirmed. Positive selection phylogenetic branching (site test) were determined in just a few cases overall (**Figure 4**).

## DISCUSSION

We examined a set of 26 MAVS protein-coding orthologs shared by the human, monkey, dog, cat, cow, mouse, and domestic yak genomes to detect positive selection signals (**Supplementary Table**). In MAVS genes with significant signals ($P < 0.05$ corrected), branch site analyses revealed evidence of positive selection along the mammalian lineage (**Supplementary Table**). Several evolutionary processes occur in animal genomes, including divergence, integration of genetic material from lineages, duplication events, and epigenesis. Divergence is one of the most well-studied evolutionary processes. On a horizontal scale, genetic transfers and duplications serve as the building blocks for developing all major adaptive immune molecular systems (54). Previously, studies on the evolution of immune genes in birds focused on the co-evolution of disease hotspots such as MAVS in influenza virus infection (Mammalian Apicomplexan Viral System) (55). They contribute to lymphocyte activation, immune system activity, T regulatory cell stimulation, and the origin, development, and immunological tolerance of autoimmunity (56). MAVS genes have been identified to exhibit positive selection in mammals (**Table 1**). We observed that the genes with the greatest overall characteristic expression in these mammalian lineages give standards similar to those reported in animals that were not chosen or were positively selected in the laboratory. Our findings suggest that pathogens are a continuous selective constraint throughout the vertebrate phylogenetic tree. According to previous research, an adaptive immune system was close to the first mammalian evolutionary transition of MAVS (Mammals Adapting to Variable Environments) (36). In the presence of viral antagonism, host antiviral factors such as MAVS can be subjected to consistent selective pressure, resulting in positive selection (i.e., accumulation of an excess of nonsynonymous changes relative to synonymous changes over evolutionary time). In the previous studies, positive selection has been shown in numerous antiviral factors that have been identified in primate genomes (57). It is anticipated that positive selection is mostly driven by adaptations to previous viral infections, with adaptive modifications having advantageous repercussions for the host to overcome viral antagonism. However, the adaptive alterations that occur from this process can potentially impact resistance or susceptibility to modern viruses. In the case of the antiviral gene Protein Kinase R (PKR), adaptive modifications at critical residues in the gene are essential drivers of PKR's capacity to withstand antagonism by modern poxviruses (57, 58), which are likely driven by ancient viruses. As a result, antiviral genes that have evolved through positive selection are excellent candidates to serve as genetic determinants of resistance or susceptibility to emerging viruses. It is thought that the MAVS

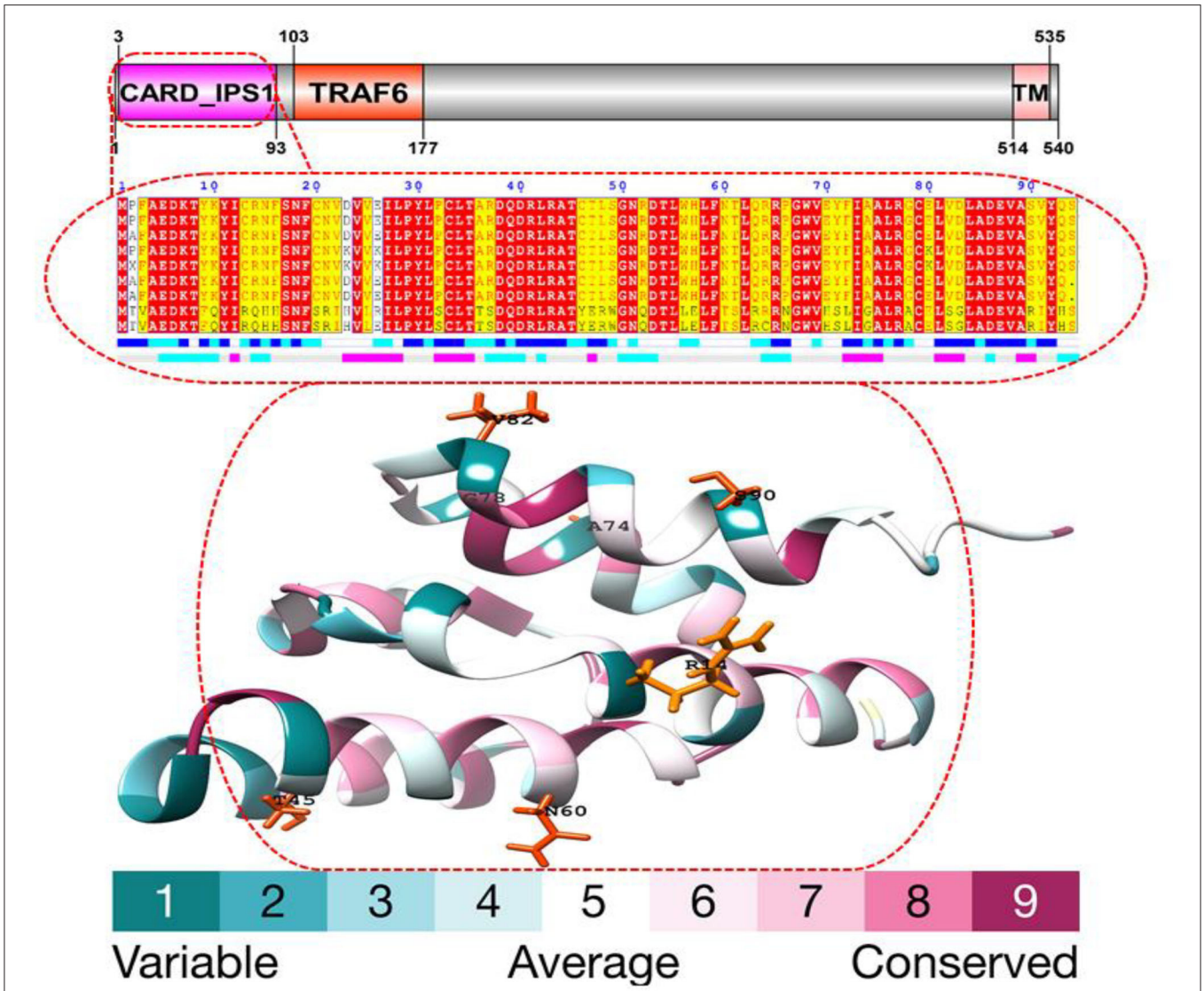


**FIGURE 1 |** Analysis of the MAVS protein structure and conserved domains. The MSA of the 20 proteins with the highest homology to MAVS (as determined by a BLAST+ search against the PDBAA database). The accessibility of a solvent is shown by a first bar below the sequence (blue represents accessible, cyan represents intermediate, and white represents buried), and the hydropathy of a solvent is represented by a second bar below the sequence (pink is hydrophobic, white is neutral, cyan is hydrophilic). Residues that are the same or similar are boxed in yellow or red. The MAVS conserved CARD domain contains positively chosen amino acid residues. The crystal structure of human MAVS as a reference and positively selected sites were drawn onto the crystal structure using the Phyre tool.

family has been split into two branches, both of which are found in all cnidarians and bilaterians, according to current knowledge (55). A positive selection evolutionary model (M8) was used to identify the difference at the codon level. An MCMC model, employed in MrBayes on the Selecton server, was used to determine the difference at the codon level (59). In both situations, values for each place were calculated. Our findings show Ig domain conservation in MAVS coding sequences following MAFFT protein alignments (**Figure 2**). These findings show that non-identical protein switches in purifying Selection areas are harmful to health and hence unlikely to be fixed during evolution (20, 40). Next, positive selection selected amino acid residues with $\omega > 1$ (**Table 1**). Comparing amino acids N60 and A74, G78 and V82 in CARD domain (**Figure 2**). Using the M8 evolutionary model, three positively chosen sites, N60 and A74, G78 and V82, were identified in MAVS, with a *dN/dS* ratio of 10.89870. Amino acid sites in other proteins under strong positive selection have developed faster than mature ones (20). The dynamic selection causes the modification to enhance protein secretion effectiveness, which is true for MAVS, unlike matured protein (60, 61). According to the research, MAVS from several primates were shown to be resistant to inactivation by the HCV protease. A single alteration inside the protease cleavage region in MAVS has been identified as the source of this resistance. These modifications prevent MAVS from being cleaved by the HCV protease. Surprisingly, most of these


**FIGURE 2 |** Positive/purifying selection was detected in MAVS homologous sequences from mammals using the human as a reference. Yellow and brown highlights represent positive selection, gray and white highlights describe the neutral selection, purple highlights on codons represent purifying selection.

modifications have occurred independently at a single residue 506, which has developed under positive selection throughout time (57). In our study we have detected.

We detected positive selection in mammalian and avian clades in the MAVS gene (**Figure 3**). Interestingly, we detected positive selection in most mammalian clades in the data set when looking at the MAVS gene. Given that multi-nucleotide mutations might lead to erroneous positive selection implications in branch-site analysis, we further verified our results using the aBSREL (42). Similar selection patterns were identified between the aBSREL and site-model (**Figure 3**). In general, the MAVS protein found little evidence of positive selection in vertebrate lineages, except in the avian group. The LRT fully supports the M8 evolutionary model's observation of no positive selection. This may be related to the absence of gene duplication events in the evolutionary history of the MAVS gene. Gene duplication is one of the evolutionary strategies that allow genomes to evolve. Positive selection occurs following a duplication event for other proteins, suggesting a relaxation of the selective pressure supporting genetic diversity (35, 62). Positively chosen sites are found in the helicase domain. The majority of the positively chosen sites in MAVS are in areas exclusive to this RLR, including a unique insertion inside the helicase domain. According to structural analysis, positively selected residues are implicated in para-influenza virus protein binding. Our findings suggest that RLRs have been involved in host-virus genetic conflict, leading to diversifying selection, and that they have shown parallel evolution at the same place in RIG-I, a position that is likely to be critical in antiviral responses.

Furthermore, among 22 mammalian species, we found strong selection signals in the hominidae clade, which resulted in 149A, 438V, and 465M codon positions. Positively chosen amino

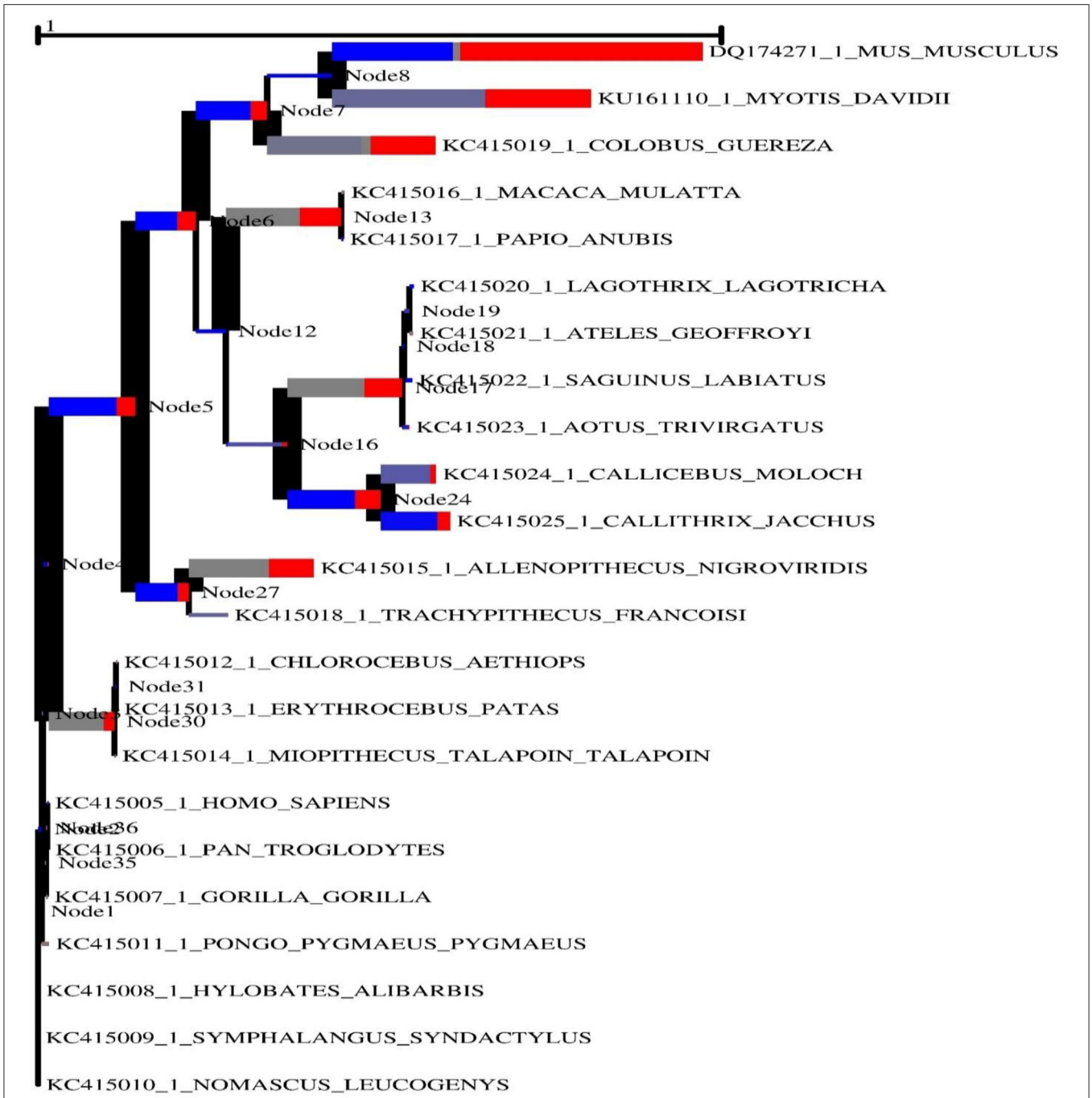


**FIGURE 3 |** The adaptive branch-site REL test for episodic diversifying selection in the MAVS gene across vertebrate species is a new approach to testing for episodic diversifying selection. To calculate the size of the phylogenetic tree, the predicted number of substitutions/nucleotides was considered. With primary red corresponding $\omega > 5$, primary blue corresponding $\omega = 0$, and corresponding gray $\omega = 1$, the hue of each color correlates to the degree of selection made for that color.

acid sites are critical for signaling. These receptors detect viral RNA and activate signal transduction *via* contact with the adaptor protein MAVS, culminating in the generation of pro-inflammatory cytokines and type I interferon.

Not just in birds but also in other vertebrate lineages throughout MAVS evolution, giving Bayesian phylogenetic methods (**Figure 4**). These findings suggest that negative selection has largely dictated PD1 atomic progress. Variations in a few motifs discovered in MAVS may be illustrated by altering the genetic basis for homologous arrangements in mammals and other animals. Purifying choice, notably inside areas compared to Ig similar domain, has pushed MAVS molecular evolution. During MAVS evolution, residues within the areas compared to each motif co-vary with each other (63, 64).


**FIGURE 4 |** The phylogenetic tree estimates various parameters (*dN/dS*, branch length) on the codon (nucleotide) alignment for MAVS gene in mammalian species. The rate variation among codons was estimated using $\omega = dN/dS$, which indicates selective pressure in Selectome database, to account for selection at the DNA level. Selectome uses the branch-site model, which estimates different dN/dS values among branches and sites.

Protein structure and function rely on coordinated amino acid interactions. Thus, identifying structural features of favorably chosen amino acid residues might be done by detecting co-evolving sites. Their physical or functional connection may have resulted in this co-evolutionary relationship. Protein co-evolution has been linked to protein stability and intermolecular

interactions (34, 40). Thus, evolution may have changed MAVS proteins. By calculating the *dN/dS* of mammalian MAVS sequences, we observed that N60 and A74, G78 and V82 of the human CARD domain might be relevant for certain earlier suggested activities. Its domains are well conserved among vertebrates, indicating that their functions are not redundant and that the selection pressure may come from MAVS specialization for immune system control. Using protein alignments for MAVS homologs as input, we discovered positively chosen co-evolving residues with considerable heterogeneity (20). These findings suggest that domain-like areas represent structural and functional components within these proteins. Using a Gaussian network, homology modeling the region similar to CARD domains. According to its projected molecular mass of 56KDa, MAVS is a mitochondrial integral outer-membrane protein that in healthy conditions forms a supramolecular complex (about 600KDa) (65). MAVS is encoded in the nuclear genome (not mtDNA) and is widely expressed in tissues and cells. Some MAVS orthologs are conserved across fish species (66). MAVS has an amino-terminal caspase activation and recruitment domain (CARD) with six helices, three of which create a flat positively charged surface and two of which form an acidic negatively charged surface (4).

## CONCLUSION

Detecting evolutionary arms races is critical for comprehending and controlling host-pathogen interactions, such as viral competition with their animal hosts. The need for innate immune activation for cellular energy output and significant metabolic reprogramming has necessitated mitochondrial integration into this arm of immunity, which has evolved to develop and increase the cross-talk between metabolism and innate immune pathways. Arms races may be identified at the molecular level by detecting rapidly changing nucleotide sequences. The purpose of this study was to determine whether or not sequence-level analyses are an adequate method for detecting what is ultimately a phenotype-level effect. These findings shed light on the adaptive development of mitochondrial antiviral proteins in mammalian species. The CARD domain in MAVS proteins are highly conserved in mammals, which may help explain its involvement in biological systems, including adaptive immunity. Due to the vast data collection and recommendations from different study areas, the evolutionary history of MAVS protein is revealed. We discovered that the evolutionary rates of mammalian and other vertebrate lineages differ. Further research into the functional ramifications of positive selection signals at the cellular and organismal levels would help distinguish between convergence and early shared vertebrate selection. Finally, the inclusion of evolutionary diversity may contribute to clarifying some of the conflicts that have developed in mammalian proteins due to a variety of experimental data. Following these findings, we propose that studies of the co-evolution of rapidly evolving immune proteins may give data compatible with the interaction between the host and pathogens.

## DATA AVAILABILITY STATEMENT

The original contributions presented in the study are included in the article/**Supplementary Material**, further inquiries can be directed to the corresponding author.

## AUTHOR CONTRIBUTIONS

HIA, GA, and MKM: data curation. HIA, GA, and BS: formal analysis and methodology. JC: funding acquisition and supervision. JC and MKM: investigation and project administration. HIA and JC: resources and visualization. HIA, MNI, and MAI: software. MKM and BS: validation. HIA and GA: writing and original draft. HIA, GA, MKM, MNI, and MAI: writing and review and editing. All authors contributed to the article and approved the submitted version.

## FUNDING

This work was supported by the GDAS project of Science and Technology Development (2019-GDASYL-0103059 and 2018GDASCX-0107).

## SUPPLEMENTARY MATERIAL

The Supplementary Material for this article can be found online at: https://www.frontiersin.org/articles/10.3389/fvets.2021.814765/full#supplementary-material

## REFERENCES

1. Medzhitov R. Recognition of microorganisms and activation of the immune response. *Nature.* (2007) 449:819. doi: 10.1038/nature06246
2. Jacobs JL, Coyne CB. Mechanisms of MAVS regulation at the mitochondrial membrane. *J Mol Biol.* (2013) 425:5009–19. doi: 10.1016/j.jmb.2013.10.007
3. Pourcelot M, Arnoult D. Mitochondrial dynamics and the innate antiviral immune response. *FEBS J.* (2014) 281:3791–802. doi: 10.1111/febs.12940
4. Yasukawa K, Koshiba T. Mitochondrial reactive zones in antiviral innate immunity. *Biochimica et Biophysica Acta (BBA)-General Subjects.* (2021) 1865:129839. doi: 10.1016/j.bbagen.2020.129839
5. Mohanty A, Tiwari-Pandey R, Pandey NR. Mitochondria: the indispensable players in innate immunity and guardians of the inflammatory response. *Journal of cell communication and signaling.* (2019) 13:303–18. doi: 10.1007/s12079-019-00507-9
6. Kawai T, Akira S. Toll-like Receptor and RIG-1-like Receptor Signaling. *Ann N Y Acad Sci.* (2008) 1143:1–20. doi: 10.1196/annals.1443.020
7. Akira S, Uematsu S, Takeuchi O. Pathogen recognition and innate immunity. *Cell.* (2006) 124:783–801. doi: 10.1016/j.cell.2006.02.015
8. Benko S, Philpott DJ, Girardin SE. The microbial and danger signals that activate Nod-like receptors. *Cytokine.* (2008) 43:368–73. doi: 10.1016/j.cyto.2008.07.013
9. Scott I. The role of mitochondria in the mammalian antiviral defense system. *Mitochondrion.* (2010) 10:316–20. doi: 10.1016/j.mito.2010.02.005
10. West AP, Shadel GS, Ghosh S. Mitochondria in innate immune responses. *Nature Reviews Immunology.* (2011) 11:389–402. doi: 10.1038/nri2975

11. Belgnaoui SM, Paz S, Hiscott J. Orchestrating the interferon antiviral response through the mitochondrial antiviral signaling (MAVS) adapter. *Curr Opin Immunol.* (2011) 23:564–72. doi: 10.1016/j.coi.2011.08.001
12. Khan KA, Marineau A, Doyon P, Acevedo M, Durette É, Gingras A-C, et al. TRK-Fused Gene (TFG), a protein involved in protein secretion pathways, is an essential component of the antiviral innate immune response. *PLoS Pathog.* (2021) 17:e1009111. doi: 10.1371/journal.ppat.1009111
13. Zerbe CM, Mouser DJ, Cole JL. Oligomerization of RIG-I and MDA5 2CARD domains. *Protein Science.* (2020) 29:521–6. doi: 10.1002/pro.3776
14. Li S, Shao Q, Zhu Y, Ji X, Luo J, Xu Y, et al. Porcine RIG-I and MDA5 signaling CARD domains exert similar antiviral function against different viruses. *Front Microbiol.* (2021) 12:677634. doi: 10.3389/fmicb.2021.677634
15. Krchlíkov,á V, Hron T, Těšick,ý M, Li T, Hejnar J, Vinkler M, et al. Repeated MDA5 Gene Loss in Birds: An Evolutionary Perspective. *Viruses.* (2021) 13:2131. doi: 10.3390/v13112131
16. Chen J, Shang S, Wu X, Zhong H, Zhao C, Wei Q, et al. Genomic analysis and adaptive evolution of the RIG-I-like and NOD-like receptors in reptiles. *Int J Biol Macromol.* (2019) 134:1045–51. doi: 10.1016/j.ijbiomac.2019.05.172
17. Kanehisa M, Furumichi M, Sato Y, Ishiguro-Watanabe M, Tanabe M. KEGG: integrating viruses and cellular organisms. *Nucleic Acids Res.* (2021) 49:D545–51. doi: 10.1093/nar/gkaa970
18. Kanehisa M, Sato Y. KEGG mapper for inferring cellular functions from protein sequences. *Protein Science.* (2020) 29:28–35. doi: 10.1002/pro.3711
19. Jabbir F, Irfan M, Mustafa G, Ahmad HI. Bioinformatics approaches to explore the phylogeny and role of BRCA1 in breast cancer. *Crit Rev Eukaryot Gene Expr.* (2019) 29:551–64. doi: 10.1615/CritRevEukaryotGeneExpr.2019030785
20. Ahmad HI, Asif AR, Ahmad MJ, Jabbir F, Adnan M, Ahmed S, et al. Adaptive evolution of peptidoglycan recognition protein family regulates the innate signaling against microbial pathogens in vertebrates. *Microb Pathog.* (2020) 147:104361. doi: 10.1016/j.micpath.2020.104361
21. Hall T, Biosciences I, Carlsbad C. BioEdit: an important software for molecular biology. *GERF Bull Biosci.* (2011) 2:60–1.
22. Thompson JD, Gibson TJ, Higgins DG. Multiple sequence alignment using ClustalW and ClustalX. *Curr Protoc Bioinformatics.* (2003) 2.3.1–22. doi: 10.1002/0471250953.bi0203s00
23. Madden T. The BLAST sequence analysis tool. *The NCBI handbook.* (2013) 2:425–36.
24. Nishimaki T, Sato K. An extension of the Kimura two-parameter model to the natural evolutionary process. *J Mol Evol.* (2019) 87:60–7. doi: 10.1007/s00239-018-9885-1
25. Hughes AL, Friedman R. The effect of branch lengths on phylogeny: an empirical study using highly conserved orthologs from mammalian genomes. *Mol Phylogenet Evol.* (2007) 45:81–8. doi: 10.1016/j.ympev.2007.04.022
26. Martin DP, Lemey P, Posada D. Analysing recombination in nucleotide sequences. *Mol Ecol Resour.* (2011) 11:943–55. doi: 10.1111/j.1755-0998.2011.03026.x
27. Martin DP, Murrell B, Golden M, Khoosal A, Muhire B. RDP4: detection and analysis of recombination patterns in virus genomes. *Virus Evol.* (2015) 1:vev003. doi: 10.1093/ve/vev003
28. Ye ZA, Moshovos A, Hauck S, Banerjee P. CHIMAERA: a high-performance architecture with a tightly-coupled reconfigurable functional unit. *ACM SIGARCH computer architecture news.* (2000) 28:225–35. doi: 10.1145/339647.339687
29. Martin D, Posada D, Crandall K, Williamson C. A modified bootscan algorithm for automated identification of recombinant sequences and recombination breakpoints. *AIDS Res Hum Retroviruses.* (2005) 21:98–102. doi: 10.1089/aid.2005.21.98
30. Weaver S, Shank SD, Spielman SJ, Li M, Muse SV, Kosakovsky Pond SL. Datamonkey 2.0: a modern web application for characterizing selective and other evolutionary processes. *Mol Biol Evol.* (2018) 35:773–7. doi: 10.1093/molbev/msx335
31. Hickey DA, Golding GB. The advantage of recombination when selection is acting at many genetic loci. *J Theor Biol.* (2018) 442:123–8. doi: 10.1016/j.jtbi.2018.01.018
32. Zhang J, Yang B, Wen X, Sun G. Genetic variation and relationships in the mitochondrial DNA D-loop region of Qinghai indigenous and commercial pig breeds. *Cell Mol Biol Lett.* (2018) 23:1–8. doi: 10.1186/s11658-018-0097-x
33. Wei X, Zhang J. A simple method for estimating the strength of natural selection on overlapping genes. *Genome Biol Evol.* (2015) 7:381–90. doi: 10.1093/gbe/evu294
34. Ahmad HI, Liu G, Jiang X, Edallew SG, Wassie T, Tesema B, et al. Maximum-likelihood approaches reveal signatures of positive selection in BMP15 and GDF9 genes modulating ovarian function in mammalian female fertility. *Ecol Evol.* (2017) 7:8895–902. doi: 10.1002/ece3.3336
35. Ahmad HI, Ahmad MJ, Adeel MM, Asif AR, Du X. Positive selection drives the evolution of endocrine regulatory bone morphogenetic protein system in mammals. *Oncotarget.* (2018) 9:18435. doi: 10.18632/oncotarget.24240
36. Asif AR, Awais M, Qadri S, Ahmad HI, Du X. Positive selection of IL-33 in adaptive immunity of domestic Chinese goats. *Ecol Evol.* (2017) 7:1954–63. doi: 10.1002/ece3.2813
37. Nylander J. *MrModeltest (version 2.2).* (2004). Available online at: http://www.abc. se/∼ nylander/.
38. Susko E, Roger AJ. On the use of information criteria for model selection in phylogenetics. *Mol Biol Evol.* (2020) 37:549–62. doi: 10.1093/molbev/msz228
39. Xia X. Nucleotide substitution models and evolutionary distances. In: *Bioinformatics and the Cell.* Springer (2018). p. 269–314.
40. Ahmad HI, Zhou J, Ahmad MJ, Afzal G, Jiang H, Zhang X, et al. Adaptive selection in the evolution of programmed cell death-1 and its ligands in vertebrates. *Aging.* (2020) 12:3516. doi: 10.18632/aging.102827
41. Ayres DL, Cummings MP, Baele G, Darling AE, Lewis PO, Swofford DL, et al. BEAGLE 3: improved performance, scaling, and usability for a high-performance computing library for statistical phylogenetics. *Syst Biol.* (2019) 68:1052–61. doi: 10.1093/sysbio/syz020
42. Ahmad HI, Afzal G, Jamal A, Kiran S, Khan MA, Mehmood K, et al. In silico structural, functional, and phylogenetic analysis of cytochrome (CYPD) protein family. *BioMed Research International.* (2021) 1–13. doi: 10.1155/2021/5574789
43. Ahmad HI, Liu G, Jiang X, Liu C, Fangzheng X, Chong Y, et al. Adaptive selection at agouti gene inferred breed specific selection signature within the indigenous goat populations. *Asian-australas J Anim Sci.* (2017). doi: 10.5713/ajas.16.0994
44. Ben Chorin A, Masrati G, Kessel A, Narunsky A, Sprinzak J, Lahav S, et al. ConSurf-DB: an accessible repository for the evolutionary conservation patterns of the majority of PDB proteins. *Protein Sci.* (2020) 29:258–67. doi: 10.1002/pro.3779
45. Glaab E, Baudot A, Krasnogor N, Schneider R, Valencia A. EnrichNet: network-based gene set enrichment analysis. *Bioinformatics.* (2012) 28:i451–7. doi: 10.1093/bioinformatics/bts389
46. Merico D, Isserlin R, Stueker O, Emili A, Bader GD. Enrichment map: a network-based method for gene-set enrichment visualization and interpretation. *PLoS ONE.* (2010) 5:e13984. doi: 10.1371/journal.pone.0013984
47. Schwede T, Kopp J, Guex N, Peitsch MC. SWISS-MODEL: an automated protein homology-modeling server. *Nucleic Acids Res.* (2003) 31:3381–5. doi: 10.1093/nar/gkg520
48. Yang J, Zhang Y. Protein structure and function prediction using I-TASSER. *Current protocols in bioinformatics.* (2015) 52:5. doi: 10.1002/0471250953.bi0508s52
49. Kelley LA, Mezulis S, Yates CM, Wass MN, Sternberg MJ. The Phyre2 web portal for protein modeling, prediction and analysis. *Nat Protoc.* (2015) 10:845–58. doi: 10.1038/nprot.2015.053
50. Wiederstein M, Sippl MJ. ProSA-web: interactive web service for the recognition of errors in three-dimensional structures of proteins. *Nucleic Acids Res.* (2007) 35:W407–10. doi: 10.1093/nar/gkm290
51. Li X-D, Chiu Y-H, Ismail AS, Behrendt CL, Wight-Carter M, Hooper LV, et al. Mitochondrial antiviral signaling protein (MAVS) monitors commensal bacteria and induces an immune response that prevents experimental colitis. *Proc Nat Acad Sci.* (2011) 108:17390–5. doi: 10.1073/pnas.1107114108
52. Celniker G, Nimrod G, Ashkenazy H, Glaser F, Martz E, Mayrose I, et al. ConSurf: using evolutionary data to raise testable hypotheses about protein function. *Isr J Chem.* (2013) 53:199–206. doi: 10.1002/ijch.201200096
53. Doron-Faigenboim A, Stern A, Mayrose I, Bacharach E, Pupko T. Selecton: a server for detecting evolutionary forces at a single amino-acid site. *Bioinformatics.* (2005) 21:2101–3. doi: 10.1093/bioinformatics/bti259

54. Sun L, Wang X, Saredy J, Yuan Z, Yang X, Wang H. Innate-adaptive immunity interplay and redox regulation in immune response. *Redox Biol.* (2020) 101759. doi: 10.1016/j.redox.2020.101759
55. Han Y, Gao H, Xu J, Luo J, Han B, Bao J, et al. Innate and adaptive immune responses against microsporidia infection in mammals. *Front Microbiol.* (2020) 11:1468. doi: 10.3389/fmicb.2020.01468
56. Arruga F, Gyau BB, Iannello A, Vitale N, Vaisitti T, Deaglio S. Immune response dysfunction in chronic lymphocytic leukemia: dissecting molecular mechanisms and microenvironmental conditions. *Int J Mol Sci.* (2020) 21:1825. doi: 10.3390/ijms21051825
57. Patel MR, Loo Y-M, Horner SM, Gale Jr M, Malik HS. Convergent evolution of escape from hepaciviral antagonism in primates. *PLoS Biol.* (2012) 10:e1001282. doi: 10.1371/journal.pbio.1001282
58. Elde NC, Child SJ, Geballe AP, Malik HS. Protein kinase R reveals an evolutionary model for defeating viral mimicry. *Nature.* (2009) 457:485–9. doi: 10.1038/nature07529
59. Stern A, Doron-Faigenboim A, Erez E, Martz E, Bacharach E, Pupko T. Selecton 2007: advanced models for detecting positive and purifying selection using a Bayesian inference approach. *Nucleic Acids Res.* (2007) 35:W506–11. doi: 10.1093/nar/gkm382
60. Biacchesi S, Leberre M, Lamoureux A, Louise Y, Lauret E, Boudinot P, et al. Mitochondrial antiviral signaling protein plays a major role in induction of the fish innate immune response against RNA and DNA viruses. *J Virol.* (2009) 83:7815–27. doi: 10.1128/JVI.00404-09
61. Findlay GD, Swanson WJ. Proteomics enhances evolutionary and functional analysis of reproductive proteins. *Bioessays.* (2010) 32:26–36. doi: 10.1002/bies.200900127
62. Tamura K, Stecher G, Peterson D, Filipski A, Kumar S. MEGA6: molecular evolutionary genetics analysis version 6.0. *Mol Biol Evol.* (2013) 30:2725–9. doi: 10.1093/molbev/mst197
63. Pritham EJ, Putliwala T, Feschotte C. Mavericks, a novel class of giant transposable elements widespread in eukaryotes and related to DNA viruses. *Gene.* (2007) 390:3–17. doi: 10.1016/j.gene.2006.08.008
64. Mclaughlin Jr RN, Young JM, Yang L, Neme R, Wichman HA, Malik HS. Positive selection and multiple losses of the LINE-1-derived L1TD1 gene in mammals suggest a dual role in genome defense and pluripotency. *PLoS Genet.* (2014) 10:e1004531. doi: 10.1371/journal.pgen.1004531
65. Koshiba T. Mitochondrial-mediated antiviral immunity. *Biochim Biophys Acta.* (2013) 1833:225–32. doi: 10.1016/j.bbamcr.2012.03.005
66. Koshiba T, Bashiruddin N, Kawabata S. Mitochondria and antiviral innate immunity. *Int J Biochem Mol Biol.* (2011) 2:257.


**Conflict of Interest:** The authors declare that the research was conducted in the absence of any commercial or financial relationships that could be construed as a potential conflict of interest.

**Publisher's Note:** All claims expressed in this article are solely those of the authors and do not necessarily represent those of their affiliated organizations, or those of the publisher, the editors and the reviewers. Any product that may be evaluated in this article, or claim that may be made by its manufacturer, is not guaranteed or endorsed by the publisher.

frontiers in Veterinary Science

ORIGINAL RESEARCH
published: 02 February 2022
doi: 10.3389/fvets.2022.822259

# Penthorum Chinense Pursh Extract Alleviates Aflatoxin B1-Induced Liver Injury and Oxidative Stress Through Mitochondrial Pathways in Broilers

*Fazul Nabi[1,2†], Weilai Tao[1†], Ruiling Ye[1], Zhenzhen Li[1], Qin Lu[1], Yangfei Shang[1], Yu Hu[1], Jiali Fang[1], Zohaib Ahmed Bhutto[2] and Juan Liu[1,3,4*]*

[1] Department of Traditional Chinese Veterinary Medicine, College of Veterinary Medicine, Southwest University, Chongqing, China, [2] Department of Poultry Science, Faculty of Veterinary and Animal Science, Lasbela University of Agriculture, Water and Marine Sciences, Uthal, Pakistan, [3] Chinese Veterinary Herbal Drugs Innovation Research Laboratory, University Veterinary Science Engineering Research Center in Chongqing, Chongqing, China, [4] Immunology Research Center of Medical Research Institute, Southwest University, Chongqing, China

OPEN ACCESS

**Edited by:**
Yung-Fu Chang,
Cornell University, United States

**Reviewed by:**
Aftab Shaukat,
Huazhong Agricultural University, China
Ali Raza Jahejo,
Shanxi Agricultural University, China
Shahid Ali Rajput,
Muhammad Nawaz Shareef University of Agriculture, Pakistan

***Correspondence:**
Juan Liu
liujrc@163.com

[†]These authors have contributed equally to this work

**Specialty section:**
This article was submitted to Animal Nutrition and Metabolism, a section of the journal Frontiers in Veterinary Science

**Received:** 25 November 2021
**Accepted:** 10 January 2022
**Published:** 02 February 2022

**Citation:**
Nabi F, Tao W, Ye R, Li Z, Lu Q, Shang Y, Hu Y, Fang J, Bhutto ZA and Liu J (2022) Penthorum Chinense Pursh Extract Alleviates Aflatoxin B1-Induced Liver Injury and Oxidative Stress Through Mitochondrial Pathways in Broilers. Front. Vet. Sci. 9:822259. doi: 10.3389/fvets.2022.822259

Aflatoxin is an important toxicant of the fungal origin and poses a threat to the poultry industry. This study was designed to reveal the underlying mechanism and protective methods against aflatoxin B1 (AFB1)-induced liver injury, oxidative stress, and apoptosis using a Traditional Chinese medicine, Penthorum chinense Pursh extract (PCPE), in broilers. A total of 164 (day-old) broilers were equally allocated to the control, AFB1 (3 mg/kg feed), positive drug (Yin-Chen-Hao Tang extract, 10 ml/kg feed), PCPE (2 g PCPE/kg), and PCPE low, medium, and high dose groups (1 g, 2 g, 3 g PCPE/kg feed, respectively). AFB1 significantly decreased the growth performance and serum immunoglobulin level, altered normal serum biochemical parameters and antioxidant activities, and induced histopathological lesions in the liver as compared to control group. Additionally, AFB1 significantly up-regulated the mRNA expression levels of apoptosis-related genes such as Bax, Bak, caspase-9, caspase-3, and p53, whereas it down-regulated the expression levels of BCL2 in the liver of broilers. The supplementation of different doses of PCPE to AFB1-affected birds significantly eased AFB1 negative effects by improving growth performance, immunoglobulin level, and oxidative capacity, and reversed oxidative stress and pathological lesions in liver. Furthermore, supplementation of PCPE to the AFB1 group reversed apoptosis by significantly down-regulating the mRNA expression levels of Bax, Bak, caspase-9, caspase-3, and p53 and up-regulating the expression levels of BCL2 in the liver of broilers. Based on these results, we conclude that supplementation of PCPE is protective and safe against oxidative stress, is anti-apoptotic, and reverses the liver damage caused by AFB1 in broilers.

**Keywords: penthorum chinense pursh extract, liver, broilers, aflatoxin B1, apoptosis**

## INTRODUCTION

Mycotoxins produced by *Aspergillus* fungi are widespread and potent type of toxicants in the poultry industry globally. Aflatoxin B1 (AFB1) is a serious threat to the poultry industry and poses a great risk to public health (1, 2). Natural or artificial AFB1-contaminated feed results in aflatoxicosis in poultry, that can subsequently lower the growth performance and immunity in broilers (3).

AFB1 toxicity has been widely studied in humans and animals for their adverse effects, such as hepatotoxic, immunotoxic, carcinogenic, mutagenic, teratogenic, and other adverse health effects on several vital organs (4, 5). AFB1 is the hazardous and commonly occurring mycotoxin in poultry which negatively impact on productivity and high susceptibility to pathogenicity in poultry (6). Aflatoxin affect on several vital organs including spleen, kidney, thymus, bursa of Fabricius among them liver is mostly affected that causes macroscopic and microscopic liver changes (3).

The liver is a vital organ with numerous functions in broilers; however, it is also the main target organ of AFB1 where aflatoxins are metabolized and converted into extremely toxic forms, thereby invading the liver, and resulting in severe hepatotoxicity. AFB1 destroys the normal structure of hepatocytes and mitochondria, subsequently altering the antioxidant system. Furthermore, autophagy eliminates impaired cellular structures and apoptosis is initiated by liver hepatocytes to maintain liver function; however, it also causes hepatotoxicity (7–9). The metabolic and toxic effects of AFB1 are principally observed in liver tissues, and previous studies have suggested that hepatic cell apoptosis leads to liver damage in poultry.

Apoptosis is the programmed cell death phenomenon which is essential for normal tissue homeostasis, and it is also associated with the development of several pathogenic diseases in animals (10, 11). In experimental models, apoptosis is performed for the validation of interventions in animals; aflatoxins induce apoptosis *via* cellular toxicity, and inhibition of carbohydrate and lipid metabolism and protein synthesis (12). In poultry, AFB1 can severely alter immunity, cause oxidative damage, and induce apoptosis and development of histopathological lesions in lymphoid tissues. Additionally, AFB1 exposure may alter the size of immune organs, thereby acclimatizing it to stress and severely altering the immune functions in broilers (13–15). Studies have reported that AFB1 can lead to renal injury, respiratory diseases, neuropathy, and liver damages through the induction of oxidative stress and apoptosis.

In the recent years, traditional Chinese medicine (TCM) or ethnomedicine is an emerging discipline. TCM is a systematic methodology for identifying various pathological biomarkers, evaluating the efficiency of herbal medicine, and finding the material basis of herbal formulas. Penthorum chinense Pursh (PCP) is a well-known TCM herbal medicine, and its main extract or ingredient has antioxidant, anti-cancer, and anti-apoptotic activities. Protection against infectious hepatitis and edema, and treatment of various liver diseases are the main functions of PCP (16–19). Our previous study showed that treatment using a PCP compound protected kidney cells from excessive apoptosis by inhibiting the mitochondrial apoptosis pathway activated by AFB1 (19). Therefore, this study was undertaken to further examine the ameliorative effects of PCP extract on oxidative stress and apoptosis through mitochondrial pathways in mycotoxin-mediated toxicity in the liver of broilers.

# MATERIALS AND METHODS

## Preparation of PCP Extract

The whole PCP grass was provided by Gulin County, Luzhou City, Sichuan Province, China. The botanical origin was identified by Professor Liu Juan, College of Veterinary Medicine, Southwest University, Chongqing, China. The whole grass was cut into small pieces, decocted with 4000 ml ethanol solution (40%), followed by reflux extraction for 120 min. The filtrate thus obtained was decompressed in a rotary vacuum evaporator at 70 °C, and subsequently dried by blowing at 30 °C to obtain a PCPE powder.

## Preparation of Positive Drug Yin-Chen-Hao Tang Extract

YCHT was prepared according to the protocol used in our previous experiment (19). Briefly, Yin chen (54 g) was mixed in 3.6 L deionized water and boiled. The solution was reduced up to 1.8 L, and then samples of gardenia (Gardenia jasminoides) and rhubarb (Rheum officinal baill) (27 and 18 g, respectively) were mixed. Total solution was again boiled for 30 min and was finally filtered. Next, the filtrate was concentrated up to 100 ml by vacuum (equivalent to 1 g herb ml $^{1}$) and stored at 4°C.

## Bird Grouping and Sample Collection

All experimental procedures agreed with the animal ethics regulations and were accepted by the Institutional Animal Care and Use Committee (IACUC) of Southwest University (IACUC-20201203). Cobb broilers (total 164) 1-day-old) were bought from a commercial hatchery (Daan, Zigong, Sichuan, China). Broilers were housed with standard hygienic and optimal conditions (temperature: 28–30°C, relative humidity (RH): 60–70%). After 7 days of acclimatization period, the broilers were equally divided in the following groups ($n = 24$ per group) with four replicates: control, AFB1, positive drug (YCHT), PCPE (2 g/kg feed), and PCPE high (3 g/kg feed), PCPE medium (2 g/kg feed), and PCPE low-dose (1 g/kg feed) groups. These herbal doses were randomly selected for the experiment. All groups were fed with AFB1 (produced by *Aspergillus flavus* NRRL3357) at 3 mg/kg feed while the positive drug group (YCHT) was fed with 8 ml/kg feed, except the control group till the research trial ended (28 days). All birds were weighed, the weekly average growth parameters, mortality, and morbidity were recorded during the experiment (day 7, 14, 21, 28). Birds were slayed by cervical dislocation; and blood and liver sampling were performed on the 14$^{th}$ and 28$^{th}$ day of the research trial for subsequent analysis.

## Analysis of Antioxidants and Oxidative Biomarkers in the Liver and Serum

Aspartate aminotransferase (AST), alanine transaminase (ALT), alkaline phosphatase (ALP), albumin (ALB), and total bilirubin (TBIL) induced in the serum were quantified using a biochemical analyzer, in accordance with manufacturer's guidelines (Beckman Instruments Inc, USA). Malondialdehyde (MDA), superoxide

dismutase (SOD), catalase (CAT), glutathione (GSH), and glutathione peroxidase (GSH-Px) activities in the liver homogenate were measured by enzyme-linked immunosorbent assay (ELISA) following specific kit instructions (Xiamen Jiahui Biotechnology Co. Ltd, Xiamen, China).

## Liver Histology

Hematoxylin and eosin (H and E) staining was performed on the liver tissues. In brief, the tissue samples were fixed in 10% formaldehyde for 24 h and placed in running water overnight. Dehydration was performed using ethanol, clearing using xylene, and embedding using paraffin wax. The sections were incised in 4–5 μm size for the preparation of slides and stained with H and E. Histopathological changes in the liver were examined under an optical microscope (Axio Scope, Germany).

## Reverse Transcription Quantitative Real-Time Polymerase Chain Reaction

The liver tissue samples were collected from each group on day 14 and 28 of the experiment for RT-qPCR analysis. PCR was performed by applying primers for individual concerned genes (**Table 1**). Total RNA extractions, cDNA synthesis, and RT-qPCR were performed according to the methods used in our previous experiments (19). The collected liver tissue sample (2–3 gm) homogenates were prepared by tissue homogenizer (T10 Basic ULTRA-TURAX ® Germany) in liquid nitrogen along with TRIzol reagent for the extraction of total RNA (1 ml/50 mg liver tissue) (Win Biosciences, Beijing, China). cDNA was synthesized using the Trans Gen cDNA kit (Biotech Co., Ltd., Beijing, China) following the protocol in a 20 μl reaction mixture (oligo $(dT)^{18}$, 2 × TS reaction mix, and 5 μg RNA), and reverse transcription was executed at 42°C for 60 min and 95°C for 3 min. The mRNA expression of genes encoding B-cell lymphoma 2 (*BCL2*), P53 (*P53*), BAX (*BAX*), BAK (*BAK1*), Caspase-9 (*CASP9*), and Caspase-3 (*CASP3*) was analyzed *via* SYBR Green I real-time fluorescent quantitative PCR system. All reactions were run at least in quadruplicate using the TransStart Green qPCR SuperMix kit (TransGen Biotech, Beijing, China) in a total 20 μl reaction volume containing 2 μl cDNA, 0.5 μl sense and antisense primers, and 10 μl SYBR Green qPCR dye with following parameters: 94°C for 30 s, 40 amplification cycles at 94°C for 5 s, 61°C for 35 s, and 72°C for 30 s. Relative quantification of each gene was performed using the comparative $2^{-\Delta\Delta CT}$ method.

## Inflammatory Mediators and Chicken Immunoglobulins Analysis in Serum

The blood serum content [interleukin (IL)-1, IL-10] was determined on day 14 and 28. Chicken immunoglobulins (IgA, IgM, and IgG) in serum was analyzed by ELISA according to the manufacture's kit instructions (Xiamen Jiahui Biotechnology Co. Ltd., Xiamen, China).

## Statistical Analyses

The data were analyzed using one-tailed analysis of variance using the SPSS software, version 20.0.0 (IBM, Armonk, NY, USA), followed by Duncan's multiple-range test. Data are represented as mean ± standard error (S.E.). Graph Pad Prism (San Diego, CA, USA) was used to generate graphs with error bars.

# RESULTS

## Serum Biochemistry

The effect of different doses of PCPE and AFB1 lead to biochemical changes in serum revealed that feed contaminated with AFB1 produced an increase in ALT, AST, ALP, and TBIL indices and decreased the total protein (TP) and ALB indices on day 14 and 28 as compared with the control. Compared to the AFB1-affected group with no PCPE administration, AFB1-affected groups administered with different doses of PCPE and positive drug showed restored biochemical changes on day 28 and a significant reversion of these levels. The most ameliorated beneficial effects were found in PCPE alone and high dose groups (3 g/kg feed). However, PCPE produced no impact on biochemical indices on day 14 when compared with the control (**Figure 1**).

## Histopathology of Liver

The effect of PCPE and AFB1 on the liver tissues histopathology was observed in broilers on day 14 and 28 in all groups. When compared with the control group, significant liver damage was observed in the AFB1 group, including intrahepatic hemorrhages, inflammatory cell infiltration and fatty degenerations, and bile duct hyperplasia of broilers. However, the supplementation of PCPE and positive drug (YCHT) to AFB1 diets inhibited the damage to the hepatic parenchyma of liver, especially in alone and high dose PCPE groups (3 g/kg feed) (**Figure 2**).

## Serum Antioxidant Parameters

The effect of different doses of PCPE and AFB1 on serum antioxidant levels on day 14 and 28 revealed that AFB1 increased serum MDA and decreased the activities and concentrations of SOD and CAT and GSH and GSH-Px ($p < 0.05$), respectively, as compared with the control group. However, the addition of different doses of PCPE and positive drug (YCHT) into diets significantly improved the antioxidant activities in serum by decreasing MDA and increasing SOD, CAT, GSH, and GSH-Px. The highly beneficial results were significantly found in PCPE alone and high dose (3 mg/kg feed) groups on $28^{th}$ day (**Figure 3**).

## mRNA Expressions of Apoptotic Genes in the Liver

To study the mechanisms of AFB1-induced apoptosis in the liver of broilers, the mRNA expression of BCL-2, Caspase-3, Caspase-9, p53, Bak, and Bax were analyzed in the liver using qRT-PCR on day 14 and 28. The mRNA expression level of BCL2 was down-regulated and the levels of CASP3, CASP9, p53, BAK1, and BAX were up-regulated in the AFB1 contaminated feed group as compared to those in the control group ($P < 0.05$). However, mRNA expression level of Caspase-3 and p53 had no significant difference on day 14 as compared to the control. In contrast,

**TABLE 1 |** Primers for quantitative real-time PCR (19).

| Target gene | Primer sequence (5′-3′) | Product length (bp) |
|---|---|---|
| Bcl-2 | F: CTGGATCCAGGACAACGGA | 19 |
| | R: GATGCAAGCTCCCACCAGAA | 20 |
| Caspase-3 | F: GAAGATCACAGCAAGCGAAGC | 21 |
| | R: CAAGAGGGCCATCTGTACCAT | 21 |
| Caspase-9 | F: CCGGAGGGATTTATGGAACAG | 21 |
| | R: CAGGCCTGGATGAAGAAGAGT | 21 |
| P53 | F: GTCCCATCCACGGAGGATTAT | 21 |
| | R: CCAGGCGGCAATAGACCTTA | 20 |
| Bak | F: GGCCATCACGAGAGATCAATG | 21 |
| | R: TCCTGTTGGTAGCGGTAGAAG | 21 |
| Bax | F: CAGATTGGAGAGGCCCTCTT | 20 |
| | R: AATCTGGTCCTGGCTGTTGC | 20 |
| GAPDH | F: CAGAACATCATCCCAGCGTC | 20 |
| | R: GGCAGGTCAGGTCAACAAC | 19 |

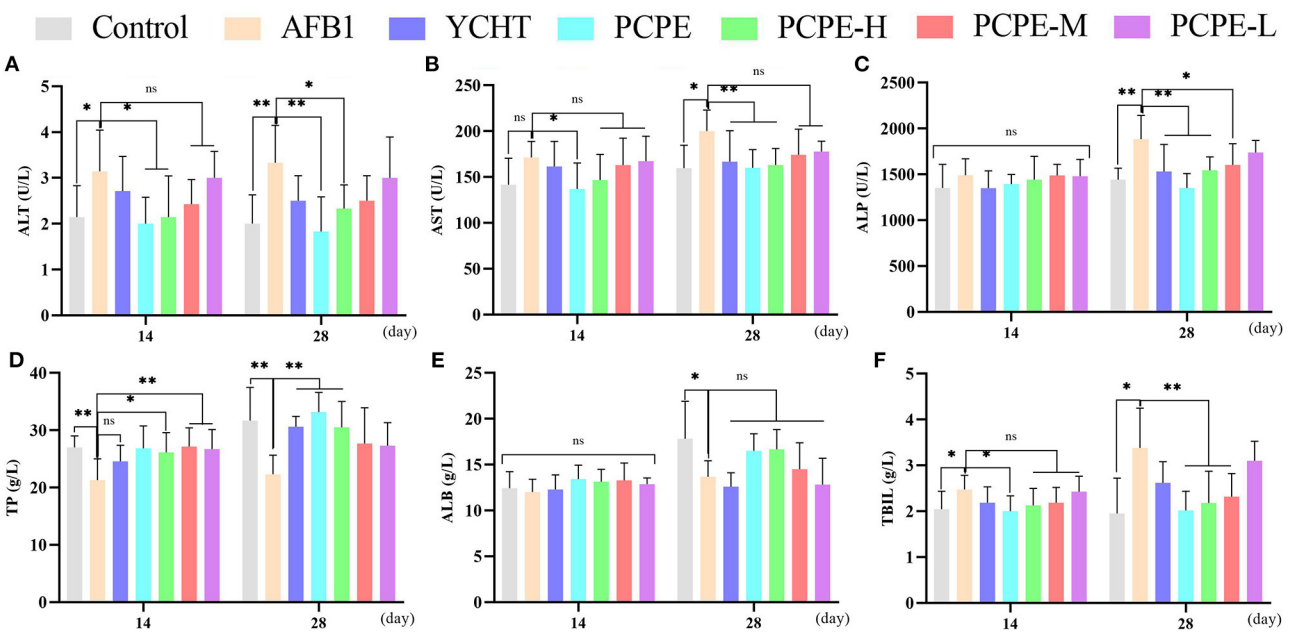


**FIGURE 1 |** Effect of PCPE on serum biochemistry of broilers feed containing AFB1 and PCPE low, medium, and high dose (1 g, 2 g, 3 g PCPE/kg feed, respectively). Values are represented as the mean ± SD. **(A)** ALT; **(B)** AST; **(C)** ALP; **(D)** TP; **(E)** ALB; **(F)** TBIL. *$P < 0.05$; **$P < 0.01$.

when AFB1 affected birds were treated with different doses of PCPE and positive drug (YCHT), the mRNA expression level of BCL2 was significantly up-regulated and the levels of CASP3, CASP9, p53, BAK1, and BAX were down-regulated on day 28 (**Figure 4**).

## Serum Immunoglobulins

The feeding diet of broilers containing AFB1 (3 mg/kg feed) significantly altered the immune response of birds on day 28 by decreasing serum IgA, IgG and IgM levels significantly as compared with that of the control group ($p < 0.05$). In contrary, the addition of PCPE and positive drug YCHT to AFB1 contaminated diet group significantly alleviated ($p < 0.05$) the toxic effect of AFB1 on serum immunoglobulin levels by increasing the IgA, IgG, and IgM content especially in PCPE alone and high dose groups (**Figure 5**).

## Effect of PCPE on Growth Performance of Broilers

The effects of AFB1 and PCPE treatments on weekly growth performance are summarized in **Figure 6**. During the experiment, the AFB1-feed contaminated (3 mg/kg feed) group showed a significantly lower final weight gain and performance with 95% morbidity and 4% mortality as compared

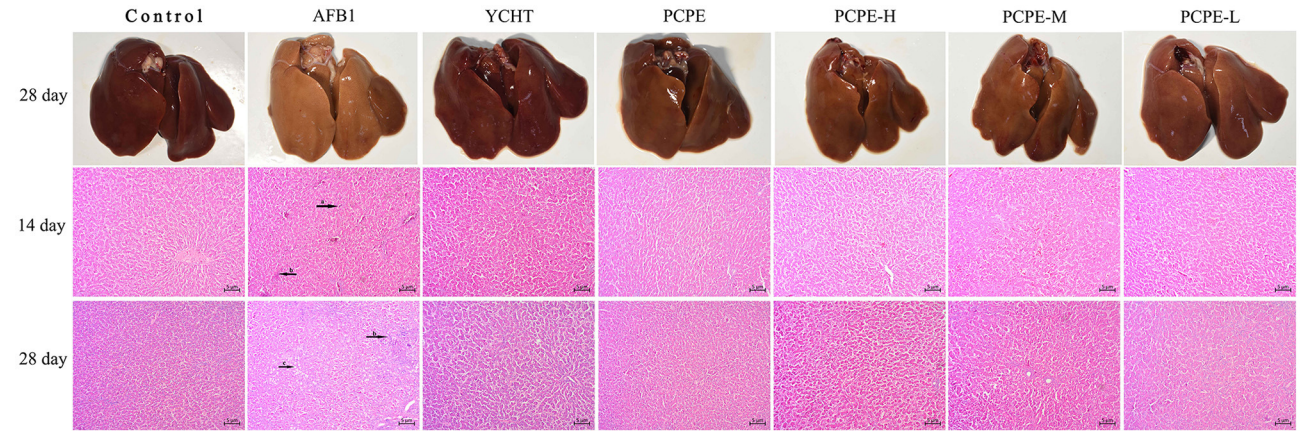


**FIGURE 2 |** Histopathological analysis of liver from different groups on day 14 and 28 in different groups of the experiment. (a) intrahepatic hemorrhages, (b) inflammatory cells infiltration and fatty degenerations, (c) bile duct hyperplasia.

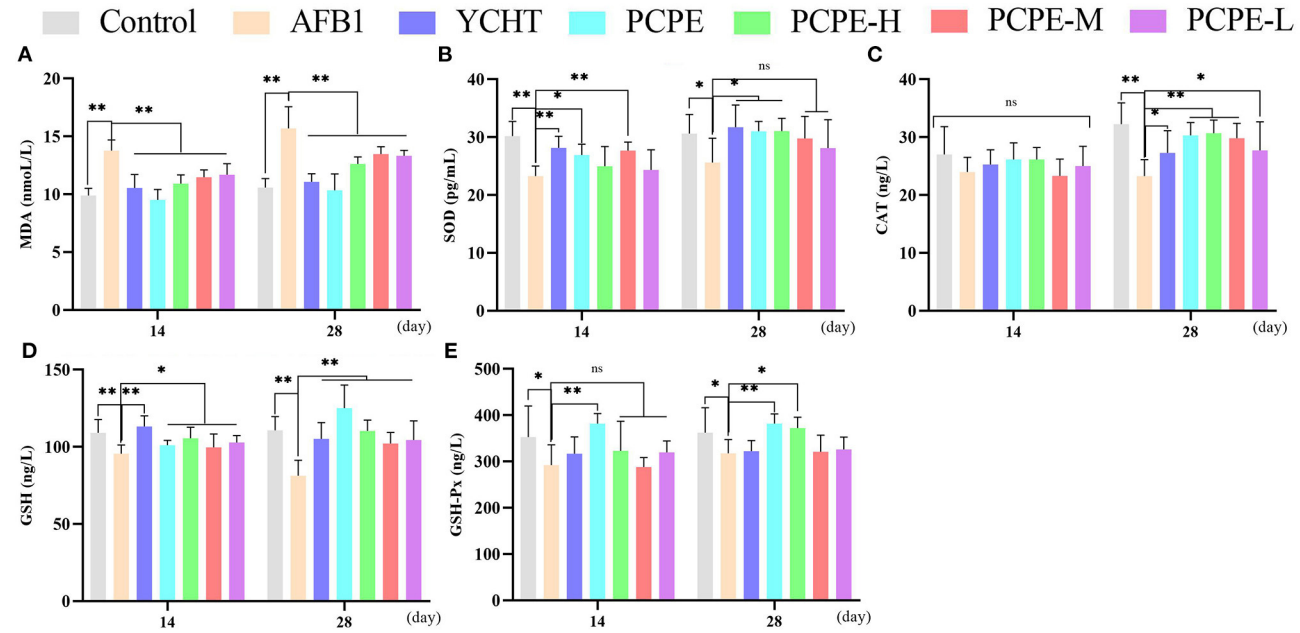


**FIGURE 3 |** Effect of PCPE on serum antioxidant parameters. Values are represented as mean ± SD. Mean values were significantly different (*$P < 0.05$; **$P < 0.01$), ns, non-significant. **(A)** MDA **(B)** SOD **(C)** CAT **(D)** GSH **(E)** GSH-Px.

with other groups ($p < 0.05$). There was a notable difference in all groups as compared with the AFB1 group. The average weight gain and performance were improved by the addition of PCPE into feed contaminated with AFB1, with a significant increase ($p < 0.05$) in weight gain and performance on day 28 as compared with the AFB1 group (**Figure 6**).

## DISCUSSION

Poultry industry involves a variety of domestic birds which are susceptible to various toxicants, likewise aflatoxins, and the presence of AFB1 in the poultry environment is a substantial risk to the poultry and its connection to the safety of food products (1). AFB1 has an impact on various biological and physiological functions of poultry birds, including oxidative stress, decreased immunity, inflammation, cell apoptosis, and liver damage (20). The liver is a vital organ responsible for the elimination and detoxification of xenobiotics and toxicants, including AFB1 (21). Earlier reported data speculated that AFB1 involved in damaging and disturbing effects on the structure and function of liver resulted in the disturbance of functional liver enzymes, oxidative stress, tissue damage, apoptosis, and finally organ failure (22, 23). Recently, Penthorum chinense Pursh, a novel folk medicine, is reported for its hepato-protective effects

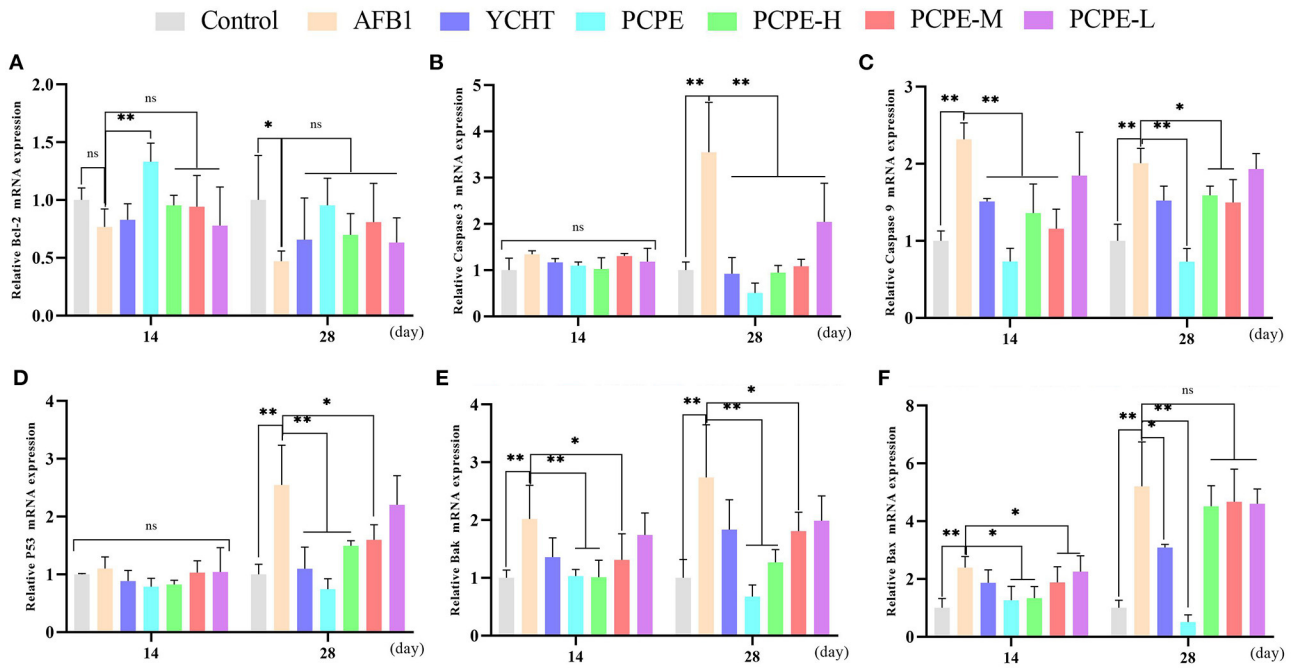


**FIGURE 4 |** Effect of PCPE on mRNA expressions of apoptosis-genes in liver of Broilers. The mRNA expressions levels of apoptosis-genes were identified by real-time PCR. All data were expressed as mean ± SD. Asterisk means significant difference ($p < 0.05$) compared to the control and AFB1 group. **(A)** Bcl-2; **(B)** Caspase-3; **(C)** Caspase-9; **(D)** P53; **(E)** Bak; **(F)** Bax.

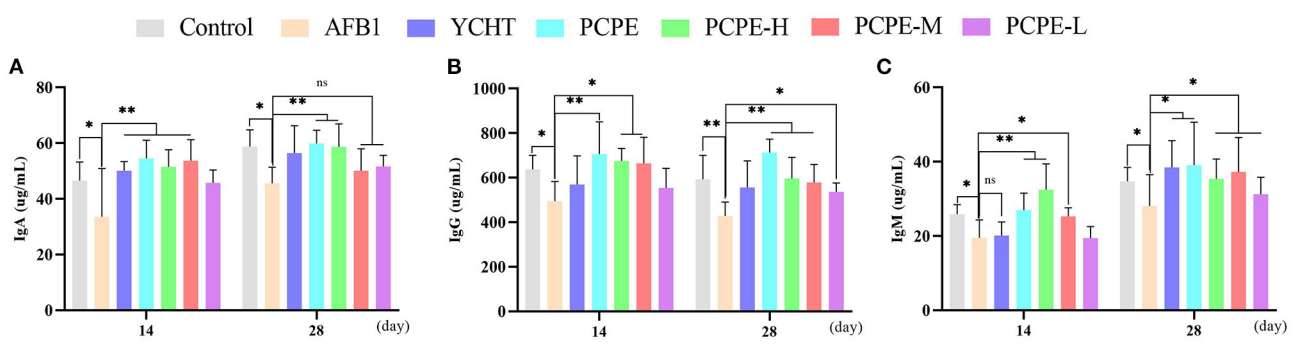


**FIGURE 5 |** Analysis of serum immunoglobulins on 14th and 28th day of experiment. Asterisk means significant difference ($p < 0.05$) compared to the control and AFB1 group (*$P < 0.05$; **$P < 0.01$, ns, non-significant). **(A)** IgA **(B)** IgG **(C)** IgM.

in a variety of pathological problems of the liver, including detoxification, anti-oxidation, promotion of xenobiotics into the blood (24–26), and can also be applied for liver intoxication due to AFB1.

The current research trial demonstrated the positive effects of PCPE in AFB1-challenged liver toxicity in broilers and investigated the mitochondrial apoptosis-concerned pathways linked with PCPE and AFB1 administration. During the current research trial, consequences of AFB1 were disturbances in the functional liver indicators, periportal fibrosis, fatty degeneration, bile duct hyperplasia, and oxidative stress enzymes, which were significantly reversed by the addition of PCPE.

The presence of functional liver indicators in the blood is connected with pathological and physiological changes in the liver (27). Hepatocytes and liver parenchyma are the important cellular components of the liver. Both structures are necessary for a variety of functions, such as metabolic, vascular, immunological, secretory, and eliminatory, along with detoxification of xenobiotics or poisons (28). These structures can be impaired by a continuous exposure of the organ toward toxicants and can result in the liberation of liver enzymes.

A majority of disease pathogenesis occur due to a variety of factors or causes, and oxidative stress is an important one amongst them, that encourages the development of diseases by unbalancing the redox homeostasis of the body. Free radicals

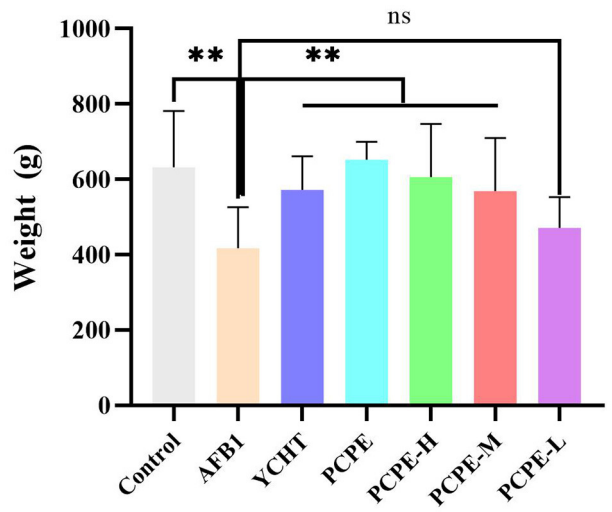


**FIGURE 6 |** Effect of PCPE on average final weight gain, growth performance of broilers whose feed diet contained AFB1 and PCPE low, medium, and high doses. The average weekly body weight of each group. $^{**}P < 0.01$.

and lipid peroxidation mechanisms can be stimulated by the impact of AFB1 and can finally trigger oxidative stress in the liver (29–31). Oxidative stress is regulated by various key components, including antioxidant enzymes (SOD, CAT), MDA, GSH, and GSH-Px. SOD is concerned with the exportation of $O2^{-}$ (32) [30], CAT has a role in cell defense, GSH and GSH-Px play a role in cell resistance, while MDA is an oxidative lipid metabolite that represents cellular injury and lipid peroxidation profile (33). Our outcomes coincide with those of previously reported studies which revealed that AFB1 can cause oxidative stress in the liver of broilers (1, 19). Further underlying mechanisms related with liver damage were validated by the apoptosis signaling pathways.

Apoptosis is important for cellular development as it finally exports the injured cells (34, 35). However, AFB1-related toxicity results in increased apoptosis that leads to liver damage (36–38). Apoptosis is governed by two signaling pathways, extrinsic and intrinsic, which are activated by either mitochondrial signal transduction or receptor-related stimuli (34, 39). It is well established that mitochondria plays an important role in controlling apoptosis as well as repairing eukaryotes for survival (40, 41). The mitochondrial membrane is covered by the BCL2 protein family which interrelates with the tumor suppressor P53. P53 is involved in the catalysis of BAK and encourages transcription-independent stimulation of BAK and BAX. Both the stimulated components are oligomerized on the mitochondrial membrane and result in permeabilization. These pathways are involved in the liberation of pro-apoptotic factors (CYC) from the mitochondria into the cytoplasm, and further stimulation of the caspase cascade family (42, 43). Finally, apoptosis is encouraged by the activation of caspase-9 and then caspase-3, which is due to the signal generated from the inside of mitochondria. In contrary, BCL2 involved in the inhibition of the stimulated BAX and BAK, results in apoptosis reversion (44). In this study, the transcription of *BCL2* was down-regulated and up-regulations were observed in *CASP3*, *CASP9, p53, BAK1, and BAX* by the addition of AFB1, while PCPE addition in the feed produced opposite effects. These results highlight that AFB1 is involved in the mitochondrial-related apoptosis (42). Thus, PCPE application prevented the liver cells from further activation of apoptosis, by reversing the mitochondrial apoptosis pathway which was triggered by AFB1 toxicant.

During the last five decades it is revealed that aflatoxins have negative effects on chicken performance development of bursa and immunity and research concluded that addition of each mg of AFB1/kg in poultry diet significantly decreased the weight gain and performance of broilers by 5% (45). It is well established that AFB1 toxicants have a bad influence on immunity and immune system is very sensitive to this toxin (46) and growth performance, along with morbidity and mortality in broilers (47, 48). Accordingly, AFB1 followed the same pattern during the current study. However, the addition of PCPE in the diet of broilers resulted in improved immunity as well as growth performance.

## CONCLUSION

PCPE administration in AFB1-challenged broilers diet had a therapeutic impact on growth and performance and reversed the pathological changes associated with AFB1 in the liver of broilers. Furthermore, PCPE prevented oxidative stress and apoptosis and delimited liver dysfunction and the imbalance in mitochondrial dynamics. Hence, PCPE produced a therapeutic impact on oxidative stress and apoptosis in AFB1-toxoid broilers. PCPE application can be a traditional medicine approach in veterinary clinics while handling mycotoxin-related toxicity in poultry. However, further studies are suggested to understanding of the link between AFB1 and intestinal mucus and permeability in poultry.

## DATA AVAILABILITY STATEMENT

The original contributions presented in the study are included in the article/supplementary material, further inquiries can be directed to the corresponding author.

## ETHICS STATEMENT

The animal study was reviewed and approved by all experiment procedures agreed with animal ethics regulations and accepted by the Institutional Animal Care and Use Committee (IACUC) of Southwest University (IACUC-20201203).

## AUTHOR CONTRIBUTIONS

WT, FN, RY, and JL conceptualized and designed the study. WT and JL analyzed and interpreted the data. WT, ZL, YS, JF, and QL performed the experiments. WT, ZB, and FN wrote the first draft of the manuscript. All authors have contributed in the revision of the manuscript, and have read and approved the submitted version.

## FUNDING

This research was funded by the Special Project for Fundamental Work of Science and Technology, Grant Number 2013FY110600-03; and special funding for Chongqing Post-Doctoral Research project 2020, number 7820100603.

## ACKNOWLEDGMENTS

All authors would specially like to appreciate and thank Professor Zhumei He, School of Life Sciences, Sun Yat-sen University, Guangzhou, China for donating the *Aspergillus flavus* NRRL3357 for the research experiment.

## REFERENCES

1. Ali Rajput S, Sun L, Zhang N, Mohamed Khalil M, Gao X, Ling Z, et al. Ameliorative effects of grape seed proanthocyanidin extract on growth performance, immune function, antioxidant capacity, biochemical constituents, liver histopathology and aflatoxin residues in broilers exposed to aflatoxin B1. *Toxins.* (2017) 9:371. doi: 10.3390/toxins9110371
2. Cheng L, Qin Y, Hu X, Ren L, Zhang C, Wang X, et al. Melatonin protects in vitro matured porcine oocytes from toxicity of Aflatoxin B1. *J Pineal Res.* (2019) 66:e12543. doi: 10.1111/jpi.12543
3. Magnoli AP, Monge MP, Miazzo RD, Cavaglieri LR, Magnoli CE, Merkis CI, et al. Effect of low levels of aflatoxin B1 on performance, biochemical parameters, and aflatoxin B1 in broiler liver tissues in the presence of monensin and sodium bentonite. *Poult Sci.* (2011) 90:48–58. doi: 10.3382/ps.2010-00971
4. Trebak F, Alaoui A, Alexandre D, El Ouezzani S, Anouar Y, Chartrel N, et al. Impact of aflatoxin B1 on hypothalamic neuropeptides regulating feeding behavior. *Neurotoxicology.* (2015) 49:165–73. doi: 10.1016/j.neuro.2015.06.008
5. Zhang N-Y, Qi M, Zhao L, Zhu M-K, Guo J, Liu J, et al. Curcumin prevents aflatoxin B1 hepatoxicity by inhibition of cytochrome P450 isozymes in chick liver. *Toxins.* (2016) 8:327. doi: 10.3390/toxins8110327
6. Fouad AM, Ruan D, El-Senousey HK, Chen W, Jiang S, Zheng C. Harmful Effects and Control Strategies of Aflatoxin B1 Produced by *Aspergillus flavus* and *Aspergillus parasiticus* Strains on Poultry: Review. *Toxins.* (2019) 11:176. doi: 10.3390/toxins11030176
7. Li S, Muhammad I, Yu H, Sun X, Zhang X. Detection of Aflatoxin adducts as potential markers and the role of curcumin in alleviating AFB1-induced liver damage in chickens. *Ecotoxicol Environ Saf.* (2019) 176:137–45. doi: 10.1016/j.ecoenv.2019.03.089
8. Xu Q, Shi W, Lv P, Meng W, Mao G, Gong C, et al. Critical role of caveolin-1 in aflatoxin B1-induced hepatotoxicity *via* the regulation of oxidation and autophagy. *Cell Death and Disease.* (2020) 11:6. doi: 10.1038/s41419-019-2197-6
9. Hua Z, Liu R, Chen Y, Liu G, Li C, Song Y, et al. Contamination of aflatoxins induces severe hepatotoxicity through multiple mechanisms. *Front Pharmacol.* (2021) 11:605823. doi: 10.3389/fphar.2020.605823
10. Brahmi D, Bouaziz C, Ayed Y, Mansour HB, Zourgui L, Bacha H. Chemopreventive effect of cactus Opuntia ficus indica on oxidative stress and genotoxicity of aflatoxin B1. *Nutr Metab.* (2011) 8:1–16. doi: 10.1186/1743-7075-8-73
11. Nagata S, Tanaka M. Programmed cell death and the immune system. *Nature Reviews Immunology.* (2017) 17:333–40. doi: 10.1038/nri.2016.153
12. Bbosa GS, Kitya D, Ogwal-Okeng J. *Aflatoxins* metabolism, effects on epigenetic mechanisms and their role in carcinogenesis. *Health.* (2013) 5:38887. doi: 10.4236/health.2013.510A1003
13. Wang F, Shu G, Peng X, Fang J, Chen K, Cui H, et al. Protective effects of sodium selenite against aflatoxin B1-induced oxidative stress and apoptosis in broiler spleen. *Int J Environ Res Public Health.* (2013) 10:2834–44. doi: 10.3390/ijerph10072834
14. Chen K, Fang J, Peng X, Cui H, Chen J, Wang F, et al. Effect of selenium supplementation on aflatoxin B1-induced histopathological lesions and apoptosis in bursa of Fabricius in broilers. *Food Chem Toxicol.* (2014) 74:91–7. doi: 10.1016/j.fct.2014.09.003
15. Liu T, Ma Q, Zhao L, Jia R, Zhang J, Ji C, et al. Protective effects of sporoderm-broken spores of ganderma lucidum on growth performance, antioxidant capacity and immune function of broiler chickens exposed to low level of aflatoxin B1. *Toxins.* (2016) 8:278. doi: 10.3390/toxins8100278
16. Hu Y, Wang S, Wang A, Lin L, Chen M, Wang Y. Antioxidant and hepatoprotective effect of penthorum chinense pursh extract against t-BHP-induced liver damage in L02 cells. *Molecules.* (2015) 20:6443–53. doi: 10.3390/molecules20046443
17. Ding Q, Jin Z, Dong J, Wang Z, Jiang K, Ye Y, et al. Bioactivity Evaluation of Pinocembrin Derivatives From Penthorum chinense Pursh Stems. *Natural Product Communications.* (2019) 14:1934578X19875892. doi: 10.1177/1934578X19875892
18. Tian X, Liu H, Qiao S, Yin H, Chen M, Hu P, et al. Exploration of the hepatoprotective chemical base of an orally administered herbal formulation (YCHT) in normal and CCl4-intoxicated liver injury rats. Part 2: hepatic disposition in vivo and hepatoprotective activity *in vitro*. *J Ethnopharmacol.* (2019) 236:161–72. doi: 10.1016/j.jep.2019.02.022
19. Tao W, Li Z, Nabi F, Hu Y, Hu Z, Liu J. Penthorum chinense pursh compound ameliorates AFB1-induced oxidative stress and apoptosis *via* modulation of mitochondrial pathways in broiler chicken kidneys. *Front Vet Sci.* (2021) 8:750937. doi: 10.3389/fvets.2021.750937
20. Wang Q, Zhang Y, Zheng N, Guo L, Song X, Zhao S, et al. Biological system responses of dairy cows to aflatoxin B1 exposure revealed with metabolomic changes in multiple biofluids. *Toxins.* (2019) 11:77. doi: 10.3390/toxins11020077
21. Corcuera LA, Vettorazzi A, Arbillaga L, Gonzalez-Peñas E, De Cerain AL. An approach to the toxicity and toxicokinetics of aflatoxin B1 and ochratoxin A after simultaneous oral administration to fasted F344 rats. *Food Chem Toxicol.* (2012) 50:3440–6. doi: 10.1016/j.fct.2012.06.048
22. Rawal S, Kim JE, Coulombe R Jr. Aflatoxin B1 in poultry: toxicology, metabolism and prevention. *Res Vet Sci.* (2010) 89:325–31. doi: 10.1016/j.rvsc.2010.04.011
23. Monson MS, Coulombe RA, Reed KM. Aflatoxicosis: lessons from toxicity and responses to aflatoxin B1 in poultry. *Agriculture.* (2015) 5:742–77. doi: 10.3390/agriculture5030742
24. Sun X, Wu A, Law BYK, Liu C, Zeng W, Qiu ACL, et al. The active components derived from Penthorum chinense Pursh protect against oxidative-stress-induced vascular injury *via* autophagy induction. *Free Radical Biology and Medicine.* (2020) 146:160–80. doi: 10.1016/j.freeradbiomed.2019.10.417
25. Wang A, Li M, Huang H, Xiao Z, Shen J, Zhao Y, et al. A review of Penthorum chinense Pursh for hepatoprotection: traditional use, phytochemistry, pharmacology, toxicology and clinical trials. *J Ethnopharmacol.* (2020) 251:112569. doi: 10.1016/j.jep.2020.112569
26. Zhao X, Li L, Zhou M, Liu M, Deng Y, He L, et al. An overview of the mechanism of penthorum chinense pursh on alcoholic fatty liver. *Evidence-Based Complementary and Alternative Medicine.* (2020) 2020:4875764. doi: 10.1155/2020/4875764
27. Lu T, Harper A, Zhao J, Corl B, LeRoith T, Dalloul R. Effects of a dietary antioxidant blend and vitamin E on fatty acid profile, liver function, and inflammatory response in broiler chickens fed a diet high in oxidants. *Poult Sci.* (2014) 93:1658–66. doi: 10.3382/ps.2013-03827
28. Mitra V, Metcalf J. Metabolic functions of the liver. *Anaesth Intensive Care.* (2009) 10:334–5. doi: 10.1016/j.mpaic.2009.03.011
29. Kanbur M, Eraslan G, Sarica ZS, Aslan Ö. The effects of evening primrose oil on lipid peroxidation induced by subacute aflatoxin exposure in mice. *Food Chem Toxicol.* (2011) 49:1960–4. doi: 10.1016/j.fct.2011.05.006
30. Li S, Tan H-Y, Wang N, Zhang Z-J, Lao L, Wong C-W, et al. The role of oxidative stress and antioxidants in liver diseases. *Int J Mol Sci.* (2015) 16:26087–124. doi: 10.3390/ijms161125942

31. Singh A, Kukreti R, Saso L, Kukreti S. Oxidative stress: role and response of short guanine tracts at genomic locations. *Int J Mol Sci.* (2019) 20:4258. doi: 10.3390/ijms20174258
32. Miao L, Clair DKS. Regulation of superoxide dismutase genes: implications in disease. *Free Radic Biol Med.* (2009) 47:344–56. doi: 10.1016/j.freeradbiomed.2009.05.018
33. Ayala A, Muñoz MF, Argüelles S. Lipid peroxidation: production, metabolism, and signaling mechanisms of malondialdehyde and 4-hydroxy-2-nonenal Oxidative medicine and cellular longevity. (2014) 2014:360438. doi: 10.1155/2014/360438
34. Cheng X, Ferrell JE. Apoptosis propagates through the cytoplasm as trigger waves. *Science.* (2018) 361:607–12. doi: 10.1126/science.aah4065
35. Nagata S. Apoptosis and clearance of apoptotic cells. *Annu Rev Immunol.* (2018) 36:489–517. doi: 10.1146/annurev-immunol-042617-053010
36. Chen Y, Feng X, Hu X, Sha J, Li B, Zhang H, et al. Dexmedetomidine ameliorates acute stress-induced kidney injury by attenuating oxidative stress and apoptosis through inhibition of the ROS/JNK signaling pathway. *Oxid Med Cell Longev.* (2018) 2018:4035310. doi: 10.1155/2018/4035310
37. Zhu L, Huang C, Yang X, Zhang B, He X, Xu W, et al. Proteomics reveals the alleviation of zinc towards aflatoxin B1-induced cytotoxicity in human hepatocyes (HepG2 cells). *Ecotoxicol Environ Saf.* (2020) 198:110596. doi: 10.1016/j.ecoenv.2020.110596
38. Frenette C, Kayali Z, Mena E, Mantry PS, Lucas KJ, Neff G, et al. Emricasan to prevent new decompensation in patients with NASH-related decompensated cirrhosis. *J Hepatol.* (2021) 74:274–82. doi: 10.1016/j.jhep.2020.09.029
39. Zhu S, Liu Y, Li Y, Yi J, Yang B, Li Y, et al. The potential risks of herbicide butachlor to immunotoxicity *via* induction of autophagy and apoptosis in the spleen. *Chemosphere.* (2022) 286:131683. doi: 10.1016/j.chemosphere.2021.131683
40. Pfanner N, Warscheid B, Wiedemann N. Mitochondrial proteins: from biogenesis to functional networks. *Nat Rev Mol Cell Biol.* (2019) 20:267–84. doi: 10.1038/s41580-018-0092-0
41. Abate M, Festa A, Falco M, Lombardi A, Luce A, Grimaldi A, et al. Mitochondria as playmakers of apoptosis, autophagy and senescence. *Semin Cell Dev Biol.* (2020) 139–53. doi: 10.1016/j.semcdb.2019.05.022
42. Estaquier J, Vallette F, Vayssiere J-L, Mignotte B. The mitochondrial pathways of apoptosis. *Adv Exp Med Biol.* (2012) 942:157–83. doi: 10.1007/978-94-007-2869-1_7
43. Bock FJ, Tait SW. Mitochondria as multifaceted regulators of cell death. *Nat Rev Mol Cell Biol.* (2020) 21:85–100. doi: 10.1038/s41580-019-0173-8
44. Ouyang Z, Yang B, Yi J, Zhu S, Lu S, Liu Y, et al. Exposure to Fluoride induces apoptosis in liver of ducks by regulating Cyt-C/Caspase 3/9 signaling pathway. *Ecotoxicol Environ Saf.* (2021) 224:112662. doi: 10.1016/j.ecoenv.2021.112662
45. Yunus AW, Razzazi-Fazeli E, Bohm J. Aflatoxin B(1) in affecting broiler's performance, immunity, and gastrointestinal tract: a review of history and contemporary issues. *Toxins.* (2011) 3:566–90. doi: 10.3390/toxins3060566
46. Saleh AA, Ebeid TA, Abudabos AM. Effect of dietary phytogenics (herbal mixture) supplementation on growth performance, nutrient utilization, antioxidative properties, and immune response in broilers. *Environ Sci Pollut Res Int.* (2018) 25:14606–13. doi: 10.1007/s11356-018-1685-z
47. Slizewska K, Cukrowska B, Smulikowska S, Cielecka-Kuszyk J. The effect of probiotic supplementation on performance and the histopathological changes in liver and kidneys in broiler chickens fed diets with aflatoxin B1. *Toxins.* (2019) 11:112. doi: 10.3390/toxins11020112
48. Wang X-h, Li W, Wang X-h, Han M-y, Muhammad I, Zhang X-y, et al. Water-soluble substances of wheat: a potential preventer of aflatoxin B1-induced liver damage in broilers. *Poultry science.* (2019) 98:136–49. doi: 10.3382/ps/pey358


**Conflict of Interest:** The authors declare that the research was conducted in the absence of any commercial or financial relationships that could be construed as a potential conflict of interest.

**Publisher's Note:** All claims expressed in this article are solely those of the authors and do not necessarily represent those of their affiliated organizations, or those of the publisher, the editors and the reviewers. Any product that may be evaluated in this article, or claim that may be made by its manufacturer, is not guaranteed or endorsed by the publisher.

frontiers | Frontiers in Veterinary Science

ORIGINAL RESEARCH
published: 07 April 2022
doi: 10.3389/fvets.2022.846700

# Regularity of Toll-Like Receptors in Bovine Mammary Epithelial Cells Induced by *Mycoplasma bovis*

*Jinghan Yang[1], Yuhui Liu[1], Changjie Lin[1], Rui Yan[1], Zhengzhi Li[1], Qiuhui Chen[1], Haiyan Zhang[1], Haojun Xu[1], Xi Chen[1], Yingyu Chen[1], Aizhen Guo[1,2] and Changmin Hu[1]**

[1] College of Veterinary Medicine, Huazhong Agricultural University, Wuhan, China, [2] State Key Laboratory of Agricultural Microbiology, Huazhong Agricultural University, Wuhan, China

Mastitis is one of the most common and significant infectious diseases in dairy cattle and is responsible for significant financial losses for the dairy industry globally. An important pathogen of bovine mastitis, *Mycoplasma bovis* (*M. bovis*) has a high infection rate, requires a long course of treatment, and is difficult to cure. Bovine mammary epithelial cells (BMECs) are the first line of defense of the mammary gland, and their natural immune system plays a critical role in resisting *M. bovis* infection. This study aimed to explore and demonstrate the regularity of Toll-like receptors (TLRs) activation during *M. bovis* infection and their function during *M. bovis* mastitis. An *in vitro* model of *M. bovis*-induced mastitis showed that the expression of IL-6, IL-8, and TNF-α increased significantly following infection. *M. bovis* infection also upregulated the expression of TLR1/2/6 on the cell membrane and TLR3/9 in the cytoplasm. There is a crosstalk effect between TLR1–TLR2 and TLR2–TLR6. Furthermore, *M. bovis* infection was found to activate the TLR1/2/6/9/MyD88/NF-κB and TLR3/TRIF/IRF signal transduction pathways, which in turn activate inflammatory factors. These findings lay the theoretical foundation for understanding the pathogenesis of *M. bovis*, permitting the development of effective measures for preventing and controlling *M. bovis* mastitis.

**Keywords: mastitis, bovine mammary epithelial cells, *M. bovis*, TLRs, pathogen-host interaction, signal pathways**

OPEN ACCESS

***Edited by:***
*Jianzhu Liu,*
*Shandong Agricultural University, China*

***Reviewed by:***
*Chuang Xu,*
*Heilongjiang Bayi Agricultural University, China*
*Yu Li,*
*Anhui Agricultural University, China*
*Xing-Ping Wang,*
*Ningxia University, China*

***Correspondence:**
*Changmin Hu*
*hcm@mail.hzau.edu.cn*

***Specialty section:***
*This article was submitted to Animal Nutrition and Metabolism, a section of the journal Frontiers in Veterinary Science*

***Received:*** *31 December 2021*
***Accepted:*** *15 February 2022*
***Published:*** *07 April 2022*

***Citation:***
*Yang J, Liu Y, Lin C, Yan R, Li Z, Chen Q, Zhang H, Xu H, Chen X, Chen Y, Guo A and Hu C (2022) Regularity of Toll-Like Receptors in Bovine Mammary Epithelial Cells Induced by Mycoplasma bovis. Front. Vet. Sci. 9:846700. doi: 10.3389/fvets.2022.846700*

## INTRODUCTION

Mastitis is a highly prevalent inflammatory disease that ranks first among diseases that affect dairy cows. It causes significant economic losses and severely impacts animal welfare and milk production (1). Bovine mastitis is caused by the co-infection of various pathogenic microorganisms, including bacteria, fungi, *Mycoplasma*, and viruses (2). Mastitis caused by *Mycoplasma bovis* (*M. bovis*) has severely restricted the development of the dairy cow breeding industry because of its long-lasting effects, fast transmission, and poor response to therapy (3).

*Mycoplasmas*, the smallest and most pleomorphic self-replicating prokaryotes, reside either on eukaryotic cell membranes or inside the cells themselves (4). *Mycoplasmas* are complex bacteria, and broad-spectrum antibiotic treatment is not effective against most *Mycoplasmas*. *Mycoplasmas* are pleomorphic due to their lack of cell walls, allowing them to quickly reach and bind to the target surface, and achieve membrane fusion with the host (5). *Mycoplasmas* contain a rich variety of hydrophobic proteins that are specifically soluble in TritonX-114-lipid associated membrane proteins (LAMPs) (6). The pathogenic mechanism of *M. bovis* is caused mainly by the host

cells' recognition of LAMPs through their TLRs, triggering an inflammatory response (7). Some *Mycoplasmas* also cause cell damage through their secretions or metabolites. *Mycoplasmas* have developed a variety of strategies to resist and manipulate the host immune system, including evading the host's immune response via surface antigen mutations. Lysnyansky (8) found that *M. bovis* can evade host immunity through variable surface lipoproteins. However, the definitive pathophysiologic mechanisms of *M. bovis* remain unclear.

Breast tissue is protected by both innate and acquired immunity. Innate immunity is dominant during the initial stages of infection, with mammary epithelial cells constituting an essential part of innate immunity. Host cells have a complete set of natural immune systems to resist the invasion of pathogenic microorganisms, called pattern recognition receptors (PRRS). These include TLRs, NOD-like receptors (NLRs), and RIG-I like receptors (RLRs) (9). TLRs are key regulators of both innate immunity and adaptive immunity and are also the best-studied family of PRRs. It has been estimated that most mammalian species have 10 to 15 types of TLRs, and that the distribution of certain TLRs varies between species. TLRs are crucial to the pathogenesis, prevention, and control of mastitis (10–13). Takeda (14) found that TLR2/TLR6 could identify the diacylated lipoprotein M161Ag (MALP404) derived from *Mycoplasma fermentum*. Other studies have shown that *M. bovis* activates the ERK1/2 MAPK pathway through TLR2 and TLR4, promotes the secretion of CXCL8, and intensifies the host's inflammatory response (15). *M. bovis* can also combine with TLR1/2 to stimulate MMP9 production, thereby worsening mastitis (16). TLR recognition mediates the activation of innate immunity to instruct the development of an effective acquired immune response. Thus far, the investigation of Toll-like receptors of bovine mammary epithelial cells induced by *M. bovis* is a breakthrough in the treatment of mastitis.

Here we established a BMECs model of *M. bovis* infection *in vitro* and studied the mechanism of the TLRs signaling pathway after *M. bovis* infection, thereby identifying the types of TLRs and triggered inflammatory signal pathways that are involved in the regulation of *M. bovis* infection. Such associations are key to furthering our understanding of the immune and pathogenic mechanisms of *M. bovis*.

# MATERIALS AND METHODS

## Cell Preparation and Co-culture With *M. bovis*

Bovine mammary epithelial cells were extracted from the mammary tissue of Holstein cows during their middle lactation period. The cells were routinely maintained in DMEM/F12 medium, supplemented with 10% fetal bovine serum (Sigma, Bedford, MA), 1% penicillin–streptomycin solution (Hyclone Logan, UT), 5 ng/mL EGF (SinoBiological, Beijing, China), and 5 μg/mL insulin and transferrin (Sigma, Bedford, MA). All cells were stored in incubators at 37°C with 5% $CO_2$. Three strains of *M. bovis* were used in this study, 39YC (clinical isolates of *M. bovis* from milk), which was identified and stored in our lab; PG45 (standard *M. bovis* strain, ATCC 25523); and HB0801 (*M. bovis* pneumonia clinical isolates from the lungs, CCTCC # M2010040) (17). *M. bovis* and BMECs were co-cultured at a ratio of 1000:1 and 500:1, respectively (18, 19).

## Immunofluorescence

Cytokeratin 18 immunofluorescence was used to identify the isolated BMECs. The BMECs were fixed in 4% paraformaldehyde and blocked with 5% BSA solution. Following incubation with the primary antibody (anti-Cytokeratin 18 antibody, Bioss) overnight at 4°C, BMECs were then incubated with a secondary antibody.

## Polymerase Chain Reaction

Total RNA was isolated using Trizol reagent (Invitrogen, CA), and cDNA was synthesized using a reverse transcription kit (+gDNA wiper) (Vazyme, Nanjing, China). We examined the MUC-1 gene to identify and distinguish BMECs from BMFBs (bovine mammary fibroblasts) (20). Specific primers for the MUC-1 gene are shown below: forward: 5′-AGATCAAGTTCAGGCCAGGAT-3′; reverse: 5′-CCAGGTTTGTATAAGAGAGGTTGC-3′.

## Quantitative Real-Time PCR

The qPCR reaction system included AceQ® qPCR SYBR Green Master Mix 5 μL, upstream primer 0.2 μL, downstream primer 0.2 μL, ROX Reference Dye1 0.2 μL, cDNA (the template obtained by reverse transcription was diluted 10 times to 50 ng/mL) 1 μL, and $ddH_2O$ 3.4 μL. The qPCR reaction program was 40 cycles at 95°C for 5 min, 95°C for 30 s, 60.5°C for 30 s, and 72°C for 30 s. The primers used for quantitative real-time PCR are shown in **Table 1**. Each gene's relative expression (cycle threshold) values were normalized based on β-actin expression. $H_2O$ wells (NTC = no-template controls) were used as negative controls. The induction values of genes mRNA expression were calculated according to the equation: fold change $= 2^{-\Delta\Delta Ct}$. All reactions were performed in triplicate on at least 3 biologic replicates. A full description of the experiments that comply with MIQE (the Minimum Information for Publication of Quantitative Real-Time PCR Experiment) can be found in the **Supplementary Material**.

## Western Blot

Confluent BMECs were lysed in ice-cold RIPA buffer with 1 mM PMSF (Vazyme, Nanjing, China). Lysate protein concentration was measured using a BCA protein assay kit (Thermo, Waltham, MA). Protein samples were denatured in boiling water for 10 min, and electrophoresed. Protein bands were transferred to a PVDF membrane and blocked using 5% skim milk in a TBST buffer. The bands were combined with primary antibodies (TLR1, Biobyt, 1:1000; TLR2, TLR9, Avivia Systems Biology, 1:1000; TLR3, Novus, 1:500; TLR6 and IκBα, Santa Cruz Biotechnology, 1:1500 and 1:1000; P65, P-P65, p-IκBα, Cell Signaling Technology, 1:1000; p-c-Jun, Bioss, 1:1000) and slowly rocked overnight at 4°C, then incubated with secondary antibodies at room temperature in TBST buffer. Signals were detected using the ECL method.

**TABLE 1 |** Primer sequences of fluorescence quantitative PCR.

| Genes | Primers sequence (5′-3′) | |
|---|---|---|
| IL-8 | F:TGAAGCTGCAGTTCTGTCAAG | R:TTCTGCACCCACTTTTCCTTGG |
| TNF-α | F:TCTTCTCAAGCCTCAAGTAACAAGC | R:CCATGAGGGCATTGGCATAC |
| IL-6 | F:CAGCAGGTCAGTGTTTGTGG | R:CTGGGTTCAATCAGGCGAT |
| TLR1 | F:ACTTGGAATTCCTTCTTCACGA | R:GGAAGACTGAACACATCATGGA |
| TLR2 | F:GGTTTTAAGGCAGAATCGTTTG | R:AAGGCACTGGGTTAAACTGTGT |
| TLR3 | F:GATGTATCACCCTGCAAAGACA | R:TGCATATTCAAACTGCTCTGCT |
| TLR4 | F:TGCTGGCTGCAAAAAGTATG | R:TTACGGCTTTTGTGGAAACC |
| TLR5 | F:CCTCCTGCTCAGCTTCAACTAT | R:TATCTGACTTCCACCCAGGTCT |
| TLR6 | F:CCTTGTTTTTCACCCAAATAGC | R:TAAGGTTGGTCCTCCAGTGAGT |
| TLR7 | F:TCTTGAGGAAAGGGACTGGTTA | R:AAGGGGCTTCTCAAGGAATATC |
| TLR9 | F:CTGACACCTTCAGTCACCTGAG | R:TGGTGGTCTTGGTGATGTAGTC |
| TLR10 | F:ATGGTGCCATTATGAACCCTAC | R:CACATGTCCCTCTGGTGTCTAA |
| MyD88 | F:ACTATCGGCTGAAGTTGTGC | R:TCCTTGCTTTGCAGGTATTC |
| TRIF | F:GGAGTCGTCCGAGCAGAAA | R:AGGATGATGAATGCCGAGTG |
| IRF3 | F:GCATCCCTTGGAAGCACG | R:CCTCCGCTAAACGCAACAC |

## Immunoprecipitation

TLR2 and TLR6 protein expression was measured after BMECs were co-cultured with *M. bovis* for 16 h, and TLR2 and TLR1 protein expression was measured after BMECs were infected with *M. bovis* for 20 h. Total cellular protein was extracted using the conventional method, and concentrations were adjusted using PBS (1 mM PMSF) after the protein concentration was measured. Equal 1 mL protein was incubated with 30 μL 50% protein A/G agarose for 1 h, after which the supernatants were collected. The TLR2 primary antibody was added at 4°C overnight, and then incubated with 20 μL protein A/G agarose on a shaker for 5 h at room temperature. Samples were centrifuged and supernatants were collected for Western blot analysis.

## Statistical Analysis

All values were written as the mean ± SD of at least three independent experiments. Statistical analysis was performed using GraphPad Prism 5.0. The *t* tests were used to identify statistically significant differences between the compared groups, and Western blot results were quantified using NIH Image J software (Bethesda, MD). ($^{*}p < 0.05$ = different; $^{**}p < 0.01$ = significantly different; $^{***}p < 0.001$ = extremely significantly different).

# RESULTS

## *M. bovis* Induced IL-6, IL-8, and TNF-α mRNA Expression in BMECs

BMECs were extracted from the mammary tissue of Holstein cows (**Supplementary Figure S1**). Under MOI conditions of 500 and 1,000, the activity of 39YC, PG45, and HB0801 in BMECs was equivalent with controls, suggesting that BMECs maintained stable activity after being infected with *M. bovis* at MOI = 500 and 1,000 (**Supplementary Figure S2**). We then measured the expression of inflammatory cytokines such as IL-6, IL-8, and TNF-α in BMECs after infection with *M. bovis* under different strains and at different MOIs (**Figures 1A–C**). All three *M. bovis* strains induced the expression of inflammatory cytokines by BMECs, and underwent consistent changes based on infection time and MOI. The up-regulated levels of inflammatory factors were more significant at MOI = 1,000 than at MOI = 500. Based on the above experimental results, we established a BMECs model of *M. bovis* infection.

## *M. bovis* Activated TLRs Expression in BMECs

Cells were harvested for total RNA extraction and the expression of TLR genes 10, 16, 20, and 24 h post-infection (hpi) was measured using PCR. As shown in **Figure 2A**, the expression of TLR2, TLR3, and TLR6 in the 39YC group increased compared with the control group at 10 hpi. Similarly, the mRNA levels of TLR2 and TLR6 were significantly higher in the 39YC and HB0801 groups than in controls. However, only TLR6 was highly expressed in the PG45 group at 16 hpi (**Figure 2B**). The mRNA of TLR1 and TLR2 were more highly expressed in the 39YC group than that in the control group, and the mRNA of TLR9 was higher in the PG45 group compared with the control group at 20 hpi (**Figure 2C**). The expression of TLR2 in the 39YC group was significantly higher than in controls (**Figure 2D**). There was also a significant difference in TLR2 and TLR9 expression between the PG45 group and the control group, the expression of TLR9 of the HB0801 group was significantly higher than that of the control group at 24 hpi (**Figure 2D**).

According to the above results (**Figure 2**), we found that the expression of TLR2, TLR3, and TLR6 were to increase at 16 hpi, and the expression of TLR1 and TLR9 were increased at 20 hpi. The expression of TLR factors at the indicated times was also detected using Western blot analysis (**Figure 3**). We found that the expression of TLR2, TLR3, and TLR6 was significantly higher than controls at 16 hpi by the three different stains *M. bovis*. TLR1 and TLR9 protein expression was significantly increased at 20 hpi.

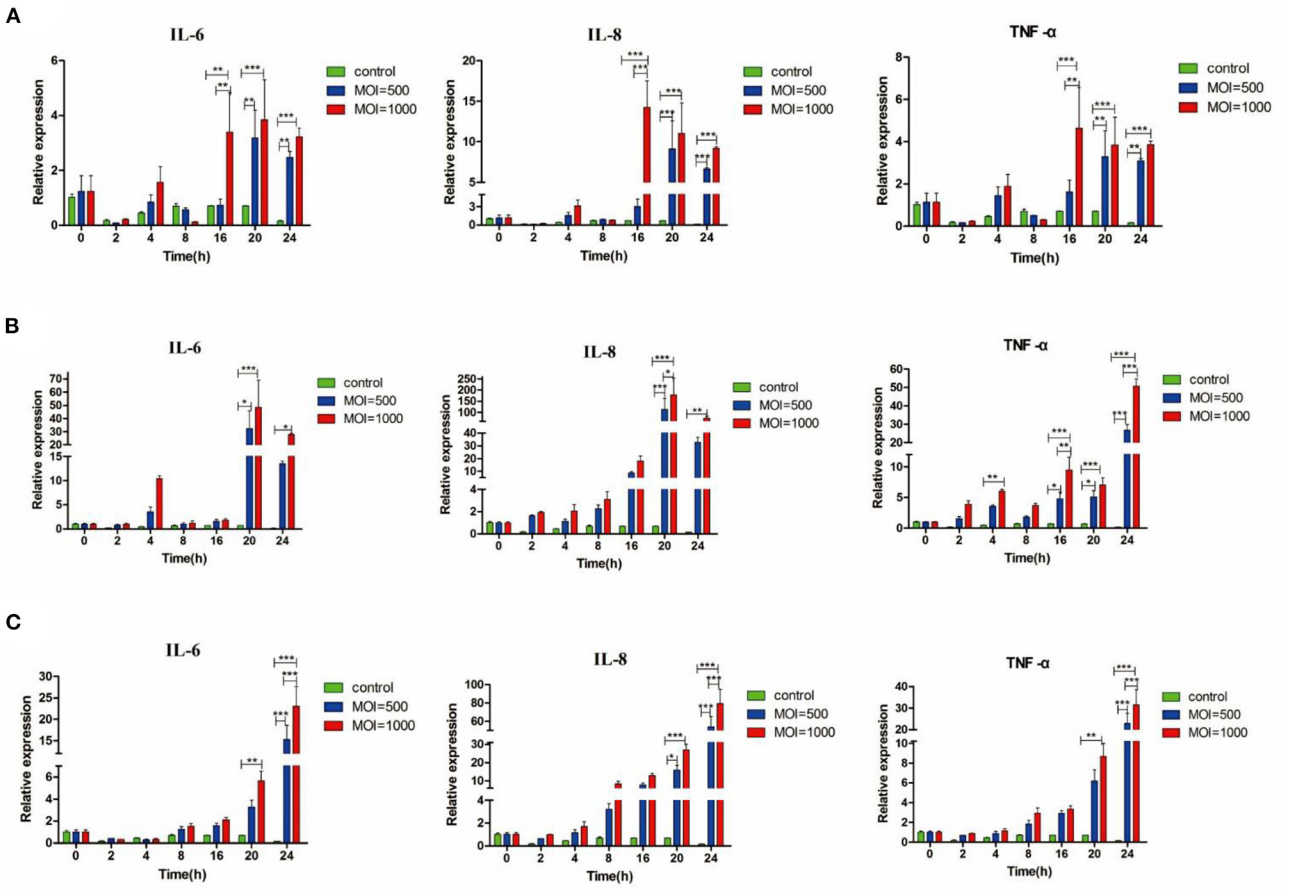


**FIGURE 1 |** *M. bovis* induced IL-6, IL-8, and TNF-α mRNA expression in BMECs. Relative expression of different cytokines from BMECs infected by three *M. bovis*, respectively, **(A)** BMECs infected by 39YC within 24 h, **(B)** BMECs infected by PG45 within 24 h, **(C)** BMECs infected by HB0801 within 24 h. $^{*}p < 0.05$, $^{**}p < 0.01$, and $^{***}p < 0.001$.

## Roles of TLR1/2/6 in BMECs Induced by *M. bovis*

To detect whether there was a crosstalk between TLR1/TLR2 and TLR2/TLR6, cells were collected at distinct time points after infection for qRT-PCR (**Figure 4A**). The upregulation of TLR1 began at 4 hpi with 39YC and lasted until 24 hpi. TLR2 began to rise at 4 hpi with 39YC, reaching its peak at 14 hpi. It then downregulated slowly but consistently at an increasing rate. The expression of TLR6 began to rise at 2 hpi with 39YC, and its rate of increase fell 20–22 hpi at a consistent and progressive rate. Similarly, the expression of TLR1 and TLR2 began to rise at 12 hpi with PG45. TLR1 expression fell at a steady increasing rate from 22 to 24 hpi, and TLR2 expression fell at a steady but increasing rate at 18–24 hpi. The expression of TLR6 began to rise at 2 hpi with PG45 and reached its peak at 16 hpi, after which the ascent rate fell until 24 hpi. The expression of TLR1 and TLR2 began to rise at 4 hpi with HB0801 and reached its peak at 20 hpi. TLR6 began to rise at 2 hpi with HB0801, after which it remained upregulated. Similar trends were observed between TLR1/TLR2, and TLR2/TLR6, so immunoprecipitation was used to verify the hypothesis that there was an interaction between TLR1/TLR2 and TLR2/TLR6. This showed that the gray values of TLR1 and TLR6 in the 39YC, PG45, and HB0801 groups were higher than that of the control and LPS groups (**Figure 4B**), which indicated that TLR1 or TLR6 can combine with TLR2 to recognize the different strains of *M. bovis* after BMECs were infected by *M. bovis*.

## Changes of Inflammatory Signaling Pathways in BMECs Induced by *M. bovis*

To detect changes in the cascade signaling pathway molecules of TLRs after *M. bovis* infection, we surveyed the relative temporal expression of MyD88, TRIF, and IRF3 using qRT-PCR analysis. The expression of TRIF in the 39YC group (**Figure 5A**) increased significantly at 10 hpi. The expression of TRIF in the PG45 and HB0801 groups increased significantly at 16 hpi (**Figure 5B**). Compared with the control group, the expression of TRIF in the 39YC group (**Figure 5C**) increased significantly ($P < 0.001$), and IRF3 expression levels in the 39YC, PG45, and HB0801 groups increased at 20 hpi ($P < 0.001$). The levels of TRIF in the 39YC and PG45 groups, and IRF3 in the PG45 group (**Figure 5D**)

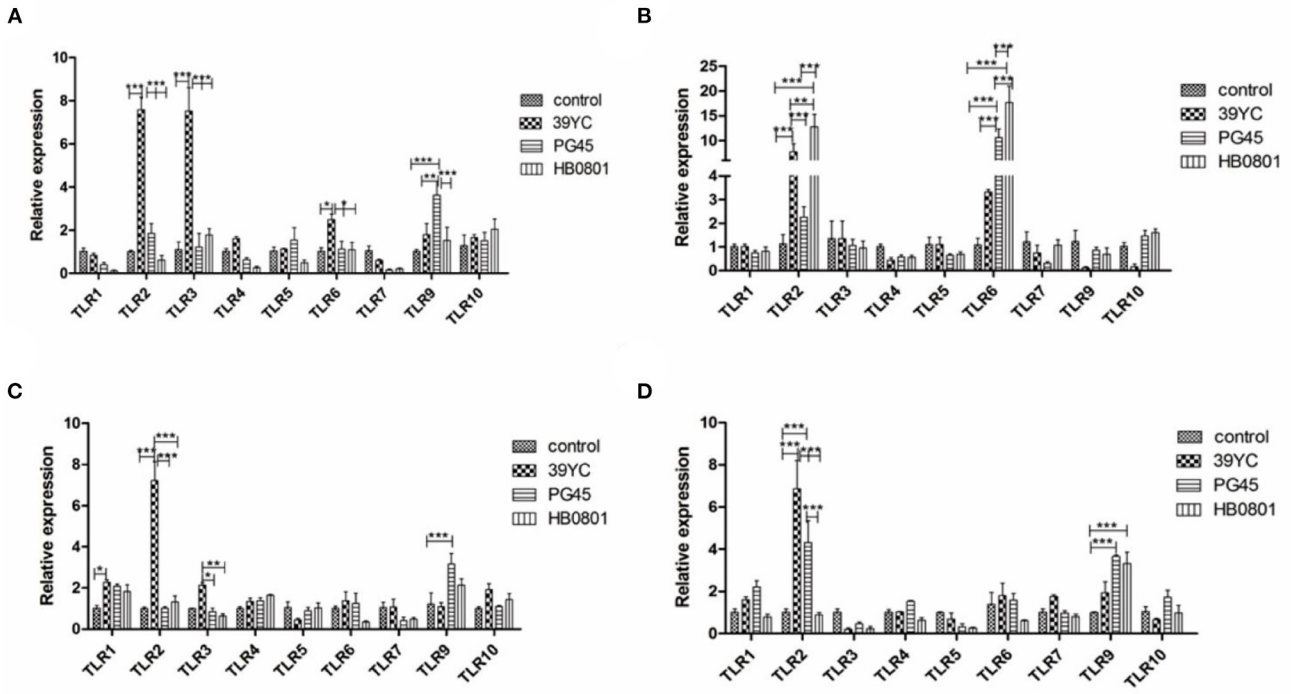


**FIGURE 2 |** *M. bovis* activated TLRs expression in BMECs. TLRs expression on BMECs induced by *M. bovis* at different time, **(A)** 10 h post-infection (hpi), **(B)** 16 hpi, **(C)** 20 hpi, **(D)** 24 hpi. $^{*}p < 0.05$, $^{**}p < 0.01$, and $^{***}p < 0.001$.

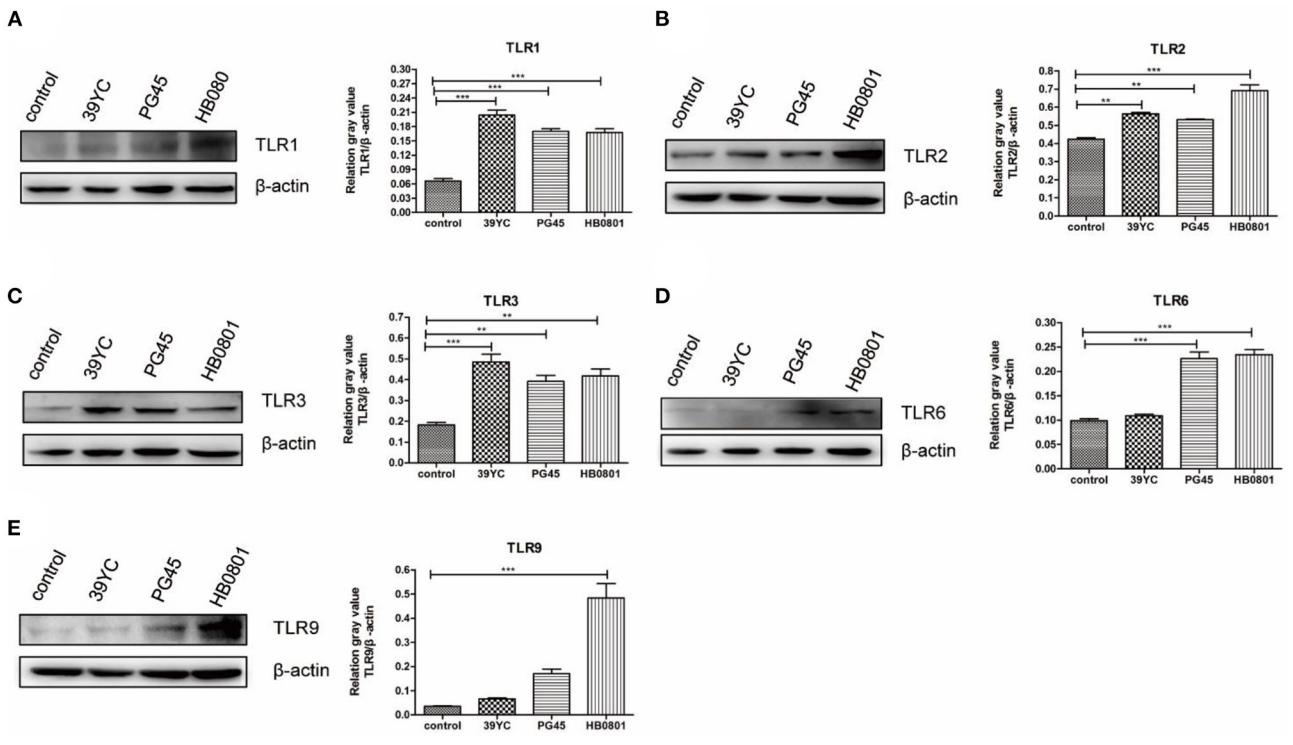


**FIGURE 3 |** *M. bovis* activated TLRs expression in BMECs. **(A–E)** The protein expression of TLR1, TLR2, TLR3, TLR6, and TLR9 from BMECs infected by *M. bovis,* **(A)** 20 h post-infection (hpi), **(B–D)** 16 hpi, **(E)** 20 hpi. $^{**}p < 0.01$, and $^{***}p < 0.001$.

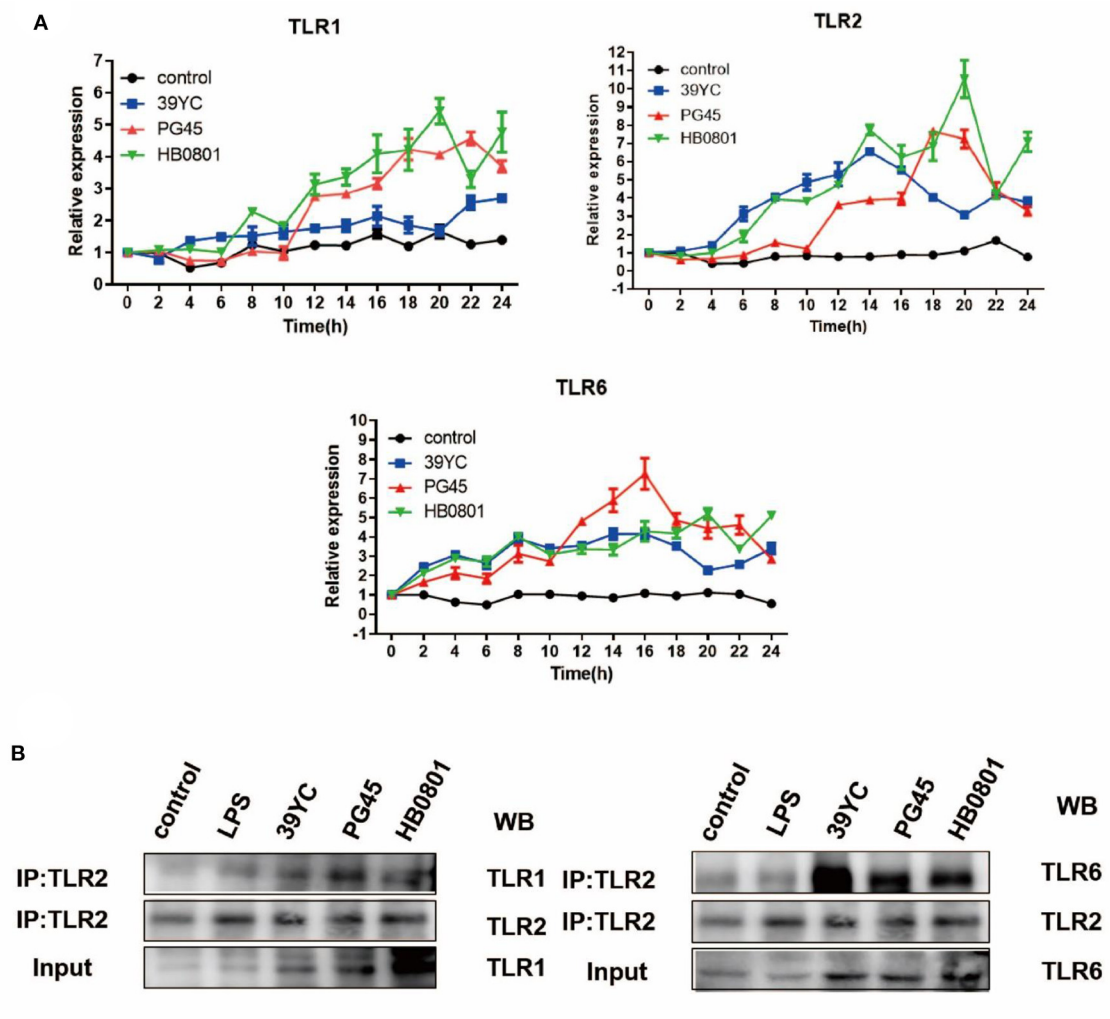


**FIGURE 4 |** Roles of TLR1/2/6 in BMECs induced by *M. bovis*. **(A)** Time-dependent mRNA expression of TLR1, TLR2, and TLR6 after BMECs infected by *M. bovis*, **(B)** Co-IP for TLR1/TLR2, TLR2/TLR6 after BMECs infected by *M. bovis*.

were higher than the control group at 24 hpi ($P < 0.001$). Regarding signaling pathways, the signaling molecules activated downstream of TLRs (NF-κB, TLR4) were analyzed using Western blot after BMECs were co-cultured with *M. bovis* for 20 h (**Figure 5E**). The results indicated that p-p65 protein levels were markedly increased in the PG45 and HB0801 groups compared with controls (**Figure 5F**). Moreover, phosphorylation of IκBα protein levels was also obviously reduced in the PG45, HB0801, and 39YC groups than the control group, representing the activation of the NF-κB signaling pathway. In addition, the phosphorylation levels of c-jun were increased in three groups, especially in the PG45 and HB0801 groups. To further investigate the role of the NF-κB pathway in mastitis, we used PDTC to treat with BMECs, an NF-κB inhibitor. The expression of IL-6 and TNF-α was markedly decreased after treatment with PDTC (**Figures 5G,H**). However, the expression of IL-8 was decreased only in the HB0801 group after treatment with PDTC (**Figure 5I**).

## DISCUSSION

As a functional part of mammary immunity, BMECs can present certain immunogenic pathogens after infection (21, 22). Our experiment showed that three strains of *M. bovis* did not impair the viability of BMECs within 24 h of infection at MOIs of 500 and 1,000. Beyond that, the changes of inflammatory factors at different time points also found that the expression of IL-6, TNF-α, and IL-8 was increased in BMECs after *M. bovis* infection and showed a change dependent on infection time and MOIs. This confirms the establishment of a stable *in vitro* BMECs inflammation model of *M. bovis*.

The expression of IL-6, a major immune and inflammatory mediator, and the IL-6 level in our experiment began to increase at 4 h post-infection (hpi). While the expression level of IL-6 was increased at 24 hpi, and it participated in the post-infection reaction, there was no increase in the early stage in Liu's

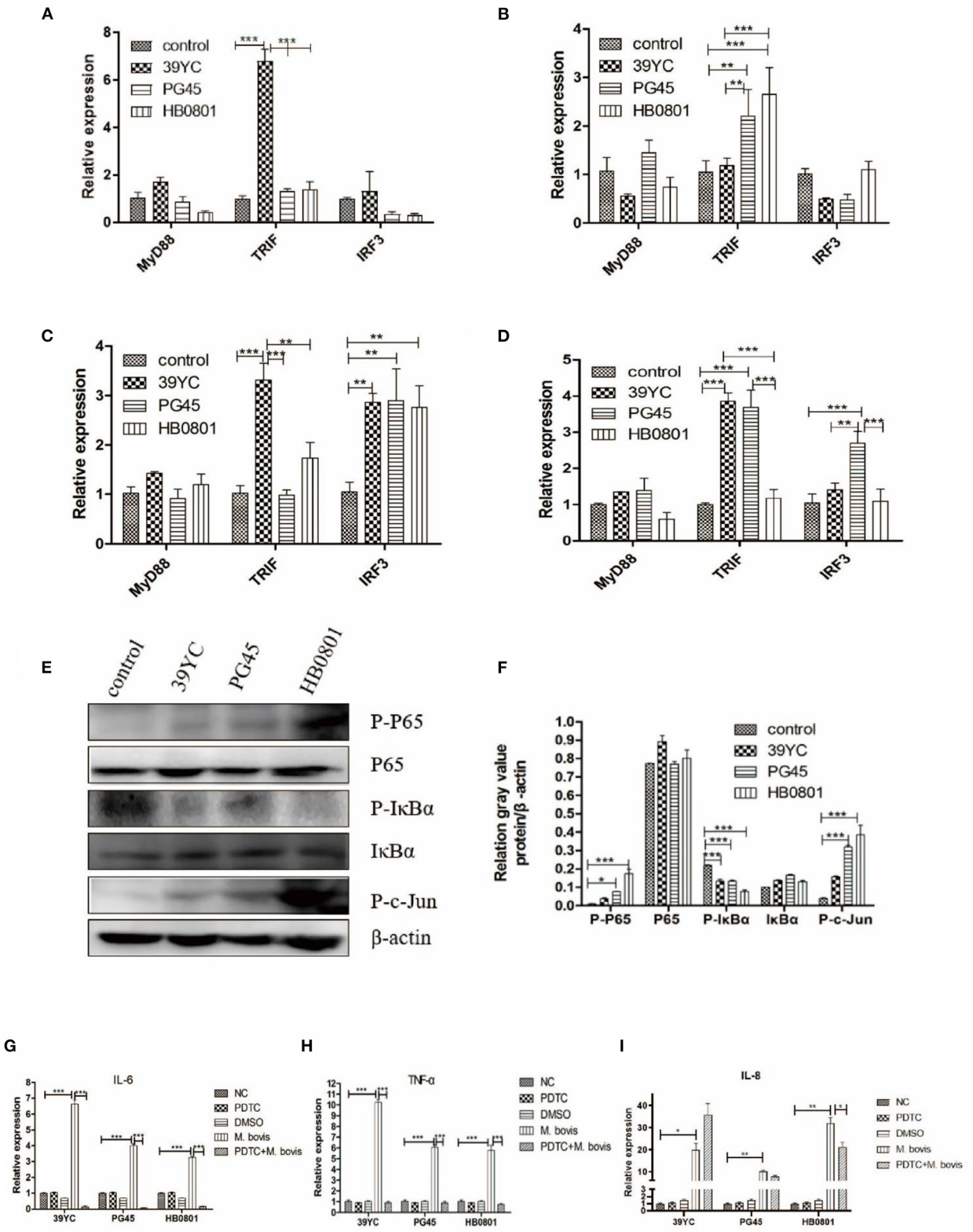


**FIGURE 5 |** Changes of inflammatory signaling pathways in BMECs induced by *M. bovis.* **(A–D)** Related factors expression of BMECs infected with *M. bovis* at different time points, **(A)** 10 h post-infection (hpi), **(B)** 16 hpi, **(C)** 20 hpi, **(D)** 24 hpi. Proteins expression of TLRs from BMECs infected by *M. bovis*, **(E)** Western Blot, **(F)** gray value analysis. Expression of IL-6, TNF-α, and IL-8 after BMECs infected by *M. bovis* and NF-κB inhibited by PDTC of qRT-PCR, **(G)** IL-6, **(H)** TNF-α, **(I)** IL-8. $^{*}p < 0.05$, $^{**}p < 0.01$, and $^{***}p < 0.001$.

study (23). This might be due to the diverse types and culture methods of both the *M. bovis* and BMECs cell lines, which can lead to differences in the virulence of *M. bovis* and the characteristics of the BMECs. TNF-α not only promoted the release of IL-8 (24), but also had the ability to activate NF-κB (25). As TNF-α is a known key inflammatory factor, and the increase of TNF-α expression following exposure to all three *M. bovis* strains confirms their pro-inflammatory effects on BMECs. IL-8 is a chemokine that recruits neutrophils to swarm to sites of infection with multiple pathogens (26). IL-8 secretion increased after *M. bovis* infection (27). All three *M. bovis* strains promoted IL-8 overexpression in the present work, an observation consistent with the findings of Zbinden et al. (28) in their own study of the BMEC immune response to *M. bovis* infection.

TLRs are pattern recognition protein receptors, and they are expressed by many immune and epithelial cells (29, 30). TLR1-10 can be expressed by bovine tissues, but the expression and distribution of TLRs differs between different tissues and cells (31). We showed here that the expression levels of TLR1, TLR2, and TLR6 increased after BMECs were infected with *M. bovis*. It is well-known that TLR1, TLR2, and TLR6 can recognize *Mycoplasma* to initiate innate immunity. The expression levels of TLR3 and TLR9 increased in this study, indicating that *M. bovis* contained some components that could be recognized by TLR3 and TLR9.

To identify the roles of TLR1/2, and TLR2/6 in BMECs in response to *M. bovis*, we measured the changes in TLRs expression at different time points after *M. bovis* infection. TLR2 forms dimers with TLR1 and TLR6 to resist the invasion of *Mycoplasma* (32). The results of the co-immunoprecipitation experiment showed TLR1 and TLR6 were better able to bind to a TLR2 primary antibody following infection with three strains of *M. bovis* compared with controls, which indicated that there was a crosstalk between TLR1/TLR2 and TLR2/TLR6. However, it remains to be further demonstrated whether dimers are formed between TLR-TLR2 and TLR2-TLR6.

Inflammatory signaling pathways are crucial to the pathogenesis of mastitis. Our experiment showed that the expression of both TRIF and downstream IRF3 was increased. The phosphorylation of IκBα protein decreased in the present work, indicating that the NF-κB signaling pathway was activated. JNK is an important member of the MAPK signaling pathway, which requires the phosphorylation of JNK to be activated. This study found that the expression of P-c-Jun protein increased after *M. bovis* infection, indicating that the activation of TLRs promoted MAPK activation. PDTC can inhibit the activation of NF-κB by inhibiting the phosphorylation process (33–36). Cell viability was not affected by 50 μM PDTC in the present work. The expression of IL-6 and TNF-α increased after BMECs were infected with *M. bovis*, then decreased after PDTC intervention,

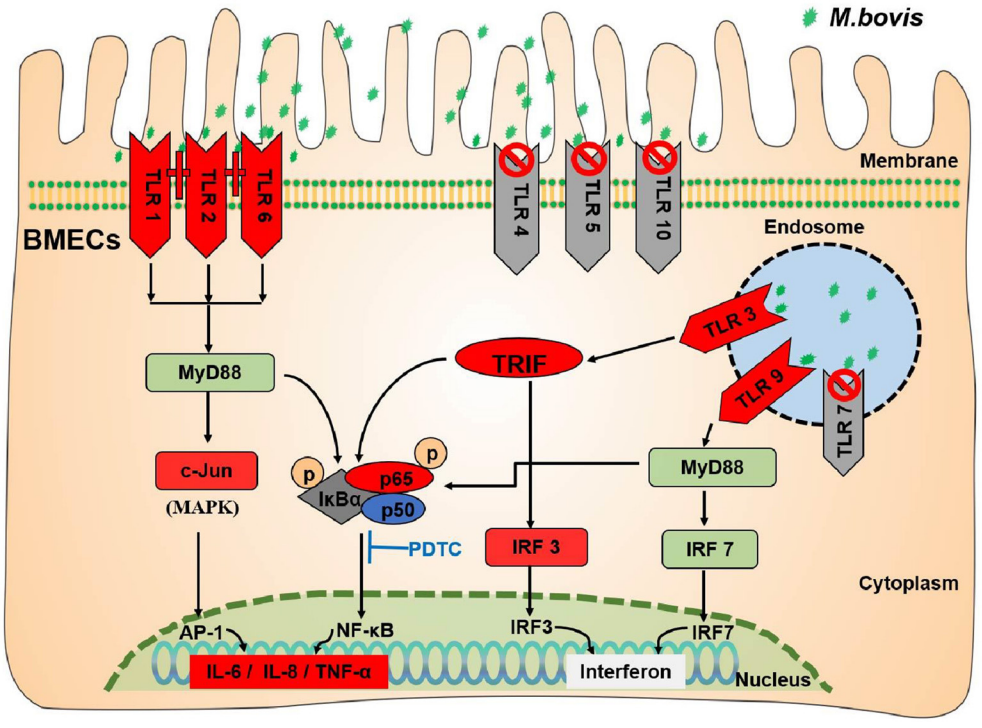


**FIGURE 6 |** TLRs signaling pathway induced by *M. bovis* infected BMECs. The green stars indicate *M. bovis*. The red (TLR1/2/6/3/9; TRIF/IRF3/c-Jun/P-P65; IL-6/IL-8/TNF-α) in the figure indicates that the expression level increased. The gray (TLR4/5/10/7) indicates that they have no effect during *M. bovis* infection. The dark gray (P-IκBα) indicates that expression decreased during *M. bovis* infection.

indicating that the expression of these inflammatory factors was associated with the NF-κB. It also indirectly explained the role of TLRs. However, the expression of IL-8 was decreased only in the HB0801 group after treatment with PDTC, increasing in the 39YC group and remaining equivocal in the PG45 group than controls. The different expression trends of IL-8 between *M. bovis* strains may represent differences in their pathogenic mechanisms. The reason for the increased IL-8 level in the 39YC group after PDTC treatment may be that *M. bovis* can regulate the secretion of IL-8 through multiple pathways (37). Other signaling pathways may also be triggered by 39YC, which dominates the regulation of IL-8 in BMECs alongside NF-κB. The specific mechanisms underlying these effects require further study. This study did have some limitations. For instance, which TLRs are related to breast lactation function and inflammation still needs to be explored in future experiments. The innate immunity NLRs caused by *M. bovis* also require further study.

## CONCLUSION

This study clearly shows that *M. bovis* infection initiates the innate immune-TLRs signaling pathway of BMECs (**Figure 6**). *M. bovis* activated TLR1, TLR2, and TLR6 on the BMECs membrane surface and TLR3 and TLR9 pattern recognition receptors in their cytoplasm. TLR2 could combine with TLR1 or TLR6 to initiate immunity. The infectious signal was transmitted downward through the action of the adaptor proteins MyD88 and TRIF, activating the inflammatory signal pathways of NF-κB and MAPK, and increasing the expression of IL-6, TNF-α, IL-8, and interferon IRF3.

## DATA AVAILABILITY STATEMENT

The original contributions presented in the study are included in the article/**Supplementary Material**, further inquiries can be directed to the corresponding author.

## AUTHOR CONTRIBUTIONS

JY and CH wrote the manuscript. YL performed the literature retrieval, designed and conducted experiments, and analyzed data. CL, RY, ZL, HX, QC, and HZ performed the literature retrieval. XC, YC, AG, and CH designed the experiments and revised the manuscript. All authors contributed to the article and approved the submitted version.

## FUNDING

This research was funded by the National Natural Science Foundation of China (Nos. 31972758 and 31101874), the special fund for the China Agriculture Research System (Beef/Yak cattle) (No. CARS-37), Key R&D Program of Hubei Province of China (No. 2020BBA055), and the Fundamental Research Funds for the Central Universities (No. 2662020DKPY014).

## ACKNOWLEDGMENTS

We thank State Key Laboratory of Agricultural Microbiology of Huazhong Agricultural University for providing a platform to conduct this study.

## SUPPLEMENTARY MATERIAL

The Supplementary Material for this article can be found online at: https://www.frontiersin.org/articles/10.3389/fvets.2022.846700/full#supplementary-material

## REFERENCES

1. Hoekstra J, Zomer AL, Rutten VPMG, Benedictus L, Stegeman A, Spaninks MP, et al. Genomic analysis of European bovine *Staphylococcus aureus* from clinical versus subclinical mastitis. *Sci Rep.* (2020) 10:18172. doi: 10.1038/s41598-020-75179-2
2. Song W, Sheng L, Chen F, Tian Y, Li L, Wang G, et al. *C.sakazakii* activates AIM2 pathway accompanying with excessive ER stress response in mammalian mammary gland epithelium. *Cell Stress Chaperones.* (2020) 25:223–33. doi: 10.1007/s12192-019-01065-0
3. Maunsell FP, Woolums AR, Francoz D, Rosenbusch RF, Step DL, Wilson DJ, et al. *Mycoplasma bovis* infections in cattle. *J Vet Intern Med.* (2011) 25:772–83. doi: 10.1111/j.1939-1676.2011.0750.x
4. He J, Liu M, Ye Z, Tan T, Liu X, You X, et al. Insights into the pathogenesis of *Mycoplasma pneumoniae* (Review). *Mol Med Rep.* (2016) 14:4030–6. doi: 10.3892/mmr.2016.5765
5. Hu X, Yu J, Zhou X, Li Z, Xia Y, Luo Z, et al. Synergism between upregulation of Rab7 and inhibition of autophagic degradation caused by *Mycoplasma* facilitates intracellular *Mycoplasma* infection. *Mol Med Rep.* (2014) 9:793–800. doi: 10.3892/mmr.2014.1907
6. You XX, Zeng YH, Wu YM. Interactions between *Mycoplasma* lipid-associated membrane proteins and the host cells. *J Zhejiang Univ Sci B.* (2006) 7:342–50. doi: 10.1631/jzus.2006.B0342
7. Shimizu T, Kida Y, Kuwano K. Ureaplasma parvum lipoproteins, including MB antigen, activate NF-{kappa}B through TLR1, TLR2 and TLR6. *Microbiology.* (2008) 154:1318–25. doi: 10.1099/mic.0.2007/016212-0
8. Lysnyansky I, Ron Y, Yogev D. Juxtaposition of an active promoter to vsp genes via site-specific DNA inversions generates antigenic variation in *Mycoplasma bovis*. *J Bacteriol.* (2001) 183:5698–708. doi: 10.1128/JB.183.19.5698-5708.2001
9. Li C, Lu L, Qi Z, Zhu Y, Su F, Zhao P, et al. Transcriptome and miRNome analysis provide new insight into host lipid accumulation, innate immunity, and viral persistence in hepatitis C virus infection *in vitro*. *Front Microbiol.* (2020) 11:535673. doi: 10.3389/fmicb.2020.535673
10. Lai JL, Liu YH, Liu C, Qi MP, Liu RN, Zhu XF, et al. Indirubin inhibits lps-induced inflammation via TLR4 abrogation mediated by the NF-κB and MAPK signaling pathways. *Inflammation.* (2017) 40:1–12. doi: 10.1007/s10753-016-0447-7
11. Lin C, Zhu Y, Hao Z, Xu H, Li T, Yang J, et al. Genome-wide analysis of lncRNA in bovine mammary epithelial cell injuries induced by *Escherichia coli* and *Staphylococcus aureus*. *Int J Mol Sci.* (2021) 22:9719. doi: 10.3390/ijms22189719
12. Tang X, Liu C, Li T, Lin C, Hao Z, Zhang H, et al. Gambogic acid alleviates inflammation and apoptosis and protects the blood-milk barrier in mastitis induced by lps. *Int Immunopharmacol.* (2020) 86:106697. doi: 10.1016/j.intimp.2020.106697

13. Liu C, Tang X, Zhang W, Li G, Chen Y, Guo A, et al. 6-Bromoindirubin-3'-Oxime suppresses lps-induced inflammation via inhibition of the TLR4/NF-κB and TLR4/MAPK signaling pathways. *Inflammation*. (2019) 42:2192–204. doi: 10.1007/s10753-019-01083-1
14. Takeda Y, Azuma M, Funami K, Shime H, Matsumoto M, Seya T. Type I interferon-independent dendritic cell priming and antitumor T cell activation induced by a *Mycoplasma* fermentans lipopeptide. *Front Immunol.* (2018) 9:496. doi: 10.3389/fimmu.2018.00496
15. Méndez-Samperio P, Belmont L, Miranda E. *Mycobacterium bovis* BCG Toll-like receptors 2 and 4 cooperation increases the innate epithelial immune response. *Arch Med Res.* (2008) 39:33–9. doi: 10.1016/j.arcmed.2007.06.019
16. Chambers MA, Whelan AO, Spallek R, Singh M, Coddeville B, Guerardel Y, et al. Non-acylated *Mycobacterium bovis* glycoprotein MPB83 binds to TLR1/2 and stimulates production of matrix metalloproteinase 9. *Biochem Biophys Res Commun.* (2010) 400:403–8. doi: 10.1016/j.bbrc.2010.08.085
17. Qi J, Guo A, Cui P, Chen Y, Mustafa R, Ba X, et al. Comparative geno-plasticity analysis of *Mycoplasma bovis* HB0801 (Chinese isolate). *PLoS ONE.* (2012) 7:e38239. doi: 10.1371/journal.pone.0038239
18. Zhang H, Zhao G, Guo Y, Menghwar H, Chen Y, Chen H, et al. *Mycoplasma bovis* MBOV_RS02825 encodes a secretory nuclease associated with cytotoxicity. *Int J Mol Sci.* (2016) 17:628. doi: 10.3390/ijms17050628
19. Gondaira S, Higuchi H, Iwano H, Nishi K, Nebu T, Nakajima K, et al. Innate immune response of bovine mammary epithelial cells to *Mycoplasma bovis*. *J Vet Sci.* (2018) 19:79–87. doi: 10.4142/jvs.2018.19.1.79
20. Strandberg Y, Gray C, Vuocolo T, Donaldson L, Broadway M, Tellam R. Lipopolysaccharide and lipoteichoic acid induce different innate immune responses in bovine mammary epithelial cells. *Cytokine.* (2005) 31:72–86. doi: 10.1016/j.cyto.2005.02.010
21. Huang Y, Shen L, Jiang J, Xu Q, Luo Z, Luo Q, et al. Metabolomic profiles of bovine mammary epithelial cells stimulated by lipopolysaccharide. *Sci Rep.* (2019) 9:19131. doi: 10.1038/s41598-019-55556-2
22. Wellnitz O, Kerr DE. Cryopreserved bovine mammary cells to model epithelial response to infection. *Vet Immunol Immunopathol.* (2004) 101:191–202. doi: 10.1016/j.vetimm.2004.04.019
23. Liu Y, Zhou M, Xu S, Khan MA, Shi Y, Qu W, et al. *Mycoplasma bovis*-generated reactive oxygen species and induced apoptosis in bovine mammary epithelial cell cultures. *J Dairy Sci.* (2020) 103:10429–45. doi: 10.3168/jds.2020-18599
24. Hasan A, Akhter N, Al-Roub A, Thomas R, Kochumon S, Wilson A, et al. TNF-α in combination with palmitate enhances IL-8 production via the MyD88- independent TLR4 signaling pathway: potential relevance to metabolic inflammation. *Int J Mol Sci.* (2019) 20:4112. doi: 10.3390/ijms20174112
25. Van Quickelberghe E, De Sutter D, Van Loo G, Eyckerman S, Gevaert K. A protein-protein interaction map of the TNF-induced NF-κB signal transduction pathway. *Sci Data.* (2018) 5:180289. doi: 10.1038/sdata.2018.289
26. Gonzalez-Aparicio M, Alfaro C. Influence of interleukin-8 and neutrophil extracellular trap (NET) formation in the tumor microenvironment: is there a pathogenic role? *J Immunol Res.* (2019) 2019:6252138. doi: 10.1155/2019/6252138
27. Shirani I, Zhang H, Zhao G, Lu S, Marawan MA, Dawood A, et al. In silico identification of novel immunogenic secreted proteins of *Mycoplasma bovis* from secretome data and experimental verification. *Pathogens.* (2020) 9:770. doi: 10.3390/pathogens9090770
28. Zbinden C, Pilo P, Frey J, Bruckmaier RM, Wellnitz O. The immune response of bovine mammary epithelial cells to live or heat-inactivated *Mycoplasma bovis*. *Vet Microbiol.* (2015) 179:336–40. doi: 10.1016/j.vetmic.2015.07.007
29. Price AE, Shamardani K, Lugo KA, Deguine J, Roberts AW, Lee BL, et al. A map of toll-like receptor expression in the intestinal epithelium reveals distinct spatial, cell type-specific, and temporal patterns. *Immunity.* (2018) 49:560–75. doi: 10.1016/j.immuni.2018.07.016
30. Li L, Acioglu C, Heary RF, Elkabes S. Role of astroglial toll-like receptors (TLRs) in central nervous system infections, injury and neurodegenerative diseases. *Brain Behav Immun.* (2021) 91:740–55. doi: 10.1016/j.bbi.2020.10.007
31. Opsal MA, Våge DI, Hayes B, Berget I, Lien S. Genomic organization and transcript profiling of the bovine toll-like receptor gene cluster TLR6-TLR1-TLR10. *Gene.* (2006) 384:45–50. doi: 10.1016/j.gene.2006.06.027
32. Love W, Dobbs N, Tabor L, Simecka JW. Toll-like receptor 2 (TLR2) plays a major role in innate resistance in the lung against murine *Mycoplasma*. *PLoS ONE.* (2010) 5:e10739. doi: 10.1371/journal.pone.0010739
33. Wang HT, Fang YQ, You P, Bao XC, Li KC, Yao J, et al. PDTC ameliorates decompression induced-lung injury caused by unsafe fast buoyancy ascent escape via inhibition of NF-κB pathway. *Undersea Hyperb Med.* (2018) 45:351–62. doi: 10.22462/05.06.2018.10
34. Guo F, Tang C, Li Y, Liu Y, Lv P, Wang W, et al. The interplay of lncRNA ANRIL and miR-181b on the inflammation-relevant coronary artery disease through mediating NF-κB signalling pathway. *J Cell Mol Med.* (2018) 22:5062–75. doi: 10.1111/jcmm.13790
35. Zhang HM, Sang XG, Wang YZ, Cui C, Zhang L, Ji WS. Role of Δ133p53 isoform in NF-κB inhibitor PDTC-mediated growth inhibition of MKN45 gastric cancer cells. *World J Gastroenterol.* (2017) 23:2716–22. doi: 10.3748/wjg.v23.i15.2716
36. Jiang JY, Liu DJ, Liu MX. The protective effect of NF-κB signaling pathway inhibitor PDTC on mice with chronic atrophic gastritis. *Scand J Gastroenterol.* (2021) 56:1131–39. doi: 10.1080/00365521.2021.1953130
37. Martínez-Neri PA, López-Rincón G, Mancilla-Jiménez R, del Toro-Arreola S, Muñoz-Valle JF, Fafutis-Morris M, et al. Prolactin modulates cytokine production induced by culture filtrate proteins of M. bovis through different signaling mechanisms in THP1 cells. *Cytokine.* (2015) 71:38–44. doi: 10.1016/j.cyto.2014.08.006


**Conflict of Interest:** The authors declare that the research was conducted in the absence of any commercial or financial relationships that could be construed as a potential conflict of interest.

frontiers | Frontiers in Veterinary Science

ORIGINAL RESEARCH
published: 12 May 2022
doi: 10.3389/fvets.2022.824785

# Genetic Characterization and Phylogenetic Analysis of Fasciola Species Isolated From Yaks on Qinghai-Tibet Plateau, China

*Xing Gao[1†], Dongjing Wang[2,3†], Zhao Zhang[1], Chuxian Quan[1], Shimeng Zhou[1], Kewei Li[1], Yan Li[1], Suonan Zhao[4], Xiangying Kong[4], Muhammad Fakhar-e-Alam Kulyar[1], Jiangyong Zeng[2,3*] and Jiakui Li[1,5*]*

[1] College of Veterinary Medicine, Huazhong Agricultural University, Wuhan, China, [2] Tibet Livestock Research Institute, Tibet Academy of Agricultural and Animal Husbandry Sciences, Lhasa, China, [3] State Key Laboratory of Hulless Barley and Yak Germplasm Resources and Genetic Improvement, Lhasa, China, [4] Haibei Agricultural and Animal Husbandry Sciences Institute, Haibei, China, [5] College of Animals Husbandry and Veterinary Medicine, Tibet Agricultural and Animal Husbandry University, Linzhi, China

OPEN ACCESS

**Edited by:**
Yung-Fu Chang,
Cornell University, United States

**Reviewed by:**
Quan Liu,
Foshan University, China
Agusto R. Luzuriaga Neira,
University of Nevada, United States

***Correspondence:**
Jiangyong Zeng
zengjiangyong@hotmail.com
Jiakui Li
lijk210@sina.com

[†]These authors have contributed equally to this work and share first authorship

**Specialty section:**
This article was submitted to Animal Nutrition and Metabolism, a section of the journal Frontiers in Veterinary Science

**Received:** 29 November 2021
**Accepted:** 22 February 2022
**Published:** 12 May 2022

**Citation:**
Gao X, Wang D, Zhang Z, Quan C, Zhou S, Li K, Li Y, Zhao S, Kong X, Kulyar MF, Zeng J and Li J (2022) Genetic Characterization and Phylogenetic Analysis of Fasciola Species Isolated From Yaks on Qinghai-Tibet Plateau, China. Front. Vet. Sci. 9:824785. doi: 10.3389/fvets.2022.824785

The present study determined the complete mitochondrial DNA (mt DNA) sequence of *Fasciola intermediate* (isolated from yaks) based on gene content and genome organization. According to our findings, the genome of *Fasciola intermediate* was 13,960 bp in length, containing 2 ribosomal RNA (rRNA) genes, 12 protein-coding genes (PCGs), and 22 transfer RNA (tRNA) genes. The A+T content of genomes was 63.19%, with A (15.17%), C (9.31%), G (27.51%), and T as the nucleotide composition (48.02%). Meanwhile, the results showed negative AT-skew (-0.52) and positive GC-skew (0.494). The AT bias significantly affected both the codon usage pattern and amino acid composition of proteins. There were 2715 codons in all 12 protein-coding genes, excluding termination codons. Leu (16.72%) was the most often used amino acid, followed by Val (12.74%), Phe (10.90%), Ser (10.09%), and Gly (8.39%). A phylogenetic tree was built using Maximum-Likelihood (ML) through MEGA 11.0 software. The entire mt DNA sequence of *Fasciola intermediate* gave more genetic markers for investigating Trematoda population genetics, systematics, and phylogeography. Hence, for the first time, our study confirmed that yaks on the Qinghai-Tibet plateau have the infestation of *Fasciola intermediate* parasite.

**Keywords: yaks, *Fasciola intermediate*, mitogenome, gene order, phylogenetic**

## INTRODUCTION

Yak is a unique bovine specie on the Qinghai-Tibet plateau, China. The Qinghai-Tibet plateau is home to around 14 million yaks (a small amount of distribution in India, Bhutan, Sikkim, Afghanistan and Pakistan) (1). The yaks are necessary for herders in this area because of their milk, wool, and meat (2). Fasciolosis is one of the most important parasitic zoonotic issue, mainly

caused by *Fasciola hepatica* (*F. hepatica*), *Fasciola gigantica* (*F. gigantica*) (3, 4). The infection occurs mostly through the oral route (5), causing emaciation, fever, hepatomegaly, cholangitis, and jaundice, and even death (5). Approximately 2.4 million humans and more than 600 million animals are infected per year, causing serious public health threats and considerable economic loss to the livestock industry (6, 7).

The sequence of mitochondrial DNA (mt DNA) is an extrachromosomal genome, commonly used as an informative genetic marker for various evolutionary studies among species due to the maternal inheritance. It includes molecular evolution, comparative population genetics, phylogenetics, and evolutionary genomics (8, 9). In most parasites, mitogenomes are ∼13 kilobases (Kb) in size as closed circular molecules (10). The mt DNA contains 36 genes, including 12 protein coding genes (PCGs) (subunits 6 of the ATPase (*atp6*), cytochrome B (*cob*), cytochrome c oxidase subunits 1–3 (*cox1–cox3*), NADH dehydrogenase subunits 1–6 and 4 L (*nad1–6* and *nad4L*), two ribosomal RNA genes encoding the small and large subunit rRNAs (*rrnL* and *rrnS*), 22 transfer RNA (tRNA) genes and a control region (CR) of variable length, known as the A+T-rich region (11, 12).

**TABLE 1 |** Position and nucleotide sequence lengths of mitochondrial genomes of *F. intermediate*, and start and stop codons for protein-coding genes as well as their tRNA gene anticodons.

| Feature | Strand | Position | Length (bp) | Initiation codon | Stop codon | Anticodon | Intergenic nucleotide |
|---|---|---|---|---|---|---|---|
| cox3 | N | 231–633 | 403 | ATG | TAA | - | 15 |
| trnH | N | 649–713 | 65 | - | - | GTG | 0 |
| cob | N | 714–1770 | 1,057 | ATA | T | - | 64 |
| nad4l | N | 1,835–2,099 | 265 | ATG | TAA | - | 133 |
| nad4 | N | 2,233–3,172 | 940 | TAG | TAA | - | 165 |
| trnQ | N | 3,338–3,404 | 67 | - | - | TTG | 11 |
| trnF | N | 3,416–3,482 | 67 | - | - | GAA | 4 |
| trnM | N | 3,487–3,553 | 67 | - | - | CAT | 47 |
| atp6 | N | 3,601–4,054 | 454 | ATC | TAA | - | 62 |
| nad2 | N | 4,117–4,624 | 508 | ATT | TAA | - | 331 |
| trnV | N | 4,956–5,020 | 65 | - | - | TAC | 13 |
| trnA | N | 5,034–5,099 | 66 | - | - | TGC | 2 |
| trnD | N | 5,102–5,167 | 66 | - | - | GTC | 65 |
| nad1 | N | 5,233–6028 | 796 | ATT | TAG | - | 54 |
| trnN | N | 6,083–6,153 | 71 | - | - | GTT | 8 |
| trnP | N | 6,162–6,230 | 69 | - | - | TGG | −2 |
| trnI | N | 6,229–6,293 | 65 | - | - | GAT | 2 |
| trnK | N | 6,296–6,363 | 68 | - | - | CTT | −1 |
| nad3 | N | 6,363–6,711 | 349 | ATA | TAG | - | 12 |
| trnS1 | N | 6,724–6,780 | 57 | - | - | GCT | 8 |
| trnW | N | 6,789–6,852 | 64 | - | - | TCA | 2 |
| cox1 | N | 6,855–8,310 | 1,456 | ATG | TAA | - | 98 |
| trnT | N | 8,409–8,477 | 69 | - | - | TGT | 441 |
| rrnL | N | 8,919–9,446 | 528 | - | - | - | 15 |
| trnC | N | 9,462–9,532 | 71 | - | - | GCA | −3 |
| rrnS | N | 9,530–10,274 | 745 | - | - | - | 47 |
| cox2 | N | 10,322–10,910 | 589 | ATG | TAA | - | 36 |
| nad6 | N | 10,947–11,376 | 430 | ATA | TAA | - | 30 |
| trnY | N | 11,407–11,474 | 68 | - | - | GTA | −1 |
| trnL1 | N | 11,474–11,539 | 66 | - | - | TAG | −3 |
| trnS2 | N | 11,537–11,600 | 64 | - | - | TGA | 5 |
| trnL2 | N | 11,606–11,670 | 65 | - | - | TAA | 4 |
| trnR | N | 11,675–11,733 | 59 | - | - | TCG | 208 |
| nad5 | N | 11,942–12,854 | 913 | ATT | TAA | - | 468 |
| trnE | N | 13,323–13,391 | 69 | - | - | TTC | 175 |
| trnG | N | 13,567–13,631 | 65 | - | - | TCC | - |

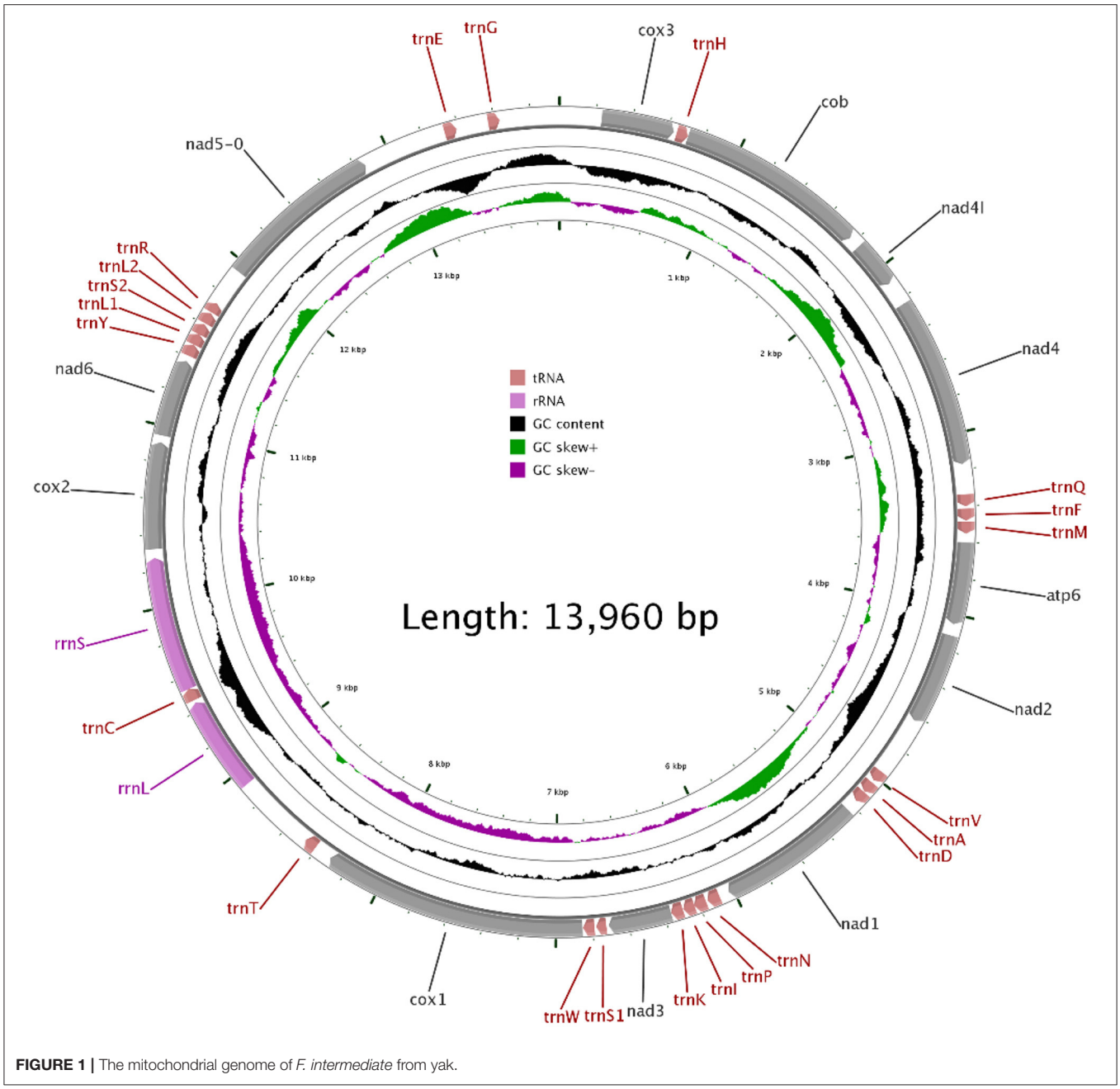


**FIGURE 1 |** The mitochondrial genome of *F. intermediate* from yak.

Previous research has identified the species of *Fasciola* in buffaloes and sheep, but not in yaks of the Qinghai-Tibet plateau. Therefore, in this study, the complete mitogenome of *F. intermediate* from yaks was initially sequenced and compared with other Trematoda mitogenomes (4). The available complete mitogenomes were used to provide insight into the phylogenetic relationship of *F. intermediate*. These findings would be valuable in order to have a better understanding of the *F. intermediate* mitogenome and the evolutionary relationships within Trematoda. The characteristics of *F. intermediate* mitogenome might be used to build appropriate genetic markers to detect Fasciola in yaks. This study might provide a basis for the accurate prevention, diagnosis, and treatment of Fasciolosis in yaks for studying the population genetic structure of *F. intermediate* in China.

## MATERIALS AND METHODS

### Samples and DNA Extraction

The *F. intermediate* samples used in this study were collected from the chopped liver of yaks (Xiahua slaughter house in Tibetan Autonomous Prefecture of Haibe, Qinghai Province, China). The samples were fixed in 75% alcohol and stored at −20°C until used for DNA extraction. Total genomic DNA was isolated by using TIANcombi DNA Lyse&Det PCR Kit [TIANGEN biotech (Beijing) Co., Ltd.].

**TABLE 2 |** Mitochondrial genome sequences of *F. intermediate*.

| Family | Taxon | Size (bp) | Accession number |
|---|---|---|---|
| Echinostomatidae | Echinostoma caproni 1 | 14,150 | AP017706.1 |
| Echinostomatidae | Hypoderaeum sp. | 14,180 | KM111525.1 |
| Echinostomatidae | Echinochasmus japonicus | 15,865 | KP844722.1 |
| Echinostomatidae | Echinostoma hortense | 15,048 | KR062182.2 |
| Echinostomatidae | Echinostoma paraensei | 20,298 | KT008005.1 |
| Echinostomatidae | Acanthoparyphium sp. | 14,191 | MG792058.1 |
| Echinostomatidae | Artyfechinostomum sufrartyfex | 14,567 | NC_037150.1 |
| Fasciolidae | Fasciola hepatica 1 | 14,462 | AF216697.1 |
| Fasciolidae | Fasciola hepatica 2 | 14,374 | AP017707.1 |
| Fasciolidae | Fasciola gigantica | 14,478 | KF543342.1 |
| Fasciolidae | Fasciola sp. | 14,453 | KF543343.1 |
| Fasciolidae | Fascioloides magna | 14,047 | KU060148.1 |
| Fasciolidae | Fasciolopsis buski | 14,833 | KX169163.1 |
| Fasciolidae | Fasciola jacksoni | 14,952 | KX787886.1 |
| Gastrodiscidae | Homalogaster paloniae 1 | 14,490 | KT266674.1 |
| Gastrodiscidae | Homalogaster paloniae 2 | 15,987 | KX169165.1 |
| Gastrothylacidae | Fischoederius elongatus | 14,120 | KM397348.1 |
| Gastrothylacidae | Gastrothylax crumenifer | 14,801 | KM400624.1 |
| Gastrothylacidae | Fischoederius cobboldi | 14,256 | KX169164.1 |
| Heterophyidae | Metagonimus yokogawai | 15,258 | KC330755.1 |
| Heterophyidae | Haplorchis taichui | 15,130 | KF214770.1 |
| Notocotylidae | Ogmocotyle sikae | 14,307 | KR006934.1 |
| Notocotylidae | Ogmocotyle sp. | 14,001 | KR006935.1 |
| Opisthorchiidae | Opisthorchis felineus | 14,277 | EU921260.2 |
| Opisthorchiidae | Metorchis orientalis | 13,834 | KT239342.1 |
| Paragonimidae | Paragonimus westermani 1 | 14,965 | AF219379.2 |
| Paragonimidae | Paragonimus westermani 2 | 14,244 | AF540958.1 |
| Paragonimidae | Paragonimus westermani complex 1 sp. | 14,103 | KM280646.1 |
| Paragonimidae | Paragonimus ohirai strain Kino | 14,818 | KX765277.1 |
| Paragonimidae | Paragonimus westermani 3 | 15,005 | KX943544.1 |
| Paramphistomatidae | Paramphistomum cervi 1 | 14,014 | KF475773.1 |
| Paramphistomatidae | Orthocoelium streptocoelium | 13,800 | KM659177.1 |
| Paramphistomatidae | Calicophoron microbothrioides | 14,028 | KR337555.1 |
| Paramphistomatidae | Paramphistomum cervi 2 | 14,023 | KT198987.1 |
| Paramphistomatidae | Explanatum explanatum | 13,968 | KT198989.1 |
| Schistosomatidae | Schistosoma mekongi | 14,072 | AF217449.1 |

## Gene Annotation and Sequence Analysis

DNA samples were randomly interrupted, the required length of DNA fragments were collected, the base "A" to 3′-end was added, DNA fragments and 3′-end were connected with "T" base special joint, and finally used for cluster preparation and sequencing.

The mitogenome of *F. intermediate* was sequenced by next-generation sequencing (NGS). Two lanes for *F. intermediate* were sequenced as 400 bp reads using Illumina MiSeq (1 GB raw). The raw data was saved by Paired-End FASTQ and generated high-quality sequences by using AdapterRemoval (version 2) and SOAPec (version 2.01) based on K-mer distribution (13).

A5-miseqv20150522 and SPAdesv3.9.0 were used to assemble high-quality second-generation sequencing data to construct contig and scaffold sequences (14, 15). Mitochondrial sequences of each splicing result were selected by Blastn (BLAST v2.2.31+), compared between the sequences with high sequencing depth and the NT library on NCBI. By mummerv3.1 software. The results of mitochondrial splicing were used for collinearity analysis. The location relationship was determined, and then gap between contig was filled (16).

The complete mitochondrial genome sequences of splicing were uploaded to MITOS web server (http://mitos.bioinf.uni-leipzig.de/) for functional annotation (17). The Genetic Code was set to 05-invertebrate; the rest was set as the default parameter by MITOS. The secondary structure of each predicted tRNA can be obtained in the MITOS web server. The complete genome circle map of mitochondria was drawn using CGview visualization software (18).

## Phylogenetic Analysis

The taxonomic status of *F. intermediate* with available Trematoda was estimated by reconstructing phylogenetic trees. The complete nucleotide sequences of 36 Trematoda and one outgroup are available at GenBank (https://www.ncbi.nlm.nih.gov/genbank/).

Nucleotide sequences of each gene and their deduced amino acid sequences were aligned separately by using https://www.novoprolabs.com/ and MEGA 11.0 (19). The phylogenetic tree was built using Maximum-Likelihood (ML) through MEGA 11.0 software. The genome information used in this study is shown in **Table 1**.

# RESULT AND DISCUSSION

## Genome Organization and Nucleotide Composition

In our study, the mitogenome of *F. intermediate* was a closed circular molecule of 13,960 bp in length (**Figure 1**). The mitogenome contained 36 typical mitochondrial genes [12 PCGs (cox1-3, nad1-6, nad4L, cob and atp6), 22 tRNAs, 2 rRNAs (rrnS and rrnL)] (**Table 2**). The mitogenome of *F. intermediate* had been submitted to the NCBI GenBank under the accession number MH621335.1. The nucleotide compositions of the mitogenome of *F. intermediate* were as follows: A =

**TABLE 3 |** Composition and skewness of *F. intermediate* mitogenome.

| Region | A% | C% | G% | T% | A+T% | G+C% | AT skew | GC skew |
|---|---|---|---|---|---|---|---|---|
| Whole genome | 15.17 | 9.31 | 27.51 | 48.02 | 63.19 | 36.82 | −0.52 | 0.494 |
| atp6 | 12.36 | 10.38 | 26.71 | 50.55 | 62.91 | 37.09 | −0.607 | 0.44 |
| cob | 14.58 | 8.81 | 27.08 | 49.53 | 64.11 | 35.89 | −0.545 | 0.509 |
| cox1 | 14.09 | 10.31 | 25.57 | 50.03 | 64.12 | 35.88 | −0.561 | 0.425 |
| cox2 | 20.75 | 10.03 | 27.38 | 41.84 | 62.59 | 37.41 | −0.337 | 0.464 |
| cox3 | 14.43 | 9.2 | 23.13 | 53.23 | 67.66 | 32.34 | −0.574 | 0.431 |
| nad1 | 13.33 | 7.55 | 30.44 | 48.68 | 62.01 | 37.99 | −0.57 | 0.603 |
| nad2 | 12.43 | 9.86 | 25.05 | 52.66 | 65.09 | 34.91 | −0.618 | 0.435 |
| nad3 | 12.36 | 8.05 | 26.44 | 53.16 | 65.52 | 34.48 | −0.623 | 0.533 |
| nad4 | 13.53 | 10.01 | 27.05 | 49.41 | 62.94 | 37.06 | −0.57 | 0.46 |
| nad41 | 13.64 | 4.92 | 29.17 | 52.27 | 65.91 | 34.09 | −0.586 | 0.711 |
| nad5-0 | 11.84 | 9.32 | 26.32 | 52.52 | 64.36 | 35.64 | −0.632 | 0.477 |
| nad6 | 11.42 | 9.79 | 26.34 | 52.45 | 63.87 | 36.13 | −0.642 | 0.458 |
| rrnL | 23.91 | 12.52 | 28.27 | 35.29 | 59.2 | 40.8 | −0.192 | 0.386 |
| rrnS | 21.91 | 12.37 | 26.75 | 38.98 | 60.89 | 39.11 | −0.28 | 0.368 |
| trnA | 16.92 | 13.85 | 30.77 | 38.46 | 55.38 | 44.62 | −0.389 | 0.379 |
| trnC | 20 | 17.14 | 27.14 | 35.71 | 55.71 | 44.29 | −0.282 | 0.226 |
| trnD | 16.92 | 10.77 | 29.23 | 43.08 | 60 | 40 | −0.436 | 0.462 |
| trnE | 19.12 | 10.29 | 23.53 | 47.06 | 66.18 | 33.82 | −0.422 | 0.391 |
| trnF | 27.27 | 12.12 | 27.27 | 33.33 | 60.61 | 39.39 | −0.1 | 0.385 |
| trnG | 18.75 | 14.06 | 23.44 | 43.75 | 62.5 | 37.5 | −0.4 | 0.25 |
| trnH | 18.75 | 10.94 | 34.38 | 35.94 | 54.69 | 45.31 | −0.314 | 0.517 |
| trnI | 18.75 | 14.06 | 32.81 | 34.38 | 53.12 | 46.88 | −0.294 | 0.4 |
| trnK | 20.9 | 11.94 | 25.37 | 41.79 | 62.69 | 37.31 | −0.333 | 0.36 |
| trnL1 | 15.38 | 13.85 | 29.23 | 41.54 | 56.92 | 43.08 | −0.459 | 0.357 |
| trnL2 | 20.31 | 14.06 | 29.69 | 35.94 | 56.25 | 43.75 | −0.278 | 0.357 |
| trnM | 28.79 | 13.64 | 19.7 | 37.88 | 66.67 | 33.33 | −0.136 | 0.182 |
| trnN | 22.86 | 14.29 | 24.29 | 38.57 | 61.43 | 38.57 | −0.256 | 0.259 |
| trnP | 22.06 | 8.82 | 30.88 | 38.24 | 60.29 | 39.71 | −0.268 | 0.556 |
| trnQ | 18.18 | 7.58 | 31.82 | 42.42 | 60.61 | 39.39 | −0.4 | 0.615 |
| trnR | 15.52 | 15.52 | 22.41 | 46.55 | 62.07 | 37.93 | −0.5 | 0.182 |
| trnS1 | 12.5 | 16.07 | 28.57 | 42.86 | 55.36 | 44.64 | −0.548 | 0.28 |
| trnS2 | 15.87 | 14.29 | 22.22 | 47.62 | 63.49 | 36.51 | −0.5 | 0.217 |
| trnT | 20.59 | 10.29 | 27.94 | 41.18 | 61.76 | 38.24 | −0.333 | 0.462 |
| trnV | 23.44 | 12.5 | 21.88 | 42.19 | 65.62 | 34.38 | −0.286 | 0.273 |
| trnW | 20.63 | 11.11 | 28.57 | 39.68 | 60.32 | 39.68 | −0.316 | 0.44 |
| trnY | 16.42 | 11.94 | 37.31 | 34.33 | 50.75 | 49.25 | −0.353 | 0.515 |

15.17%; T = 48.02%; G = 27.51%; and C = 9.31%. The whole mitogenome of *F. intermediate* was biased toward AT nucleotides (63.19%) (**Table 3**). All genes were encoded on the minority (N) strand (**Table 2**). There was a 10 bp overlap between genes in five locations: trnP/trnI, trnK/nad3, trnC/rrnS, trnY/trnL1, and trnL1/trnS2.

## PCGs and Codon Usage

The mitogenome of *F. intermediate* had 12 typical PCGs, containing seven NADP genes (nad1-6 and nad4L), one ATP gene (atp6) and four cytochrome genes (cox1-3 and cob) (**Figure 1**). The region of PCGs was 8,160 bp in size. The PCGs started with ATG (cox1-3, nad4L), ATA (cob, nad3, nad6), TAG (nad4), ATC (atp6), ATT (nad1-2, nad5), and nine PCGs, terminated by TAA (cox1-3, atp6, nad2, nad4, nad5, nad6 and nad4L). The nad1 and nad3 used TAG as a stop codon whereas the cob terminated by a single T (**Table 2**).

The pattern of codon usage and relative synonymous codon usage (RSCU) in the *F. intermediate* mt DNA was studied. A total of 2,716 amino acids were encoded by the *F. intermediate* mitogenome, including the termination codes. The most frequently used amino acids were Leu (16.72%), followed by Val (12.74%), Phe (10.90%), Ser (10.09%) and Gly (8.39%) (**Table 4** and **Figure 2**).

**TABLE 4 |** The codon number and relative synonymous codon usage in *F. intermediate* mitochondrial protein coding genes.

| Amino acid | Codon | Count | RSCU | Amino acid | Codon | Count | RSCU | Amino acid | Codon | Count | RSCU | Amino acid | Codon | Count | RSCU |
|---|---|---|---|---|---|---|---|---|---|---|---|---|---|---|---|
| Phe(F) | UUU | 284 | 1.92 | Ser(S) | UCU | 128 | 3.24 | Tyr(Y) | UAU | 118 | 1.90 | Cys(C) | UGU | 89 | 1.93 |
| | UUC | 12 | 0.08 | | UCC | 5 | 0.13 | | UAC | 6 | 0.10 | | UGC | 3 | 0.07 |
| Leu(L) | UUA | 72 | 0.38 | | UCA | 5 | 0.13 | End (*) | UAA | 1 | 2 | Trp(W) | UGA | 14 | 0.31 |
| | UUG | 308 | 1.62 | | UCG | 20 | 0.51 | | UAG | 0 | 0 | | UGG | 77 | 1.69 |
| Leu(L) | CUU | 62 | 3.35 | Pro(P) | CCU | 57 | 2.68 | His(H) | CAU | 43 | 1.91 | Arg(R) | CGU | 38 | 2.87 |
| | CUC | 3 | 0.16 | | CCC | 3 | 0.14 | | CAC | 2 | 0.09 | | CGC | 0 | 0 |
| | CUA | 1 | 0.05 | | CCA | 5 | 0.24 | Gln(Q) | CAA | 6 | 0.55 | | CGA | 5 | 0.38 |
| | CUG | 8 | 0.43 | | CCG | 20 | 0.94 | | CAG | 16 | 1.45 | | CGG | 10 | 0.74 |
| Ile(I) | AUU | 99 | 1.89 | Thr(T) | ACU | 53 | 3.03 | Asn(N) | AAU | 45 | 1.88 | Ser(S) | AGU | 77 | 2.66 |
| | AUC | 6 | 0.11 | | ACC | 3 | 0.17 | | AAC | 3 | 0.12 | | AGC | 2 | 0.07 |
| Met(M) | AUA | 28 | 0.48 | | ACA | 2 | 0.11 | Lys(K) | AAA | 13 | 0.55 | | AGA | 7 | 0.24 |
| | AUG | 88 | 1.52 | | ACG | 12 | 0.69 | | AAG | 34 | 1.45 | | AGG | 30 | 1.03 |
| Val(V) | GUU | 246 | 2.84 | Ala(A) | GCU | 81 | 3.38 | Asp(D) | GAU | 59 | 1.97 | Gly(G) | GGU | 147 | 2.58 |
| | GUC | 11 | 0.13 | | GCC | 5 | 0.21 | | GAC | 1 | 0.03 | | GGC | 5 | 0.09 |
| | GUA | 24 | 0.28 | | GCA | 4 | 0.17 | Glu(E) | GAA | 10 | 0.32 | | GGA | 18 | 0.32 |
| | GUG | 65 | 0.75 | | GCG | 6 | 0.25 | | GAG | 53 | 1.68 | | GGG | 58 | 1.02 |

## A+T Skewness and Transfer RNAs

In the mitogenome of *F. intermediate*, the skew of AT was negative and the skew of GC was positive, indicating an obvious bias toward the use of T and A (**Table 3**). Like most mt DNA, the *F. intermediate* mitogenome contained a set of 22 tRNAs genes. The tRNAs ranged in size from 57 to 71 bp. All the tRNA genes were present on the N strand and all the tRNA genes had the typical cloverleaf structure (**Figure 3**).

## Phylogenetic Analysis

The phylogenetic relationship was analyzed based on the concatenated nucleotide sequences of 12 PCGs from 36 Trematoda and one outgroup. The result of analyses, generated a consistent tree topologies (**Figure 4**).

In this study, the ML analyses showed that each superfamily in the tree formed a monophyletic clade. Obviously, *F. hepatica, F. intermediate,* and *F. gigantica* clustered in one branch in the phylogenetic tree with high nodal support values (**Figure 4**), indicating that *F. hepatica, F. intermediate,* and *F. gigantica* have a sister group relationship. Additionally, the phylogenetic analyses revealed that *F. hepatica*, *F. intermediate,* and *F. gigantica* were grouped into one clade in fascioliases within Trematoda, which was consistent with a previous study (4).

## Comparative mt Genomic Analyses With *F. hepatica, F. intermediate*, and *F. gigantica*

The complete mitogenome sequences in this study (*F. intermediate*, *Fi*, MH621335.1) were 493, 414, and 518 bp shorter than *F. intermediate* from bovine (*fin*, KF543343.1, 14453 bp), *F. hepatica* (*Fh*, AP017707.1, 14374 bp), and *F. gigantica* (*Fg*, KF543342.1, 14478 bp), respectively. A comparison of the nucleotide sequences of each mt gene and the amino acid sequences, conceptually translated from all mt protein-encoding genes of the four flukes, as shown in **Tables 5**, **6**. The sequence difference across the entire mitogenome was 182 nucleotide substitutions between *Fi* and *Fin*, 1, 432 nucleotide substitutions between *Fi* and *Fh*, and 197 nucleotide substitutions between *Fi* and *Fg.* The difference across amino acid sequences of the 12 protein-coding was 42 amino acid substitutions between the *Fi* and *Fin*; 270 amino acid substitutions between *Fi* and *Fh*; and 44 amino acid substitutions between *Fi* and *Fg*, respectively.

# DISCUSSION

Fasciolosis is a zoonotic disease belonging to water-borne trematodes. The previous studies showed the prevalence of fasciolosis in Africa with the highest range in cattle (1.2–91.0%) and the lowest in sheep (0.19–73.7%). In America the highest range was in goats (24.5–100%) and the lowest in cattle (3.0–66.7%) in America. In Asia the highest range in cattle (0.71–69.2%) and lowest in goat (0.0–47.0%). In Australia, the highest range was in cattle (26.5–81.0%), and the lowest range was in sheep (5.5–52.2%). While in Europe, the highest range was in cattle (0.12–86.0%) and the lowest in goats (0.0–0.8%) (20).

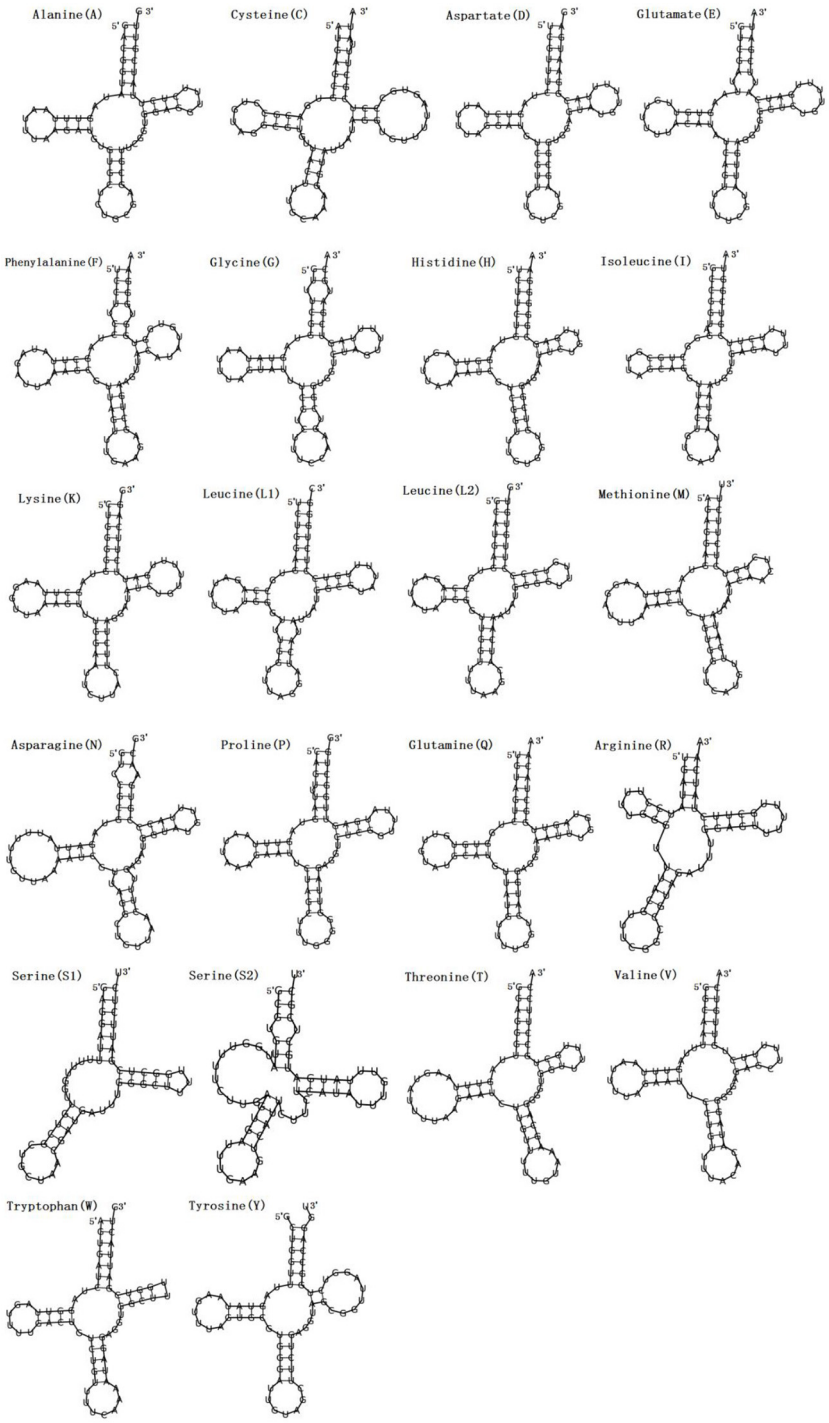


**FIGURE 2 |** Secondary structures of the 22 transfer RNA genes of *F. intermediate* tRNAs (labeled with the abbreviations of their corresponding amino acids).

Annually 2000 million dollars are lost because of helminthic infection (21).

*F. hepatica* and *F. gigantica* are considered two effective species in the genus Fasciola. However, the researchers found that there was also an "intermediate type" of Fasciola (*F. intermediate*). This "intermediate type" of Fasciola was first discovered in Japan and was subsequently reported in China and South Korea (22). Many studies on Fascioliasis have limited information about the Fasciola types in yaks. Genome-based molecular identification has been more commonly employed

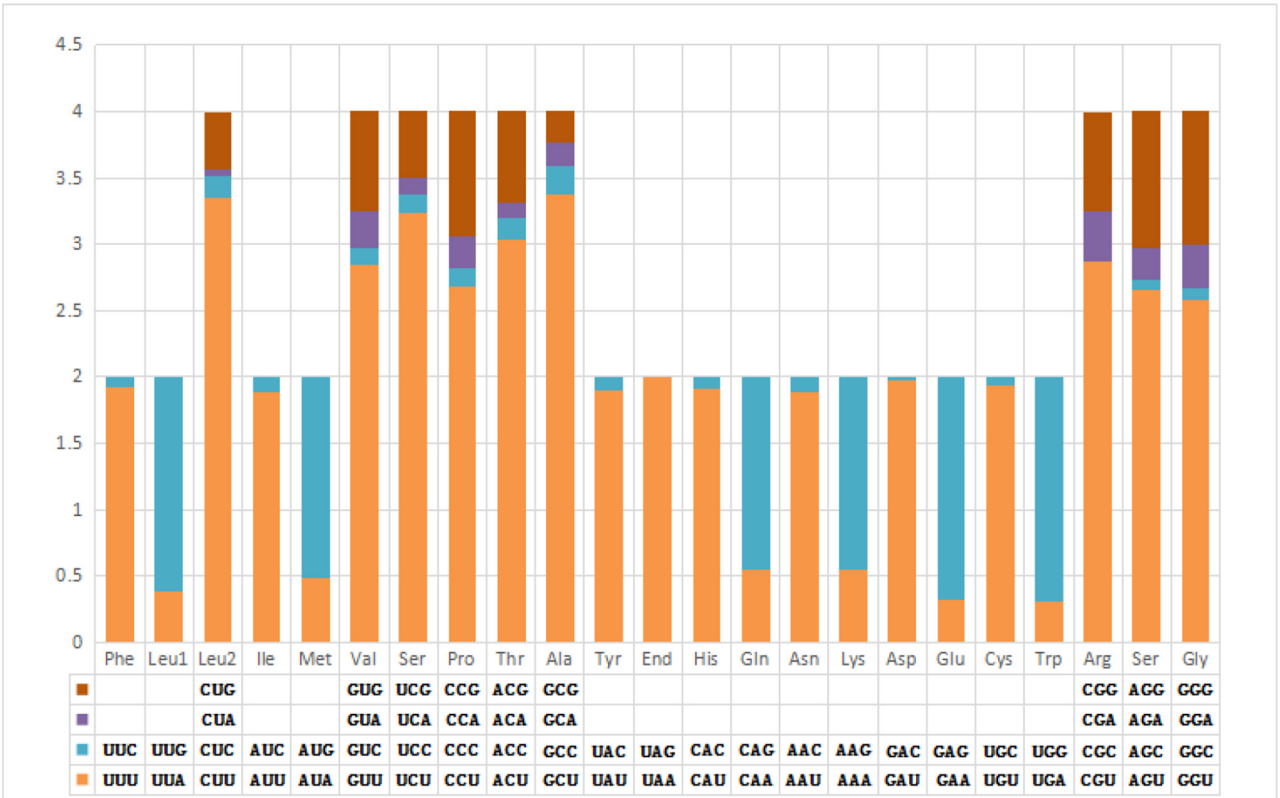


**FIGURE 3 |** Relative synonymous codon usage in *F. intermediate* mitogenome.

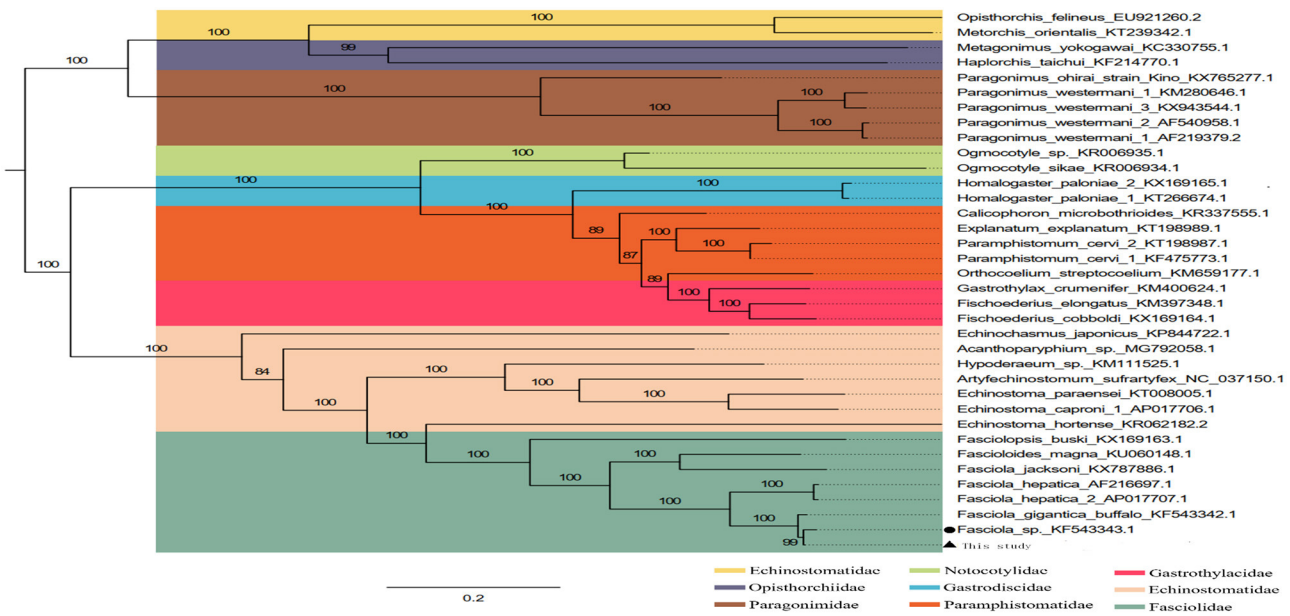


**FIGURE 4 |** Inferred phylogenetic relationship among the *F. intermediate*. The phylogenetic tree was inferred from the nucleotide sequences of mitogenome by using ML methods (Numbers on branches indicate ML).

**TABLE 5 |** The sequence differences of nucleotide (nt) in each mt gene among *F. intermediate*, *F. gigantica* and *F. hepatica*.

| Gene/Region | Nt sequence length | | | | Nt difference | | |
|---|---|---|---|---|---|---|---|
| | ***Fi* (this study)** | ***Fin* (KF543343.1)** | ***Fh* (AP017707.1)** | ***Fg* (KF543342.1)** | ***Fi/Fin*** | ***Fi/Fh*** | ***Fi/Fg*** |
| atp6 | 519 | 519 | 519 | 519 | 29 | 77 | 15 |
| nad1 | 903 | 903 | 903 | 903 | 27 | 67 | 0 |
| nad2 | 867 | 867 | 867 | 867 | 31 | 103 | 0 |
| nad3 | 357 | 357 | 357 | 357 | 20 | 37 | 0 |
| nad4 | 1,269 | 1,269 | 1,272 | 1,269 | 42 | 65 | 20 |
| nad4L | 273 | 273 | 273 | 273 | 0 | 23 | 5 |
| nad5 | 1,566 | 1,566 | 1,566 | 1,566 | 1 | 204 | 28 |
| nad6 | 453 | 453 | 453 | 453 | 0 | 64 | 18 |
| cox1 | 1,542 | 1,542 | 1,542 | 1,542 | 5 | 143 | 26 |
| cox2 | 603 | 603 | 603 | 603 | 1 | 65 | 10 |
| cox3 | 642 | 642 | 642 | 642 | 1 | 83 | 17 |
| cytb | 1,113 | 1,113 | 1,113 | 1,113 | 2 | 90 | 23 |
| rrnL | 986 | 986 | 987 | 986 | 0 | 99 | 10 |
| rrnS | 769 | 769 | 763 | 771 | 0 | 92 | 10 |
| trna | 1,417 | 1,413 | 1,426 | 1,414 | 23 | 171 | 11 |
| at-loop1 | 176 | 176 | 187 | 174 | 0 | 49 | 4 |
| at-loop2 | 329 | 841 | 732 | 841 | – | – | – |

**TABLE 6 |** Amino acid (aa) sequence differences in each mt gene among *F. intermediate, F. gigantica,* and *F. hepatica*.

| Gene/Region | Number of aa | | | | aa difference | | |
|---|---|---|---|---|---|---|---|
| | ***Fi* (this study)** | ***Fin* (KF543343.1)** | ***Fh* (AP017707.1)** | ***Fg* (KF543342.1)** | ***Fi/Fin*** | ***Fi/Fh*** | ***Fi/Fg*** |
| atp6 | 172 | 172 | 172 | 172 | 9 | 25 | 6 |
| nad1 | 300 | 300 | 300 | 300 | 9 | 20 | 0 |
| nad2 | 288 | 288 | 288 | 288 | 5 | 31 | 0 |
| nad3 | 118 | 118 | 118 | 118 | 1 | 9 | 0 |
| nad4 | 422 | 422 | 423 | 422 | 10 | 38 | 7 |
| nad4L | 90 | 90 | 90 | 90 | 0 | 4 | 1 |
| nad5 | 521 | 521 | 521 | 521 | 1 | 58 | 5 |
| nad6 | 150 | 150 | 150 | 150 | 0 | 9 | 11 |
| cox1 | 513 | 513 | 513 | 513 | 4 | 24 | 3 |
| cox2 | 200 | 200 | 200 | 200 | 0 | 10 | 1 |
| cox3 | 213 | 213 | 213 | 213 | 1 | 25 | 5 |
| cytb | 370 | 370 | 370 | 370 | 2 | 17 | 5 |

to identify biological types in recent years due to advances in biotechnology. mt DNA is an ideal genetic marker due to the simple and stable structure, reflecting the maternal genetic background (23).

Our study showed that *F. intermediate* from yak and *F. intermediate* from bovine belonged to the same branch and it was to be similar to *F. gigantica* compared with the *F. hepatica* through phylogenetic analysis. We compared the whole mitochondrial genome between *Fi, Fin, Fg, and Fh.* The results showed that *Fi* was no base site mutations in rrnL and rrnS compared with *Fin,* 10 base site mutations in rrnL and rrnS compared with *Fg*. Compared with *Fh*, *Fi* there were 99 base site mutations in rrnL and 92 base site mutations in rrnS, respectively. Hence, it would be the ideal genetic marker to distinguish the three species of Fasciola. Meanwhile, *Fi* had a deletion of nearly 500 bp in the AT-loop area, compared with *Fin*, *Fg,* and *Fh*, which may be due to the adaptability to plateau for *Fi.*

## CONCLUSION

In this study, we sequenced the complete 13,960 bp mitogenome of *F. intermediate* from yaks, in which 36 genes (12 PCGs, 22tRNA genes and 2 rRNA genes) were located as a typical of

Trematoda mitogenome. All PCGs were initiated by ATN codon, the cob genes had incomplete stop codons consisting of just T, and the other 11 PCGs stop with the canonical TAA or TAG. The AT-skew were negative, and the GC-skew were positive in the mitogenomes of *F. intermediate,* consistent with most sequenced Trematoda. The phylogenetic analyses support that *F. intermediate* from yaks was the same as the *F. intermediate* from bovine. This study would provide a basis for the accurate prevention, diagnosis, and treatment of Fasciolosis in yaks.

## DATA AVAILABILITY STATEMENT

The datasets presented in this study can be found in online repositories. The names of the repository/repositories and accession number(s) can be found in the article/supplementary material.

## ETHICS STATEMENT

The samples were collected under the permission of the relevant institutions. All procedures were approved and performed by Laboratory Animals Research Centre of Hubei province and Qinghai province in P.R. China, and the Ethics Committee of Huazhong Agricultural University, China (Permit number: 4200695757). All animal experiments and procedures were conducted under the relevant procedures of Proclamation of the Standing Committee of Hubei People's congress (PSCH No. 5), China.

## AUTHOR CONTRIBUTIONS

XG, JZ, and JL conceived and designed the study. XG, SZ, ZZ, KL, and XK executed the experiment and analyzed the sera and tissue samples. XG, SZ, CQ, and YL analyzed the data. XG and DW finished the first draft. MK finished the revision. All authors interpreted the data, critically revised the manuscript for important intellectual contents, and approved the final version.

## FUNDING

This study was supported by the Chinese Agricultural Research Systems (CARS-37) and the major science and technology projects of Tibet Autonomous Region (XZ202101ZD0002N).

## REFERENCES

1. Li JK, Li K, Shahzad M, Han ZQ, Nabi F, Gao JF, et al. Seroprevalence of Bluetongue virus in domestic yaks (*Bos grunniens*) in Tibetan regions of China based on circulating antibodies. *Trop. Anim. Health Prod.* (2015) 47:1221–3. doi: 10.1007/s11250-015-0853-0
2. Li K, Gao J, Shahzad M, Han Z, Nabi F, Liu M. Seroprevalence of Toxoplasma gondii infection in yaks (*Bos grunniens*) on the Qinghai-Tibetan Plateau of China. *Vet Parasitol.* (2014) 205:354–6. doi: 10.1016/j.vetpar.2014.07.014
3. Nyindo M, Lukambagire AH. Fascioliasis: an ongoing zoonotic trematode infection. *Biomed Res Int.* (2015) 2015:1–8. doi: 10.1155/2015/786195
4. Liu GH, Gasser RB, Young ND, Song HQ, Ai L and Zhu XQ. Complete mitochondrial genomes of the 'intermediate form' of Fasciola and Fasciola gigantica, and their comparison with F. hepatica. *Parasites & Vectors.* (2014) 7:150. doi: 10.1186/1756-3305-7-150
5. Biu AA, Ahmed MI, Mshelia SS. *Economic assessment of losses due to parasitic diseases common at the Maiduguri abattoir, Nigeria*. African Scientist. (2006).
6. Piedrafita D, Spithill TW, Smith RE, Raadsma HW. Improving animal and human health through understanding liver fluke immunology. *Parasite Immunol.* (2010) 32:572–581 doi: 10.1111/j.1365-3024.2010.01223.x
7. Chen JX, Chen MX, Ai L, Xu XN, Jiao JM, Zhu TJ. An outbreak of human fascioliasis gigantica in Southwest China. *PLoS ONE.* (2013) 8: e71520 doi: 10.1371/journal.pone.0071520
8. Boore JL. Animal mitochondrial genomes. *Nucleic Acids Res.* (1999) 27:1767–80. doi: 10.1093/nar/27.8.1767
9. Liu QN, Zhu BJ, Dai LS, Wei GQ and Liu CL. The complete mitochondrial genome of the wild silkworm moth, *Actias selene*. *Gene*. (2012) 505:291–9. doi: 10.1016/j.gene.2012.06.003
10. Dai LS, Zhu BJ, Liu QN, Wei GQ and Liu CL. Characterization of the complete mitochondrial genome of *Bombyx mori* strain H9 (Lepidoptera: Bombycidae). *Gene*. (2013) 519:326–34. doi: 10.1016/j.gene.2013.02.002
11. Wolstenholme DR. Animal mitochondrial DNA: structure and evolution. *Int Rev Cytol.* (1992) 141:173–216. doi: 10.1016/S0074-7696(08)62066-5
12. Gissi C, Iannelli F, Pesole G. Evolution of the mitochondrial genome of Metazoa as exemplified by comparison of congeneric species. *Heredity*. (2008) 101:301–20. doi: 10.1038/hdy.2008.62
13. Mikkel S. Adapter Removal v2: rapid adapter trimming, identification, read merging. *BMC Res Notes.* (2016) 9:88. doi: 10.1186/s13104-016-1900-2
14. McLean JS, Lombardo MJ, Ziegler MG, Novotny M, Yee-Greenbaum J, Badger JH. Genome of the pathogen Porphyromonas gingivalis recovered from a biofilm in a hospital sink using a high-throughput single-cell genomics platform. *Genome Res.* (2013) 23:867–77. doi: 10.1101/gr.150433.112
15. Coil D, Jospin G, Darling AE. A5-miseq: an updated pipeline to assemble microbial genomes from Illumina MiSeq data. *Bioinformatics.* (2015) 31:587–9. doi: 10.1093/bioinformatics/btu661
16. Toro M, Philippou A, Arboleda S, Puerta M. Mean-field semantics for a process calculus for spatially-explicit ecological models. *Electron Proc Theor Comput*. (2016) 79–94. doi: 10.4204/EPTCS.204.7
17. Bernt M, Donath A, Juhling F, Externbrink F, Florentz C, Fritzsch G, et al. (2013). MITOS: Improved *de novo* metazoan mitochondrial genome annotation. *Mol Phylogenet Evol.* 69:313–9. doi: 10.1016/j.ympev.2012.08.023
18. Beatson SA, das Graças de Luna M, Bachmann NL, Alikhan NF, Hanks KR, Sullivan MJ. Genome sequence of the emerging pathogen Aeromonas caviae. *J Bacteriol.* (2011) 193:1286–7. doi: 10.1128/JB.01337-10
19. Tamura K, Stecher G, Kumar S. *MEGA 11: Molecular Evolutionary Genetics Analysis Version 11. Mol Biol Evol.* (2021). doi: 10.1093/molbev/msab120
20. Mehmood K, Zhang H, Sabir AJ, Abbas RZ, Ijaz M, Durrani AZ. A review on epidemiology, global prevalence and economical losses of fasciolosis in ruminants[J]. *Microb Pathog.* (2017) 109:253–62. doi: 10.1016/j.micpath.2017.06.006
21. Mungube EO, Bauni SM, Tenhagen BA, Wamae LW, Nginyi JM, Mugambi JM. The prevalence and economic significance of Fasciola gigantica and

Stilesia hepatica in slaughtered animals in the semi-arid coastal Kenya. *Trop Anim Health Prod.* (2006) 38:475–83. doi: 10.1007/s11250-006-4394-4

22. Zeng MH, Lan Z, Guo XR. Analysis of polymorphic sites in the large and small ribosomal subunit sequences of the "intermediate" Fasciola [J]. *Heilongjiang Animal Husbandry and Veterinary Medicine.* (2020) 09:85—8.
23. Tang MT, Zhou Y, Liu YH. Molecular identification of Fasciola in Dali Prefecture, Yunnan Province. *Chin J Biol.* (2019) 14:525–9.

**Conflict of Interest:** The authors declare that the research was conducted in the absence of any commercial or financial relationships that could be construed as a potential conflict of interest.

**Publisher's Note:** All claims expressed in this article are solely those of the authors and do not necessarily represent those of their affiliated organizations, or those of the publisher, the editors and the reviewers. Any product that may be evaluated in this article, or claim that may be made by its manufacturer, is not guaranteed or endorsed by the publisher.

# Advantages of publishing in Frontiers

**OPEN ACCESS**
Articles are free to read for greatest visibility and readership

**FAST PUBLICATION**
Around 90 days from submission to decision

**HIGH QUALITY PEER-REVIEW**
Rigorous, collaborative, and constructive peer-review

**TRANSPARENT PEER-REVIEW**
Editors and reviewers acknowledged by name on published articles

**Frontiers**
Avenue du Tribunal-Fédéral 34
1005 Lausanne | Switzerland

**Visit us:** www.frontiersin.org
**Contact us:** frontiersin.org/about/contact

**REPRODUCIBILITY OF RESEARCH**
Support open data and methods to enhance research reproducibility

**DIGITAL PUBLISHING**
Articles designed for optimal readership across devices

**FOLLOW US**
@frontiersin

**IMPACT METRICS**
Advanced article metrics track visibility across digital media

**EXTENSIVE PROMOTION**
Marketing and promotion of impactful research

**LOOP RESEARCH NETWORK**
Our network increases your article's readership